Open Research Online

The Open University's repository of research publications
and other research outputs

Preparation of Bimetallic Catalysts by Surface Organometallic Chemistry

Thesis

How to cite:

Marshall, Robert (1999). Preparation of Bimetallic Catalysts by Surface Organometallic Chemistry. PhD thesis The Open University.

For guidance on citations see FAQs.

© 1998 Robert Marshall

https://creativecommons.org/licenses/by-nc-nd/4.0/

Version: Version of Record

Link(s) to article on publisher's website:
http://dx.doi.org/doi:10.21954/ou.ro.00010216

Copyright and Moral Rights for the articles on this site are retained by the individual authors and/or other copyright owners. For more information on Open Research Online's data policy on reuse of materials please consult the policies page.

oro.open.ac.uk

UNRESTRICTED

PREPARATION OF BIMETALLIC CATALYSTS BY SURFACE ORGANOMETALLIC CHEMISTRY

Robert Marshall, B.Sc.

A thesis submitted for the degree of Doctor of Philosophy

DATE OF SUBMISSION: 30 SEPTEMBER 1998
DATE OF AWARD: 22 JANUARY 1999

The Open University
Department Of Chemistry

September, 1998

ProQuest Number: C717918

All rights reserved

INFORMATION TO ALL USERS
The quality of this reproduction is dependent upon the quality of the copy submitted.

In the unlikely event that the author did not send a complete manuscript and there are missing pages, these will be noted. Also, if material had to be removed, a note will indicate the deletion.

ProQuest C717918

Published by ProQuest LLC (2019). Copyright of the Dissertation is held by the Author.

All rights reserved.
This work is protected against unauthorized copying under Title 17, United States Code
Microform Edition © ProQuest LLC.

ProQuest LLC.
789 East Eisenhower Parkway
P.O. Box 1346
Ann Arbor, MI 48106 – 1346

Abstract

Surface organometallic chemistry (SOMC) has been used to prepare a range of bimetallic catalysts. This work reports, for the first time, the preparation of alumina supported palladium iron and platinum iron catalysts by reaction of ferrocene with a reduced monometallic catalyst. In addition, alumina supported and carbon supported platinum tin and alumina supported palladium tin catalysts were prepared using this technique using tetrabutyl tin. The catalysts were characterised using a range of techniques to determine the extent of the interaction between the two metals. Hydrogen chemisorption, TEM, EDX and cyclic voltammetry provide evidence of such an interaction and indicate that the catalysts consist of bimetallic particles. This provides evidence for a selective reaction between the organometallic precursor and the parent metal. Mössbauer, EPR and EXAFS spectroscopies have been used to examine the effect of different reducing and oxidising environments on the structure of a PdFe catalyst. These suggest, that in air, the particles exist as palladium with an overlayer of FeO_x. The alumina supported catalysts were tested for the gas phase catalytic hydrogenation of 1,3-butadiene and crotonaldehyde. The results show, that the addition of the second metal, can modify the activity and selectivity of the parent catalyst towards these reactions, in particular PtFe which shows an enhanced activity for both. Comparison of the range of carbon supported platinum tin catalysts with different loadings towards the electrooxidation of carbon monoxide has shown a significant effect on the addition of a quarter of a monolayer coverage of tin. On further addition of tin, there is little further change in the electrochemical properties or indeed the number of exposed platinum sites. Comparison of a catalyst prepared using SOMC and another, of similar loading, prepared using hydrolysis/precipitation suggests that the SOMC exhibits a greater level of control over the electrocatalytic properties.

Acknowledgments

I would like to sincerely thank Dr. Eleanor M. Crabb for her help and encouragement throughout the duration of this work.

In addition, I would also like to thank the following people who have contributed at various stages of this work: Prof. Frank Berry, Mr. Karl Whittle and Mr. Neil Bailey for their help with the Mössbauer and EXAFS experiments; Dr. Charlie Harding for collecting the EPR spectrum; Mr. Gordon Oates for writing the computer software used for the surface area measurements; the technical staff of the Chemistry Department – Messrs. Gibbs, Jeffs, Leslie and Patel – for their technical expertise throughout; Ms Naomi Williams and the staff of the Open University Electron Microscopy Centre for their help with the electron microscopy work; Dr. Dave Thompsett and Mr. Alex Gunner for obtaining the electrochemical data described in Chapter 5; and Dr. Mike Mortimer for reading the final draft of this thesis.

The funding of The Open University, The Nuffield Foundation and EPSRC is gratefully acknowledged.

Table of Contents

CHAPTER 1

Introduction

1.1 Introduction and scope of the thesis

This thesis is concerned with the preparation, characterisation and testing of a range of bimetallic catalysts prepared using surface organometallic chemistry (SOMC). The main aim of this work has been to extend the range and applications of catalysts prepared using this method and in doing so, to develop a greater understanding of the technique and the catalysts themselves. Investigations have concentrated on two main systems: firstly, a series of MM'/Al_2O_3 bimetallic catalysts (where M is Pd or Pt, and M' is Fe or Sn) and, secondly, a range of Pt/C catalysts modified with Sn.

After this brief introductory chapter, the thesis is divided into a further four main chapters. The remainder of this chapter briefly reviews bimetallic catalysts, their benefits and how they work, and gives a overview of what is meant by surface organometallic chemistry. Chapter 2 describes the experimental methods used during the work; this includes a description of the preparation of both the monometallic and bimetallic catalysts and details of the techniques used to characterise these catalysts. A brief summary of the theory of the techniques and the experimental procedures used is given. The procedures and apparatus used in the experiments to evaluate catalyst performance are also described. The results are reported and discussed in Chapters 3 to 5. Each chapter begins with a brief literature review of the relevant area. Chapter 3 is concerned with the preparation and characterisation of γ-alumina supported palladium and platinum monometallic and bimetallic catalysts. Catalytic evaluation of these materials is

discussed in Chapter 4. Two reactions were used to probe the activity of these catalysts: i) the hydrogenation of 1, 3-butadiene and (ii) the hydrogenation of crotonaldehyde. Both reactions are of industrial importance and have been studied quite extensively; however, few reports exist concerning the application of bimetallic catalysts prepared by SOMC towards these particular reactions. Chapter 5 describes the research carried out on the PtSn/C system. This was performed in collaboration with Johnson Matthey plc. Results are presented for the preparation and characterisation of a range of PtSn/C catalysts. A variety of traditional characterisation techniques (such as TEM and chemisorption) were used along with electrochemical evaluation using linear potential sweep cyclic voltammetry and CO electrooxidation.

1.2 Background

It is not the intention here to present an introduction to catalysis (see for example, [1-4]), rather the following paragraphs contain a brief summary of the concepts which highlight the need for the preparation of bimetallic catalysts using SOMC.

Bimetallic catalysts

Bimetallic catalysts have attracted scientific interest since the 1950's when it was established that an improvement in activity, selectivity and/or lifetime may be observed for a catalytic reaction on addition of a second metal component to a monometallic catalyst. One of the best known and most intensively studied

applications of bimetallic catalysts is the use of platinum-rhenium catalysts for catalytic reforming reactions. A wide range of bimetallic catalysts have now been investigated and many examples exist in the literature where improvements in catalyst performance have been observed [5]. The earliest theory proposed to account for the bimetallic phenomena involved charge transfer between the two metallic elements and was known as the Rigid Band Theory (RBT) [4]. Although this theory was successful in explaining certain metal combinations (such as the Pd-Au pair) the theory was eventually discarded with the advent of techniques able to study the density of states profiles of the metal systems. Today, the properties of bimetallic catalysts are usually explained in terms of geometric or electronic modification of the catalyst surface and Chapter 3 discusses these ideas further.

Bimetallic catalysts are typically prepared by either impregnation (which can be either co- or successive impregnation) or by a precipitation reaction. However, these methods often lead to a non-homogeneous catalyst where a mixture of phases may be present. These phases may consist of bimetallic particles, alloy particles or separate particles of the individual metals and often a mixture of oxidation states of the metals, thus making characterisation of bimetallic catalysts a difficult proposition. High temperature treatments are often required for formation of the bimetallic or alloy particles thus promoting the unwanted sintering of the particles. Furthermore, these methods of preparing bimetallic catalysts are not always reproducible from one preparation to another. Thus a reproducible method of preparing bimetallic catalysts which leads to a

homogeneous and single phase catalyst is sought, preferably without the use of high temperature treatments. Among the attempts to achieve this goal include the use of bimetallic carbonyl compounds such as $Co_2Rh_2(CO)_{12}$ [6] where the carbonyl complex is decomposed and reduced on the surface of a support producing small alloy particles; however, this technique has not been used extensively. There also exist a group of reactions which can be described as 'controlled surface reactions'. These reactions are similar in that they involve the deposition of a second metal onto the surface of a preprepared monometallic catalyst but differing in the mode of deposition. One method uses hydrogen chemisorbed on the surface of the first metal to reduce a second metal and another uses the difference in the redox potentials of the two metals to deposit the second metal onto the surface of the first metal. These two methods have been successfully applied in the example of Pt-Au bimetallic catalysts [7]. A third 'controlled surface reaction' involves the use of surface organometallic chemistry to deposit one metal onto the surface of another. It is this method that is chosen in the present work to prepare bimetallic catalysts. In the following paragraphs an introduction to surface organometallic chemistry will be given although the bulk of the review of this area will be presented in Chapter 3. It is useful to note at this stage that in this work the term alloy is avoided, instead the term bimetallic particle is preferred which is taken to denote a particle which contains two metallic elements. It should also be noted that the term bimetallic particle used here implies that two metallic elements are involved, however the characterisation studies presented later investigate if this was the case or whether

metal oxide particles exist instead. However for simplicity the term bimetallic particle will be retained.

Surface Organometallic Chemistry

The use of surface organometallic chemistry to prepare bimetallic catalysts is a relatively new procedure with the first reports appearing in the literature in the mid-1980's. The technique involves the modification of a monometallic catalyst by addition of a second metal which is introduced in the form of an organometallic species. This species is believed to react preferentially with hydrogen preadsorbed on the surface of the first metal, thus forming particles which contain the two metals in intimate contact. In the present work tetrabutyl tin and ferrocene have been used to deposit Sn and Fe, respectively, on supported monometallic Pd or Pt catalysts. In principle the technique allows greater control of the final composition and structure of the catalyst particles than is currently possible using conventional techniques of bimetallic catalyst preparation. As a consequence it may be possible to prepare catalysts for a specific reaction rather than the sometimes empirical nature of catalyst choice used today.

It should be evident from the above discussion of the SOMC approach that a well-defined monometallic catalyst is required. The preparation and characterisation of these monometallic catalysts is thus important to the overall method.

1.3 References

1 Bond, G. C., "Heterogeneous Catalysis and Applications." Oxford University Press, Oxford, 1987.

2 Farrauto, R. J., and Bartholomew, C. H., "Fundamentals of Industrial Catalytic Processes." Blackie Academic & Professional, London, 1997.

3 Bond, G. C., and Ponec, V., *Stud. Surf. Sci. Cat.*, **95**, Elsevier, Amsterdam, (1995).

4 Foger, K., *in* "Catalysis: Science and Technology" (J. R. Anderson and M. Boudart, Eds.) **6**, Springer-Verlag, Amsterdam, 1984.

5 Sinfelt, J. H., "Bimetallic catalysts, discoveries and concepts." Wiley, New York, 1983.

6 Anderson, J. R., and Mainwaring, D. E., *J. Catal.* **35**, 162 (1974).

7 Dumas, J. M., Geron, C., Hadrane, H., Marecot, P., and Barbier, J., *J. Mol. Cat.* **77**, 87 (1992).

8 Ryndin, Y. A., Yermakov, Y. I., *in* "Surface Organometallic Chemistry: Molecular Approaches to Surface Catalysis" (J. M. Basset *et al.*, Eds.), p. 127, Kluwer Academic Publishers, Dordrecht, 1988.

CHAPTER 2

Experimental

2 Introduction

This chapter describes the experimental procedures used throughout the course of this research. The first section (Section 2.1) describes the methods of preparation for both the monometallic and bimetallic catalysts. Section 2.2 describes the techniques used to characterise the catalysts, including a brief outline of the theory of the techniques and experimental procedures used. The theory and procedures used in the electrochemical evaluation of the carbon supported platinum based catalysts are described in Section 2.3. The final section describes the testing procedures used to probe the activity of the catalysts (Section 2.4).

A full list of the chemicals and reagents used during the preparation, characterisation and testing of the catalysts is given in Appendix 1.

2.1 Catalyst Preparation

Supports

The support materials used for the catalysts were γ-alumina, an important support used widely for commercial catalysts [1], and a carbon furnace black, a commonly used support for electrode applications [2]. The structures and properties of these support materials can be found in the literature [3-5].

The γ-alumina support was received as cylindrical pellets. These were ground in a mortar and pestle and sieved to give support grains in the range 250 μm to 500 μm; the grains were calcined in a programmable muffle furnace at 773 K for 1 h and stored in a desiccator until required. The BET surface area of the calcined support was 180 $m^2 g^{-1}$ and the pore volume of the support, as determined by wetting until water was no longer absorbed, was found to be 1.5-2.0 $cm^3 g^{-1}$.

The carbon support, Vulcan XC72R, a furnace carbon black with a BET surface area of 240 $m^2 g^{-1}$, was supplied by Johnson Matthey plc.

2.1.1 Monometallic catalysts

The palladium and platinum monometallic catalysts supported on γ-alumina were prepared using a wet impregnation technique. This widely used technique is described in detail in various reviews published on catalyst preparation methods for example, [1, 6-8] and will be described only briefly here. The aim of impregnation is to distribute the active metal phase in the most efficient way on the surface of the support in order to obtain a large surface area of the active phase thereby maximising the area available for adsorption of reactants. The support material is contacted with a suitable solution of a salt of the metal to be deposited. The object is to fill the pores of the support with a solution of the metal salt of sufficient concentration to give the desired loading. During the

impregnation and subsequent drying step the metal salt is deposited onto the support. Wet impregnation typically performed for salts which have a low solubility, involves *wetting* the support material with the metal salt solution by adding an amount of solution greater than the pore volume of the support. After contacting the support with the metal salt solution for a sufficient length of time, the catalyst preparation is typically completed by a *drying* stage to remove the solvent, and a *calcination* stage to decompose the metal salt precursor to the supported metal or metal oxide.

The Pd and Pt salts chosen were the acetylacetonato complexes of the metals, ($Pd(CH_3COCHCOCH_3)_2$ and $Pt(CH_3COCHCOCH_3)_2$). The complex was dissolved in excess toluene and added to the calcined γ-alumina. A ratio of approximately 1.0 g γ-alumina to 2.5 cm^3 toluene was found to give reproducible results. The solvent was allowed to evaporate from the metal salt/γ -alumina mixture over several hours at room temperature, then the impregnated γ-alumina was dried at 383 K overnight and further calcined for 1 h at 623 K (for the palladium containing catalysts) or 473 K (for the platinum containing catalysts). The metal loading of the catalysts can be expressed in terms of weight% (wt%) of the support if it is assumed that (i) all of the metal complex added was absorbed by the γ-alumina support, and (ii) that there is no loss of metal under the relatively mild calcination conditions. The actual metal content was accurately determined by elemental analysis (ICP-AES) and any difference

observed between the nominal loading and the actual loading is discussed in the results chapters.

Different palladium salts (dinitrodiammine palladium, $(Pd(NO_2)_2(NH_3)_2$, and ammonium tetrachloropalladate, $(NH_4)_2PdCl_4$,) were used to prepare monometallic Pd catalysts in order to examine the effect of different metal precursors on the final catalyst. These particular catalysts were prepared by impregnating alumina with an excess of a solution of the appropriate salt and, after a length of time in contact at room temperature, the catalyst preparation was completed by drying at 383 K (16 h) and calcination at 623 K (1 h).

The carbon supported platinum (Pt/C) monometallic catalyst was kindly supplied by Johnson Matthey plc. Its preparation, details of which have been published in the patent literature [9], involves the hydrolysis/precipitation reaction of the platinum salt chloroplatinic acid (H_2PtCl_6) on a carbon support at 373 K. After removal of the solvent (demineralised water) the Pt/C was then reduced in a flow of hydrogen.

In addition to the Pd and Pt monometallic catalysts it was also necessary to prepare both Fe/Al_2O_3 and Sn/Al_2O_3 samples for comparison. These were prepared by a wet impregnation technique using solutions of iron nitrate ($Fe(NO_3)_3.9H_2O$) and tin octoate ($C_{16}H_{30}O_4Sn$) respectively. Both impregnated samples were dried at 383 K overnight and then calcined at 623 K for 1 h.

2.1.2 Bimetallic catalysts

Surface organometallic chemistry (SOMC) was used to prepare the bimetallic catalysts listed below in Table 2.1. The principles behind this method of preparing bimetallic catalysts were discussed in Chapter 1 and will be discussed in greater length in Chapter 3.

Table 2.1 List of bimetallic catalysts prepared using surface organometallic chemistry.

γ-alumina supported	carbon supported
$PdFe/Al_2O_3$	PtSn/C
$PdSn/Al_2O_3$	
$PtFe/Al_2O_3$	
$PtSn/Al_2O_3$	

2.1.2.1 Apparatus

The apparatus used to prepare the bimetallic catalysts by SOMC is shown schematically in Figure 2.1. It was constructed from a series of interconnected lengths of 1/8" PTFE tubing. A Pyrex reactor and a saturator vessel (H. Bambauch & Company Ltd.) were connected to the apparatus by Swagelok coupling fittings (North London Valve & Fitting Company Ltd.). The Pyrex

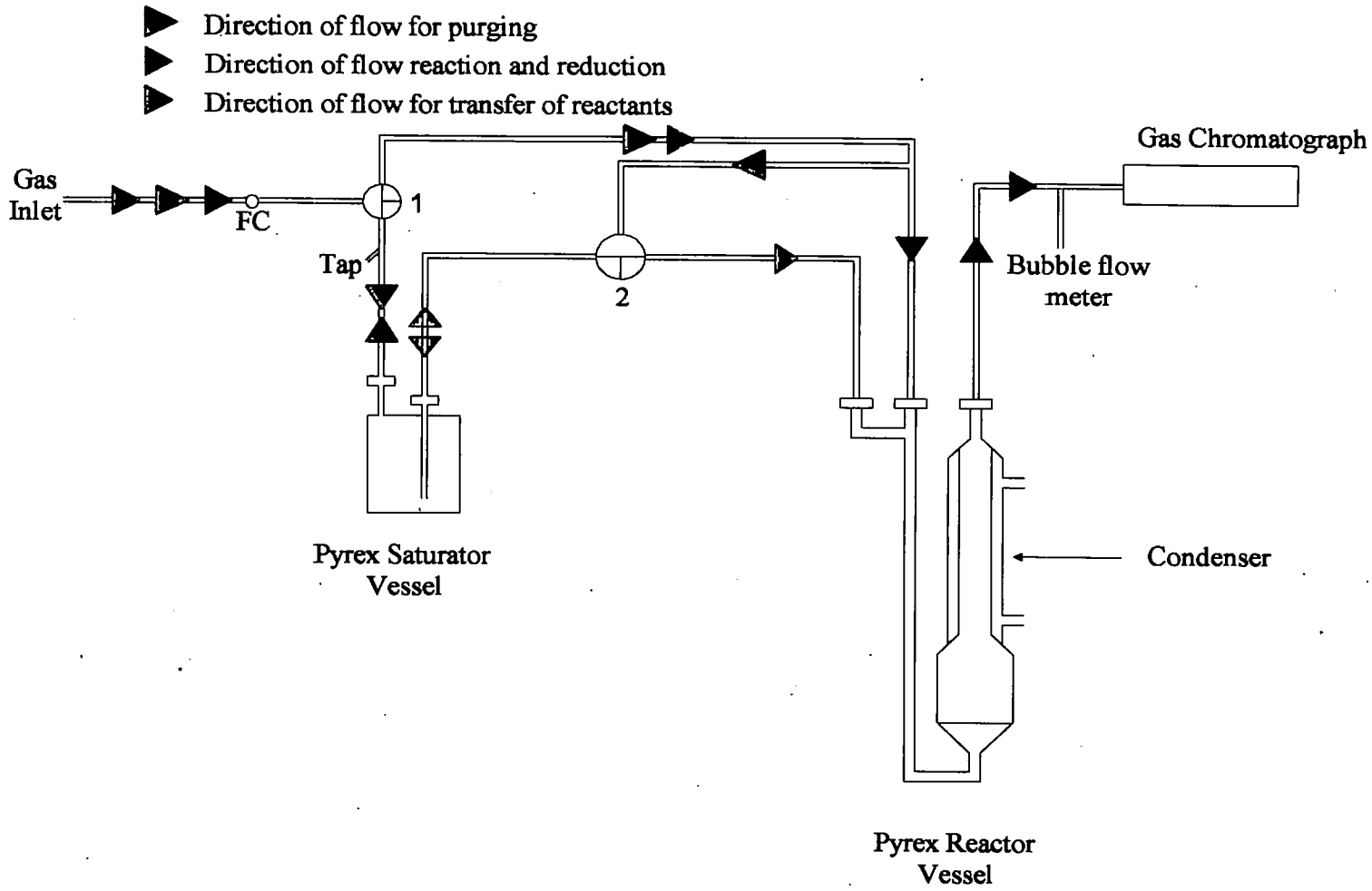

Figure 2.1 Schematic diagram of apparatus used for preparation of bimetallic catalysts by SOMC.

reactor was fitted with a condenser tube so that cooling water could be circulated to minimize loss of the solvent by vaporisation. Two three-way valves (Hoke) and a tap were included in the apparatus to allow the system to be purged of air. The apparatus was designed to allow the reduction of a parent monometallic catalyst followed by purging and transfer of a solution from the Pyrex saturator vessel into the Pyrex reactor vessel without exposure to air.

Gas flow was controlled by a Jones Chromatography flow controller (model 1000A110ABF) (represented by FC in Figure 2.1) with the flow measured at the point shown on the diagram by a bubble flow meter. The reactor was heated using a programmable homemade vertical tube furnace controlled by a Eurotherm Model 818. Sampling of the effluent gases from the reactor was achieved by feeding a length of PTFE tubing from the exit of the reactor into an AI Cambridge GC94 gas chromatograph equipped with a flame ionisation detector and fitted with a 15% Apiezon L on Chrompac 80/100 mesh column (1/8", 8 m) operating at 338 K.

2.1.2.2 Preparation procedure

A known mass of monometallic catalyst (prepared in the manner described in Section 2.1.1) was loaded into the Pyrex glass reactor vessel, which was then attached to the apparatus shown in Figure 2.1. The catalyst was reduced in hydrogen at a flow rate of 100 $cm^3 min^{-1}$. The reduction program consisted of an

initial ramp of 1 K min^{-1} from room temperature to the required reduction temperature; 623 K for the palladium catalysts and 473 K for the platinum catalysts. This temperature was maintained for 3 hours before the reactor was cooled to room temperature at a rate of 1 K min^{-1}.

With the catalyst in the reduced state, a surface organometallic reaction was carried out to prepare the bimetallic catalyst. The organometallic precursor selected was either tetrabutyltin for the tin bimetallics or ferrocene for the iron bimetallics. The amount of the precursor added was calculated to provide a given coverage of the first metal surface assuming that all the precursor added would react and that the dispersion of the monometallic catalysts was known. The precursor was added to the Pyrex saturator vessel with a volume of heptane to give a ratio of 2.5 cm^3 solvent to 1.0 g catalyst. Then bypassing the reactor, by turning valve 2 and opening the tap, the apparatus was purged with nitrogen for several minutes to remove air from the system. Once purged the direction of the gas flow was changed - by closing the tap and switching valve 1 - to pump the contents of the saturator into the reactor containing the reduced monometallic catalyst. The gas was then switched to hydrogen which was bubbled through the reactor at 100 cm^3 min^{-1} for 24 hours. The reaction was monitored by analysing alkyl species in the gas stream exiting the reactor. The solvent level was topped up as necessary by adding heptane to the saturator vessel, purging the system as described above and then pumping the solvent into the reactor vessel. After 24 hours at room temperature the reactor was heated to 343 K using an

electromantle heater; the temperature of the catalyst was monitored using a thermocouple inserted in a thermocouple well situated near the catalyst bed. Online sampling of the reaction products was continued during this period. After a further 8 hours the heat was removed and the flow of water through the condenser discontinued so that the remaining solvent could evaporate. Once dry, the catalyst was discharged from the reactor, washed in heptane to remove any unreacted organometallic precursor of the second metal, filtered and dried. The dried catalyst was then reloaded into the reactor and reduced using the same procedure as the initial reduction process.

2.2 Methods of Catalyst Characterization

The monometallic and bimetallic catalysts were characterized using a range of physical and chemical techniques to gain information on their structure. Several books and reviews describe the common methods of catalyst characterisation (for example, [10-12]). Some of the most commonly used techniques in catalyst characterisation are chemisorption studies, electron microscopy and temperature-programmed reduction. Many of the techniques are relatively straightforward to perform; however, analysis is often not straightforward and the conclusions can be uncertain.

The characterisation techniques used in this work are described in the following sections. In each section, after a brief introduction, the theory behind the

technique will be discussed followed by a description of the apparatus and the experimental procedures used.

2.2.1 Surface area measurements

2.2.1.1 Introduction

For each catalyst the total surface area of the catalyst and the dispersion (defined as the ratio of the number of metal atoms on the surface to the total number of metal atoms) of the noble metal were obtained. The total surface area was determined using nitrogen physical adsorption. Metal dispersion was obtained via chemical adsorption of hydrogen as well as carbon monoxide onto the metal surface.

2.2.1.2 Theory

Adsorption

It is well known [13] that a gas will be adsorbed onto a solid surface due to the forces acting between the surface and the gas. Depending on the nature of the interaction between the solid (adsorbent) and gas (adsorbate) and the temperature, the adsorption can be described as either *physical adsorption* or *chemical adsorption* [13].

Physical adsorption is due to the attraction that exists between a molecule and a surface resulting from intermolecular forces. The strength of the adsorption relates to the physical properties of the adsorbate and depends little on the chemical nature of the solid. This adsorption is not specific and can be used for the determination of the total surface area of a solid. Multilayer adsorption is possible where an adsorbed layer can build up on the initially adsorbed layer.

Chemical adsorption is a very specific interaction and can only occur if the adsorbate is capable of forming a chemical bond with an active site on the surface of the solid. Thus by choosing an adsorbate which adsorbs on the metal surface and not the support surface, chemical adsorption can be used to determine just the specific surface area of the supported metal, rather than the total surface area of the support and metal surface combined.

The extent of adsorption of a gas by a solid depends on a number of factors including the surface area of the solid sample, the temperature, the pressure of the gas and the chemical nature of both the solid and the gas. Of particular interest is the relationship between the quantity of gas adsorbed by the solid surface at constant temperature and the relative pressure of the gas with which it is in equilibrium: this is called the adsorption isotherm. The isotherm that derives from the adsorption of a gas by a porous material is commonly referred to as a

type II isotherm after the original classification of the five main types of isotherm by Brunauer, L. Deming, W. Deming and Teller [14].

Total surface area measurements

The principal method of determining the total surface area of a catalyst is via physical adsorption isotherm measurements. If the conditions under which a complete adsorbed layer of gas, averaging one molecule thick, can be established and the area per molecule of the gas is known (A_m), then the number of moles of gas adsorbed (n_m), determined from the adsorption isotherm, gives the surface area, A as follows:

$$A = n_m A_m L \tag{2.1}$$

where L is the Avogrado constant.

The most useful model used for determining the value for the monolayer capacity and hence, the total surface area was proposed by Brunauer, Emmett and Teller (BET) in 1938 [15]. This is based on the kinetic model of the process of *chemical adsorption* presented by Langmuir [16] which can be extended to cover *physical adsorption.*

The monolayer volume can be calculated using the BET equation derived from their theoretical model [15]:

$$\frac{V}{V_m} = \frac{c(p/p^o)}{(1-p/p^o)(1+(c-1)p/p^o)} \qquad (2.2)$$

where V is the volume of gas adsorbed for a given mass of adsorbent at the equilibrium pressure p; V_m is the monolayer capacity; p is the equilibrium pressure; p^o is defined as the pressure of the adsorbate over its condensed phase at the adsorption temperature and c is a constant related to the net heat of adsorption.

Rearranging this equation gives:

$$\frac{p}{V(p^o-p)} = \frac{1}{V_m c} + \frac{c-1}{V_m c}\left(\frac{p}{p^o}\right) \qquad (2.3)$$

If the solid is a porous material then V/V_m plotted against p/p^o gives a type II isotherm and $p/V(p^o-p)$ plotted against p/p^o gives a straight line with gradient, s equal to $(c-1)/V_m c$ and intercept i equal to $1/V_m c$.

Solving these two equations simultaneously gives V_m and c:

$$V_m = \frac{1}{s+i} \qquad c = \frac{s}{i} + 1 \tag{2.4}$$

The number of adsorbed molecules in the monolayer, n_m, can be calculated from the volume of the monolayer according to the equation (2.5):

$$n_m = V_m / V_m^{\theta} \tag{2.5}$$

where V_m^{θ} is the molar volume of an ideal gas. The total surface area can thus be calculated according to equation (2.1).

Any condensable inert gas can be used for the determination but the molecules should be small and roughly spherical, so that all the interior surface area of a porous solid is contacted. For these reasons the adsorbate used is usually nitrogen. The physical adsorption of nitrogen will be fairly weak and detectable only at low temperatures, thus the surface area is measured at 77 K. It is assumed that A_m, the average area occupied by one nitrogen molecule in the completed monolayer, is 0.162 nm^2 [17, 18].

Using nitrogen as the adsorbate, the BET equation can be used over a range of relative pressures p/p^o between approximately 0.05 and 0.3. Between these

values the BET equation is linear; at lower values the data becomes less accurate and at higher values the complexities associated with multilayer adsorption become apparent [18].

Metal Surface area (or dispersion) measurements

Determination of the metal surface area or, more usefully, dispersion is not as straightforward as determination of the total surface area. The procedure involves the selective chemisorption of an adsorbate gas onto the surface metal atoms and not onto the catalyst support surface. It is then possible to determine the metal dispersion from the isotherm obtained. However, careful consideration must be given to the choice of adsorbate gas depending on the metal to be investigated. For palladium and platinum most workers have used either carbon monoxide or hydrogen [19] due to the unambiguous stoichiometry of the chemisorption. In the present work we have used both hydrogen and carbon monoxide chemisorption for the determination of metal dispersion. It is assumed that hydrogen dissociatively adsorbs on both metals and that carbon monoxide is associatively adsorbed on platinum (CO chemisorption was not used for palladium catalysts).

From the adsorption isotherm obtained from selective chemisorption on the metal surface, by plotting the quantity of gas adsorbed onto the catalyst versus p/p^o, it is possible to calculate the dispersion of the active metal component on the surface

of the support. For both hydrogen and carbon monoxide chemisorption this is possible by extrapolating the isotherm to the region of zero pressure; the volume adsorbed at this point is denoted Q^o. This figure is then inserted into either equation (2.6) to give H/M, the ratio of hydrogen atoms adsorbed to the total number of metal atoms, or equation (2.7) to give CO/M, the ratio of CO molecules adsorbed to the total number of metal atoms:

$$H/M = \left(\frac{2Q^0}{Mass.\left(\frac{\%M}{RMM} \right)} \right) \tag{2.6}$$

$$CO/M = \left(\frac{Q^0}{Mass.\left(\frac{\%M}{RMM} \right)} \right) \tag{2.7}$$

where *Mass* is the mass of sample (g); *% M* is the percentage metal in the sample (expressed as a % by weight) and *RMM* is the relative molecular mass of the metal component.

The factor of 2 in the numerator in equation (2.6) derives from the assumption that hydrogen is dissociatively adsorbed on the catalyst surface. If it is assumed that one hydrogen atom is chemisorbed per surface metal atom then H/M x 100 % will give the percentage of the metal atoms on the surface i.e. the dispersion.

Similarly CO/M x 100 % gives the dispersion from the CO chemisorption experiments.

2.2.1.3 Apparatus

Figure 2.2 shown below is schematic for the apparatus that was constructed for the determination of surface area. The volumetric vacuum system was made of glass and all taps were gas-tight greaseless taps (J. Young), fitted with PTFE 'O' rings.

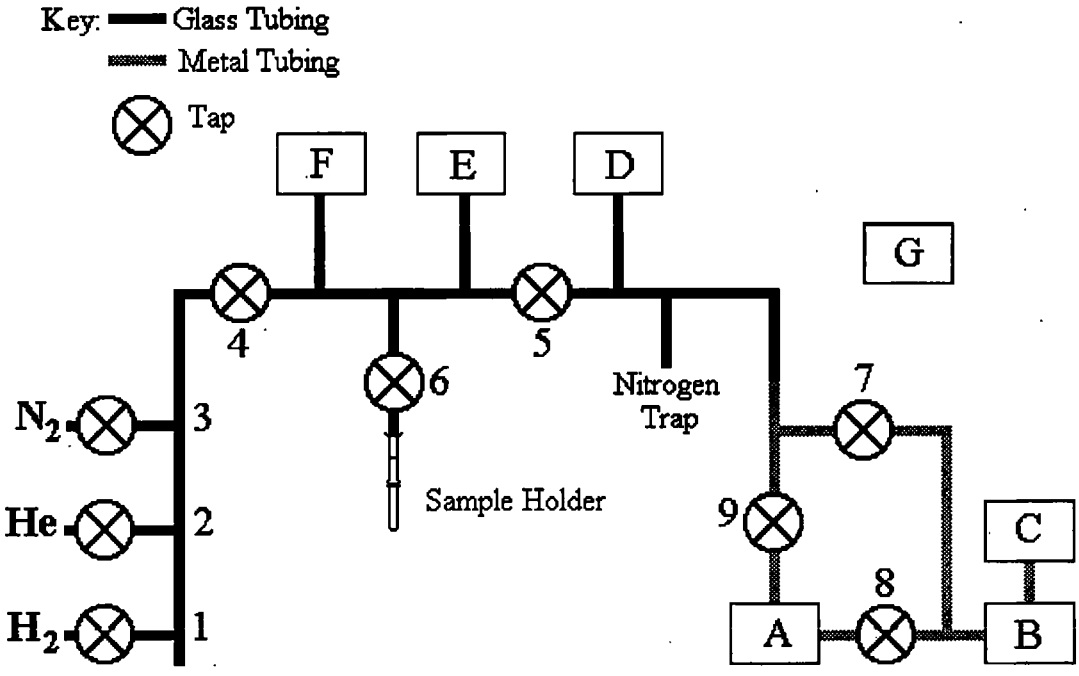

Figure 2.2 Schematic diagram of apparatus used for determination of catalyst surface area and dispersion. Each box containing a letter will be defined in the text below.

Figure 2.3 below shows in greater detail the main section of the vacuum apparatus including the volumes V_d, V_n, V_s and V_x.

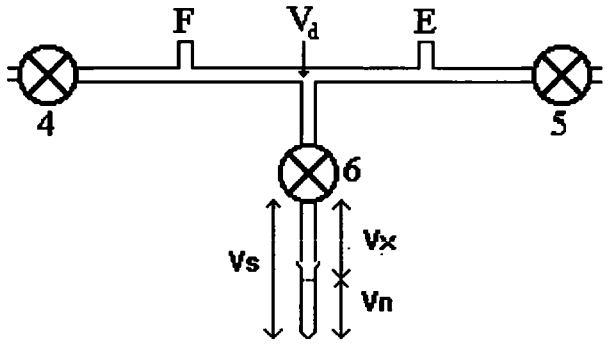

Figure 2.3 Schematic diagram showing position of V_d, V_n, V_s and V_x on vacuum line apparatus.

The sample was placed into a Pyrex sample chamber which was clipped to the system using a ball and socket joint (J. Young) with a silicone 'O' ring. A sinter was placed above the sample chamber to prevent catalyst particles being sucked up into the system. Samples in the sampleholder were heated using a home-made vertical heating column controlled by a Zenith variable transformer. The system was evacuated by an Edwards Air Cooled Diffusion pump [A] backed up by an Edwards Two way Rotary Pump [B]; together these allowed a vacuum of 10^{-5}/ 10^{-6} mbar to be achieved. A trap containing liquid nitrogen was situated on the line leading to the pumps to prevent any unwanted products from contaminating the pumps. The pressure in the vacuum line was measured by means of two

pressure gauges attached to the line; an Edwards Active Pirani Gauge [C] reads the pressure in the range 100 to 10^{-3} mbar and an Edwards Active Inverted Magnetron [D] gauge reads the pressure in the 10^{-3} to 10^{-8} mbar range. Regular heating of the vacuum line by means of a hot air blower was necessary to keep the system dry.

Helium and nitrogen gas cylinders were attached to the line via taps 2 and 3 respectively, and either hydrogen or carbon monoxide gas cylinders were attached via tap 1. These were prevented from over pressuring the line by means of mini-pressure regulators. The pressure of the gases in the dosing volume was measured by two Edward Barocel Capacitance Barometers positioned as shown, [E, F]. [E] measured the pressures in the range 0 to 1 000 mbar and [F] in the range 0 to 10 mbar. All pressures measured by the pressure gauges were displayed by an Edwards Active Gauge Controller [G].

The apparatus was calibrated by expansion of nitrogen from the dosing volume into two bulbs of known volume. The sample volume was then calibrated by gas expansion from the calculated dosing volume. Each procedure to determine V_d, V_s and V_n was repeated several times and the individual values obtained were averaged to give the values used in the calculations. The full procedure used and calculations made are given in Appendix 2A.

2.2.1.4 Experimental procedure

i) Total surface area measurement

A sample (approximately 0.1 g) of the solid was loaded into the dry, clean sampleholder and attached, with the sinter in place, to the vacuum line. Typically each sample was then outgassed at room temperature for about 17 h followed by heating to 523 K for 1 h. Outgassing was essential to ensure that any water or other gases present had desorbed from the catalyst surface. If this is not done, slow desorption during the experiment may lead to errors. After removing the furnace, outgassing was continued as the sample was allowed to return to room temperature. The vacuum attained was typically in the region of 10^{-5}-10^{-6} mbar. Particular attention was taken to maintain a standard outgassing routine, with respect to duration, temperature and final pressure, in order to be able to legitimately compare results from separate experiments.

With taps 4, 5 and 6 closed, the sampleholder was immersed in a Dewar containing liquid nitrogen up to a pre-etched mark on the sampleholder. This level was kept constant by continually topping up the dewar. Nitrogen gas was then admitted into the dosing volume by opening taps 3 and 4 and the dosing pressure recorded (P_d^1). The temperature of the dosing volume was also recorded (T_1) using a thermocouple attached to the vacuum line for this purpose. Tap 6 was then opened a pre-determined amount and the nitrogen allowed to expand

into the sample volume and adsorb onto the sample. On reaching equilibrium (indicated by constant pressure) tap 6 was closed and the equilibrium pressure recorded (P_e^1). Successive expansions were performed with increasing dosing pressure until sufficient adsorption points had been acquired. Typically seven points were taken with dosing pressures 50, 75, 100, 150, 200, 250 and 300 mbar.

It is assumed in the treatment of the data that the volume of sample in the sampleholder was zero. For more accurate results it was possible to calculate the actual volume that the sample occupied. The procedure to obtain a true value of V_s is identical to that outlined in Appendix 2A to calibrate the sample volume V_s for the empty sampleholder, except that the sampleholder now contained the sample and helium gas was used as the adsorbate. Helium does not adsorb onto the solid surface. The procedure was performed after the sample was outgassed, prior to the BET procedure, again outgassing the sample for a further 15 minutes to remove the helium before carrying on.

The data points obtained from the BET experiment were processed using a personal computer program to solve the BET equation giving the total surface area in $m^2 g^{-1}$. The theory behind these calculations is given in Appendix 2B.

To validate the calibration of the apparatus and the procedure used, a standard sample of graphitized carbon black with a known total surface area (71.3 $m^2 g^{-1}$ ±

2.7 $m^2 g^{-1}$ was available (obtained from the National Physical Laboratory, UK). In addition, the surface area of the γ-alumina was confirmed (180 $m^2 g^{-1}$) by experiment.

ii) Metal surface area or dispersion measurements

Approximately 0.1 g of the catalyst sample to be examined was loaded into the calibrated sampleholder and attached to the vacuum line. The sample was then outgassed at 523 K for 1 h before cooling to room temperature. This was followed by reduction under a static pressure (750 mbar) of hydrogen for 30 min at 623 K for the Pd containing catalysts, or 473 K for the Pt containing catalysts. After 30 min tap 5 was then opened to remove the hydrogen from the sampleholder and dosing volume; the sample was then outgassed for a further 30 min at the same temperature. Outgassing was continued once the furnace was removed while the sample cooled down. Once cool, taps 4, 5 and 6 were closed and hydrogen was admitted to the line (opening tap 1). Note that if the BET experiment for determination of the total surface area was to be performed on the same sample, this was carried out before the chemisorption experiment after the initial outgassing of the sample and before the reduction procedure. The data for the isotherm were obtained by successive expansion of either hydrogen or carbon monoxide onto the sample at room temperature. It should be noted that, as discussed by Chou *et al.* [20], there are three stages of *sorption* of hydrogen on palladium. These stages are the chemisorption of hydrogen on the surface of the

Pd crystallite, followed by penetration of hydrogen into the sublayers of the crystallite to form the α-phase palladium hydride and finally diffusion into bulk crystallites to form β-phase palladium hydride. Therefore, when determining the Pd metal surface area low pressures of hydrogen were used to prevent the formation of α- and β-phase palladium hydride thus avoiding overestimation of the number of metal atoms on the surface. This problem is not encountered when determining platinum surface areas since Pt does not form a β-hydride phase and so higher hydrogen pressures could be used. Thus, typically 7 or 8 data points were collected in each experiment with values of P_d^n between 1 mbar and 12 mbar for the palladium samples and between 1 mbar and 750 mbar for platinum catalysts. The CO chemisorption experiment on the Pt-based catalysts used pressures of between 1 mbar and 400 mbar. Again the data points obtained were processed by a personal computer program which generated Q^o and hence dispersion values using either equation (2.6) or (2.7). Details of the calculation are provided in Appendix 2C.

Again validation of the calibration and the experimental procedure was possible due to access to a platinum catalyst with a known dispersion (0.5 wt% Pt/Al_2O_3, Micrometrics, dispersion 29.5 ± 5%).

2.2.2 Mössbauer spectroscopy

2.2.2.1 Introduction

Mössbauer Spectroscopy (sometimes known as nuclear γ-ray resonance spectroscopy) is a spectroscopic technique which has generally not achieved wide use for the study of catalyst structure principally because only a small number of catalytically active elements display the so called Mössbauer effect. Nevertheless, it is possible to identify phases, determine oxidation states and derive structural information by interpretation of the data obtained from the Mössbauer experiment.

Details of Mössbauer spectroscopy and its application to catalysis, mainly applied to catalysts containing iron (^{57}Fe) or tin (^{119}Sn), can be found in the literature [21-25]. The theory of the technique and the experimental procedure is described in the following sections.

2.2.2.2 Theory

Mössbauer spectroscopy accurately analyses the energy levels of a nucleus and therefore reflects the chemical and electronic environment surrounding the nucleus [21, 22]. It does this by utilising the phenomenon known as the Mössbauer effect. This effect is best understood by considering the two cases

shown in Figure 2.4. Initially in both cases a radioactive nucleotide decays into a nucleus in an excited state. This can further decay into a nucleus in the ground state by emission of a γ-ray. The radioactive nucleotide or source is chosen so that it decays to the same nucleus as the sample under study. Thus for ^{57}Fe Mössbauer spectroscopy the radioactive nucleotide used is usually ^{57}Co which decays to ^{57}Fe by capture of an electron. The fate of the emitted γ-ray will differ depending on the environment of the excited nucleus. In case (a) if one considers the excited nucleus to be free and able to vibrate, then the emitted γ-ray will not be absorbed by another similar nucleus, in the ground state, due to the recoil energy involved. However in case (b) if the excited nucleus is in a solid lattice and is held rigidly in place so the atom cannot recoil as if it were free, the recoil energy is taken up by the vibrations of the lattice as a whole. Also, if conditions were such that the recoil energy of the photon emission and absorption is significantly smaller than the energy of the lattice vibrations, then it is possible that a fraction of the photons emitted by the source nucleus will be reabsorbed by the nucleus in the absorber. This is the Mössbauer effect and forms the basis for Mössbauer spectroscopy. In the case of ^{57}Fe spectroscopy the absorber nucleus will be a ground state ^{57}Fe nucleus in the sample under study.

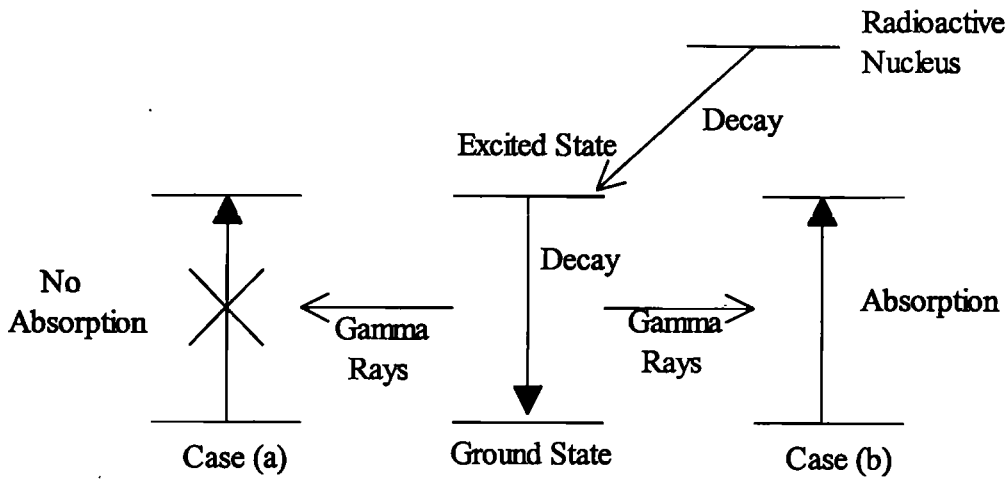

Figure 2.4 Representation of decay of excited nucleus by emission of γ-ray and subsequent fate of emitted γ-ray.

For ^{57}Fe the energy of the transition between the excited state and the ground state is 14.4 keV.

In the Mössbauer experiment the emitted γ-ray energy is modulated by imparting a Doppler velocity to the source of γ-rays so that γ-rays of discrete energies can be resonantly absorbed by absorber nuclei.

The Mössbauer spectrum consists of a proportional count of the number of γ-rays transmitted by the sample versus the velocity of the sample and peak(s) are observed where resonance occurs. The main parameters that can be obtained in the Mössbauer experiment are the isomer shift, the quadrupole splitting and the magnetic hyperfine splitting. The isomer shift reflects the coloumbic interaction

between the positively charged nucleus and the negatively charged s-electrons surrounding the nucleus and gives a measure of the oxidation state of the absorber atom (^{57}Fe in our case). In oxidic compounds of iron one usually only encounters high spin configurations of Fe^{2+} and Fe^{3+}. Fe^{2+} usually displays an isomer shift of about 1.2 to 2 mms^{-1} and Fe^{3+} from about 0.4 to 1.1 mms^{-1} (both high spin).

2.2.2.3 Apparatus

A standard Mössbauer instrument was used. The γ-ray source was mounted on a vibrator and the desired range of γ-ray energies was achieved by vibrating the source at a velocity in the range of a few millimetres per second. The instrument is shown schematically in Figure 2.5 below.

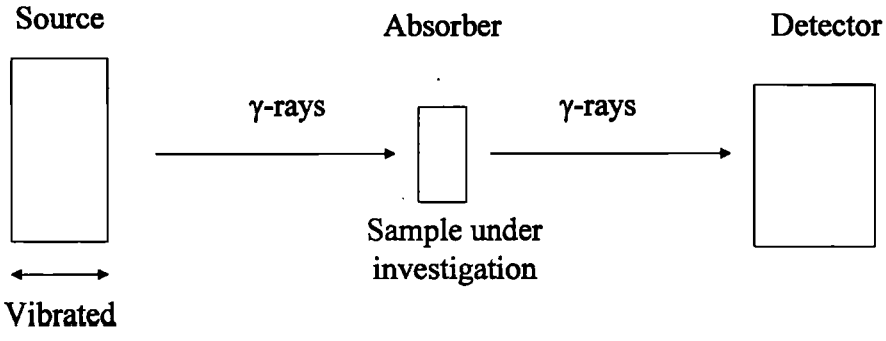

Figure 2.5 Schematic diagram of the layout of the Mössbauer spectroscopy experiment.

The γ-ray source used was a ^{57}Co/Rh matrix source embedded in a resin. A glass vessel was used to contain the sample under investigation and is shown in Figure 2.6. The glass vessel was connected via 1/8" PTFE tubing and a three-way tap (Omnifit) to a hydrogen line. The vessel allowed collection of Mössbauer data after reducing the catalyst sample without exposure of the sample to air. The vessel was fitted with aluminised mylar windows transparent to γ-rays. The sample was reduced by placing the glass vessel in a vertical tube furnace controlled by a Eurotherm Controller (Model 818).

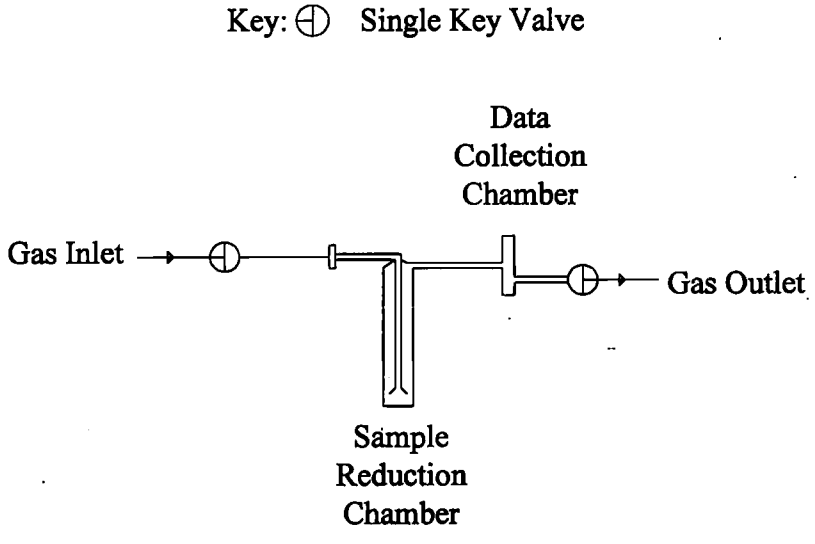

Figure 2.6 Diagram of the glass sample vessel used for Mössbauer spectroscopy.

2.2.2.4 *Experimental procedure*

A small amount of catalyst (approximately 0.5 g) was loaded into the glass vessel and then reduced at 623 K (at a ramp rate 1 K min^{-1}, then held for 3 hours at 623 K) in flowing hydrogen (100 cm^3 min^{-1}). After the sample had cooled to room temperature, the three-way taps at either end of the glass vessel were closed and the hydrogen flow discontinued. Collection of the Mössbauer data was achieved by placing the glass vessel in the Mössbauer collection apparatus. After collecting the data for 14 days the data was processed and analysed using specialised software (kindly supplied by the University of Iceland).

A standard Mössbauer spectrum was obtained from an iron foil and all isomer shifts values are quoted relative to this. The spectra of ferrocene and $FeCl_3$ were also collected for comparison.

2.2.3 X-ray powder diffraction

2.2.3.1 *Introduction*

X-ray powder diffraction (XRD) has been used routinely for the characterisation of crystalline solids for many years. However, application of the technique in catalysis has been more restricted due to the limited crystallinity of most supported metal catalyst systems. In addition the loading of the active metal

phase in a typical metal catalyst is usually below the threshold of sensitivity of the technique. A further limitation is that only relatively large particles can be examined due to the severe X-ray line broadening in the case of small particles so, therefore, a well dispersed catalytic phase will not be observed. Nevertheless in favourable circumstances, where the catalyst displays a degree of crystallinity and where the phases under investigation are present in sufficient quantities it is possible to extract structural information, such as phase composition and crystallite size, from an XRD pattern [26, 27].

2.2.3.2 Theory

XRD uses the principle of diffraction [28]. When a X-ray beam strikes an atom the interaction between the X-rays and the electrons in the atom results in scattering of the X-rays in all directions. A crystal is comprised of regular arrays of atoms, which cause diffraction of the X-rays, analogous to diffraction experiments with a diffraction grating. In practice a crystal is more complicated than a grating since it has a 3-D array of atoms and is considered in terms of reflecting parallel planes. These parallel planes cause diffraction of monochromatic X-rays, producing diffraction lines. If the diffracted X-rays are in phase then constructive interference will occur and if they are out of phase then destructive interference will occur. For constructive interference to occur the path difference must be a multiple of the wavelength as expressed by Bragg's law [29]:

$$n\lambda=2d\sin\theta \qquad (2.8)$$

where n is an integer, λ is the wavelength of the incident x-ray beam, d is the interplanar spacing and θ is the angle of reflection. Thus Bragg's law imposes a stringent condition on the angles at which a reflection may occur. Each crystalline solid has its own characteristic X-ray powder pattern which, in many cases, may be used as a finger print in identification.

2.2.3.3 Apparatus

The X-ray powder diffraction patterns were obtained using a Siemens D5000 Diffractometer. A CuKα radiation source filtered by a nickel filter was used.

2.2.3.4 Experimental procedure

The catalyst samples were pressed flat on a plastic plate and placed in the diffractometer. The samples were scanned from $4° < 2\theta < 70°$ at room temperature. The recorded patterns were matched against existing powder patterns using the Joint Committee on Powder Diffraction Standards (JCPDS) file.

2.2.4 Extended X-ray absorption fine structure

2.2.4.1 Introduction

Extended X-Ray Absorption Fine Structure (EXAFS) is a technique which has found prominence more recently in the field of catalyst characterisation [32-36]. Information about the local structure around a particular atom, such as the distance to the nearest neighbour, the type and number of neighbours, can be drawn from EXAFS data. It should be noted that EXAFS gives an average picture of the environment around a particular atom so therefore, unlike other techniques such as XRD, it is not necessary for the sample to have an ordered structure. The theory of the technique and a discussion of the mathematical modelling used to interpret the data obtained from the experiment are available in the literature [37].

2.2.4.2 Theory

The principle behind the technique relies on the scattering of photoelectrons by atoms in the unit cell. If an atom absorbs an X-ray it emits a photoelectron with a certain energy which upon encountering neighbouring atoms in the lattice can be scattered. Due to the wave nature of the photoelectron, the emitted electrons and the back scattered electrons can interfere constructively or destructively depending on the wavelength of the electron, the distance between the emitting

and scattering atom and the phase shift caused by the scattering. This interference can be observed in the X-ray absorption spectrum. However the extraction of meaningful information from EXAFS data is not always a straightforward and unambiguous task. A typical X-ray absorption spectrum is shown in Figure 2.7 and three distinct segments can be identified: (i) the pre-edge absorption region, (ii) the absorption edge where the X-rays are of sufficient energy to eject an electron from the K- or L-shell of the atom and (iii) the post-absorption edge region. The oscillations observed in the post-edge absorption region of the X-ray absorption are known as EXAFS.

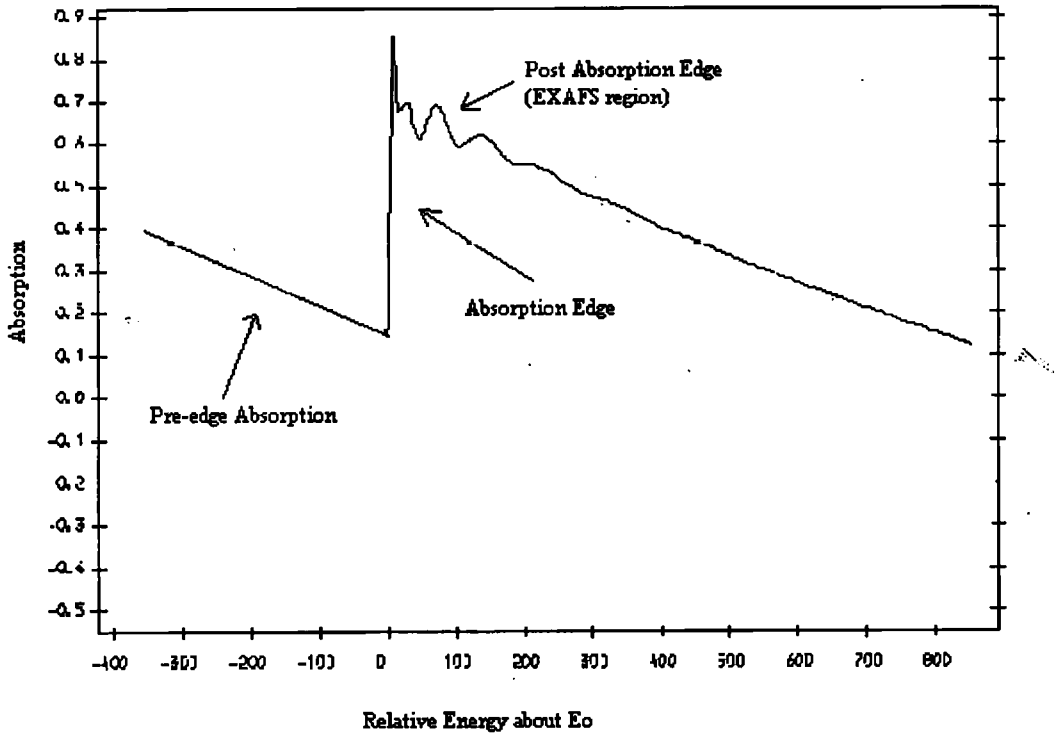

Figure 2.7 Typical X-ray absorption spectrum.

The raw X-ray absorption spectrum without any data analysis does supply some information. The intensity of the wiggles observed in the so called fine structure region of the spectrum goes up if the number of neighbours increases, the number of oscillations depends inversely on interatomic distances and the step height of the edge jump is proportional to the number of atoms in the sample. The EXAFS spectrum is obtained from the X-ray absorption spectrum by subtracting the background and the edge jump to leave the fine structure spectrum. The EXAFS signal is the product of a sine function and the backscattering amplitude F(k) divided by k where k is the wave number. Fourier transformation is used to decompose the spectrum into the different contributions from individual interactions. Detailed information on the procedures used to analyse the X-ray absorption spectrum is given below in Section 2.2.4.5.

2.2.4.3 Apparatus

EXAFS experiments at the Pd K-edge, Fe K-edge and Sn K-edge were performed at station 9.2 at the Synchrotron Radiation Source (SRS) of the Central Laboratory of the Research Councils (CLRC) at Daresbury, UK. The storage ring operated at 2 GeV with an average beam current of 200 mA and the monochromator was the double crystal Si (220).

Where it was necessary to reduce a catalyst and to record the EXAFS data without the catalyst being exposed to air, then the catalyst was reduced in a U-

tube glass reactor which could then be isolated by means of three-way taps (Omnifit) at either end of the reactor. The sample was then taken into a dry glove box and loaded into a sampleholder under air and moisture free conditions. The samples were then stored in a glass vacuum dessicator until required.

The sampleholders consisted of three circular sheets of aluminium each with a 2.5 cm x 1.5 cm window (see Figure 2.8). The outer two sheets had circular groves (plate 1) in which rubber 'O'-rings were placed. The middle layer (plate 2) contained the sample in the window with two circular sheets of transparent mylar placed on either side. The outer plates then completed the sandwich all held together by fours screws. The sampleholder was designed in order to seal the samples in an air and moisture free environment once prepared.

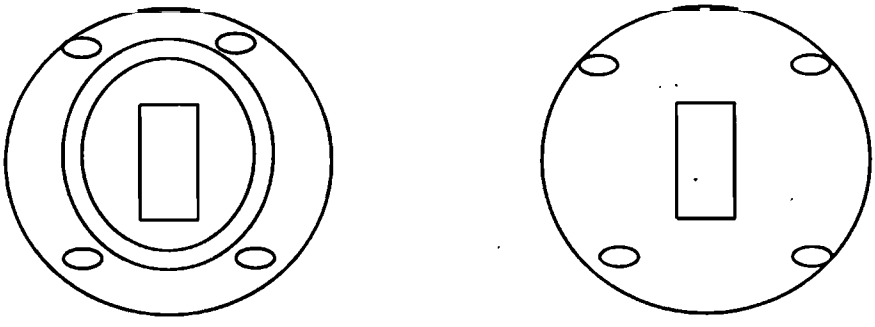

PLATE 1 PLATE 2

Figure 2.8 Circular aluminium plates used for storing EXAFS samples.

2.2.4.4 Experimental procedure

The spectra were obtained in the fluorescence mode and the average time to obtain a spectrum was approximately 45 minutes. For several samples more than one spectrum was recorded in order to improve the quality of the data by increasing the signal to noise ratio.

The following procedure was used to obtain the EXAFS data. First, the ionising chamber was filled with the necessary gas partial pressure for the edge under investigation and then placed between the X-ray beam and the sample. The position of the beam was then recorded by burning a spot on a piece of photographic paper. A laser was then lined up with the position of the beam and the catalyst sample positioned correctly using the laser beam. The fluorescence detector was placed in position so that a sufficient number of counts was obtained. For each different edge investigated the monochromator was set to the correct position. Before recording a set of data it was checked that the correct energy range was being scanned to ensure that the X-ray absorption edge jump was obtained. After these procedures were fulfilled it was possible to obtain an X-ray absorption spectrum of the sample under investigation. Pd, Fe and Sn foils were available to record the phase shift and intermetallic bond distance of the individual elements.

2.2.4.5 *Treatment of EXAFS data*

Analysis of EXAFS is relatively complex. Overall the initial procedure removes the background spectrum to leave only the EXAFS oscillations. The computer program EXBACK was used to achieve the background subtraction. This multistep process initially involved determining the absorption edge (E_o) where the EXAFS oscillations start; this then allowed energy rescaling with E_o defined as the point of zero energy. The pre-edge absorption was fitted to a linear polynomial function and extrapolated across the EXAFS region (Figure 2.9).

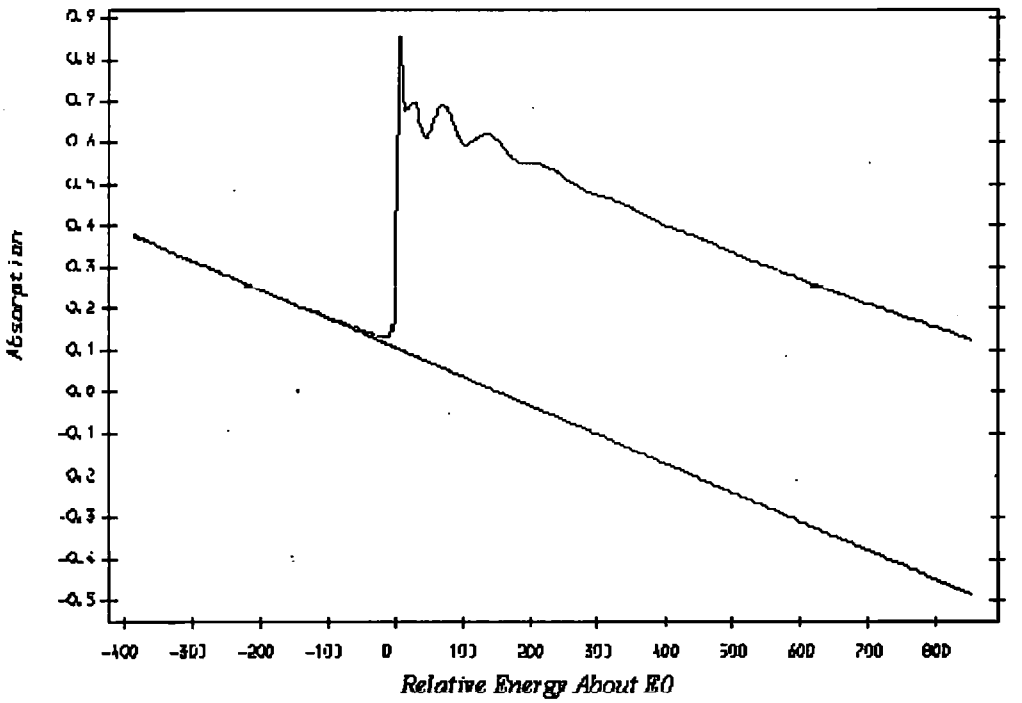

Figure 2.9 Representation of pre-absorption edge fitting procedure.

The post-edge absorption was fitted to a set of polynomials which model μ^o, the atomic absorption factor. This should pass smoothly through the EXAFS

oscillations which effectively models the post-edge as it would appear without the EXAFS oscillations (Figure 2.10).

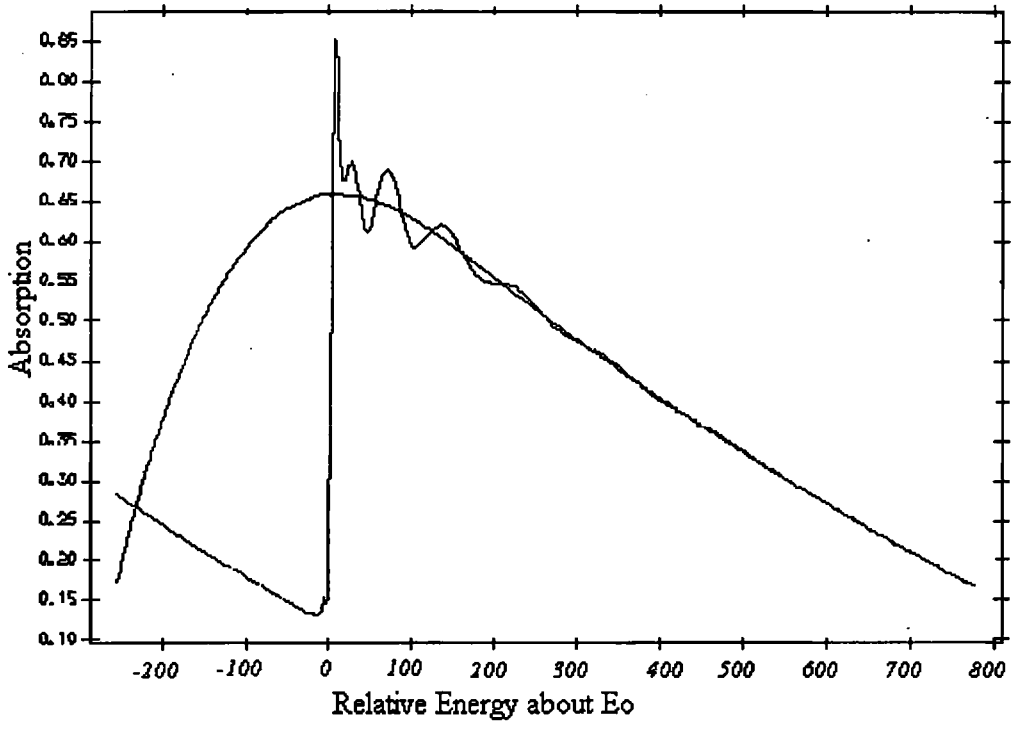

Figure 2.10 Post-absorption edge fitting procedure.

After subtracting the pre-edge and post-edge backgrounds to leave only the EXAFS oscillations, the x-axis was then converted from energy space (E) into photoelectron wave vector space (k) where $k = (2\pi/\lambda)$ and λ is the electron wavelength (Figure 2.11).

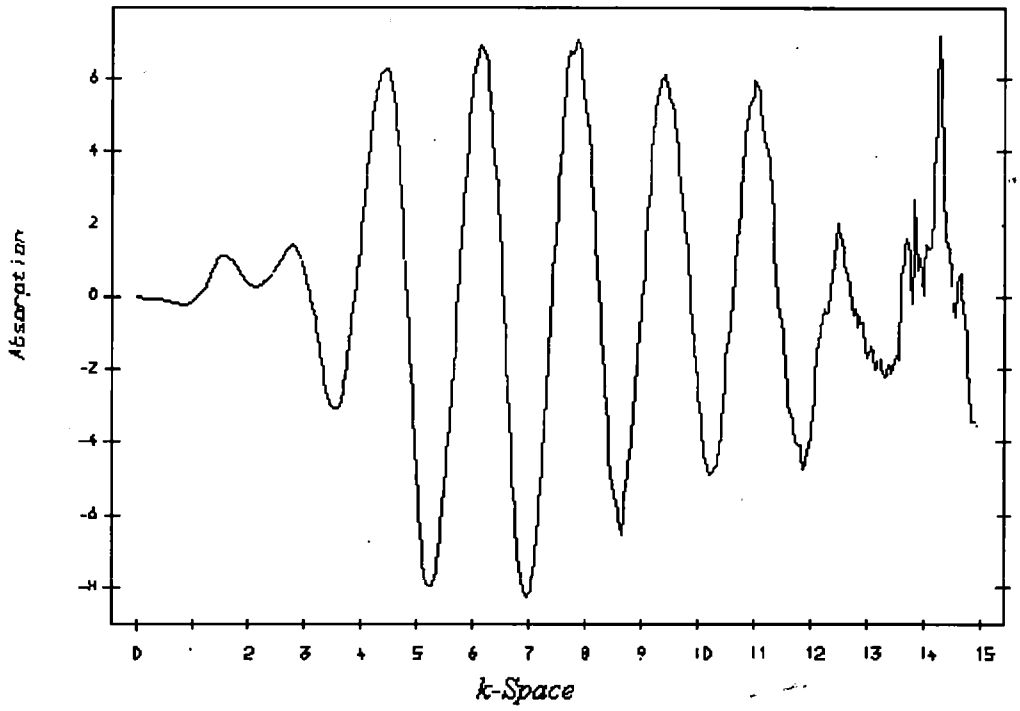

Figure 2.11 EXAFS oscillations after subtraction of pre- and post- absorption backgrounds.

A Fourier transformation using a k^3 weighing factor (to enlarge the oscillations at large k) then produces a radial distribution function which displays peaks at certain distances away from the core atom. After calculating atomic potentials and the phase shifts of the elements involved, the Fourier transformed EXAFS data can then be used to extract structural information about the sample under investigation, such as the type of neighbouring atoms, interatomic distances and co-ordination numbers. This step involved developing a theoretical model of the structure which was iterated by computational methods to match, as closely as possible, the experimental data using a series of curve fitting procedures. This procedure was achieved using the program EXCURV92. This program simulates

EXAFS spectra using rapid wave theory from the parameters of the radial shells of atoms surrounding the central atom. The parameters which were refined to obtain the best fit were the interatomic distance (R), the coordination number (N), the atom type (T), the Debye Waller factor (σ) and E_o.

One disadvantage of EXAFS is that it is essential to obtain good quality data, which is not always possible, if a good quality fit is to be achieved. Often as k increases the data becomes increasingly noisy and it may only be possible to obtain a fit to the first coordination sphere around the central atom. Errors from the fitting procedure can be as large as 10-30% for coordination numbers and 10% for interatomic distances.

2.2.5 Temperature-programmed reduction

2.2.5.1 Introduction

Temperature-programmed reduction (TPR) is a relatively simple technique used commonly in catalyst characterization. The first review article of the technique appeared in the early 1980's [38]. TPR can be used to characterise the phases present in a catalytic system and gives information about the reducibility of the metal component [39]. An interesting application of TPR is in the field of bimetallic catalysts. The reduction profile gained from supported bimetallic catalysts often, when compared with the TPR profiles of the respective

monometallic catalysts, can reveal whether the two metals are in close contact [40, 41].

2.2.5.2 Theory

TPR is a thermal-analytical technique in which the composition of a gas stream, usually a dilute hydrogen mixture, is monitored as it passes over a sample as the temperature of the sample is raised linearly.

The reduction of a metal oxide (MO_n), involves the dissociative adsorption of hydrogen onto the metal oxide surface and can be written as:-

$$MO_n\,(s) + nH_2\,(g) \rightarrow M\,(s) + nH_2O\,(g) \qquad (2.9)$$

Hence, the degree of reduction of a metal oxide can be measured as a function of temperature, as hydrogen gas is passed over the sample.

2.2.5.3 Apparatus

A schematic diagram of the TPR apparatus is shown in Figure 2.12. The experiment involved flowing a 10 % H_2 in N_2 gas mixture through the reference arm of a kathrometer detector of a gas chromatograph (Varian Model 3700) operating at 323 K and then through the sample under investigation. The sample

was placed in a 8 mm quartz U-tube attached via Chemcon PTFE fittings. The sample was heated using a homemade vertical tube furnace controlled by a Eurotherm model 818 temperature programmer. The gas mixture returned, via a copper drying tube containing silica gel, to the other arm of the kathrometer. Consumption of hydrogen (and therefore reduction) was easily detected as a voltage imbalance between the two arms of the kathrometer. The gas flow was measured as it left the detection system using a bubble flow meter. The current from the detector was collected, processed and analysed using commercial software (purchased from Pico Technology Ltd.).

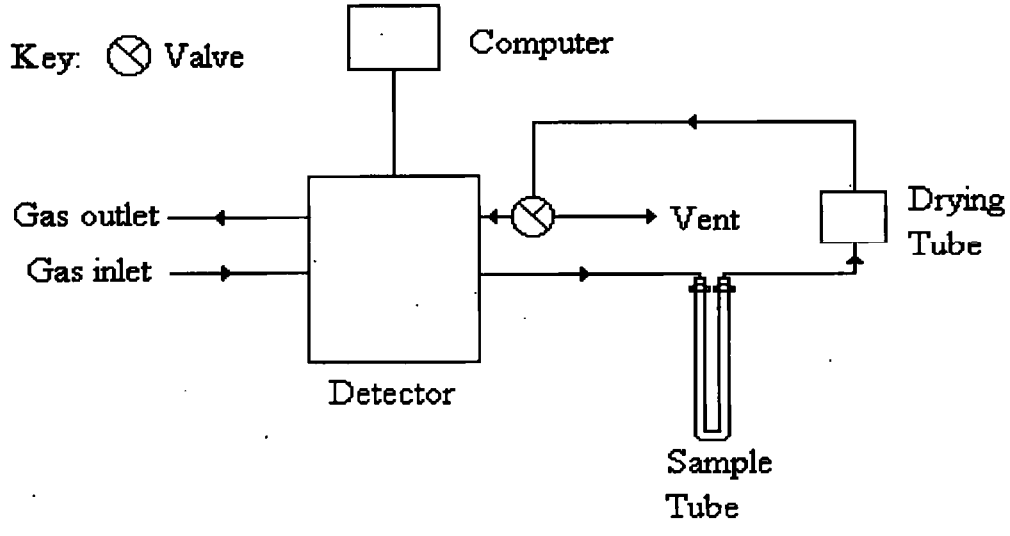

Figure 2.12 Schematic diagram of apparatus used for TPR experiment.

2.2.5.4 Experimental procedure

In the TPR experiment a small amount of sample (approximately 25 mg) was added to a quartz glass U-tube, supported between two quartz wool plugs. The U-tube was attached to the apparatus and placed in a dewar filled with liquid nitrogen. The 10% H_2 in N_2 gas mixture was started at a flow of 20 cm^3 min^{-1} and the system purged for about 20 min before the detector was switched on. To commence data collection the U-tube containing the sample was removed from the dewar of liquid nitrogen and then placed in the centre of a programmable furnace. Once the sample had warmed to room temperature the sample was heated to 1073 K at 10 K min^{-1}. A plot of hydrogen consumption versus temperature was obtained.

2.2.6 Transmission electron microscopy

2.2.6.1 Introduction

Transmission electron microscopy (TEM) is one of the most widely used physical techniques used to examine catalysts. It allows the direct observation of catalyst samples under high magnification and the size and shape of metal particles can easily be obtained. It is also possible to determine the elemental composition of the samples under investigation. This was particularly important

in the current research in order to help determine if individual particles are bimetallic in nature.

The theory of TEM can be found in the literature [42] and a number of excellent examples of the skillful application of TEM applied to bimetallic catalysts are also available [43-47]. The main disadvantage of the technique is that it is not possible to investigate catalysts under operating conditions. This is because the sample for microscopy has to situated in an evacuated chamber so that the coherent electron beam is not altered in any way. The samples also have to be exposed to air, even if only for a short period, before being inserted into the microscope so it is not possible to examine the catalysts in a reduced state.

2.2.6.2 Theory

In the TEM instrument the electrons are generated in the electron gun by heating a filament by passing a current (filament current) through it to a temperature at which it emits electrons. These electrons are accelerated by applying an electric potential between the filament and an anode plate facing the filament. A fraction of these electrons pass through a hole in the centre of the anode and are focused into a narrow beam by a series of lenses and apertures. This beam is allowed to strike the surface of the sample at which point the electrons are decelerated and scattered by collisions with atoms in the sample material. In TEM an image of the sample is formed by electrons which penetrate and pass through the sample.

X-rays emitted by the impact of the electrons on the sample are characteristic of the atoms which emit them, and their relative intensities depend on the concentrations of the emitting elements. Therefore, it is possible, by measuring the quantity of emitted X-rays and their respective wavelengths, to perform in most cases qualitative elemental microanalysis. This is known as Energy Dispersive X-ray analysis (EDX). Such quantitative microanalysis is, however, only possible when a sufficient number of X-rays are emitted.

2.2.6.3 Apparatus

The instrument used for TEM analysis was a JEOL 2000fx Transmission Electron Microscope fitted with a side entry port. The microscope was fitted with a Lanthanum Hexaboride (LaB_6) crystal filament and was equipped with the necessary detector for detecting X-rays and therefore could be used for EDX analysis using the commercially available Quantum Kevex Instrument. It was possible to obtain electron micrographs of the catalysts using a camera which was fitted beneath the image screen. The negatives used for the electron micrographs were obtained from Agfa Scienta EM film (6.5 cm x 9 cm) and were printed on Ilford photographic paper.

2.2.6.4 Experimental Procedure

The samples for TEM were prepared as follows according to the method described in the literature [48, 49]. A small amount of catalyst sample was added to a glass ampoule containing methanol and placed in an ultrasonic bath for approximately 10 minutes. This caused a dispersion to form above the bulk of the catalyst material. A carbon coated copper grid (3 mm, 200 mesh) was dipped in this solution and the solvent allowed to evaporate from the copper grid. The grid was then placed into the microscope.

Routine analysis was performed at an accelerating voltage of 200 kV and the images were obtained in the bright tilt mode. For each sample a number of photographs were obtained at various magnifications and particle size analysis obtained by measuring the diameter of a sufficient number of particles. Analysis of the composition of individual particles by EDX was achieved by adjusting the electron beam to small spot mode and focusing the beam on individual areas of catalyst.

2.2.7 Electron paramagnetic resonance

2.2.7.1 Introduction

Electron paramagnetic resonance (EPR) spectroscopy is a study of molecules containing unpaired electrons by observing the magnetic fields at which they come into resonance with monochromatic radiation. Since the technique is limited to materials containing unpaired electrons, only a small number of catalytic active elements are applicable to the technique. However under favourable circumstances this highly sensitive technique can reveal information about oxidation states, electronic configuration and coordination of the paramagnetic ion.

2.2.7.2 Theory

The theory of EPR is covered in several books [50, 51] and only the very basic details will be given here. If one considers Figure 2.14 which depicts electron spin levels in a magnetic field then the difference between the energy levels of an α electron ($m_s = + 1/2$) and a β electron ($m_s = - 1/2$) in a magnetic field B is ΔE and

$$\Delta E = g\mu_B B \qquad (2.10)$$

where g is known as the g-factor and μ_B is the magnetic moment.

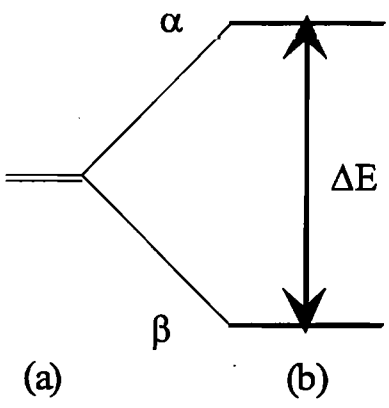

Figure 2.13 Electron energy levels (a) in the absence of an applied magnetic field and (b) in the presence of an applied magnetic field.

In EPR the sample is irradiated with microwave radiation and since, $\Delta E = h\nu$ where h is Plank's constant and ν is the frequency, then strong absorption of radiation occurs when the following relationship is met:

$$h\nu = g\mu_B B \qquad (2.11)$$

The EPR spectrum is obtained by varying the magnetic field B and the g-factor can be determined by monitoring the resultant absorption. The most important information obtained from EPR spectra is gained from the hyperfine structure where the individual resonance lines are split into different components. The hyperfine structure arises from the magnetic field from nuclear magnetic

moments within the paramagnetic species. By comparison of the EPR spectrum obtained from the sample under investigation with data obtained from standards and the literature it is possible to obtain structural and electronic information.

2.2.7.3 Apparatus

The EPR spectra were recorded using a Varian E-line Century Series spectrometer operating in the X-band region.

2.2.7.4 Experimental procedure

No facility was available to record the spectrum with the catalyst after reduction or under a hydrogen atmosphere, hence the spectrum was collected after exposing the sample to air. The data was collected for 4 minutes at 123 K with a modulation frequency of 100 kHz and was scanned over a field range up to 5 000 Gauss with 9.16 GHz.

2.2.8 Elemental analysis

Elemental analysis was performed by Medac Ltd, Brunel University, by Inductively Coupled Plasma Atomic Emission Spectroscopy (ICP-AES) and the units are expressed as wt%.

2.3 Electrochemical Evaluation

2.3.1 Introduction

This section describes the electrochemical procedures performed on the carbon supported platinum and platinum tin catalysts. The main technique used is known as cyclic voltammetry (CV) and the theory and application of this technique can be found in several books (see for example, [52, 53]). The technique can be applied for qualitative as well as quantitative analysis of almost all types of surface processes involving electron transfer. CV is an electroanalytical technique that has been successfully applied for the study of electrooxidation of small molecules such as CO, methanol and formaldehyde over carbon supported catalysts (for example, [54, 55]). Two main CV procedures have been performed during this research to analyse the catalysts. As the major goal in preparing the tin doped catalysts was to improve the CO tolerance of the Pt (the reason for this will be described in detail in Chapter 5), the electrooxidation of CO (usually called CO oxidative stripping) on the PtSn/C catalysts was examined. In this procedure, CO is adsorbed onto the surface of the electrode containing the catalyst and the potential increased until the CO is oxidised. Comparison of the CO electrooxidation peak allows evaluation of the relative activities of the different catalysts. Second, the CV technique known as linear potential sweep cyclic voltammetry (LPSCV) was performed for the catalysts in this work [52]. Measurement of the electrical charge at the working

electrode provides information on the oxidation/reduction properties of the catalyst surface and in particular, allows the extent of the interaction between the Pt and Sn in the bimetallic catalysts to be determined. LPSCV is often compared to the combination of the gas phase procedures of temperature programmed reduction, oxidation and desorption which involve monitoring the redox/desorption properties of the metal as a function of temperature [39]. LPSCV records the same properties but as a function of applied potential.

A useful application of CV is that it allows quantitative determination of the electrochemical surface areas (eca) of platinum catalysts, where the eca represents the maximum accessible active area of the catalyst. In addition, CV has the advantage of being an *in situ* technique. The CV experiments described here were performed at the Johnson Matthey Technology Centre, Sonning Common.

2.3.2 Theory

CV involves scanning the potential (V) of an electrode containing the sample under investigation at a constant rate between two potential limits, either once or cyclically following a triangular waveform, and recording the corresponding current (I) as a function of applied potential. The curve obtained (known as the voltammogram) is characteristic of the nature of the metal and any adsorbed species.

At this stage it may be useful to discuss a typical voltammogram obtained from a LPSCV procedure for a polycrystalline Pt electrode (Figure 2.14), as this will highlight many of the aspects of the technique which will be mentioned when discussing the appropriate results. Note, in the following discussion, the applied potential (V) is with reference to the *Reversible Hydrogen Electrode* (RHE). At 0 V, it is believed that a monolayer (ML) of hydrogen is adsorbed on the Pt and similarly a monolayer of oxygen is believed to be formed at 1.5 V [56].

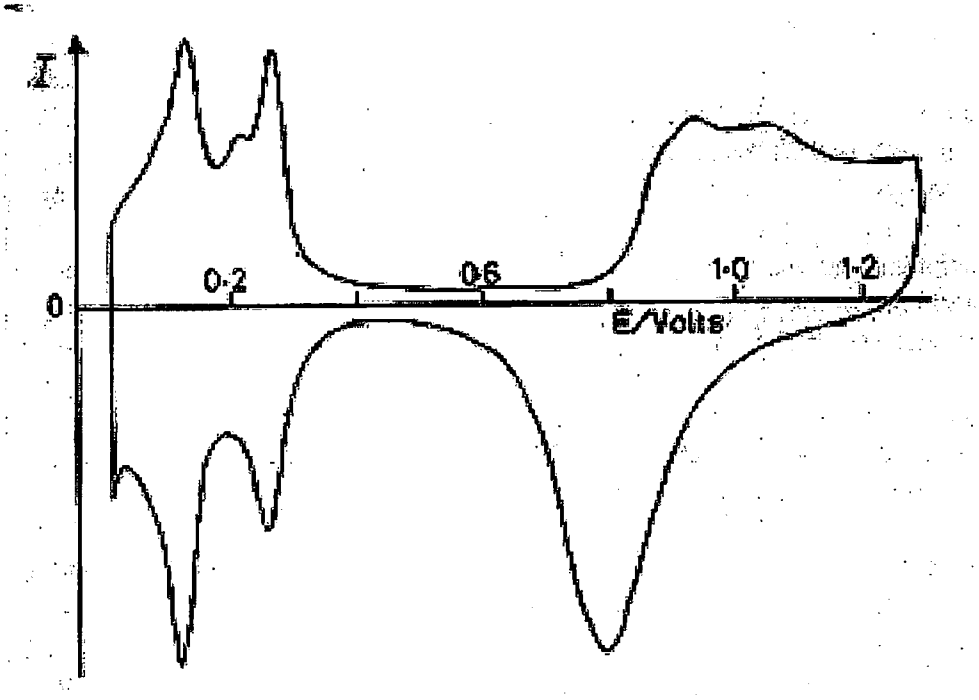

Figure 2.14 Characteristic voltammogram obtained after LPSCV procedure on polycrystalline Pt electrode.

The voltammogram can be divided into three sections.

i) Region I (0.05 V to 0.4 V) corresponds to the adsorption and desorption of hydrogen according to the reversible reaction (2.12):

$$H^+ + e^- \leftrightarrow H_{ads} \qquad (2.12)$$

where H_{ads} indicates an adsorbed hydrogen atom.

ii) In region II (0.4 to 0.65 V) no electrochemical reactions occur and the small current observed is due to the charge of the double layer and is known as the double layer region. This is a non-faradaic current which is not caused by the oxidation of adsorbed hydrogen but is rather mainly the result of the capacitive current caused by charging of the carbon support and, to a lesser extent, the platinum surface.

iii) Region III (0.65 to 1.5 V) corresponds to the adsorption and desorption of oxygen according to the reversible reaction (2.13):

$$Pt + H_2O \leftrightarrow PtO_{ads} + 2H^+ + 2e^- \qquad (2.13)$$

where PtO_{ads} represents an adsorbed oxygen atom on the Pt surface.

Therefore, the regions of most interest in the voltammogram are region I where reactions involving hydrogen occur and region III where reactions involving oxygen take place. The line with $I > 0$ is known as the anodic sweep and the line

with $I < 0$ as the cathodic sweep. In both the anodic and cathodic sweeps of region I, two peaks are observed at the same potential [57]. These are generally attributed to 'strongly' and 'weakly' adsorbed hydrogen species where the strongly adsorbed species is attributed to the adsorption of hydrogen on Pt(110) faces and the weakly adsorbed species attributed to adsorption on the Pt(100) [58]. Clearly this situation is analogous to gas phase chemisorption of hydrogen where the presence of strongly and weakly bound hydrogen has been established. In addition, a third intermediate species has been observed during potentiodynamic anodic oxidation of the adsorbed hydrogen, which is not observed in the cathodic region under quasi-equilibrium conditions. It has been suggested that the third species arises from hydrogen adsorption on Pt(111) crystal face [59], or it could result from a surface interaction between strongly and weakly bound hydrogen [60]. In region III the oxygen adsorption appears at a more positive potential than the peak associated with oxygen desorption, indicating that reaction (2.13) is not truly reversible probably due to a reconstruction of the Pt surface resulting in a more stable surface [61].

In addition the Pt catalyst surface area (and hence crystallite size) can be determined from the total coulombic charge required for hydrogen deposition, after correcting for double layer charging. This assumes that there is 1.305×10^{15} Pt atoms/cm^2 and that each surface Pt atom accommodates one hydrogen atom [62, 63]. Such measurement of H adsorption is an established method for determining real Pt surface area, however, several assumptions must be made

about (i) the distribution of crystal faces exposed and (ii) about which atoms in these faces are accessible to adsorb hydrogen. The charge associated with deposition of a monolayer of H has been commonly taken to be 0.21 mC/real cm^2 Pt, a value justified on the predominance of the Pt(100) plane or equal distribution of the three low index planes [57]. Different charges are associated with other planes.

Similarly, the CO electrooxidation peak area (see Chapter 5) can also be used for determining real Pt areas. During electrooxidation of CO_{ads} a charge of 0.42 mC/cm^2 Pt is passed and measurement of the charge allows evaluation of Pt surface areas [64]. This procedure is an electrochemical method of testing the activity of electrocatalysts. The procedure involved adsorbing CO on the catalyst surface and increasing the electrode potential until the CO was oxidised. This was indicated by an increase in the current and the activity of the catalysts were compared by the potential at which the reaction starts (known as the *onset potential*) and the potential at which the reaction is at a maximum (the *peak potential*).

This technique of measuring metal surface area is believed to be more realistic than the physical methods such as XRD and TEM which can only measure particles over a certain minimum diameter and so do not directly measure the true metal surface area. In this respect electrochemical methods (and gas chemisorption) have the advantage in that all the Pt sites that are accessible to the

electrolyte are measured. It has been shown that only the first few atomic layers are involved in processes involved in cyclic voltammetry thus confirming the technique as a surface technique [65, 66].

The limited use of CV in catalysis research is due to the nature of cyclic voltammetry. It is restricted to studying unsupported metal catalysts or, as in this research, metals supported on electrically conducting substrates (i.e., carbon). Alumina and silica, commonly used as support for metal catalysts, are inapplicable to the technique because of their insulating properties.

2.3.3 Apparatus

The apparatus and procedure used for the cyclic voltammetry are described in [67]. The apparatus used for the experiments is shown in the photograph in Figure 2.15. For CV and the electrochemical area determinations a standard three-chamber glass cell was used. 1 cm^2 buttons were punched from the pre-Nafion™ impregnated electrode sheets containing the catalyst and were 'wet-up' using 2-propanol and subsequent H_2O boil and placed in the middle chamber of the cell shown in Figure 2.15. The electrode buttons were held in a fully flooded cell using a gold clip. The counter electrode was gold foil (contained in the right hand side chamber) and a flooded palladium gas-diffusion electrode strip with flowing hydrogen, a Reversible Hydrogen Electrode (RHE) was used as the reference (contained in the left hand side chamber). The cell was filled with 1 M

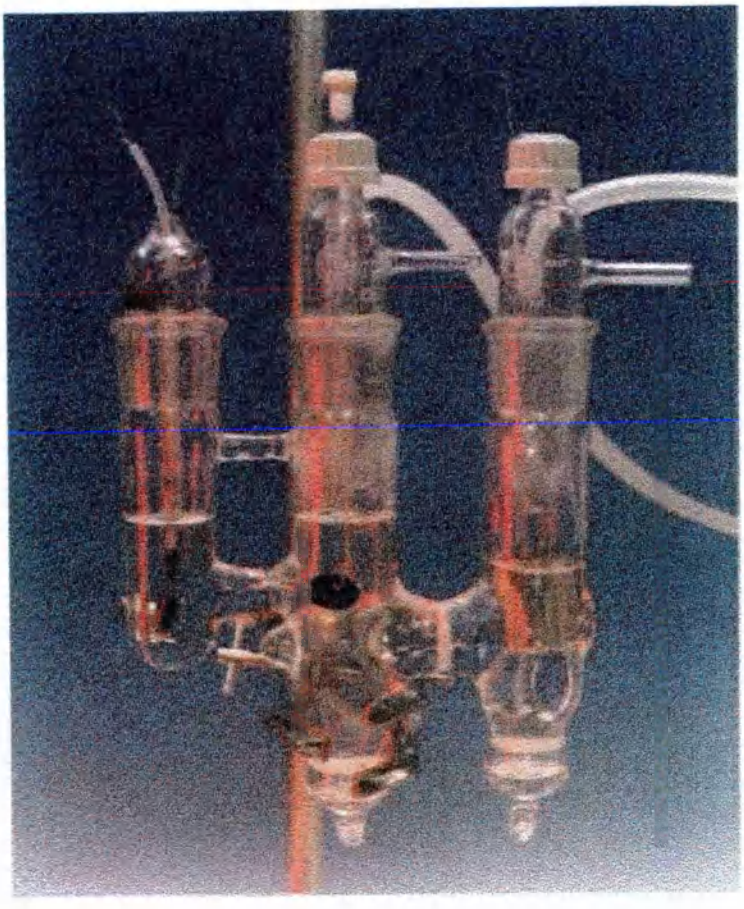

Figure 2.15 Three-chamber glass cell used for cyclic voltammetry experiments.

H_2SO_4 and maintained at 303 K by immersion in a water bath. Gases were passed over the electrode by means of the gas lines connected to the cell.

2.3.4 Experimental Procedure

The electrodes were fabricated (described in [67]) using a filter transfer technique onto wetproofed carbon paper (Stackpole PC206). The loading of the buttons were 1 mg (Pt) cm^{-2} and the PTFE loadings were 30%. Nafion™ impregnation was applied by a brush coating method using a soluble Nafion™ solution. After immersing the electrode in the electrolyte filled three-chamber cell, CO was passed over the electrode for 15 minutes, followed by nitrogen for a further 30 minutes while holding the button at 5 mV. Then the electrode was cycled between 0.01 and 1.2 V vs the Reversible Hydrogen Electrode (RHE) at a sweep rate of 10 mVs^{-1}. Comparison of the anodic charge passed during the first cycle with that for the second gave the charge associated with CO monolayer electrooxidation.

2.4 Catalyst Testing

The catalytic properties of the alumina supported catalysts prepared in this research have been evaluated for two separate test reactions. These were:

i) Hydrogenation of crotonaldehyde

ii) Hydrogenation of 1,3- butadiene

The hydrogenation reactions were studied in the gas phase using continuous flow microreactor systems operated at atmospheric pressure. The following section will describe the apparatus and procedures used during the catalyst testing experiments. Please note, for the sake of brevity, the term *standard reduction procedure* will be used to describe the reduction of a catalyst in a 10 % H_2 in N_2 gas mixture at 623 K or 473 K for the palladium or platinum catalysts respectively. The temperature controlled reduction consisted of a initial ramp of 1 K min^{-1} to the required reduction temperature, which was maintained for 3 h, before returning to room temperature at 1 K min^{-1}.

2.4.1 Crotonaldehyde Hydrogenation

2.4.1.1 Apparatus

A schematic diagram of the apparatus is shown in Figure 2.16.

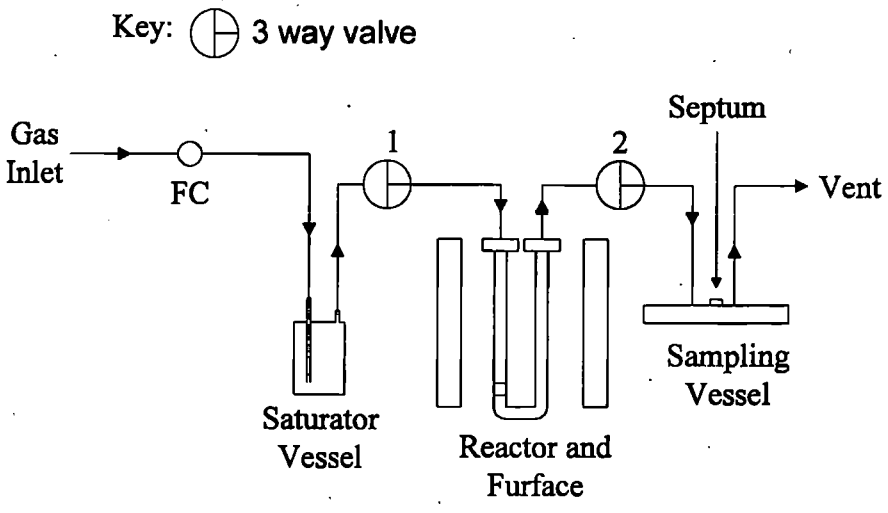

Figure 2.16 Schematic diagram of the apparatus used for crotonaldehyde hydrogenation.

The glass vessels shown above were linked by 1/8" PTFE tubing and could be isolated from each other by three-way key valves (Omnifit). Chemcon and Swagelok fittings were used to attach the U-tube reactor and the saturator vessel to the PTFE tubing, respectively. The catalyst sample was held at the bottom of the Pyrex U-tube reactor (length 10 cm, diameter 8 mm) by a glass wool plug. 10 % H_2 in N_2 gas mixture was supplied to the system via a Jones Chromatography Flow Controller (Model 1000A110ABF) (represented by FC in Figure 2.16) and the flow measured using a bubble flow meter. A Lenton Furnace controlled by a Eurotherm Controller (Model 902) was used to heat the catalyst to the desired temperature during the reduction procedure and the catalytic reaction.

Effluent in the gas phase was collected in a glass sampling vessel, fitted with a septum, to allow samples to be withdrawn periodically and analysed by a flame ionisation detection gas chromatograph (Pye Unicam PU4500) fitted with a fused silica capillary column (25 m, 0.53 mm i.d., 1.0 μm film) operating at 333 K. Helium was used as the carrier gas and was further purified by an oxygen trap. The data collected was analysed by a Waters 740 Data Module.

2.4.1.2 Experimental Procedure

Approximately 0.1 g of the catalyst sample was weighed into the U-tube reactor and reduced according to the standard reduction procedure at a H_2/N_2 gas mixture flow of 60 cm^3 min^{-1}. The U-tube reactor containing the catalyst was then isolated by closing taps 1 and 2, and a known amount of crotonaldehyde added to the glass saturator vessel. The saturator was then purged with the 10 % H_2 in N_2 gas mixture, for about 10 minutes, to avoid exposing the reduced catalyst to air. The saturator was then placed in an ice bath and taps 1 and 2 opened. A stream of 10 % H_2 in N_2 (60 cm^3 min^{-1}) saturated with crotonaldehyde vapour at 273 K was then passed through the catalyst bed. 10 μl samples of the effluent gases were withdrawn through the septum in the sampling vessel on a regular basis and analysed by GC. The retention times of the products were compared to those of known standards. The testing protocol used involved maintaining the catalyst at a constant temperature and monitoring the effluent in the gas stream over a prolonged period of time.

Full details of the reaction conditions (temperature, duration etc.) will be given with the results.

2.4.2 1,3-Butadiene Hydrogenation

2.4.2.1 Apparatus

The apparatus used for 1,3-butadiene hydrogenation is shown in Figure 2.17.

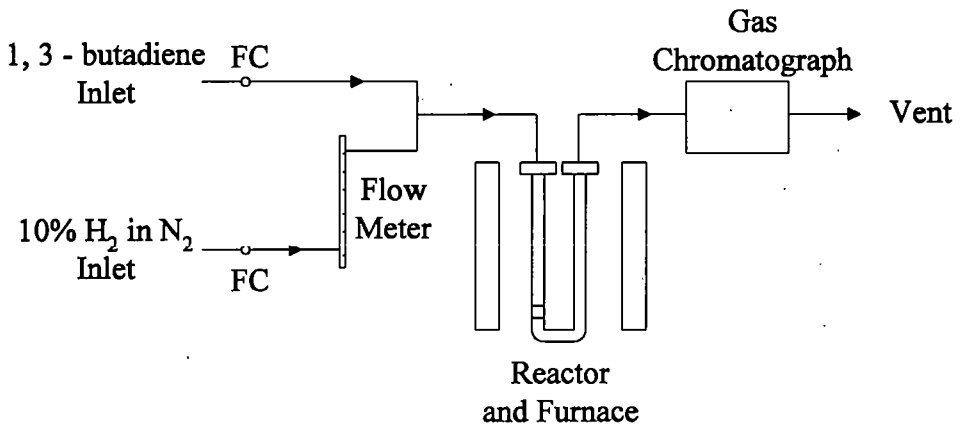

Figure 2.17 Schematic diagram of the apparatus used for hydrogenation of 1,3-butadiene.

A Pyrex U-tube reactor was connected to the 1/8" PTFE gas lines using Chemcon fittings. 10 % H_2 in N_2 and 1,3-butadiene were delivered to the system via a needle valve (Hoke) (FC in diagram) and a calibrated flow meter (Porter

Instruments) and a Jones Chromatography flow controller (model 1000A110ABF) respectively. The two gases were mixed at a T-piece and passed into the U-tube containing the catalyst. The 10 % H_2 in N_2 gas mixture and 1,3-butadiene were shown to mix efficiently by analysing the number of counts under the 1,3-butadiene peak on the GC trace over a number of runs.

Sampling of the effluent gases exiting the reactor was achieved online via a six port sampling valve connected to a flame ionisation detection gas chromatograph (Ai Cambridge GC94) with a 0.19 % Picric Acid on Graphpac (1/8", length 2 m) column operating at 323 K.

2.4.2.2 Experimental Procedure

Approximately 0.1 g of catalyst sample was loaded into the U-tube reactor and mounted on a glass wool plug. The 10 % H_2 in N_2 gas mixture was switched on at a flow of 60 cm^3 min^{-1} and the catalyst reduced using the standard reduction procedure. The furnace was then set to the required reaction temperature, depending on the catalyst, and the flow of 1,3-butadiene was started (5 cm^3 min^{-1}). An initial sample was taken after 1 minute, sampling thereafter at 20 minute intervals. The products were analysed at a constant temperature for approximately 400-500 minutes.

2.5 References

1 Foger, K., *in* "Catalysis: Science and Technology" (J. R. Anderson and M. Boudart, Eds.), p 227, Springer-Verlag, Amsterdam, 1984.

2 Attwood, P.A., McNicol, B.D., and Short, R.T., *J. Appl. Electrochem.* **10,** 213 (1980).

3 Stiles, A.B., "Catalysts Supports and Supported Catalysts: Theoretical and Applied Concepts." Butterworths, Boston, 1987.

4 Saraswati, V., Rao, G.V.N., and Rama Rao, G.V., *J. Mater. Sci.* **22,** 2529 (1987).

5 Smisek, M., and Cerny, S., "Active Carbon- Manufacture, Properties and Applications." Elsevier, Amsterdam, 1970.

6 Berebi, G., and Bernusset, Ph., *in* "Preparation of Catalysts" (B. Delmon, P.A. Jacobs and G. Poncelet, Eds.), Elsevier, Amserdam, 1976.

7 Scharwz, J.A., Contescu, C., and Contescu, A., *Chem. Rev.* **95,** 477 (1995).

8 Gonzalez, R.D., and Miura, H., *Catal. Rev.-Sci. Eng.* **36,** 145 (1994).

9 Keck, L., Buchanan, J., and Hards, G., US Patent, 5 068 161, (1991).

10 J. M. Thomas and R.M. Lambert, (Eds.) "Characterisation of Catalysts." John Wiley & Sons, New York, 1980.

11 Niemantsverdriet, J.W., "Spectroscopy in Catalysis, An Introduction." VCH, Weinheim, 1995.

12 Stytsenko, V.D., *Appl .Cat. A: Gen.* **126,** 1 (1995).

13 Gregg, S.J., and Sing, K.S.W., "Adsorption, Surface Area and Porosity." Academic Press, London, 1982.

14 Brunauer, S., Deming, L.S., Deming, W.S., and Teller, E., *J. Am. Chem. Soc.* **62**, 1723 (1940).

15 Brunauer, S., Emmett, P.H., and Teller, E., *J. Am. Chem. Soc.* **60**, 309 (1938).

16 Langmuir, I., *J. Am. Chem. Soc.* **38**, 2221 (1916).

17 Davis, R.T., De Witt, T.W., and Emmett, P.H., *J. Phys. Chem.* **51**, 1232 (1947).

18 Thorsteinson, E.M., Wilson, T.P., Young, F.G., and Kasal, P.H., *J. Catal.* **52**, 116 (1978).

19 Aben, P.C. *J. Catal.*, **10**, 224 (1968).

20 Chou, S.-C., Lin, S.-H., and Veh, C.-T., *J. Chem. Soc., Faraday Trans.* **91**, 949 (1995).

21 Greenwood, N.N., and Gibb, T.C., "Mössbauer Spectroscopy." Chapman and Hall, London, 1971.

22 Bancroft, G.M., "Mössbauer Spectroscopy, An Introduction for Inorganic Chemists and Geochemists." McGraw-Hill, London, 1973.

23 Lázár, K., *Struct. Chem.* **2**, (37)245 (1990).

24 Lázár, K., Nimz, M., Lietz, G., Völter, J., and Guzci, L., *Hyperfine Interactions* **41**, 657 (1988).

25 Niemantsverdriet, J.W., van Kaam, J.A.C., Flipse, C.F.J. and Van Der Kraan, A.M., *J. Catal.* **96**, 58 (1985).

26 Moroz, É.M., *Kinetika I Kataliz* **34**, 31 (1993).

27 Gonzalez, R.D., and Miura, H., *Catal. Rev.-Sci. Eng.* **36**, 145 (1994).

28 Azaroff, L.V., and Buerger, M.J., "The Powder Method in X-Ray Crystallography." McGraw-Hill, New York, 1958.

29 Bragg, W.L., *Proc. Roy. Soc.* **89A**, 248 (1913).

30 Johnson, P., and Wells, P.B., *Radiat. Phys. Chem.* **45**, 393 (1995).

31 Inoue, T., Tomishige, K., and Iwasawa, Y., *J. Chem. Soc., Faraday Trans.* **92**, 461 (1996).

32 Harada, M., Asakura, K., Ueka, Y., and Toshima, N., *J. Phys. Chem.* **97**, 9730 (1992).

33 Sanchez Sierra, M.C., García Ruiz, J., Grazia Proietta, M., and Blasco, J., *J. Mol. Cat. A: Chem.* **108**, 95 (1996).

34 Cowes, J.W., and Meehan, P., *Physica B* **208 & 209**, 665 (1995).

35 Lynch, J., *J. de Physique IV* **4**, C9-253 (1994).

36 El Abed, A., El Qebbaj, S.E., Guérin, M., Kappenstein, C., Dexpert, H., and Villain, F., *J. Chim. Phys.* **94**, 54 (1997).

37 Teo, B.K., "EXAFS: Basic Principles and Data Analysis." Springer-Verlag, Berlin-Heidelberg, 1986.

38 Hurst, N.W., Gentry, S.J., Jones, A., and McNicol, B.D., *Catal. Rev.- Sci. Eng.* **24**, 233 (1982).

39 Jones, A., and McNicol, B.D., "Temperature-Programmed Reduction for Solid Materials Characterisation." Dekker, New York, 1986.

40 Juszczyk, W., Pielaszek, J., Karpinski, Z., and Pinna, F., *Appl. Cat. A: Gen.* **144**, 281 (1996).

41 Pinna, F., Selva, M., Signoretto, M., Strukul, G., Boccuzzi, F., Benedetti, A., Canton, P., and Fagherazzi, G., *J. Catal.* **150**, 356 (1994).

42 Heidenreich, R.D., "Fundamentals of Transmission Electron Microscopy." Wiley-Interscience, New York, 1974.

43 Huang, Z., Fryer, J.R., Park, C., Stirling, D., and Webb, G., *J. Catal.* **159**, 340 (1996).

44 Lamber, R., Jaeger, N.I., Trunschhke, A., and Miessner, H., *Catal. Lett.* **11**, 1 (1996).

45 Neri, G., Pietropaolo, R., Galvagno, S., Milone, C., and Schwank, J., *J. Chem. Soc., Faraday Trans.* **90**, 2803 (1994).

46 Neri, G., Donato, A., Milon, C., Pietropaolo, R., and Schwank, J., *Mats. Chem. and Phys.* **44**, 145 (1996).

47 Baird, T., *in* "Specialist Periodical Reports: (Catalysis)" (G.C. Bond and G. Webb, Eds.), Vol. 5, p. 172, Royal Society of Chemistry, London, 1982.

48 Adams, C.R., Benesi, H.A., Curtis, R.M., and Meisenheimer, R.G., *J. Catal.* **1**, 336 (1962).

49 Zou, W., and Gonzalez, R.D., *J. Catal.* **133**, 202 (1992).

50 Atherton, N. M., "Electron Spin Resonance." Ellis and Horwood Limited, Chichester, 1973.

51 Wertz, J. E., and Bolton, J. R., "Electron Spin Resonance Theory and Practical Applications." McGraw-Hill, New York, 1972.

52 Noel, M., and Vasu, K. I., "Cyclic Voltammetry and the Frontiers of Electrochemistry." Aspect Publications Ltd., London, 1990.

53 Oldham, H. B., and Myland, J. C., "Fundamentals of Electrochemical Science." Academic Press, Inc., London, 1994.

54 Markovic, N.M., Widelôv, A., Ross, P.N., Monteiro, O.R., and Brown, I.G., *Catal. Lett.* **43**, 161 (1997).

55 Lamy-Pitara, E., El Ouazzani-Benhima, L., Barbier, J., Cahoreau, M., and Caisso, J., *Appl. Cat.* **81**, 47 (1992).

56 de Bruijin, F. A., Kuster, B. F. M., and Marin, G. B., *Appl. Cat. A: Gen.*, **145**, 351 (1996).

57 Brummer, S. B., *J. Phys. Chem.* **69**, 562, (1965).

58 Lamy-Pitara, E., and Barbier, J., *Appl. Cat. A: Gen.* **149**, 49 (1997).

59 Will, F. G., *J. Electrochem. Soc.* **112**, 451 (1965).

60 Kinoshita, K., Lundquist, J., and Stonehart, P., *J. Catal.* **31**, 325 (1973).

61 Christensen, P. A., and Hamnett, A., "Techniques and Mechanisms in Electrochemistry." Blackie Academic and Professional, Glasgow, 1994.

62 Bett, J., Kinoshita, K., Routsis, K., and Stonehart, P., *J. Catal.* **29**, 160 (1973).

63 Trassatti, S., and Petrii, O.A., *J. Electroanal. Chem.* **327**, 353 (1992).

64 Bett, J., Kinoshita, K., Routsis, K., and Stonehart, P., *J. Catal.* **29**, 160 (1973).

65 Biegler, T., Rand, D. A. J., and Woods, R., *J. Electroanal. Chem.* **29**, 269 (1971).

66 Rand, D. A. J., and Woods, R., *J. Electroanalyt. Chem. Interfacial Electrochem.* **36**, 57 (1972).

67 "High Performance, Low Cost Membrane Electrode Assemblies for Solid Polymer Fuel Cell", Hards, G.A., Ralph, T.R., and Cooper, S.J., ETSU Report/FCR/002, December 1992.

Appendix 1 List of reagents and chemicals

Table 2.2 Chemicals used during catalyst preparation.

Chemical	Formula	Supplier	Purity
γ-alumina	Al_2O_3	ACZO300	-
Carbon black	C	Cabot Co.	-
Palladium bis-(acetylacetonato)	$Pd(CH_3COCHCOCH_3)_2$	Johnson Matthey	99%
Dinitrodiammine-palladium	$Pd(NO_2)_2(NH_3)_2$	Johnson Matthey	99%
Ammonium tetrachloro-palladate	$(NH_4)_2\ PdCl_4$	Johnson Matthey	99.9%
Platinum bis-(acetylacetonato)	$Pt(CH_3COCHCOCH_3)_2$	Johnson Matthey	99%
Tetrabutyltin	$Sn(C_4H_9)_4$	Aldrich	98%
Ferrocene	$Fe(C_5H_5)_2$	Aldrich	98%
Tin octoate	$C_{16}H_{30}O_4Sn$	Sigma	95%
Iron nitrate	$Fe(NO_3)_3.9H_2O$	Aldrich	98+%
Heptane	C_7H_{16}	Aldrich	99+%
Toluene	$C_6H_5CH_3$	Aldrich	min.99%
Nitrogen	N_2	Air Products	99.99%
Hydrogen	H_2	Air Products	99.99%

Table 2.3 Chemicals used for catalyst testing.

Chemical	Formula	Supplier	Purity
10 % H_2 in N_2 gas mixture		Air Products	
Crotonaldehyde	$CH_3CHCHCHO$	Aldrich	99+%
1,3-butadiene	C_4H_6	Aldrich	99+%
Butane	C_4H_{10}	EDT Research	10.1% in N_2
Butyraldehyde	CH_3CH_2CHO	Aldrich	99.5%
Butanol	$CH_3CH_2CH_2CH_2OH$	BDH	99%
Crotyl alcohol	$CH_3CHCHCH_2OH$	Aldrich	97%
Helium	He	BOC	99.99%

Table 2.4 Chemicals used in catalyst characterisation.

Chemical	Formula	Supplier	Purity
Carbon Monoxide	CO	BDH	99.5%
Iron (III) Chloride	$FeCl_3.6H_2O$	Aldrich	97%
Methanol	CH_3OH	Rectapor	99%

Appendix 2

(A) Experimental procedure for determining V_d, V_s, V_x and V_n

This section describes the procedure used to calibrate the volumes (V_d, V_s, V_x *and* V_n) of the vacuum line used for determination of the surface area and dispersion of the catalysts samples in this work. These volumes are shown in Figure 2.3.

The volume of the vacuum line between taps 4, 5 and 6 is known as the dosing volume (V_d). This volume was calculated by gas expansion using two glass bulbs of known volumes (V_1) and (V_2), (determined by weighing with distilled, deionised water several times and taking the average values). Each glass bulb was attached in turn to the vacuum line and outgassed to a final pressure of approximately 10^{-5} mbar. Nitrogen gas was admitted into the dosing volume (with taps 4, 5 and 6 closed) and the dosing pressure, P_{d1}, recorded. Tap 6 was then opened a pre-determined amount to allow nitrogen into the bulb and the equilibrium pressure recorded (P_{e1}) (with tap 6 closed) once equilibrium had been attained. The first bulb was then removed and second glass bulb attached to the line. The procedure outlined above was then repeated for the second bulb to give P_{d2} and P_{e2}. The dosing volume was then calculated using the equation:

$$V_1 - V_2 = V_d\left(\frac{P_{d1}}{P_{e1}} - \frac{P_{d2}}{P_{e2}}\right) \qquad (2.14)$$

assuming that the temperature of the dosing volume (T_d) was equal to the temperature of the sample volume (T_s). The dosing volume and the glass bulb are wrapped with glass wool to maintain isothermal conditions.

Once the dosing volume had been calculated, values of V_s, V_n and V_x were measured where V_s is the volume of the section of glass below tap 6 including the sampleholder and the sinter (i.e. the sample volume), V_n is the volume below the pre-etched mark on the sampleholder and V_x is the volume between the between tap 6 and the pre-etched mark on the sampleholder (see Figure 2.3).

The empty sampleholder and sinter were attached to the line and outgassed to a pressure of approximately 10^{-5} mbar. Nitrogen was then admitted into the dosing volume and the pressure recorded (P_d). Tap 6 was then opened and the pressure allowed to equilibrate before closing tap 6 and noting the new equilibrium pressure (P_e). From the gas laws it is possible calculate V_s from the equation below:

$$V_s = V_d\left(\frac{P_d}{P_e} - 1\right) \tag{2.15}$$

again assuming T_s is equal to T_d

Furthermore, if the sampleholder was immersed in liquid nitrogen up to a pre-etched mark and tap 6 reopened then P_e decreased further until a new equilibrium pressure was reached.

If this new pressure is denoted P_n then:

$$V_n = \left(V_d + V_s\right)\left(\frac{P_e}{P_n} - 1\right)\left(\frac{T_n}{T_d - T_n}\right) \tag{2.16}$$

where T_n is the temperature of the liquid nitrogen (77 K).

(B) Treatment of Data from the BET Experiment

The data collected during the BET experiment can be used to determine the total surface area of a porous solid conforming to a type II isotherm.

The quantity of gas in the dosing volume (Q_1^n) is given by:

$$Q_1^n = \frac{V_d}{RT_d}\left(P_d^n - P_e^{n-1}\right) \tag{2.17}$$

where P_d^n is the pressure in dosing volume for point n and P_e^{n-1} is the equilibrium pressure for the previous expansion.

The quantity of gas in the gas phase after adsorption (Q_2^n), is given by:

$$Q_2^n = \frac{P_e^n}{R}\left(\frac{V_d + V_x}{T_d} + \frac{V_n}{T_n}\right) \tag{2.18}$$

where P_e^n is the equilibrium pressure for point n.

Therefore the quantity of gas *adsorbed* onto the catalyst after each doping (Q_3^n) is:

$$Q_3^n = \left(\sum_1^n Q_1^n\right) - Q_2^n \tag{2.19}$$

Q_3^n plotted against $\frac{P_e}{P^o}$ (where p^o is the saturation vapour pressure at adsorption temperature) should give a type II isotherm. $\frac{P_e^n}{Q_3^n\left(P_d^n - P_e^n\right)}$ plotted against $\frac{P_e}{P^o}$ should give a straight line with intercept $\frac{1}{V_m c}$ and gradient $\frac{c-1}{V_m c}$. Adding the values of the gradient and intercept gives $\frac{1}{V_m}$ where V_m is the volume of adsorbed gas in the completed monolayer. Given V_m, then using equation (2.5) the number of adsorbed molecules in the monolayer, n_m, can be calculated.

Finally the total surface area (A) per gram of catalyst can be calculated from the following equation:

$$A = n_m A_m L / M \tag{2.20}$$

where M is mass of catalyst in grams.

(C) Treatment of Data from the Chemisorption Experiment

Q_1^n and Q_3^n are as defined in the treatment of data for the BET experiment.

However Q_2^n is now defined as:

$$Q_2^n = \frac{P_e^n}{R}\left(\frac{V_d}{T_d} + \frac{V_s}{T_s}\right) \tag{2.21}$$

where all other values are as defined above.

Plotting Q_3^n against p/p^o gives an adsorption isotherm from which Q^o can be obtained by extrapolating the isotherm to the region of zero pressure. This value can be inserted into either equation (2.6) or (2.7) to give the dispersion.

CHAPTER 3

Preparation and characterisation of γ-alumina supported bimetallic catalysts, MM'/Al_2O_3 where M = Pd or Pt and M' = Fe or Sn

3.1 Introduction

The preparation and characterisation of the γ-alumina supported catalysts will be presented in this Chapter. As stated previously one of the main aims of the present work is to extend the range of organometallic precursors available for use in SOMC. Thus the main emphasis of the work reported in this chapter is to examine the use of the organometallic sandwich type π-complex ferrocene, $Fe(C_5H_5)_2$ as a precursor to prepare a range of $PdFe/Al_2O_3$ and $PtFe/Al_2O_3$ catalysts. A range of $PdSn/Al_2O_3$ and $PtSn/Al_2O_3$ catalysts were also prepared using the more traditional tetraalkyl precursor. Preparation of the monometallic catalysts will be considered initially before a discussion of the preparation of the bimetallic materials.

The catalysts were characterised using a number of different techniques. The main aims of the characterisation were (i) to determine whether a selective reaction had occurred between the organometallic precursor of the second metal and the reduced surface of the parent metal; and (ii) to determine the morphology of the 'bimetallic' catalysts, both reduced and after exposure to air. As stated previously it is assumed that during the SOMC reaction bimetallic particles are produced, however it is not clear what will happen on exposure to air; that is, which species will be oxidised and whether the metals will remain in contact. It was with these objectives in mind that the materials were characterised. Characterisation in particular focussed on the $PdFe/Al_2O_3$ system. The materials were studied using X-ray diffraction (XRD), hydrogen chemisorption, temperature-programmed reduction (TPR), transmission electron microscopy and

energy dispersive X-ray analysis (TEM/EDX), extended X-ray absorption fine structure (EXAFS), Mössbauer and electron paramagnetic resonance (EPR) spectroscopy. It should, however, be noted that the loading of the second metal was usually very low (< 0.5 wt%) with possibly only an atomic overlayer present (at most), and so characterisation was a difficult task.

Evaluation of these alumina supported catalysts will be presented in Chapter 4 for the hydrogenation of crotonaldehyde and 1,3-butadiene.

In order to provide a context for the discussion in this chapter a review of SOMC is first presented. Specific comments with regards to features of the present work are included in this review.

3.2 Preparation of bimetallic catalysts using surface organometallic chemistry

As was discussed in Chapter 1, traditional methods used for the preparation of bimetallic catalysts can often lead to the two metals being deposited at different sites on the support, e.g., [1, 2]. Since any bimetallic interaction only occurs when the two metallic components are in contact rather than existing as separate particles, it is desirable to develop a preparation method in which the deposition of the second metallic component preferentially takes place on the surface of the first metal particle. SOMC provides one such route depending on a controlled surface reaction between an organometallic precursor of the second metal and the surface of the first.

A range of bimetallic catalysts prepared using SOMC have been reported in the literature and a review has been written on the subject [3]. Typically the parent catalyst has been a group VIII element (such as Rh or Pt) supported on Al_2O_3 or SiO_2 and the second metal has been a group VIII or a IVB metal, such as Ni, Ge or Sn. This technique as a method for the preparation of bimetallic catalysts is relatively new with the majority of work reported since 1984 when a number of groups simultaneously described new preparative routes for bimetallic particles by reaction of a group IVA alkyl metal compound with a supported metallic surface of Rh, Pt or Ni [4-6]. Travers *et al.* [4] reported the preparation of RhSn catalysts supported on alumina and silica, by reaction of tetrabutyl tin with metallic Rh. From chemisorption and electron microscopy experiments they concluded that the tin was selectively deposited on the Rh particles and not on the support. Similarly Margitfalvi *et al.* [5] reported the preparation of PtSn bimetallic catalysts supported on Al_2O_3 using this technique, this time using tetraethyl tin to deposit Sn onto the surface of the platinum particles. Nuzzo *et al.* [6] reported the reaction of volatile group IIIA and IVA organometallic compounds with the reduced surface of alumina or silica supported Ni. Prior to this, however, a similar reaction was reported by Ryndin *et al.* to deposit Pd and Pt onto a Mo/SiO_2 catalyst by reaction of $Pd(\pi\text{-}C_3H_5)_2$ and $Pt(\pi\text{-}C_3H_5)_2$ in pentane, with the reduced surface of Mo/SiO_2 [7]. As far as we are aware this is one of the first reported bimetallic catalysts prepared by a SOMC method. A similar reaction was also used to deposit Ni onto NiO using dicyclopentadienyl nickel [8]. Since these initial studies a wider range of bimetallic catalysts have been prepared using SOMC; a selection of the studies using SOMC to modify supported Pd and Pt catalysts is listed in Table 3.1.

Table 3.1 Examples of literature containing reports of Pd- and Pt-based bimetallic catalysts prepared by SOMC.

Parent Metal	Support	Second Metal	Organometallic Precursor	Reference
Pd	Al_2O_3	Ge, Sn, Pb, Sb	$M(C_4H_9)_x$	[9]
Pd	SiO_2	Ni	$Ni(C_5H_5)_2$	[10]
Pt	Al_2O_3	Sn	$Sn(C_4H_9)_4$	[11]
Pt	Al_2O_3	Sn	$Sn(C_2H_5)_2$	[12, 13]
Pt	SiO_2	Ru	$Ru(\pi\text{-}C_5H_5)_2$	[14]

Reaction Mechanism

The mechanism involved in the SOMC preparation of bimetallic catalysts proposed is generally agreed upon by all workers in the area [3, 12]. However, before it is discussed, it is first useful to briefly re-outline the typical experimental procedure used to prepare catalysts by SOMC. The reaction between the organometallic precursor and the reduced monometallic catalyst is allowed to occur for a period of time at a chosen temperature, under hydrogen, before washing the catalyst in a solvent to remove any unreacted organometallic species. Finally, a reduction treatment is performed to complete the preparation.

A survey of the literature reveals at least two different ways in which the reaction between the organometallic precursor $M'R_n$ (M is Ge, Sn, Pb, Se, Zn and R is CH_3, C_2H_5, C_4H_9) and the surface of the reduced supported metal, M (M= Rh, Ru, Pt/ support) may occur:

i) Under an inert atmosphere the organometallic complex can react with the surface of a metal on which hydrogen has been preadsorbed. This approach was favoured by Margitalvi [5].

ii) Alternatively the reaction can occur in the presence of a partial pressure of hydrogen under either static or dynamic conditions. This was the method used in the research work described in this thesis.

The reaction generally occurs in an inert solvent such as benzene or an alkane. Once adsorbed on the surface in the presence of hydrogen, hydrogenolysis of the metal-alkyl bonds in the surface organometallic complex can occur, with elimination of RH and formation of the bimetallic particle.

It has been proposed, and indeed there is considerable evidence, that the reaction proceeds by the following mechanism (reactions (3.1) and (3.2)):

$$M\text{-}H + M'R_n \rightarrow M\text{-}M'R_{(n-x)} + xRH \qquad (3.1)$$

$$M\text{-}M'R_{(n-x)} + H_2 \rightarrow M\text{-}M' + (n\text{-}x)RH \qquad (3.2)$$

It is believed that reducing the monometallic catalyst (M) produces hydrogen sites adsorbed on the parent metal (M-H). Reaction of the organometallic species ($M'R_n$) is believed to proceed preferentially with the hydrogen preadsorbed on the first metal to produce an organometallic species ($M\text{-}M'R_{(n-x)}$) with a hydrocarbon species evolved in the gas phase (RH) (reaction (3.1)). Depending on the exact nature of R, the organometallic species ($M\text{-}M'R_{(n-x)}$) may possibly cover a number of surface metal atoms [15]. Further reaction, in the

presence of hydrogen, results in the stepwise hydrogenolysis of the remaining alkyl groups of the second metal, yielding a metallic particle with the two metals (M-M') in intimate contact (reaction (3.2)). It has been reported in some cases that, by exhibiting careful control over the reaction conditions, complete hydrogenolysis of the alkyl groups can be prevented resulting in the formation of a "stable or metastable intermediate surface complex" [16]. Our experimental procedure was such that total hydrogenolysis should occur, however, and so the formation of this type of surface complex is not relevant to the present work.

In principle, by controlling the amount of the second metal introduced in the form of the organometallic species, it is possible to deposit a known amount of the second metal onto the surface of the first metal. Assuming that all of the second metal introduced is deposited on the first metal and that the surface dispersion of the first metal is known, it is therefore possible to control the coverage of the surface sites of the parent monometallic catalyst by the second metal. This predicted coverage of the first metal by the second can be described in terms of monolayer coverage of the second metal. Maximum coverage occurs when all the surface sites of the parent metal are covered by the second metal; that is, when a complete monolayer of the second metal is present on the surface of the first metal. Further addition of the second metal may result in the build up of multilayers. Travers *et al.* have reported that a $Sn(C_4H_9)_4$ precursor can be added to give a nominal $Sn/Rh_{surface}$ ratio of 2.4 on their Rh/Al_2O_3 catalysts [4]. However, in contrast to this, Basset *et al.* suggest that for SnRh catalysts each surface Rh atom can only graft 0.8 $Sn(C_4H_9)_x$ fragments and that the amount of Sn fixed does not depend on the initial concentration of Sn organometallic

species but instead on the amount of surface Rh atoms [15]. The second metal may alternatively penetrate into the bulk of the parent metal particles thus leaving fresh exposed sites available for deposition of the second metal.

It is generally agreed that, for a parent metal supported on Al_2O_3 and SiO_2, and when the amount of the organometallic complex added corresponds to less than a monolayer, the organometallic species reacts preferentially with the reduced metal surface and not with the support surface [4, 15]. However, when an excess of the organometallic species is added, the SOMC reaction with the support has also been shown to occur to give for example, a species like $=Si\text{-}O\text{-}Sn(C_4H_9)_3$ [16, 17]. In this case the organometallic species is only physically adsorbed and can be easily removed by washing in solvent [16]. Several 'control' studies between Ge and Sn containing precursors and both silica and alumina supports have, however, shown no reaction at room temperature and no deposition of the second metal [4, 9]. It can be noted that under certain conditions, such as higher temperatures, tetrabutyl tin may react with the oxide support.

From reactions (3.1) and (3.2) above, it can be seen that alkyl species (RH) are also evolved from the hydrogenolysis of the metal-alkyl bond. Observation of these alkyl species in the gas phase provides a convenient way of monitoring the reaction (by gas chromatography). An interesting study has been published by Didillon *et al.* [16] where they monitored the products in the gas phase of the SOMC reaction between Rh/SiO_2 and $Sn(C_4H_9)_4$ at a number of different $Sn/Rh_{surface}$ ratios. They observed butane and ethane in the gas phase and found generally that the yield of ethane, a product of the hydrogenolysis of butane,

decreased as the reaction proceeded. This was taken to suggest that the Sn was depositing initially on the sites on the Rh particles active for hydrogenolysis. Similarly the ethane yield was suppressed as the $Sn/Rh_{surface}$ ratio was increased. This highlights the theory that some metals are believed to exhibit a preference for deposition on specific sites on the surface of the parent metal particle. For example, Coq *et al.* have postulated that in the deposition of Sn onto Rh particles using $Sn(C_4H_9)_4$, the Sn deposits preferentially on the sites of lowest coordination first, such as corners or edges, before filling the flatter surface planes [18]. This 'site specificity' may have the consequence of exhibiting further control in catalytic reactions by selectively poisoning reactions where the active sites are these low coordination sites thereby changing the selectivity to reactions which occur on the flat planes of metal particles.

Another attractive aspect of SOMC is that any combination of metals can be used as long as an organometallic species is readily available. Indeed it is possible to reverse the observed surface segregation in a particular combination of metals. For example, PtRu catalysts are usually enriched at the surface with Pt, however by deposition of ruthenocene on Pt it is possible to prepare catalysts with the surface enriched in Ru [14]. In this case the catalyst was stable at 600 K although heat treatment at 750 K results in diffusion of Ru into the bulk [14].

Clearly by examining the literature, two general types of organometallic species have been used in SOMC; either metal alkyl complexes such as tetrabutyl tin, or organometallic sandwich type complexes such as nickelocene or ruthenocene. The latter are not always described as SOMC by the authors; although they are

believed to react by a similar mechanism. For example, nickel is believed to be deposited onto palladium by the decomposition of nickelocene in the presence of hydrogen according to reaction (3.3) [10]:

$$(C_5H_5)_2Ni + 2H_{ads} = Ni + 2C_5H_6 \qquad (3.3)$$

The exact nature of the surface reaction and any surface intermediates still remains unclear. Both types of organometallic precursor have been used to prepare the bimetallic catalysts using SOMC in the present work.

As stated earlier the main emphasis of the work reported in this chapter will examine the use of ferrocene, $Fe(C_5H_5)_2$, to deposit Fe on the surface of Pd or Pt particles. During the course of this work a report of the use of ferrocene in the preparation of bimetallic catalysts appeared in the literature [19] although no attempt, other than electron probe microanalysis (EPMA), was used to characterise the egg-shell PdFe bimetallic catalyst prepared. This route rather than utilizing a controlled surface reaction between preadsorbed hydrogen and the ferrocene appears to involve impregnation of the ferrocene throughout the Pd particle followed by selective deposition on the surface during the reduction process. EPMA data clearly indicates that the Pd and Fe are only associated after reduction at 600 K. To date, and to our knowledge, no reports have been published describing the use of SOMC to prepare $PtFe/Al_2O_3$ bimetallic catalysts using ferrocene. Other sandwich type organometallic species have been used in other studies; for example ruthenocene, $Ru(C_5H_5)_2$, was used in the preparation of $PtRu/SiO_2$ catalysts [14] and Renouprez *et al.* [10] prepared $PdNi/SiO_2$

catalysts using a SOMC method (although they did not report it as such) by reaction of $Ni(C_5H_5)_2$ with Pd/SiO_2 in a preparation closely related to the method used here.

The most reproducible results have stressed that the monometallic parent catalyst should be fully reduced in the first step of the reaction and that the reaction relies on the selective interaction between hydrogen preadsorbed on the monometallic particles, although a few studies have reported the reaction between the organometallic complex and the unreduced surface of the metal (e.g., [20]). Recently, Margifalva *et al.* [13] published a detailed account of the SOMC reaction between unreduced Pt or Pt with adsorbed oxygen with tetraethyltin. They suggest that the reaction still proceeds although, significantly, the formation of ethylene and water, instead of ethane as expected, was observed. They proposed the following reaction mechanism (reaction (3.4)):

$$PtO_z + zSn(C_2H_5)_4 \rightarrow Pt_x[Sn(C_2H_5)_2]_x + 2zC_2H_4 + zH_2O \quad (3.4)$$

In conclusion, SOMC has provided a new method of preparing bimetallic catalysts containing the two metals in intimate contact, which relies on the selective reaction between an organometallic complex with the hydrogen sites preadsorbed on a parent monometallic catalyst. The new generation of catalytic materials produced have shown interesting catalytic properties for a variety of reactions.

3.3 The palladium and platinum monometallic catalysts

The initial stage in the preparation of a bimetallic catalyst by SOMC is the preparation of a well-defined monometallic surface. Thus the first objective of the present work was to prepare and characterise the alumina supported Pd and Pt catalysts as fully as possible using the techniques at our disposal. This work is described in the following sections. The main attributes sought in these 'parent' monometallic catalysts include a reasonably high dispersion of the active metal and a well-defined particle size, however, central to the preparation of the monometallic catalysts was the development of a reproducible preparation technique.

Hydrogen chemisorption, TEM/EDX, XRD, EXAFS, TPR and elemental analysis were used to characterise the monometallic catalysts. The theory of these techniques and the experimental procedures used were outlined in Chapter 2.

The monometallic catalysts were prepared by a simple wet impregnation reaction [21-24]. A range of commercial Pd precursors were available and the impregnation and activation conditions were investigated, varying the choice of solvent, the duration of the impregnation step and the temperature and duration of the calcination step until a 'standard' preparation technique was chosen. This method was then used throughout the work for the preparation of alumina supported Pd and extended to the preparation of the Pt monometallic catalysts.

3.3.1 Preparation of monometallic catalysts by impregnation of alumina with palladium bis-(acetylacetonato) or platinum bis-(acetylacetonato)

Table 3.2 summarises the results of hydrogen chemisorption studies for Pd/Al_2O_3 catalysts prepared using various Pd precursors. They indicate that Pd catalysts prepared from palladium bis-(acetylacetonato) ($Pd(acac)_2$), dissolved in an excess of toluene (1.0 g support/3.0 cm^3 metal salt solution), display the highest dispersion of the catalysts prepared using the different Pd precursors.

Table 3.2 Summary of hydrogen chemisorption results obtained from 4 wt% Pd/Al_2O_3 catalysts prepared using various Pd precursors using a wet impregnation technique.

Precursor	Nominal Pd loading /wt%	H/M
$Pd(acac)_2$	4	0.39
Pd (chloride)	4	0.35
Pd (nitrate)	4	0.31

As well as producing reasonably well dispersed catalysts, the use of metal (acac) precursors in the preparation of monometallic catalysts has the added advantage of the use of a chloride-free precursor thus avoiding the possible detrimental effects of chloride species on the properties of the catalysts. Moreover, the chloride containing precursor was not considered further due to a significant decrease in the total surface area of the catalyst after preparation. The Pd

(nitrate) precursor was observed to produce a catalyst with an inhomogeneous appearance and thus was not considered further. A similar comparison between the use of $Ru(acac)_3$ and ruthenium nitrosyl nitrate has been reported [25] and from EXAFS studies it was concluded that the $Ru(acac)_3$ precursor produced a more dispersed catalyst, agreeing with the present results.

As mentioned above, the main criterion in the choice of a preparation technique is that it should provide a reproducible method of dispersing the noble metal homogeneously on the surface of the support. The following experiments indicated that this was achieved using the $Pd(acac)_2$ precursor.

i) Two separate samples were prepared with the same metal loading using identical preparation procedures. Hydrogen chemisorption data confirmed that the dispersion, and hence mean particle size, of both catalysts was the same within experimental error.

ii) To examine if the noble metal was deposited evenly throughout the batch, three different samples of the same catalyst were analysed by hydrogen chemisorption. The dispersion obtained from the three samples was the same in each case confirming that the Pd was deposited on the support homogeneously throughout the batch.

The effect of calcination and reduction temperature on the final dispersion was also investigated. A 4 wt% Pd/Al_2O_3 catalyst was prepared as normal, using Pd $(acac)_2$, and calcined, then reduced at either 573 K, 623 K or 673 K. It was found that dispersion varies with the temperature of activation and that the maximum dispersion was achieved at 623 K. Therefore this temperature was

used for calcination and reduction of all the alumina supported Pd and Pt catalysts hereafter.

A mechanism has been proposed for the deposition of $Pd(acac)_2$ on to a low surface area alumina support [26]. The mechanism involves bond formation between the oxygen of a terminal hydroxyl group of alumina with $Pd(acac)_2$ and adsorption of acetylacetone (acacH) on the support (reaction (3.5) below). IR and EXAFS studies have provided evidence for the proposed mechanism [27].

$$Al\text{-}OH + Pd(acac)_2 \rightarrow Al\text{-}O\text{-}Pd(acac) + acacH \qquad (3.5)$$

Decomposition of the organic fragment occurred at elevated temperatures to leave Pd on the support. EXAFS analysis indicated that the Pd atoms were preferentially located on octahedral sites on the alumina surface and the Pd coordination number, also determined by analysis of EXAFS data, indicated that, even after high temperature calcination (973 K), a highly dispersed palladium oxide phase was present [29].

The Pt/Al_2O_3 catalysts were similarly prepared using platinum bis-(acetylacetonato), $Pt(acac)_2$.

All the alumina supported palladium and platinum catalysts discussed in this and the following chapter were prepared using the metal acac precursor.

3.3.2 Characterisation of the monometallic catalysts

Although Pd/Al_2O_3 and Pt/Al_2O_3 catalysts have been extensively characterised in the literature the results of the characterisation of the monometallics prepared in this work are discussed to allow comparison to be made with the bimetallic materials, as well as to provide information about the catalysts themselves.

The monometallic catalysts were characterised using a number of techniques. Emphasis will be given to describing the characterisation results for just a selection of the Pd/Al_2O_3 and Pt/Al_2O_3 catalysts that were investigated. These are summarised in Table 3.3.

Table 3.3 Summary of Pd/Al_2O_3 and Pt/Al_2O_3 catalysts under discussion in this section. The nominal loading is also given.

Catalyst	Nominal loading /wt%	Assay / wt%
Pd/Al_2O_3	1.0	ND
Pd/Al_2O_3[1]	2.0	1.8
Pd/Al_2O_3	3.0	ND
Pd/Al_2O_3	4.0	ND
Pd/Al_2O_3	8.0	ND
Pt/Al_2O_3[1]	1.0	0.7

Notes. [1]. Assay determined using ICP-AES. ND Assay not determined.

From the above table it can be seen that the metal assay is lower than the nominal loading, probably due to loss of the metal precursor during the impregnation of the support with the metal salt. It was noted that a small quantity of the Pd or Pt precursor was retained on the side of the glass vessel used for impregnation after evaporation of the solvent and thus was not deposited on the support.

3.3.2.1 Hydrogen chemisorption and surface area measurements

The chemisorption data for a selection of Pd and Pt catalysts are listed in Table 3.4.

Table 3.4 Hydrogen chemisorption data for a range of Pd/Al_2O_3 and Pt/Al_2O_3 catalysts prepared by impregnation of alumina with $Pd(acac)_2$ or $Pt(acac)_2$

Catalyst	Assay / wt%	H/M	Uptake H_2 / moles (x 10^{-5})	Volume-area mean particle diameter / nm [2]
Al_2O_3	-	0	0	-
Pd/Al_2O_3 [1]	1	0.56	2.7	2.0
Pd/Al_2O_3	1.8	0.45	4.3	2.5
Pd/Al_2O_3 [1]	4	0.25	4.8	4.5
Pd/Al_2O_3 [1]	8	0.18	6.8	6.3
Pt/Al_2O_3	0.7	1.1	3.2	1.0

Notes. [1]. Nominal loading. [2]. Calculated using equation (3.6).

The chemisorption data can also be used to estimate the average metal particle size. The dispersion, *H/M*, is related to the volume-area mean diameter (d_{va}) as shown in equation (3.6) [28]:

$$H/M = \frac{6\left(V_m/a_m\right)}{d_{va}} \qquad (3.6)$$

where a_m is the effective average area occupied by a metal atom in the surface and V_m is the volume per metal atom in bulk. For both Pd and Pt a value of 1.13 nm is quoted in the literature for 6 (V_m/a_m) [28]. The average particle sizes (in nm) derived from the hydrogen chemisorption data are displayed in Table 3.4.

It was confirmed that the alumina support, after calcination and reduction, did not chemisorb H_2 at room temperature. It can therefore be assumed that the hydrogen adsorbed by the catalysts must be adsorbed on the metal particles. It is possible, however, that after dissociatively adsorbing on the metal surface the hydrogen may migrate onto the surface of the support in the process known as spillover [29]. In the discussion of the results, this is taken to be negligible. The data from Table 3.4 for the range of Pd/Al_2O_3 catalysts is plotted in Figure 3.1 displaying the variation of average particle diameter size and dispersion with loading of Pd on the support. It is clear that increasing the metal content decreases the dispersion of the catalysts, i.e. higher average particle sizes are obtained at higher metal loadings. This trend is expected and has been found in many other studies; for example Ho *et al.* reported a similar variation in the dispersion of a range of Pd/Al_2O_3 catalysts with various metal loadings [30].

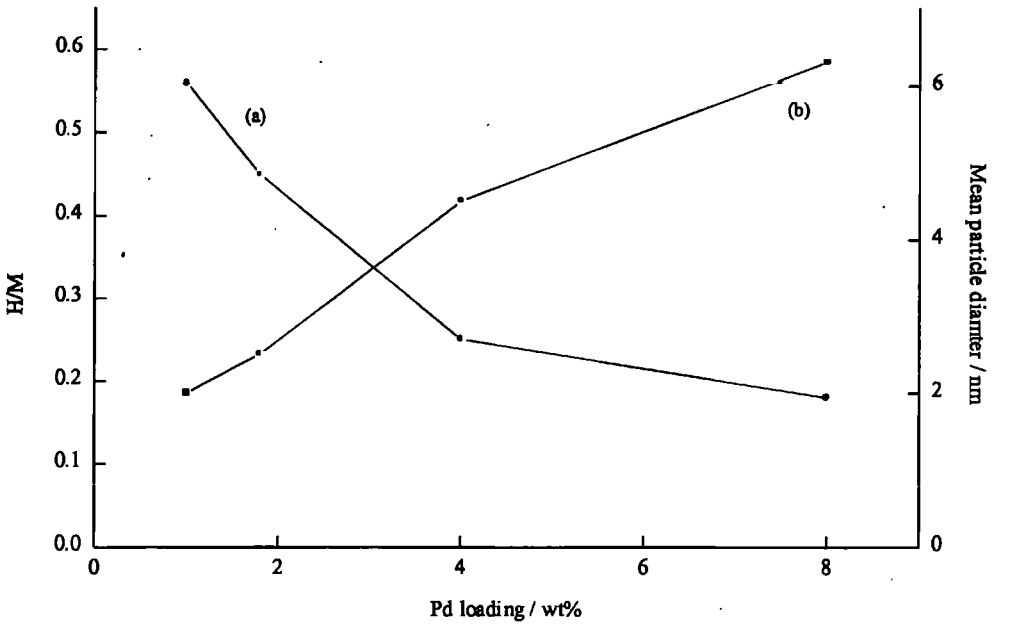

Figure 3.1 Variation of (a) dispersion (H/M) and (b) average particle size diameter with loading of Pd on support.

Only Pt/Al_2O_3 catalysts with metal loadings less than 1 wt% were prepared in this research; chemisorption data indicates that these catalysts are highly dispersed and indeed H/M values greater than 1 were observed. This has been observed previously in other studies (and with different metals) and is attributed to multiple adsorption of hydrogen atoms on certain Pt sites, when Pt is highly dispersed [28, 31]. Indeed EXAFS studies have confirmed that high dispersion values are due to $H/M_{surface}$ stoichiometries greater than unity [32].

The total surface area of the catalyst samples was also determined in order to ascertain if an alteration in surface area resulted from impregnation of the

alumina (with surface area 180 m^2g^{-1}) with Pd or Pt. For example, a decrease in surface area may occur if the noble metal accumulates around the entrances to the support surface pores physically blocking these entrances. A decrease in surface area may have a deleterious effect on the properties of the catalyst as the maximum level of metal that can be loaded on the support is limited by surface area. The total surface area was not found to change on addition of the Pd or Pt beyond experimental error. It should be noted, however, that the surface area was not determined for every catalyst; only a selection of samples were checked to confirm that no decrease in surface area was observed.

3.3.2.2 Transmission electron microscopy and energy dispersive X-ray analysis (TEM/EDX)

A representative electron micrograph for the 1.8 wt% Pd/Al_2O_3 catalyst is shown in Figure 3.2. The Pd particles are clearly distinguishable from the lighter coloured support material and are mostly spherical in nature. The particle size distribution obtained by counting over 200 particles is shown in Figure 3.3.

The particles counted varied between 3-7 nm in diameter, although it is clear from Figure 3.3 that the majority of particles observed are in the range 4-5 nm. This suggests that the Pd $(acac)_2$ precursor used in this work is thus effective in producing a dispersed catalyst with a reasonably narrow particle size range.

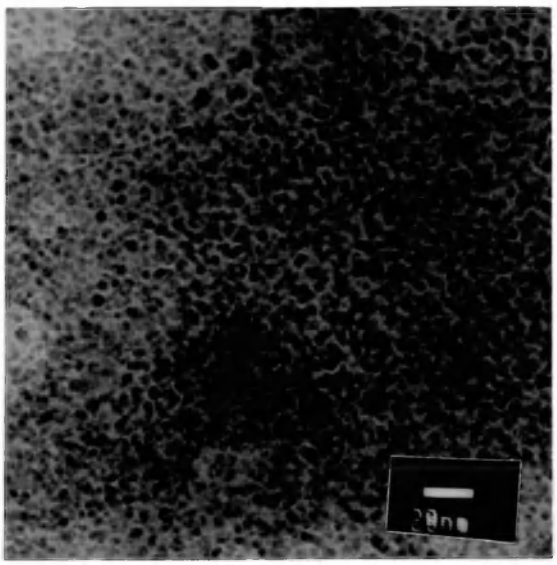

Figure 3.2 Representative electron micrograph of 1.8 wt% Pd/Al_2O_3 catalyst prepared by impregnation of alumina with Pd $(acac)_2$.

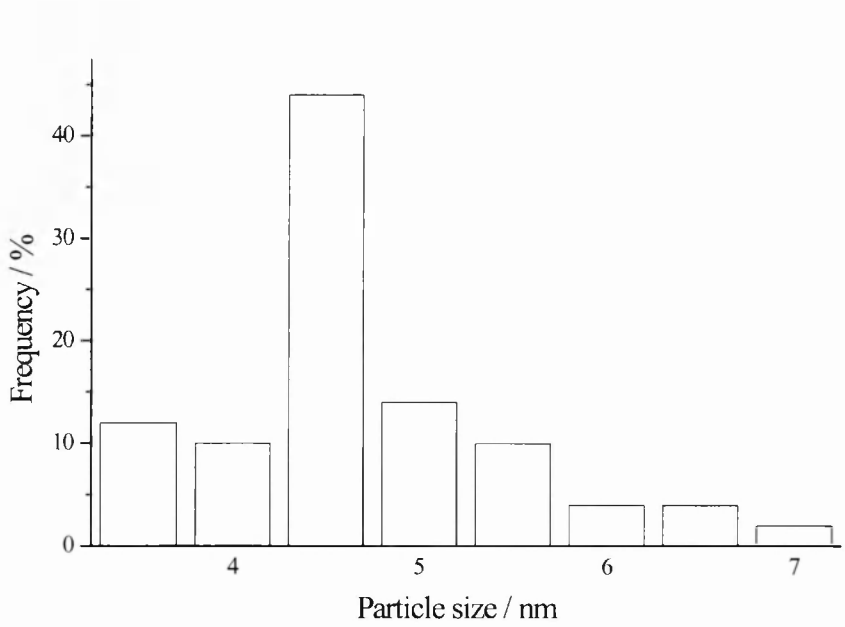

Figure 3.3 Histogram of particle size distribution for 1.8 wt% Pd/Al_2O_3 catalyst.

The mean particle size can be calculated from equation (3.7) to give a value of 4.9 nm.

$$\phi_{AV} = \frac{\sum_i n_i \phi_i}{\sum_i n_i} \qquad (3.7)$$

where n_i is the number of particles with diameter ϕ_i.

The particle size determined by TEM is larger than the value calculated from hydrogen chemisorption (2.5 nm). It is thought likely that TEM overestimates the mean particle size. From the histogram shown in Figure 3.3 it would appear that no particles under 2.5 nm were observed, however, EDX evidence (described in the next paragraph) indicates that Pd particles smaller than 2.5 nm are present. Chemisorption has the advantage that every particle is accessible and will therefore be 'counted'. Hence the value of 2.5 nm obtained from chemisorption is believed to be a more meaningful value for the mean particle size.

Energy dispersive X-ray (EDX) analysis of areas of the support where no metal particles were observable by the microscope even at high magnification, indicated the presence of further Pd. This confirms the presence of metal particles beyond the resolution of our microscope. The average particle size calculated by determining the mean of the particles measured in the electron micrographs is thus not a true indication of the average size of all the particles and should be taken to be a maximum value.

No metal particles can be seen in the electron micrograph of the 0.7 wt% Pt/Al_2O_3 catalyst (not shown) however EDX analysis of the catalysts confirmed the presence of Pt thus suggesting that the platinum catalyst is highly dispersed. This confirms the result from hydrogen chemisorption which indicated the presence of highly dispersed Pt particles.

3.3.2.3 X-ray powder diffraction (XRD)

XRD has been used to identify the phases present in the monometallic catalysts. Figure 3.4 displays the pattern obtained for the 4 wt% Pd/Al_2O_3 with the powder pattern of the alumina support shown for comparison. Note that the X-ray diffractometer used for this work had no *in situ* capability so the diffraction patterns were recorded at room temperature after exposure of the catalysts to air. The alumina support is shown to be poorly crystalline and is matched to JCPDS file number 29-1486. Additional reflections are observed in the powder pattern of the Pd/Al_2O_3 catalyst which can be matched to the JCPDS file number 6-0515 for PdO. Indeed PdO is the only PdO_x species formed without using extreme conditions: PdO_2 crystallites have only been observed at high oxygen pressure [33]. Therefore in air, XRD indicates that the alumina supported palladium exist as metal oxide particles. Below 3 wt% Pd/Al_2O_3 no Pd phase was observed in the XRD powder pattern indicating that a dispersed metal (oxide) phase is present, with an average crystallite size smaller than can be observed by XRD.

Similarly XRD powder patterns of the 0.7 wt% Pt/Al_2O_3 catalyst (not shown) did not show the presence of any Pt containing phase. Again this would be expected

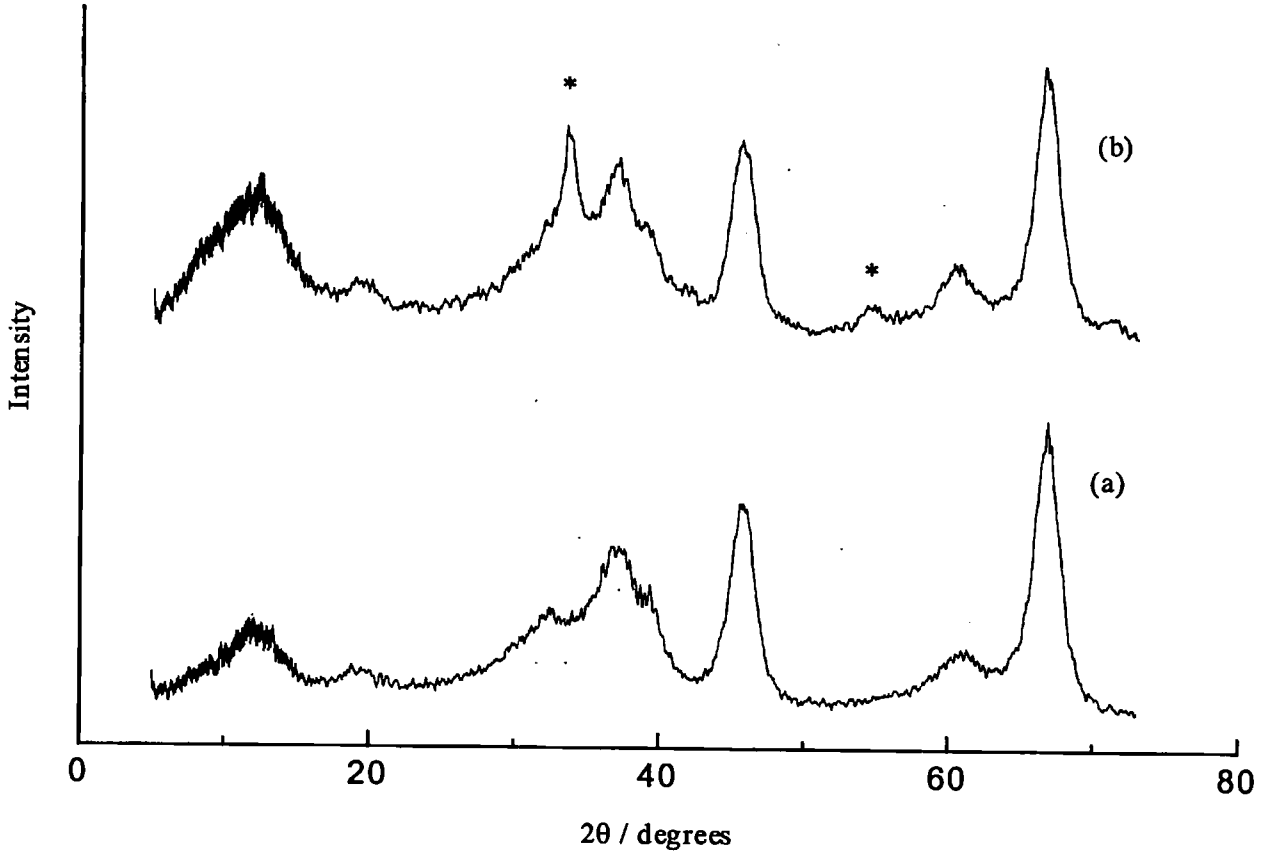

Figure 3.4 XRD powder pattern of (a) alumina support, (b) 4 wt% Pd/Al_2O_3.

since both the hydrogen chemisorption and TEM results indicate that the low loaded Pt/Al_2O_3 catalyst is highly dispersed and therefore will be XRD 'invisible'. Previous literature studies indicate that Pt particles will also be oxidised in air, although, in contrast to Pd, many PtO_x species are known to exist and many have been identified on the surface of catalyst supports. Hwang and Yeh observed Pt_sO (where Pt_s indicates a surface Pt atom), PtO, PtO_2 and $PtAl_2O_4$ species on Pt/Al_2O_3, with the formation of these species dependent on the Pt dispersion and oxidation conditions [34]. In addition Mill *et al.* reported that highly dispersed Pt/Al_2O_3 is rapidly oxidised in air to form PtO_2 [35]. Therefore it can be assumed that, in air, a PtO_x species exists on the alumina support.

3.3.2.4 Extended X-ray absorption fine structure (EXAFS)

EXAFS studies were performed at the Pd K-absorption edge (usually referred to as the K-edge) for the 1.8 wt% Pd/Al_2O_3 catalyst at different stages of the preparation procedure and under a variety of reduction and calcination conditions. The samples examined are summarised in Table 3.5. Pd/Al_2O_3-1 refers to the sample after impregnation with $Pd(acac)_2$ and low temperature drying for 16 h at 383 K. Pd/Al_2O_3-2 and -3 refer to sample 1 after a variety of higher temperature treatments at 623 K. Pd/Al_2O_3-2 is the sample obtained after calcining Pd/Al_2O_3-1 for 1 h at 623 K and Pd/Al_2O_3-3 is obtained after calcining Pd/Al_2O_3-1 (623 K, 1 h) followed by a reduction treatment at 623 K for 1 h. This sample most closely reflects the pretreatment of the monometallic catalysts before the SOMC reaction. It should be noted that the reduced sample was

transferred from the glass reactor into a homemade sample holder (described in Chapter 2, Section 2.2.4) in a dry box in an attempt to prevent exposure of the catalyst to air or moisture and then stored in a vacuum dessicator until required. The samples were stored in the sample holders for several weeks before analysis. Details of the experimental procedures used to obtain the X-ray absorption spectra and the data analysis procedures were given in Chapter 2, Section 2.2.4.

Table 3.5 1.8 wt% Pd/Al_2O_3 monometallic catalysts examined by EXAFS at Pd K-edge. Sample Pd/Al_2O_3-3 was transferred to homemade sample holders after reduction without exposure to air.

Sample	Conditions
Pd/Al_2O_3-1	Dried (383 K, 16 h) after impregnation
Pd/Al_2O_3-2	Dried, calcined (623 K, 1 h)
Pd/Al_2O_3-3	Dried, calcined (623 K, 1 h) then reduced (623 K, 1 h)

The Fourier transformed EXAFS and the best fit curves are shown in Figures 3.5-3.7 for each of the samples listed above in Table 3.5. In all cases it was only possible to fit the first coordination shell, which is taken to mean the nearest neighbouring atoms to the absorber atom, due to the low signal to noise ratio of the data obtained and only the k range 3 $Å^{-1}$ to 10 $Å^{-1}$ was analysed. The results from the best fit are listed in Table 3.6 below with the number of runs collected and summed for each sample. Errors usually associated with EXAFS analysis are estimated to 10 -30 % for the coordination numbers and 10 % for the interatomic distance [36]. A notable feature of the fitted data is an increase of

the Debye-Waller factor (Table 3.6), relative to the Pd foil, for the supported Pd catalysts indicating a disordered structure of the small Pd particles.

Table 3.6 Fitted EXAFS data from 1.8 wt% Pd/Al_2O_3 monometallic catalysts. Treatment conditions are given in Table 3.5.

Sample	Contribution	Coordination Number / N	R / Å	$2\sigma^2$ /Å(x 10^{-4})	No. of Runs
Pd foil	Pd-Pd	12	2.73	11	1
Pd/Al_2O_3-1	Pd-O	4.2	2.00	13	2
Pd/Al_2O_3-2	Pd-O	6.0	2.02	15	1
Pd/Al_2O_3-3	Pd-O	1.2	2.00	28	2

A 12 μm Pd foil was fitted satisfactorily agreeing with literature data for the known structure of metallic Pd [37]. Pd/Al_2O_3-1, the sample obtained after the impregnation step and low temperature drying procedure before any high temperature heat treatment, was fitted to 4.2 Pd-O pairs at 2.00 Å. This is in general agreement with a similar study [27] of alumina impregnated with Pd $(acac)_2$ (0.7 wt% Pd) dried at 373 K, which was fitted to 5.0 Pd-O pairs at 1.98 Å. The authors attributed this to Pd surrounded by a regular acetylacetonato framework anchored to the support.

Pd/Al_2O_3-2 is the calcined sample and the EXAFS data was fitted to 6.0 Pd-O pairs at 2.02 Å. Thus the main effect of calcining Pd/Al_2O_3-1 is to increase the number of Pd-O contributions. It has previously been shown that oxidation of Pd

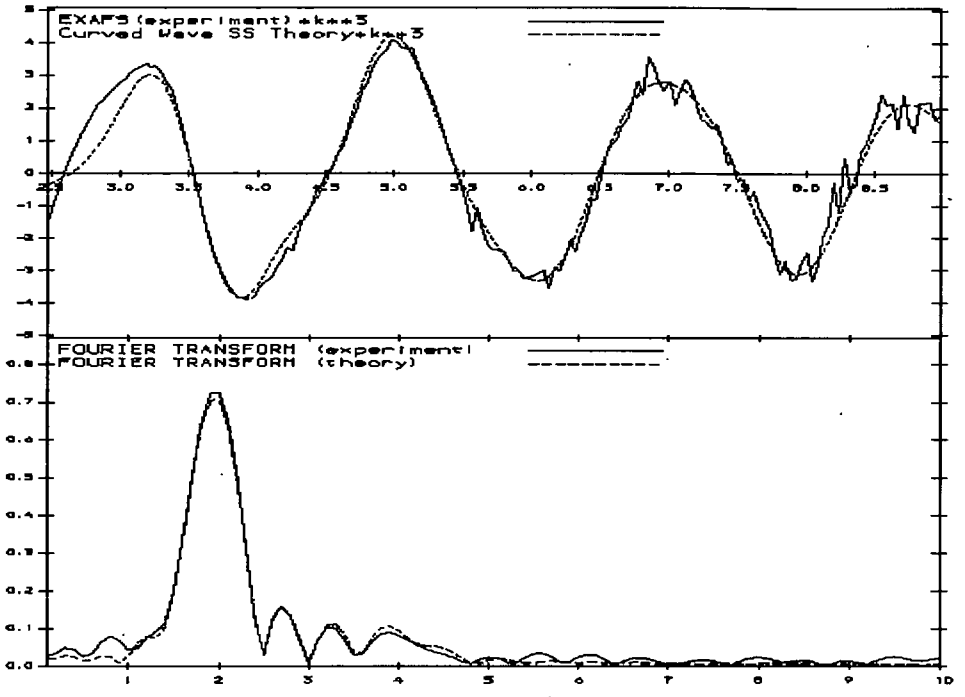

Figure 3.5 Fourier transform of Pd K-edge EXAFS recorded from Pd/Al_2O_3-1.

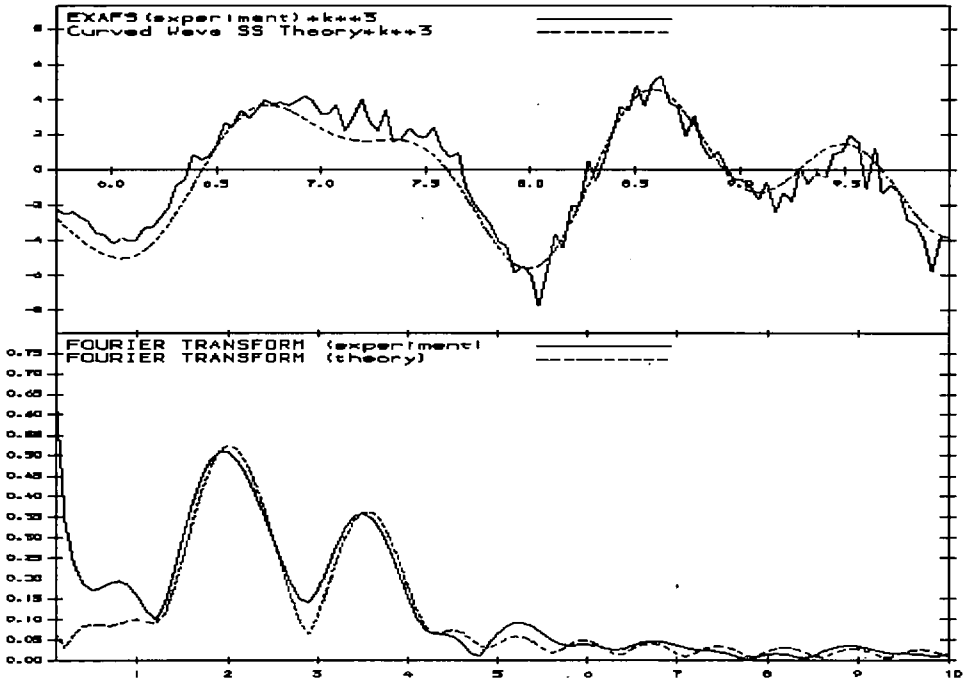

Figure 3.6 Fourier transform of Pd K-edge EXAFS recorded from Pd/Al_2O_3-2.

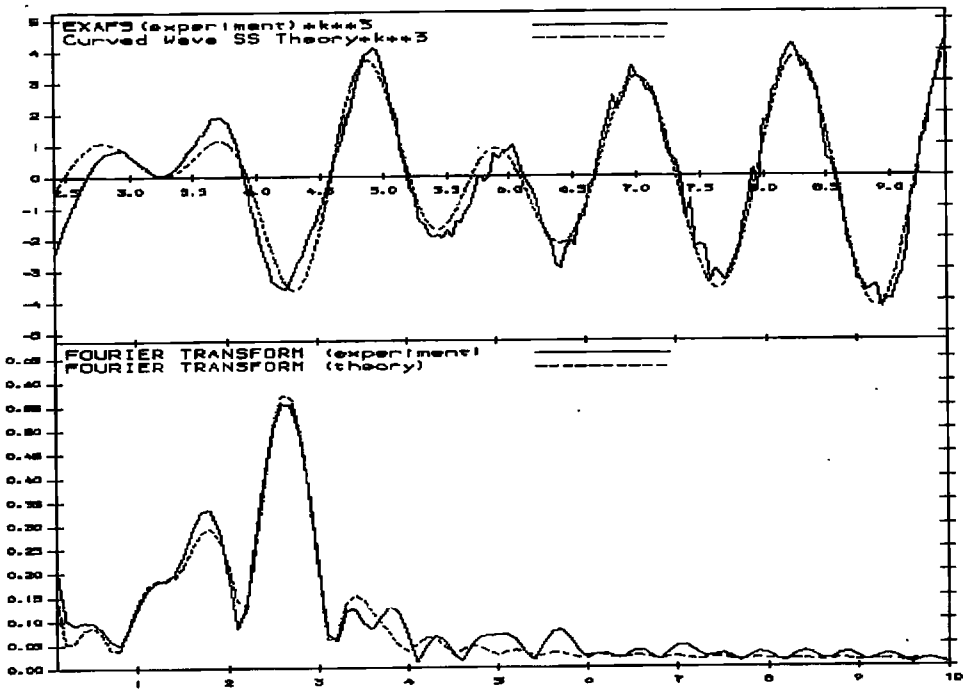

Figure 3.7 Fourier transform of Pd K-edge EXAFS recorded from Pd/Al_2O_3-3.

the Debye-Waller factor (Table 3.6), relative to the Pd foil, for the supported Pd catalysts indicating a disordered structure of the small Pd particles.

Table 3.6 Fitted EXAFS data from 1.8 wt% Pd/Al_2O_3 monometallic catalysts. Treatment conditions are given in Table 3.5.

Sample	Contribution	Coordination Number / N	R / Å	$2\sigma^2$ Å(x 10^{-4})	No. of Runs
Pd foil	Pd-Pd	12	2.73	11	1
Pd/Al_2O_3-1	Pd-O	4.2	2.00	13	2
Pd/Al_2O_3-2	Pd-O	6.0	2.02	15	1
Pd/Al_2O_3-3	Pd-O	1.2	2.00	28	2

A 12 μm Pd foil was fitted satisfactorily agreeing with literature data for the known structure of metallic Pd [37]. Pd/Al_2O_3-1, the sample obtained after the impregnation step and low temperature drying procedure before any high temperature heat treatment, was fitted to 4.2 Pd-O pairs at 2.00 Å. This is in general agreement with a similar study [27] of alumina impregnated with Pd $(acac)_2$ (0.7 wt% Pd) dried at 373 K, which was fitted to 5.0 Pd-O pairs at 1.98 Å. The authors attributed this to Pd surrounded by a regular acetylacetonato framework anchored to the support.

Pd/Al_2O_3-2 is the calcined sample and the EXAFS data was fitted to 6.0 Pd-O pairs at 2.02 Å. Thus the main effect of calcining Pd/Al_2O_3-1 is to increase the number of Pd-O contributions. It has previously been shown that oxidation of Pd

results in an increased coordination number of oxygen around the Pd atom [38]. Other characterisation techniques (for example, XRD) indicate that the Pd in calcined Pd/Al_2O_3 exists as the metal oxide phase, PdO.

Calcination and then reduction of Pd/Al_2O_3-1 gives Pd/Al_2O_3-3 and a decrease in the number of Pd-O contributions. From our TPR results, and previous literature studies concerned with the reduction of Pd catalysts, it would be anticipated that Pd would be reduced to the metallic state under our reduction conditions. For example, a similar EXAFS study of alumina supported Pd confirmed that Pd is completely reduced to the metallic state after *in situ* reduction [39]. A significant decrease in the number of Pd-O contributions is observed in our experiment although the fitted data indicates that the Pd-O contribution does not fully decrease to zero as would be anticipated if PdO was fully reduced to metallic Pd. This may be due, given the limitations of the equipment available, to some partial oxidation occurring following the reduction treatment. As stated previously sample Pd/Al_2O_3-3 most closely reflects the pretreatment conditions given to the monometallic Pd catalyst before the SOMC reaction, that is, the sample is prepared for the SOMC reaction by calcination and then reduction at 623 K. In the absence of any further evidence to the contrary we shall assume that the surface is fully reduced after reduction at 623 K.

No EXAFS data were collected at the Pt L_{III}-edge of the 0.7 wt% Pt/Al_2O_3.

3.3.2.5 *Temperature-programmed reduction (TPR)*

TPR was used to probe the reducibility of the Pd monometallic catalysts. An extensive literature exists concerning TPR of Pd-based catalysts; for example, it is known that in a stream of hydrogen, PdO is reduced to Pd metal below room temperature [40]. Although the exact temperature of reduction varies between studies, it is generally believed to occur between 200 and 273 K. The low reduction temperature of the PdO phase indicates that the reduction of PdO is thermodynamically favourable. A unique feature of Pd TPR profiles is the existence of a negative peak, due to evolution of hydrogen, at temperatures around 373 K. This is attributed to decomposition of the phase known as β-palladium hydride (β-PdH) which is formed when Pd is reduced in hydrogen. The hydride decomposes as the temperature is raised releasing the dissolved hydrogen.

Figure 3.8 displays the TPR profile for the monometallic 4 wt% Pd/Al_2O_3 catalyst monitored in the range 77 K to 1073 K.

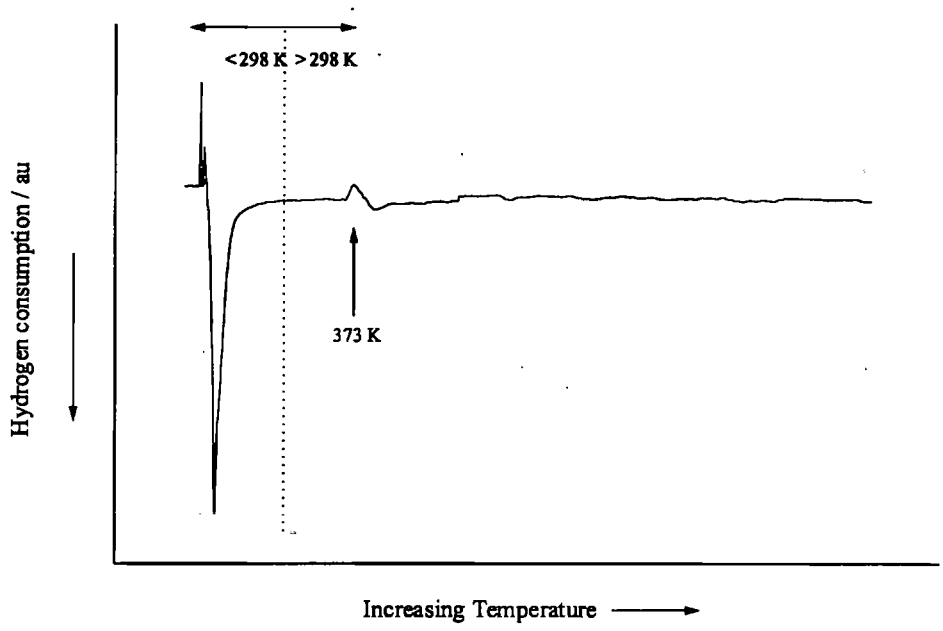

Figure 3.8 TPR profile for 4 wt% Pd/Al_2O_3 catalyst.

The TPR profile of the alumina support was also collected (not shown) which displays a flat line indicating that no reduction of the alumina takes place in the temperature range studied. Any reduction peaks observed in the Pd/Al_2O_3 profile must thus be attributed to the metal. The TPR profile of the Pd catalyst agrees well with that expected from the literature. The spike(s) observed shortly after the start of collection of the data is an inherent electronic feature observed when the U-tube vessel containing the catalyst is removed from the flask containing liquid nitrogen and is due to a rapid change in temperature of the hydrogen/nitrogen gas mixture as it passes over the TCD filaments. This was confirmed by carrying out a 'blank' reduction with no catalyst in the reactor. The main reduction peak can be seen below room temperature and a negative peak is also clearly visible at about 370-380 K, as determined by monitoring the

temperature of the sample as the experiment progressed. As a guide the point at which the temperature heating program was commenced, at 298 K, is marked on the reduction profile. The main hydrogen uptake is generally associated with the reduction of PdO, hydrogen absorption by the reduced Pd and adsorption of hydrogen on the metallic surface. As mentioned previously, the negative peak observed is due to the desorption products from the decomposition of β-PdH. In addition, desorption of weakly bound H from the Pd surface occurs at this temperature. A further peak at a higher temperature has been reported in a number of Pd TPR studies [41] and attributed to desorption of strongly adsorbed hydrogen; however, it is not observed in the present work. In summary, the TPR confirms the XRD data that the Pd exists as the metal oxide phase when exposed to air. This phase is easily reduced to Pd metal in a stream of 10 % H_2 in N_2 at temperatures below room temperature in agreement with previous literature data.

No TPR of the Pt/Al_2O_3 monometallic catalyst was collected.

3.3.3 Conclusions from the preparation and characterisation of monometallic Pd/Al_2O_3 and Pt/Al_2O_3 catalysts

Alumina supported Pd and Pt monometallic catalysts have been prepared by an impregnation technique utilising the metal bis-(acetlyacetonato) salt dissolved in an excess of toluene. A range of precursors were initially investigated and the metal $(acac)_2$ precursor was found to give a reasonable dispersion and a homogeneous deposition of the active metal on the support surface. Both

supported metals are believed to exist as the metal oxide in air but can be easily reduced to the metal by reduction in hydrogen.

The initial investigations concerning the preparation of the monometallic catalysts were focused on the Pd/Al_2O_3 catalysts. After this preparation was found to be satisfactory the technique was applied, without modification, to the preparation of Pt/Al_2O_3 catalysts. The monometallic catalysts thus prepared and characterised were then used as the basis for the preparation of bimetallic catalysts by surface organometallic chemistry.

3.4 The bimetallic PdM/Al_2O_3 and PtM/Al_2O_3 catalysts (where M = Fe or Sn) prepared using SOMC

This section will describe the preparation and characterisation of the bimetallic catalysts prepared by SOMC. A selection of the bimetallic catalysts studied is given in Table 3.7.

Table 3.7 Summary of MM'/Al_2O_3 bimetallic catalysts (where M = Pd or Pt and M' = Fe or Sn) prepared by SOMC.

Catalyst (MM'/Al_2O_3)	Coverage M' / ML	Assay M / wt%	Assay M' / wt%	Nominal M' loading / wt%
$PdFe/Al_2O_3$	0.5	4	ND	0.25
$PdSn/Al_2O_3$	0.5	4	ND	0.52
$PdFe/Al_2O_3$	0.5	1.8	0.23	0.24
$PdSn/Al_2O_3$	0.5	1.81	0.37	0.46
$PtFe/Al_2O_3$	0.5	0.73	0.23	0.26
$PtSn/Al_2O_3$	0.5	0.79	0.36	0.43

ND: Not determined.

The catalysts can be identified using the code *n wt% MM'/Al_2O_3* which corresponds, unless stated otherwise, to addition of 0.5 monolayer (ML) of M' to a n wt% M/Al_2O_3 catalyst. For example, 1.8 wt% $PdFe/Al_2O_3$ represents the bimetallic catalyst prepared by addition of 0.5 ML Fe to a 1.8 wt% Pd/Al_2O_3 monometallic catalyst. Catalysts with a coverage other than 0.5 ML were prepared although only the 0.5 ML catalysts are considered here. All the bimetallic catalysts discussed here were prepared by surface organometallic chemistry. The MFe/Al_2O_3 catalysts were prepared using ferrocene and the MSn/Al_2O_3 catalysts using tetrabutyl tin.

A key aim of this work is to extend the range of precursors available for the preparation of bimetallic catalysts using SOMC. Thus the work described in this

section will concentrate mainly on the use of ferrocene as a precursor and characterisation of the iron-containing materials. Tetraalkyl tin species, have been widely used in the preparation of bimetallic Sn catalysts, described in the introduction to this chapter, and will not be considered here in any great detail.

The experimental procedures for preparing both the tin and the iron catalysts were discussed in some detail in Chapter 2.

3.4.1 Preparation of bimetallic catalysts by SOMC

The parent monometallic catalysts were chosen to have reasonable dispersion and between 0.7-4.0 wt% Pd or Pt. Based on the dispersion and assuming that the second metal reacts selectively with the Pd or Pt surface, the amount of the precursor required to give the desired coverage was calculated.

The precursor was dissolved in n-heptane and added under nitrogen to the pre-reduced parent monometallic catalyst. Hydrogen was then bubbled through the system and the progress of the reaction followed by analysis of the gas phase.

A 'control' experiment was performed with alumina for each precursor in order to determine the extent of reaction, if any, with the support. Reactions were carried out between the alumina support and both ferrocene ($Fe(C_5H_5)_2$)and tetrabutyl tin ($Sn(C_4H_9)_4$) employing the same conditions used in the preparation of the bimetallic catalysts. The amount of organometallic introduced to the support corresponded to ca. 0.5 wt% of the support, which is similar to the

loading of the second metal in the bimetallic catalysts. The reaction was allowed to continue at 298 K for 24 h and then 343-353 K for 7-8 h. Analysis (by GC) of the gas phase leaving the reactor did not indicate the evolution of alkyl species from the reaction. After the typical reaction time the samples were washed in heptane to remove any remaining unreacted organometallic complexes from the support. The samples were then dried and reduced. Elemental analysis of the samples given in Table 3.8 indicated that only a negligible amount of Sn (less than 100 ppm) was deposited agreeing with reports in the literature [9].

Table 3.8 Assay data obtained from Sn/Al_2O_3 and Fe/Al_2O_3 samples prepared using organometallic precursors.

Sample	wt% metal introduced	Assay metal / wt%
$Al_2O_3 + Sn(C_4H_9)_4$	0.5	<< 0.001
$Al_2O_3 + Fe(C_5H_5)_2$	0.5	0.05

The results for iron, however, indicate that some iron is deposited on the alumina using ferrocene. The absence of any gas phase species during the 'reaction' suggests that the deposition of iron may in fact be due to decomposition of any impregnated or residual ferrocene, during the reduction treatment rather than a controlled surface reaction using SOMC. That the colour of the ferrocene solution remained essentially unchanged during the reaction again suggests little reaction occurred. It can be concluded that under the reaction conditions used only a small amount of Fe or Sn is deposited on the surface of the alumina

support. Thus, any Fe or Sn deposited on M/Al_2O_3 is likely to be on the surface of the metal rather than the support.

With reference to Table 3.7, and comparing the nominal loading of the second metal with the assay determined by ICP-AES, it is clear that almost all of the Fe introduced to the monometallic catalysts was successfully deposited. A slight loss of Sn was observed when using the $Sn(C_4H_9)_4$ precursor which may be due to some of the Sn complex leaving the reactor in the hydrogen stream before reaction with the catalyst.

Before the characterisation of the bimetallic catalysts is considered, it is useful to consider a few further features relating to the preparation of the Fe-containing catalysts. Reaction of ferrocene with the pre-reduced catalyst could be monitored in a number of ways. First, GC analysis showed the presence of an alkyl species in the gas phase. Although it was not possible to unambiguously identify this species it is reasonable to suggest that it is a cyclic C_5H_x moiety, probably C_5H_6. A typical reaction profile is shown in Figure 3.9. After a short induction period the evolution of the C_5 species rises rapidly to a maximum after about 1 h of reaction. From this point the yield of the alkyl species decreases slowly so that after 24 h only small quantities are evolved, indicating that at 298 K the reaction has neared completion. However heating the reactor to 343-353 K results in further evolution of cyclic C_5 in the gas phase until after about 8 h no further products are observed.

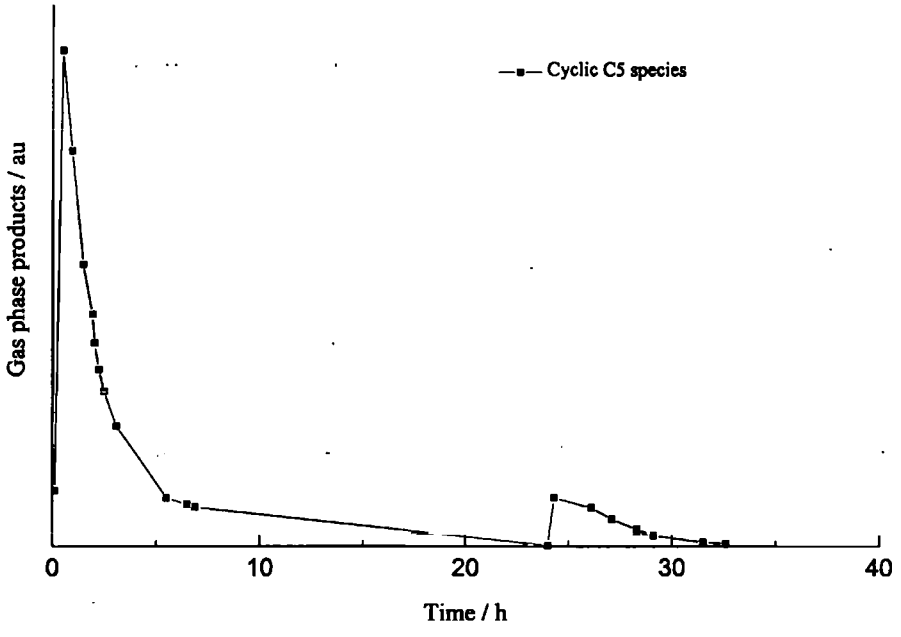

Figure 3.9 Reaction profile from preparation of a $PdFe/Al_2O_3$ catalyst.

On dissolving ferrocene in heptane an orange solution was formed allowing a second more qualitative method for determining the extent of reaction. As the reaction progressed the colour of the solution slowly became less intense, and after 24 h only a very pale orange colouration remained disappearing completely (to the naked eye) after heating to 353 K.

Evolution of the cyclic C_5 species suggests that the hydrogenolysis of the Fe-C_5H_5 bond occurs. The fact that no significant reaction occurred with the alumina in the presence of gas phase hydrogen suggests that the ferrocene is reacting with adsorbed hydrogen on the metal surface.

Thus a reaction similar to that for nickelocene [10] can be postulated (3.8):

$$Fe\text{-}(C_5H_5)_2 + 2H_{ads} \rightarrow Fe + 2C_5H_6 \qquad (3.8)$$

To our knowledge this is the first report of the use of ferrocene to deposit Fe on to the surface of another metal using SOMC. Miura has recently reported the use of ferrocene to prepare eggshell $PdFe/Al_2O_3$ catalysts based on a method using the selective chemical vapour deposition of mobile metal compounds [19]. In this work the prereduced catalysts were impregnated with a benzene solution of ferrocene, or ruthenocene. For ruthenocene with just a silica support, the ruthenocene vapourised when the dried catalyst was heated in hydrogen and condensed downstream of the catalyst bed before it could be reduced. The remaining catalyst contained only traces of ruthenium. When a similar preparation was tried using Pt/SiO_2, the ruthenocene decomposed to metallic Ru on the Pt during the reduction step and most of the Ru remained. Miura suggests that the Pt catalyses the decomposition of ruthenocene to metallic Ru. When ruthenocene is heated it migrates on the support surface and through the gas phase due to its high vapour pressure. When it migrates on a Pt particle in a hydrogen stream it catalytically decomposes and Ru metal is deposited on the Pt, the precursor ligands being easily hydrogenated. When this technique was extended to egg-shell Pd/Al_2O_3 catalysts and ferrocene, after the initial impregnation and drying steps, the iron was found to be distributed throughout the pellet. However, after hydrogen reduction the Fe was distributed in the outer layer with the Pd. It is not clear whether this method works by the same mechanism as the controlled surface reaction using SOMC.

Characterisation of the bimetallic catalysts will now be considered. In addition to the techniques used to characterise the monometallic catalysts, Mössbauer and EPR spectroscopy were also used to characterise the bimetallic catalysts.

3.4.2 Characterisation of bimetallic catalysts prepared by SOMC

3.4.2.1 Hydrogen chemisorption and surface area measurements

Before the hydrogen chemisorption data for the bimetallic catalysts are discussed, the chemisorption of hydrogen on Sn and Fe will be considered. It is well established that hydrogen adsorption is not observed on Sn, whereas it has been shown to occur on Fe. However, under our experimental conditions it was found that, after reduction at 623 K, monometallic Fe/Al_2O_3 or Sn/Al_2O_3 did not chemisorb hydrogen at room temperature. Vannice *et al.* have similarly demonstrated that hydrogen chemisorption does not occur on reduced Fe/C catalysts at 300 K [42] and that a higher temperature (473 K) was required for hydrogen chemisorption on MgO supported Fe [43]. The hydrogen uptake by the bimetallic catalysts can therefore be attributed solely to the noble metal.

The hydrogen chemisorption results for a range of the bimetallic catalysts prepared in this work are collected in Table 3.9, along with the data for the monometallic parent catalysts, for ease of reference.

Immediate inspection of the data indicates a decrease in the volume of hydrogen adsorbed by the bimetallic catalysts compared to the parent monometallic

Table 3.9 Chemisorption data for a selection of bimetallic catalysts prepared by SOMC. Data also listed for monometallic catalysts used as 'parent' for bimetallic catalysts.

Catalyst	Monometallic H/M	Hydrogen uptake / moles (x 10^{-5})	Second Metal coverage/ ML	Bimetallic H/M	Hydrogen uptake / moles (x 10^{-5})	Surface Area / m^2g^{-1}
1.8 wt% $PdFe/Al_2O_3$	0.45	4.8	0.5	0.34	2.91	196.6
1.8 wt% $PdSn/Al_2O_3$	0.45	4.8	0.5	0.16	1.48	-
0.7 wt% $PtFe/Al_2O_3$	1.1	2.9	0.5	0.41	1.07	174.1
0.7 wt% $PtSn/Al_2O_3$	1.1	2.9	0.5	0.44	1.13	-

catalysts. This indicates that the number of surface sites available for hydrogen adsorption decreases upon addition of the second metal. This can be interpreted as evidence for the deposition of the second metal onto the surface of the first metal, covering some of the metal sites available for hydrogen adsorption. These findings are similar to the results obtained for a range of Ru/Al_2O_3 monometallic and RuM/Al_2O_3 bimetallic catalysts (with M = Ge, Sn, Pb) prepared by SOMC [44], in which, a decrease in hydrogen chemisorbed was also observed after addition of the second metal.

It should be mentioned that other interpretations could also explain the decrease in adsorbed hydrogen observed after addition of the second metal. An increase in the Pd or Pt particle size would also result in a decrease in the dispersion of the noble metal. However, TEM measurements, (discussed in the next section), indicate that this is unlikely since the increases in particle sizes required for such a dramatic decrease in the amount of hydrogen chemisorbed were not observed. Decreased chemisorption after a high temperature reduction treatment is also characteristic of the existence of a *strong metal support interaction* (SMSI) [45]. There is now strong evidence to show that this state occurs when part of the support covers part of the surface of the metal particles, thus decreasing the number of metal sites available for hydrogen chemisorption [46]. However, this state is usually associated with reduction at higher temperatures than used in this work, and when reducing metals on certain 'reducible' supports such as titania and niobia. Alumina is not considered to be a 'reducible' support and it is reasonable to suggest that a *SMSI* state is not responsible for the observed reduction in the hydrogen chemisorbed.

It is also possible that the reaction conditions used to prepare the bimetallic catalysts alter the structure of the monometallic catalyst in a manner that would result in a decrease in the hydrogen chemisorbed. To test this possibility a 4 wt% Pd/Al_2O_3 catalyst was subjected to the same experimental procedure for the preparation of the bimetallic catalysts by SOMC except that no organometallic precursor was included in the reaction. Comparison of the catalyst before and after the experimental procedure by hydrogen chemisorption indicated that no change in dispersion was observed.

It can be concluded that the decrease in hydrogen chemisorption observed after addition of Fe or Sn to either Pd/Al_2O_3 or Pt/Al_2O_3 catalysts by SOMC is unlikely to be due to an increase in noble metal particle size, the existence of a *SMSI* state, or the reaction conditions used to prepare the bimetallic catalyst. The changes observed in the dispersion are attributed to the deposition of the second metal onto the surface of the first metal decreasing the number of sites available for hydrogen chemisorption.

Considering the data for the Pt mono- and bi-metallic catalyst in Table 3.9, it can be seen that the 0.7 wt% Pt/Al_2O_3 catalyst had an initial dispersion of 100 % whereas upon addition of half a monolayer of either Fe or Sn, a decrease in the dispersion is seen, to 41 and 44 %, respectively. This is consistent with the model of the second metal depositing on the surface of the Pt particles. A decrease by half of the number of exposed Pt atoms (since 0.5 ML of second metal), should result in a decrease in the dispersion of about half, as observed. However, it maybe that such a coverage model is perhaps a little simplified.

Indeed the chemisorption data for the Pd catalysts is not so straightforward. For example, the initial dispersion of the 1.8 wt% Pd/Al_2O_3 catalysts was 45 % which decreases to 34 % when 0.5 ML of Fe is added, or to 16 % upon addition of 0.5 ML of Sn. Neither result represents a decrease in the dispersion by a factor of 2. The larger decrease observed for the $PdSn/Al_2O_3$ compared to the $PdFe/Al_2O_3$ may be due to the larger atomic radius of Sn compared to that of Fe. This may result in the Sn preventing hydrogen adsorption on not only the Pd atom on which it is deposited but also the neighbouring Pd atoms as well. However, the difference in atomic radius of Sn compared with Fe is probable not significant enough for this explanation to be valid. It is also possible that the heat of adsorption of hydrogen on palladium is affected to a different extent by Fe and Sn (a ligand type effect) although no attempt was made to investigate this. At present it is not apparent why the dispersion decreases to a greater extent for the Sn-doped Pd catalyst compared with the Fe-doped catalyst, or indeed why different results were observed for the Pt and Pd catalysts.

In order to determine how reproducible the preparation method was, two further experiments were carried out. First, two batches of a 1.8 wt% $PdFe/Al_2O_3$ catalyst were prepared using the same parent monometallic 1.8 wt% Pd/Al_2O_3 catalyst and identical procedures. In each case a sufficient amount of ferrocene was added to give nominally half a monolayer of Fe on the Pd surface. Hydrogen chemisorption was used to determine the dispersion of the catalyst before and after addition of the Fe. It was found that the dispersion of the reduced bimetallic catalyst was the same in each case indicating that the second metal was deposited on the first metal in a reproducible manner. Second, it was

also examined whether the second metal was deposited on the surface of the monometallic particles in a homogeneous manner. To test this, the hydrogen uptake for three separate samples from the same batch of bimetallic catalyst $PdFe/Al_2O_3$ (1.8 wt% Pd, 0.5 ML Fe) was determined by chemisorption. The uptake of hydrogen was the same for each sample, indicating that the second metal was indeed deposited evenly on the surface of the Pd particles throughout the catalyst batch.

Total BET surface area measurements were made for a selection of the bimetallic catalysts and it was confirmed that no decrease in the surface area was observed after deposition of the second metal.

3.4.2.2 Transmission electron microscopy and energy dispersive X-ray analysis (TEM/EDX)

Figures 3.10 and 3.11 display representative electron micrographs of the 1.8 wt% PdM/Al_2O_3 bimetallic catalysts where M = Fe and Sn, respectively. The particle size distribution are shown in Figures 3.12 and 3.13. The corresponding average particle size in each case was calculated from equation (3.7) and the results are given in Table 3.10.

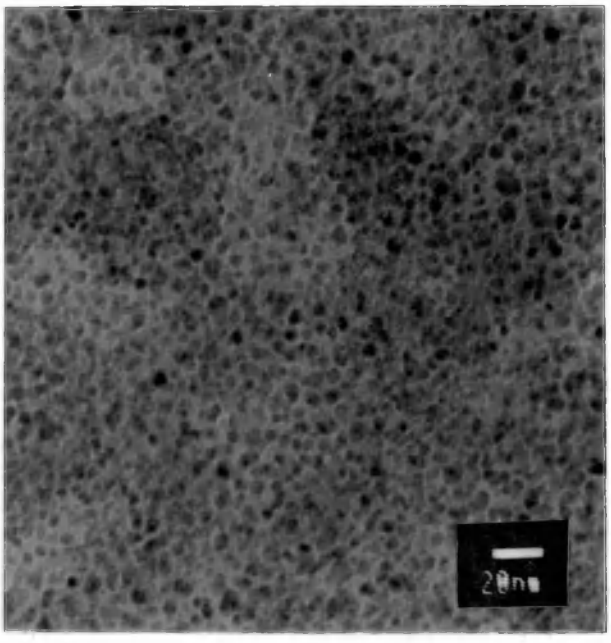

Figure 3.10 Representative electron micrograph of $PdFe/Al_2O_3$ prepared by addition of half a monolayer of Fe to 1.8 wt% Pd/Al_2O_3.

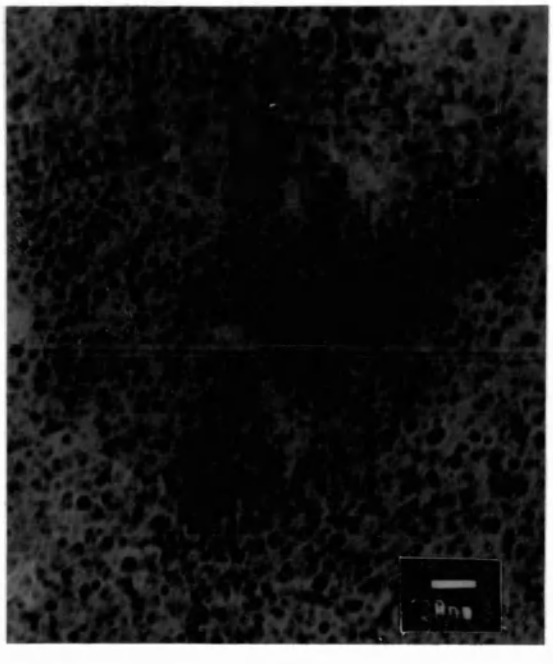

Figure 3.11 Representative electron micrograph of $PdSn/Al_2O_3$ prepared by addition of half a monolayer of Sn to 1.8 wt% Pd/Al_2O_3.

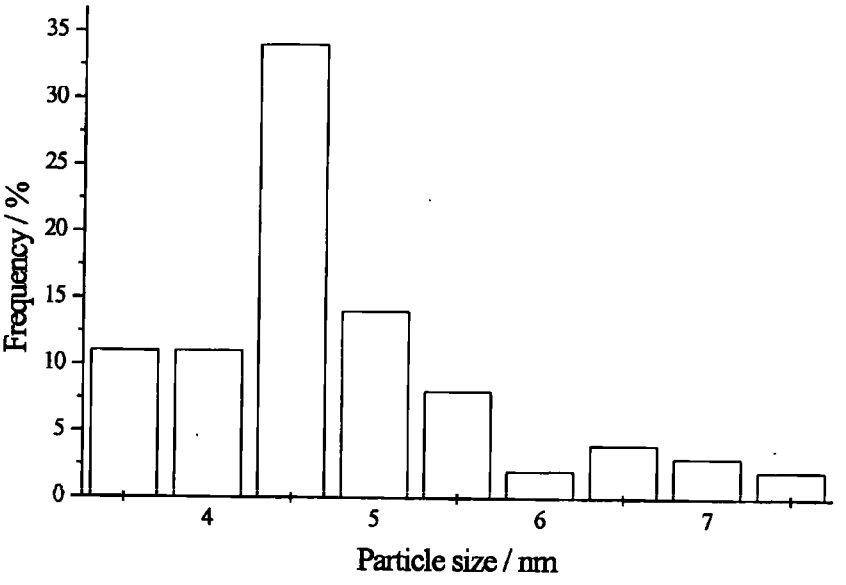

Figure 3.12 Particle size distribution from 1.8 wt% $PdFe/Al_2O_3$ catalyst.

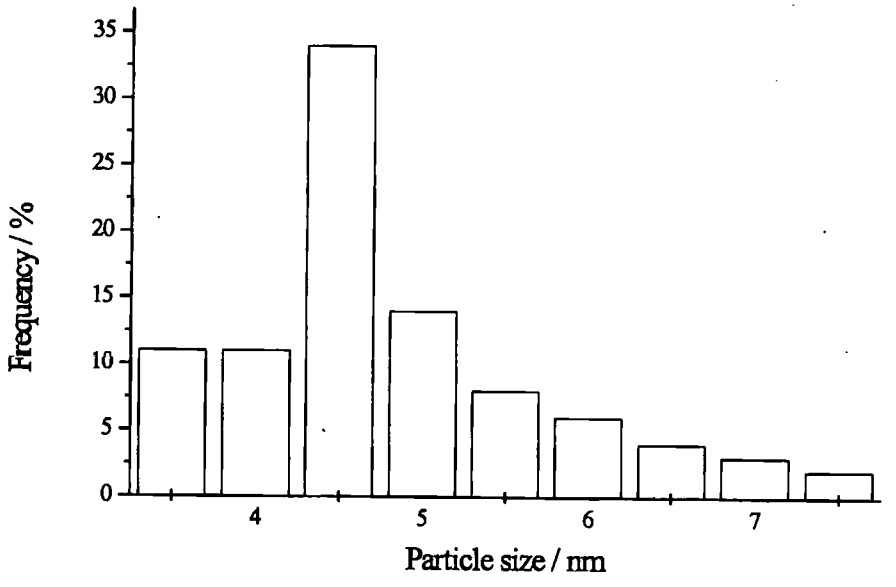

Figure 3.13 Particle size distribution from 1.8 wt % $PdSn/Al_2O_3$ catalyst.

Table 3.10 Particle size analysis from 1.8 wt% $PdFe/Al_2O_3$ and $PdSn/Al_2O_3$ bimetallic catalysts prepared by SOMC.

Catalyst	Particle size distribution / nm	Average particle size / nm
1.8 wt% $PdFe/Al_2O_3$	3-7	5.0
1.8 wt% $PdSn/Al_2O_3$	3-7.5	5.1

The average particle size of the monometallic catalyst was 4.9 nm, hence no significant increase in particle size is observed upon addition of the second metal. This would be expected if the second metal is being deposited in an atomic overlayer. The comments made in Section 3.3.2.2 are also relevant in that these figures should be taken as maximum values since no particles under 3.0 nm were observed. However, EDX analysis did indicate the presence of metallic particles in areas of the support where no particles were observable.

EDX analysis proved a valuable tool in confirming the presence of bimetallic particles in the prepared catalysts. By decreasing the size of the electron beam it was possible to focus on individual metal particles on the surface of the support. Analysis of these individual particles provided evidence for the two metals coexisting in the same particle. For example, the EDX analysis of an individual particle from the bimetallic PdFe catalyst is shown in Figure 3.14. The lines characteristic of Fe and Pd are clearly visible. No quantitative analysis was attempted because of the low count rate. By examining a large number of

particles by EDX no isolated particles of the second metal were observed on the support.

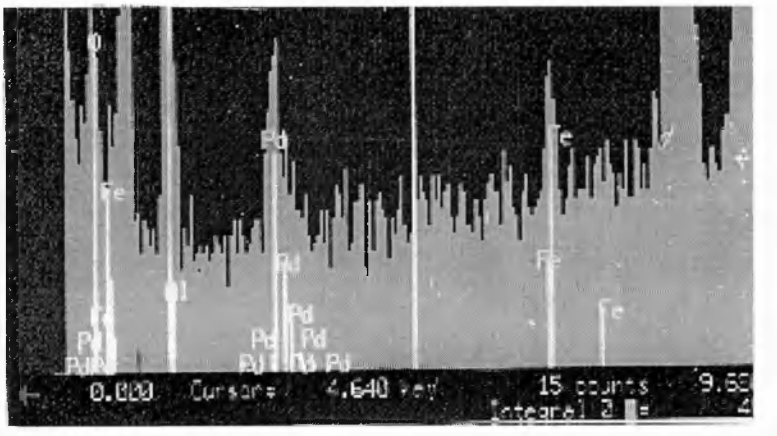

Figure 3.14 EDX analysis from 1.8 wt% $PdFe/Al_2O_3$ catalyst.

Similarly the EDX analysis of the 1.8 wt% $PdSn/Al_2O_3$ catalyst also confirmed the presence of the two metals in contact in the same particle.

It was not possible to obtain either electron micrographs or EDX analysis for the Pt-based bimetallic catalysts due to the small particle size of these catalysts. As with the monometallic catalysts this would indicate that the bimetallic catalysts exist in a highly dispersed state.

3.4.2.3 X-ray powder diffraction (XRD)

The XRD powder patterns of the 4 wt% $PdFe/Al_2O_3$ and $PdSn/Al_2O_3$ bimetallic catalysts are shown in Figure 3.15 with that for the 4 wt% Pd/Al_2O_3 catalyst repeated from Figure 3.4. No PdFe or PdSn bimetallic phase was observed,

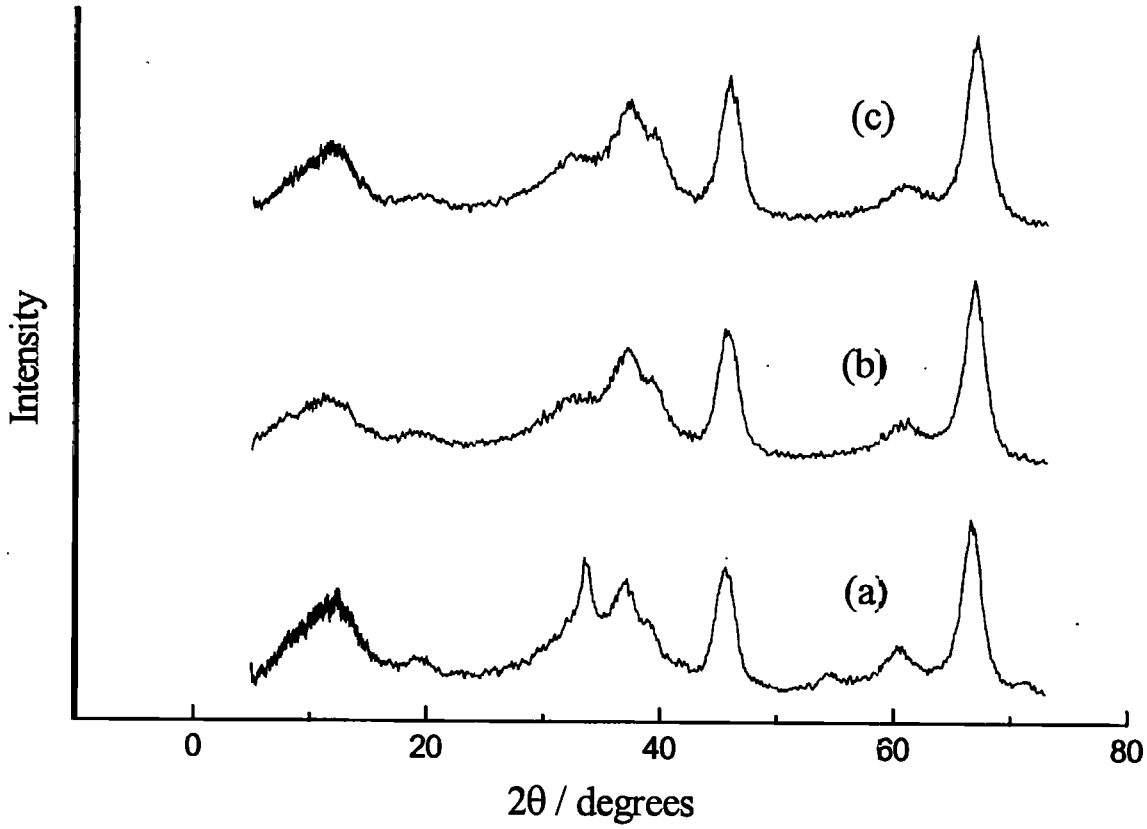

Figure 3.15 XRD powder patterns of (a) 4 wt% Pd/Al_2O_3, (b) 4 wt% $PdFe/Al_2O_3$, (c) 4 wt% $PdSn/Al_2O_3$.

although this was not unexpected considering the low loadings of the second metal. The most notable feature of the XRD patterns of the individual bimetallic catalysts is a marked decrease in the intensity of the reflections associated with PdO compared to the monometallic catalyst. This indicates a decrease in the amount of PdO present in the bimetallic catalysts. This provides indirect evidence for the existence of bimetallic particles.

No Pt-containing phase was observed in the XRD powder diffraction patterns (not shown) of the 0.7 wt% $PtSn/Al_2O_3$ and $PtFe/Al_2O_3$ bimetallic catalysts indicating that as for the monometallic catalyst, highly dispersed Pt phases were present which were 'invisible' to XRD.

3.4.2.4 Extended X-ray absorption fine structure (EXAFS)

The EXAFS data for the 1.8 wt % Pd/Al_2O_3 monometallic catalyst, used as the basis for the 1.8 wt% $PdFe/Al_2O_3$ and $PdSn/Al_2O_3$ bimetallic catalysts, was discussed in Section 3.3.2.4. Sample Pd/Al_2O_3-3 (Table 3.5) corresponds closely to the state of the monometallic Pd catalyst before the SOMC reaction and the EXAFS results for the bimetallic catalysts will be compared with those for this sample. The EXAFS data from both the Fe- and Sn-doped Pd bimetallic catalysts obtained at the Pd K-edge will be discussed first, followed by those obtained at the Fe K-edge and Sn K-edge. Finally, Sn K-edge EXAFS studies of the low loaded $PtSn/Al_2O_3$ catalyst will be considered.

The bimetallic catalysts were examined at different stages of preparation and after different treatments. It should be noted that no suitable PdFe, PdSn and PtSn alloy standards were available so no phase or amplitude transfers were made and these values were calculated from first principles using EXCURV92. A summary of the catalysts is given in Table 3.11 below.

Table 3.11 Summary of PdM/Al_2O_3 (where M = Fe or Sn) bimetallic catalysts examined by EXAFS prepared by addition of 0.5 ML Fe or Sn to a 1.8 wt% Pd/Al_2O_3 catalyst.

Catalyst	Treatment
$PdFe/Al_2O_3$-1	After SOMC, no heat treatment, unexposed
$PdFe/Al_2O_3$-2	Reduced, unexposed
$PdFe/Al_2O_3$-3	Exposed, reduced, exposed
$PdSn/Al_2O_3$-1	After SOMC, no heat treatment, unexposed
$PdSn/Al_2O_3$-2	Reduced, unexposed
$PdSn/Al_2O_3$-3	Exposed, reduced, exposed

PdM/Al_2O_3-1 corresponds to the sample obtained after the SOMC reaction without any heat treatment. PdM/Al_2O_3-2 is sample 1 after a reduction treatment (623 K, 3 h) in flowing hydrogen and PdM/Al_2O_3-3 is sample 1 after exposure to air followed by a reduction procedure (623 K, 3 h) then exposed to air again. Samples 1 and 2 were transferred in a dry box into sample holders and stored in a vacuum desiccator until required.

The results from the first shell fitting of each catalyst are listed in Table 3.12 below:

Table 3.12 Results from EXAFS data at the Pd K-edge of $PdFe/Al_2O_3$ and $PdSn/Al_2O_3$ catalysts prepared by SOMC.

Catalyst	Contribution	Coordination Number/ N	R / Å	$2\sigma^2$ / Å(x 10^{-4})	No. of runs
Pd/Al_2O_3-1	Pd-O	1.2	2.00	28	2
$PdFe/Al_2O_3$-1	Pd-O	1.5	1.98	7	2
$PdFe/Al_2O_3$-2	Pd-O	1.8	2.00	21	3
$PdFe/Al_2O_3$-3	Pd-O	1.9	1.99	18	2
$PdSn/Al_2O_3$-1	Pd-O	2.2	2.00	19	2
$PdSn/Al_2O_3$-2	Pd-O	1.5	1.99	22	2
$PdSn/Al_2O_3$-3	Pd-O	1.6	2.00	10	2

The Pd K-edge EXAFS data and corresponding Fourier transforms from the $PdFe/Al_2O_3$-1 and $PdSn/Al_2O_3$-1 bimetallic samples removed from the reactor after SOMC prior to any reduction treatment are shown in Figures 3.16 and 3.17. In each case the EXAFS oscillations and Fourier transforms are similar indicating at this stage that the Pd environment is similar and the best fit is again to a Pd-O interaction with the coordination number of 2.2 for the Sn-doped sample and 1.5 for the Fe-doped sample. Moreover, the EXAFS oscillations for these two samples are very similar to those of the parent monometallic sample, Pd/Al_2O_3-3, indicating that little alteration had occurred to the primary

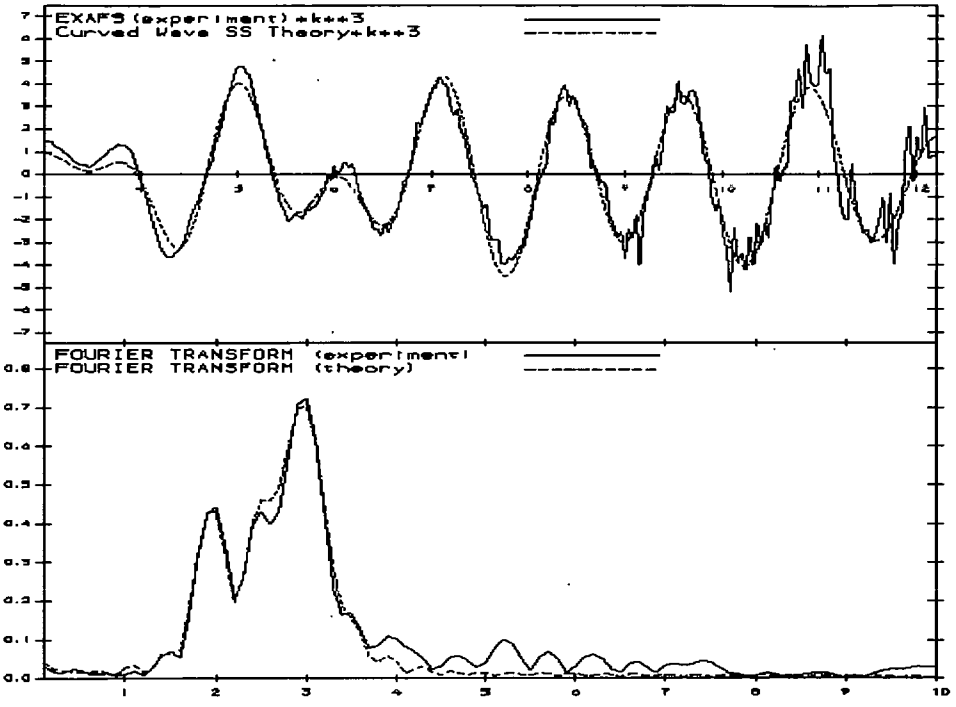

Figure 3.16 Fourier transform of Pd K-edge EXAFS recorded from $PdFe/Al_2O_3$-1.

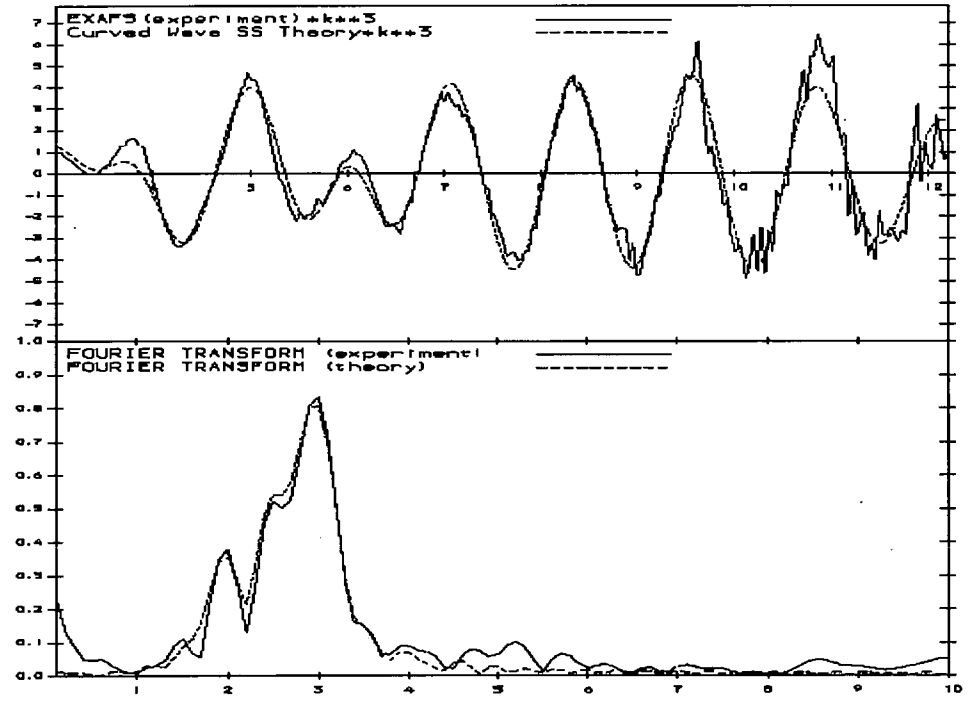

Figure 3.17 Fourier transform of Pd K-edge EXAFS recorded from $PdSn/Al_2O_3$-1.

coordination sphere of the Pd absorber in the bimetallic sample compared to the monometallic catalyst. At this stage of the preparation, previous studies have reported the existence of a stable surface organometallic moiety [16] which was identified as a $[Rh_sSn(n\text{-}C_4H_9)_2/SiO_2]$ species by EXAFS analysis. In the EXAFS data this may be observed by the presence of a carbon atom in the coordination sphere of the absorber metal. This was not observed in our measurements and is consistent with complete hydrogenolysis of the organometallic precursor occurring in our preparation method. Reduction of these samples at 623 K gave samples $PdFe/Al_2O_3$-2 and $PdSn/Al_2O_3$-2 and the EXAFS oscillations and corresponding Fourier transforms are shown in Figure 3.18 and 3.19, respectively. Again a Pd-O contribution is observed for each catalyst with a low coordination number (< 2.2). The fitted data for the reduced catalyst is very similar to the data from the unreduced catalyst. Exposure of $PdFe/Al_2O_3$-2 and $PdSn/Al_2O_3$-2 to air after reduction gave samples $PdFe/Al_2O_3$-3 and $PdSn/Al_2O_3$-3 with the EXAFS data and the Fourier transforms shown in Figure 3.20 and 3.21, respectively. The coordination number, $N_{Pd\text{-}O}$ increases slightly after exposure to air otherwise the fitted data is very similar to the data for the reduced samples.

The results obtained from the same catalysts at Fe K-edge and Sn K-edge will now be discussed. The data obtained at the absorption edge of the second metal was of poor quality so that only data in the k range 3 to 9 $Å^{-1}$ was analysed; fitting to the first coordination shell only was justified. Table 3.11 summarises the treatment conditions for the catalysts investigated.

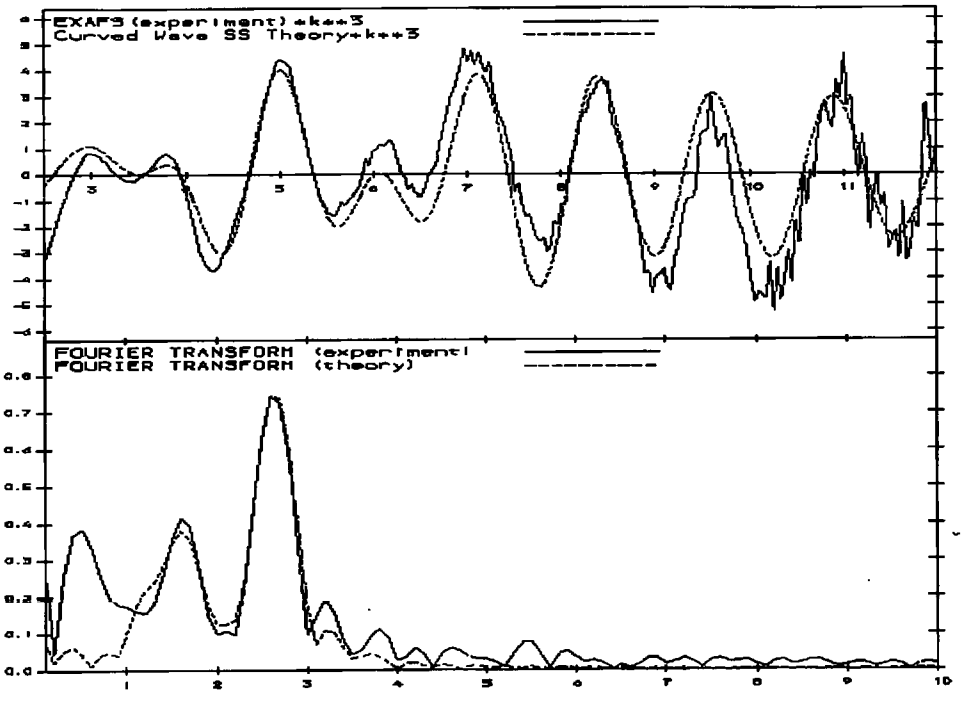

Figure 3.18 Fourier transform of Pd K-edge EXAFS recorded from $PdFe/Al_2O_3$-2.

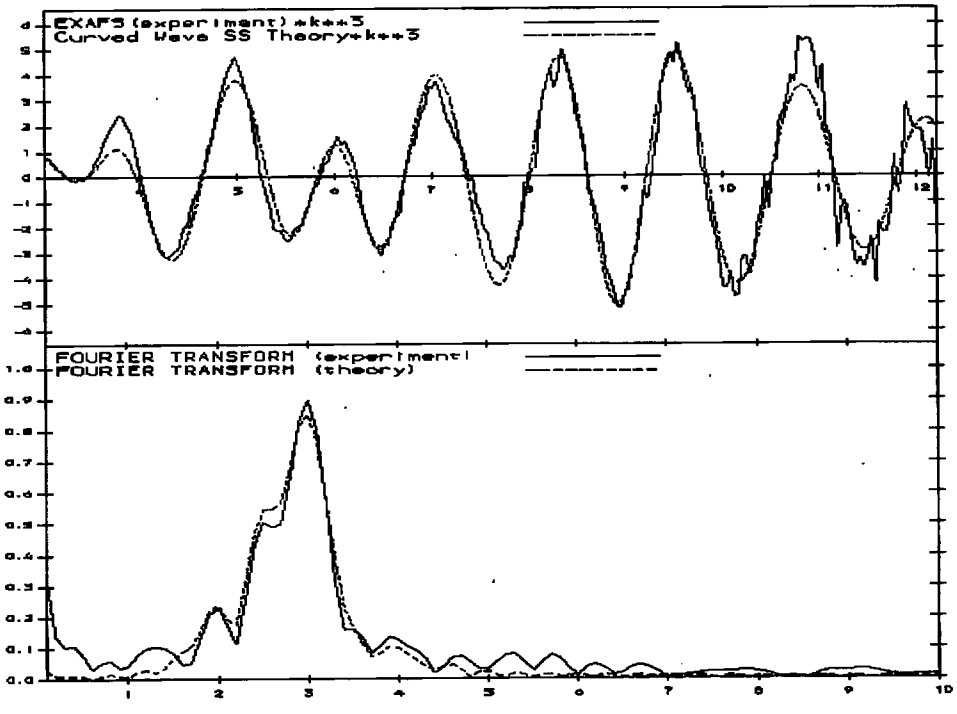

Figure 3.19 Fourier transform of Pd K-edge EXAFS recorded from $PdSn/Al_2O_3$-2.

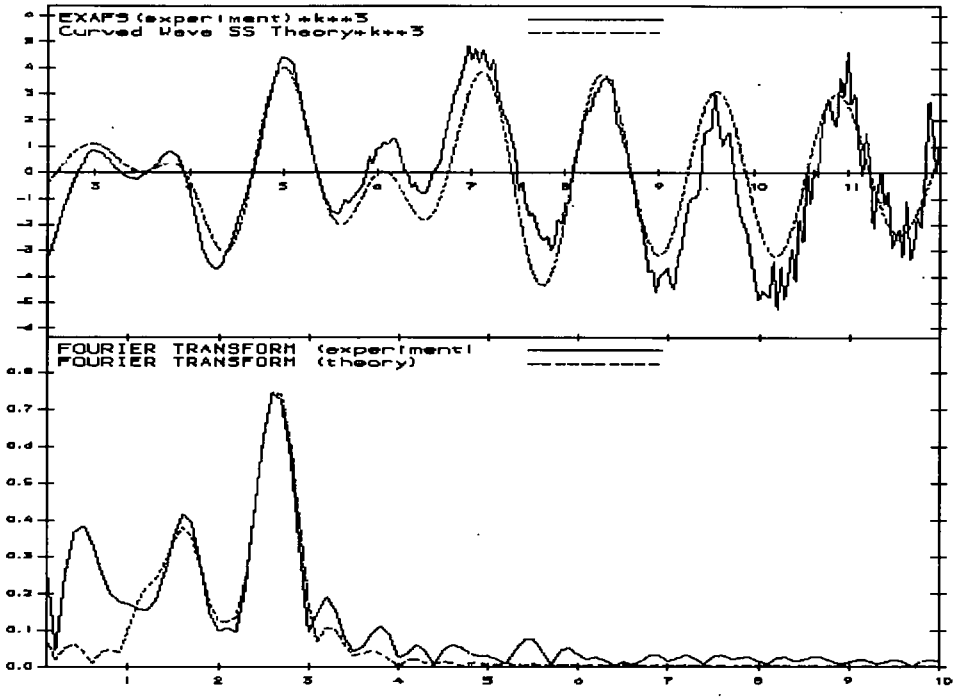

Figure 3.20 Fourier transform of Pd K-edge EXAFS recorded from $PdFe/Al_2O_3$-3.

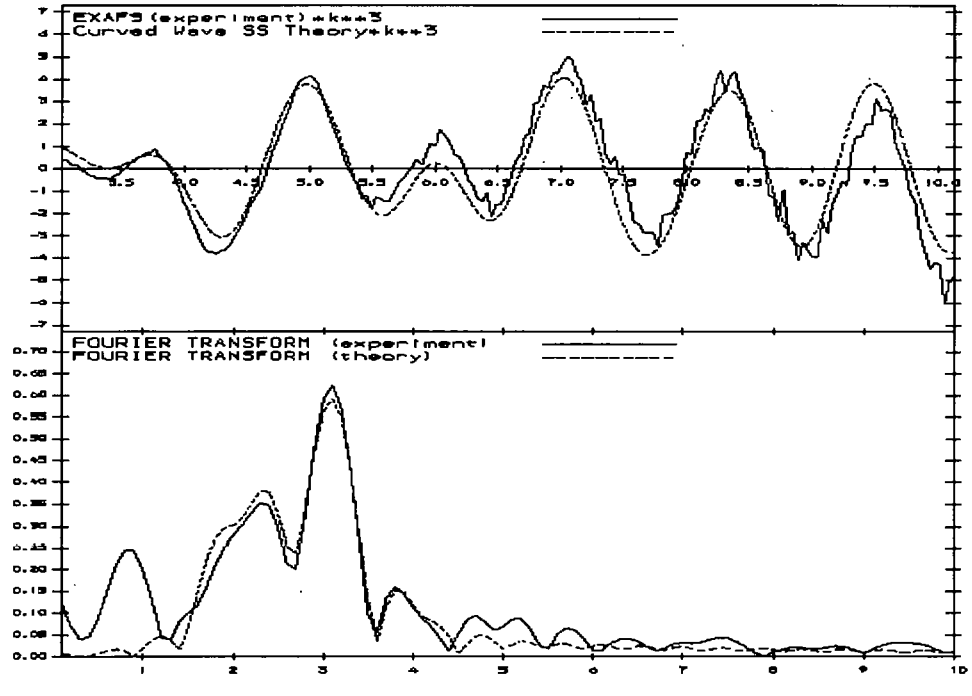

Figure 3.21 Fourier transform of Pd K-edge EXAFS recorded from $PdSn/Al_2O_3$-3.

Figures 3.22-3.24 display the Fe K-edge EXAFS data and corresponding Fourier transforms for samples $PdFe/Al_2O_3$-1 to -3 and Table 3.13 displays the best fit EXAFS data for the Fe K-edge data.

Table 3.13 Results from EXAFS data at the Fe K-edge of $PdFe/Al_2O_3$ bimetallic catalysts prepared by addition of 0.5 ML Fe to 1.8 wt% Pd/Al_2O_3 by SOMC.

Catalyst	Contribution	Coordination Number / N	R / Å	$2\sigma^2$/ Å (x 10^{-4})	No. of runs
$PdFe/Al_2O_3$-1	Fe-O	8.7	1.94	37	1
$PdFe/Al_2O_3$-2	Fe-O	8.3	1.95	43	1
$PdFe/Al_2O_3$-3	Fe-O	7.5	1.96	35	1

Again all three sample display similar EXAFS and Fourier transform profiles with the main contribution in the Fe K-edge EXAFS spectra of this series of 1.8 wt% $PdFe/Al_2O_3$ catalysts fitted to a shell at 1.94-1.96 Å away from the absorber atom. This interatomic distance is consistent with the literature value for the Fe-O bond in Fe_2O_3 [47]. It is clear, therefore, that the iron component in the bimetallic catalysts exists in an oxidised state. No significant alteration in coordination number is observed upon reduction of the catalyst, indicating either that the reduction temperature (623 K) is not sufficient to reduce the catalysts or that after reduction the Fe is reoxidised by the presence of air in the sampleholders. Again due to the poor quality of data we were unable to determine if Pd was present in the coordination sphere of Fe.

Figures 3.25-3.27 display the Sn K-edge EXAFS data and the corresponding Fourier transforms for samples $PdSn/Al_2O_3$-1 to -3 and Table 3.14 displays the best fit EXAFS data for the Sn K-edge data.

Table 3.14 Results from EXAFS data at the Sn K-edge of $PdSn/Al_2O_3$ bimetallic catalysts prepared by addition of 0.5 ML Sn to 1.8 wt% Pd/Al_2O_3 by SOMC.

Catalyst	Contribution	Coordination Number / N	R / Å	$2\sigma^2$/ Å (x 10^{-4})	No. of runs
$PdSn/Al_2O_3$-1	Sn-O	4.4	2.04	9	3
$PdSn/Al_2O_3$-2	Sn-O	5.1	2.06	13	5
$PdSn/Al_2O_3$-3	Sn-O	3.3	2.04	10	2

All the 1.8 wt% $PdSn/Al_2O_3$ samples display similar EXAFS and corresponding Fourier transforms which indicate the presence of oxygen in the immediate environment of Sn. The two Sn oxides commonly formed, SnO and SnO_2, can be distinguished by comparison of the known crystal structure. SnO has four Sn-O pairs at 2.22 Å and SnO_2 has the same number of Sn-O pairs at 2.05 Å and 2 Sn-O pairs at 2.06 Å [47]. Comparison of this data with our results suggest that the Sn species exists as SnO_2. The known PdSn bond distance is ~ 2.8 Å but due to the poor quality of the data it was not possible to unambiguously locate Pd in the shell around Sn.

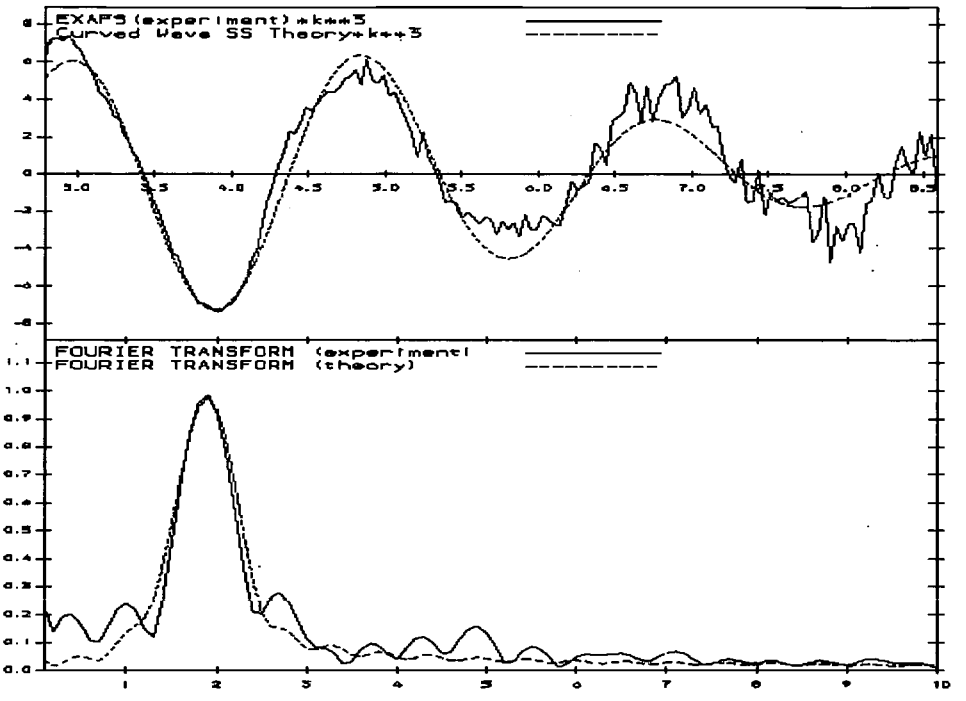

Figure 3.22 Fourier transform of Fe K-edge EXAFS recorded from $PdFe/Al_2O_3$-1.

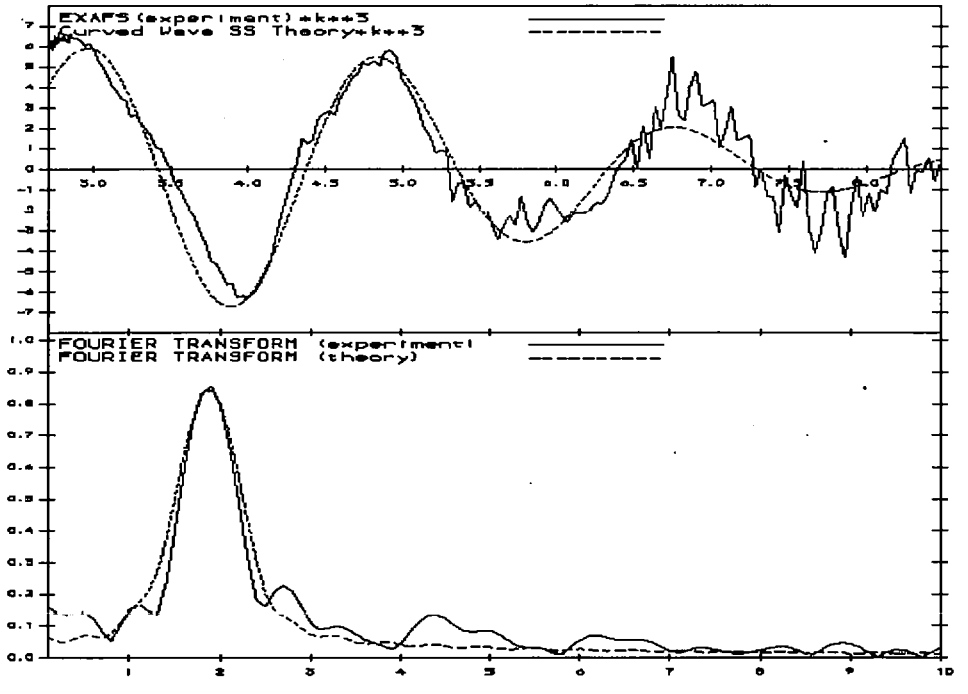

Figure 3.23 Fourier transform of Fe K-edge EXAFS recorded from $PdFe/Al_2O_3$-2.

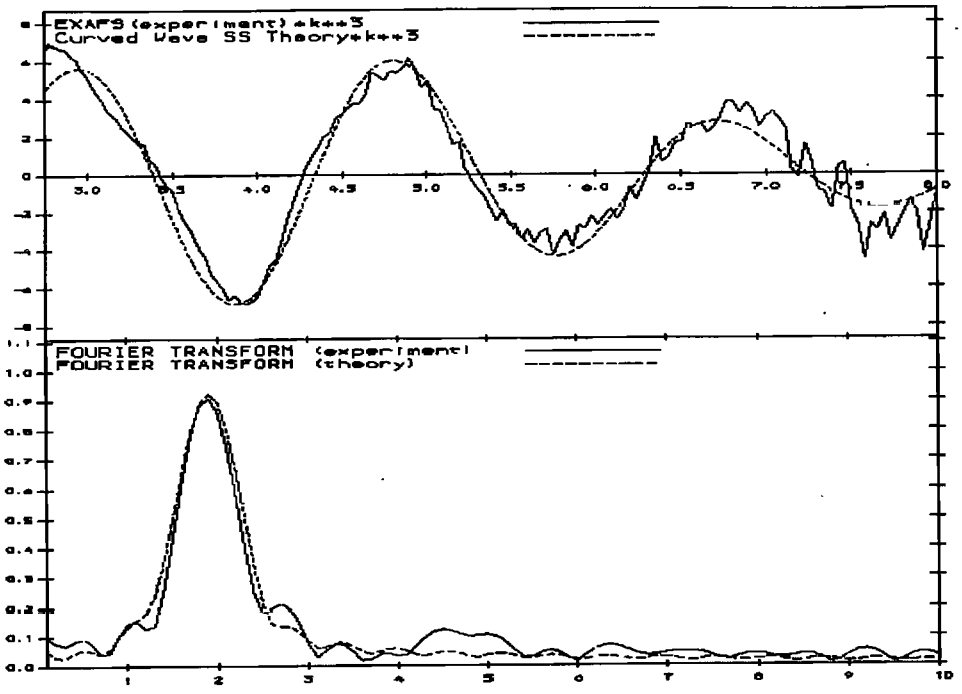

Figure 3.24 Fourier transform of Fe K-edge EXAFS recorded from $PdFe/Al_2O_3$-3.

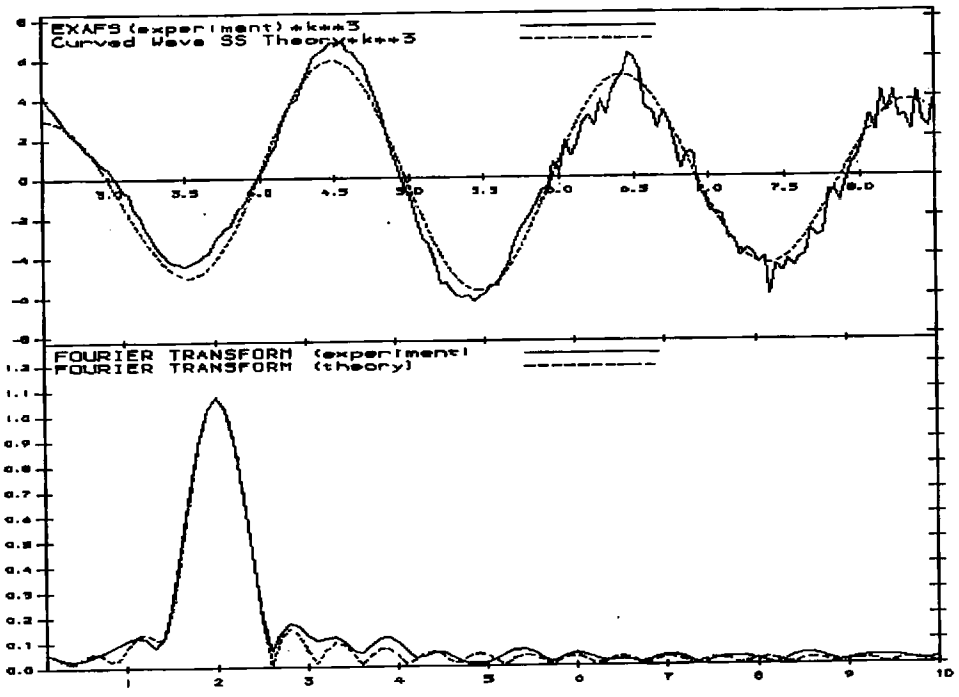

Figure 3.25 Fourier transform of Sn K-edge EXAFS recorded from $PdSn/Al_2O_3$-1.

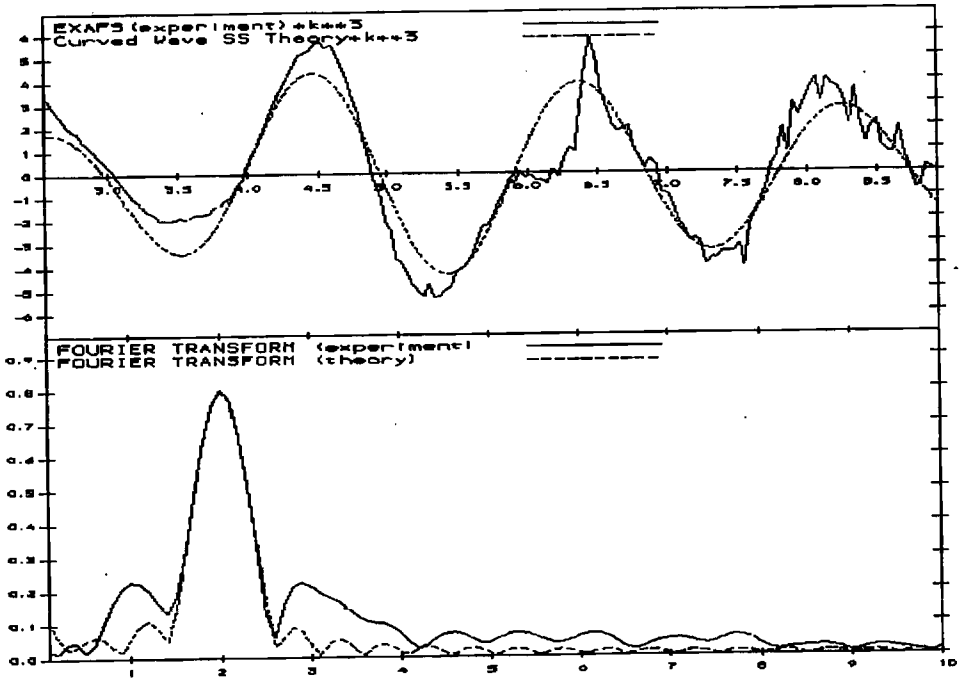

Figure 3.26 Fourier transform of Sn K-edge EXAFS recorded from $PdSn/Al_2O_3$-2.

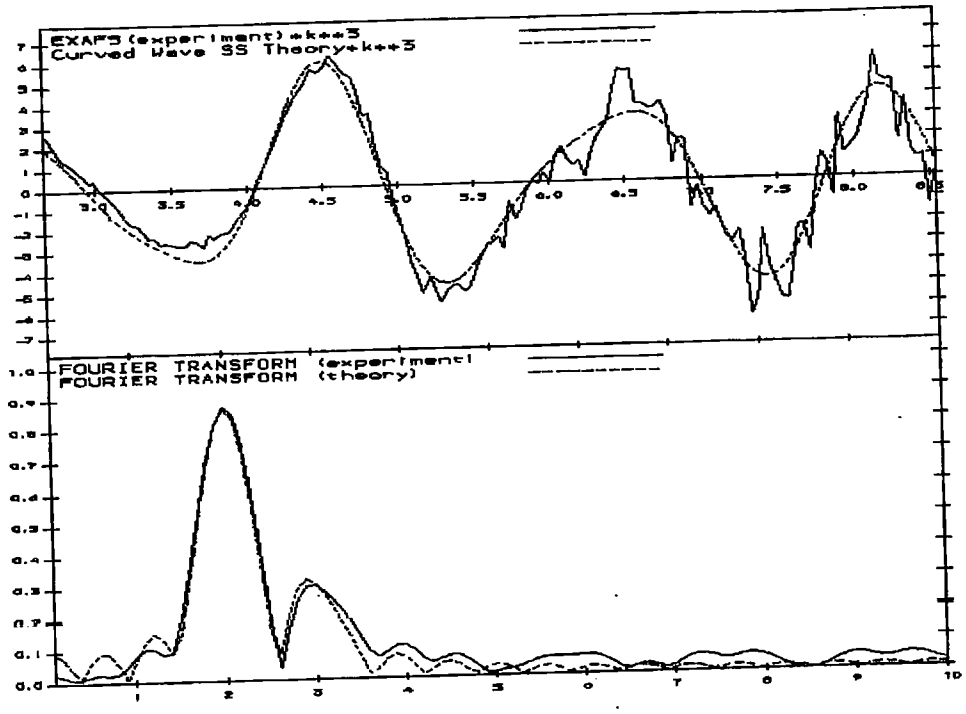

Figure 3.27 Fourier transform of Sn K-edge EXAFS recorded from $PdSn/Al_2O_3$-3.

EXAFS studies of $PtSn/Al_2O_3$ bimetallic catalysts at Sn K-edge

EXAFS studies of a 0.7 wt% $PtSn/Al_2O_3$ bimetallic catalyst, prepared by SOMC, at the Sn K-edge are presented in this section. Table 3.15 lists the $PtSn/Al_2O_3$ catalysts examined by EXAFS after different pretreatments.

Table 3.15 Summary of $PtSn/Al_2O_3$ bimetallic catalysts examined by EXAFS at Sn K-edge prepared by addition of 0.5 ML Sn to 0.7 wt% Pt/Al_2O_3.

Catalyst	Treatment
$PtSn/Al_2O_3$-1	After SOMC, no heat treatment, unexposed
$PtSn/Al_2O_3$-2	Reduced, unexposed
$PtSn/Al_2O_3$-3	Reduced, exposed

$PtSn/Al_2O_3$-1 is the sample obtained from the reactor after the SOMC reaction with no reduction treatment. Sample -2 is the sample obtained after reduction of sample -1 (623 K, 3 h) and sample -3 is sample -2 after exposure to air. $PtSn/Al_2O_3$-1 and -2 were transferred to sample holders in a dry box. The raw EXAFS data and corresponding Fourier transforms for the three $PtSn/Al_2O_3$ samples are shown in Figures 3.28-3.30 and the results from the best fit are listed in Table 3.16.

Table 3.16 Results from EXAFS data at the Sn K-edge of $PtSn/Al_2O_3$ bimetallic catalysts prepared by addition of 0.5 ML Sn to 0.7 wt% Pt/Al_2O_3 by SOMC.

Catalyst	Contribution	Coordination Number / N	R / Å	$2\sigma^2$ / Å (x 10^{-4})	No. of runs
$PtSn/Al_2O_3$-1	Sn-O	5.8	2.05	4	1
$PtSn/Al_2O_3$-2	Sn-O	6.2	2.05	17	1
$PtSn/Al_2O_3$-3	Sn-O	6.7	2.04	14	1

Reference to Figures 3.28-3.30 indicate that the EXAFS data and corresponding Fourier transforms are almost identical in each case. The data in the above table indicates that the nearest neighbour to the Sn absorber is oxygen in all three samples and the Sn-O interatomic distance is equivalent to the bond distance in SnO_2. The results are similar to the results of the Sn doped Pd/Al_2O_3 catalysts which also indicate that the Sn exists as a SnO_2 species. Exposure of $PtSn/Al_2O_3$-2 to air resulted in an increase in Sn-O coordination number as expected. No Pt-Sn interaction could be observed as only the first coordination shell could be fitted.

No EXAFS data at the Pt L_{III}-edge was collected from the above $PtSn/Al_2O_3$ sample or the Pt L_{III}-edge and Fe K-edge of the $PtFe/Al_2O_3$ catalyst.

In summary, studies at the Pd K-edge of bimetallic 1.8 wt% $PdFe/Al_2O_3$ and $PdSn/Al_2O_3$ catalysts indicate the presence of oxygen atoms in the immediate

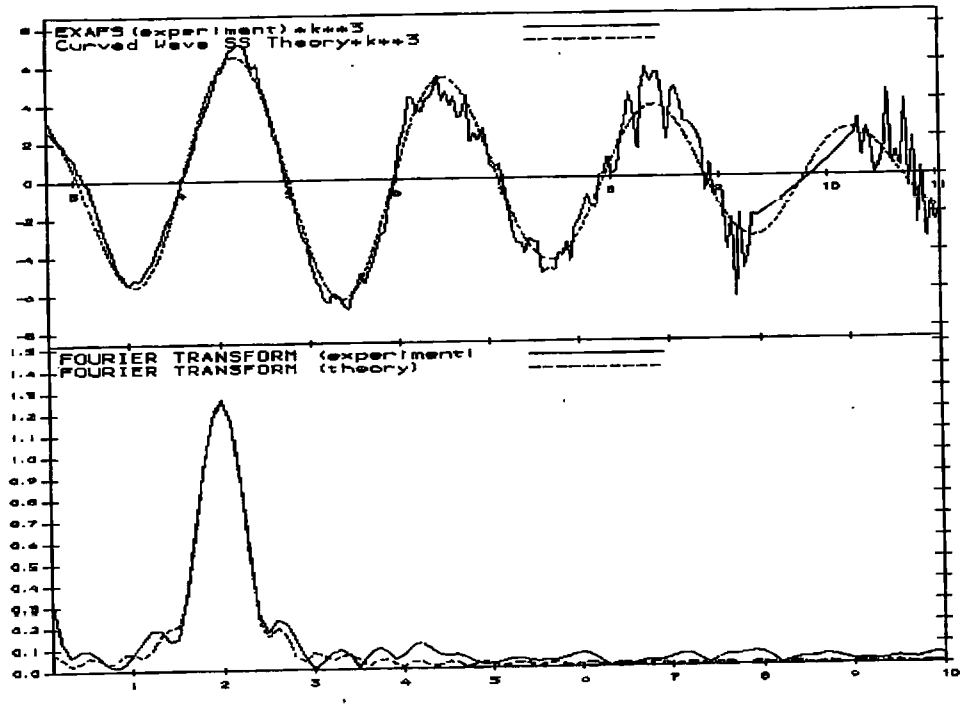

Figure 3.28 Fourier transform of Sn K-edge EXAFS recorded from $PtSn/Al_2O_3$-1.

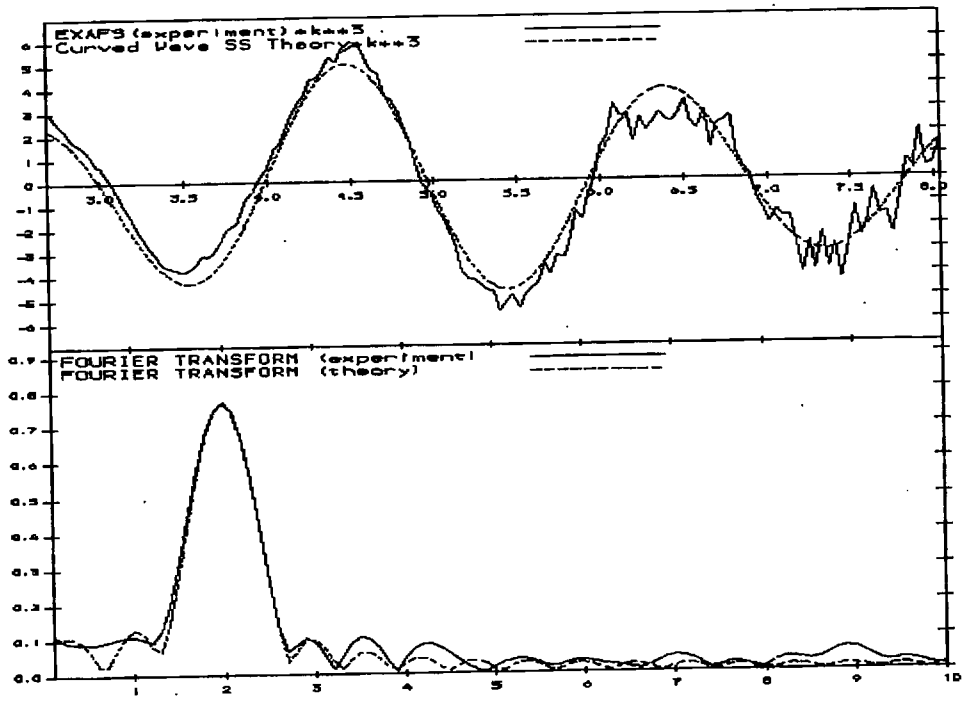

Figure 3.29 Fourier transform of Sn K-edge EXAFS recorded from $PtSn/Al_2O_3$-2.

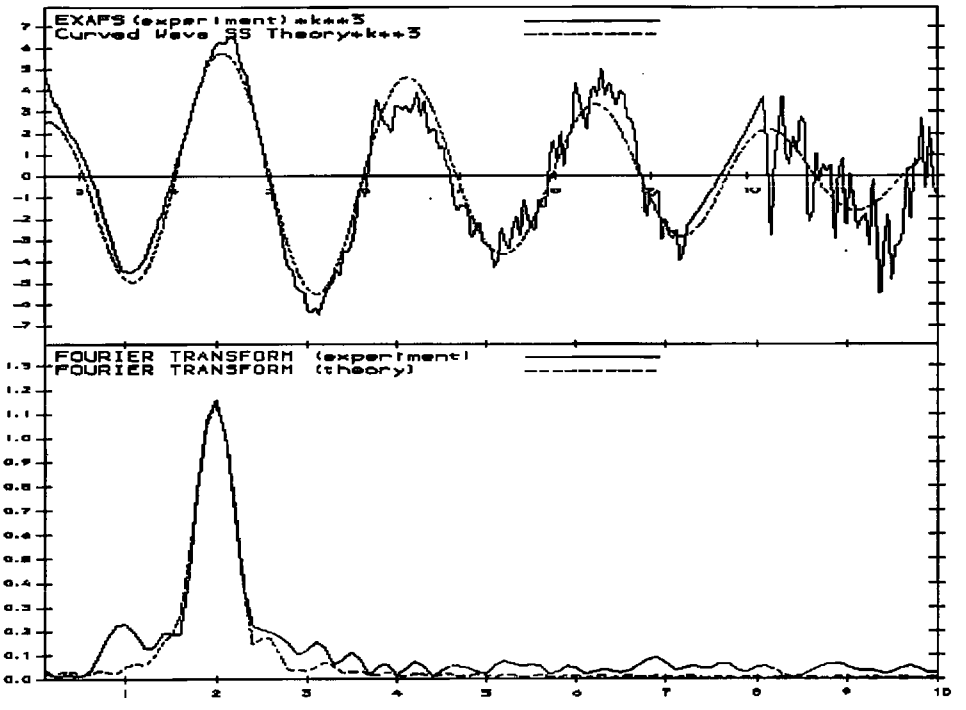

Figure 3.30 Fourier transform of Sn K-edge EXAFS recorded from $PtSn/Al_2O_3$-3.

Table 3.16 Results from EXAFS data at the Sn K-edge of $PtSn/Al_2O_3$ bimetallic catalysts prepared by addition of 0.5 ML Sn to 0.7 wt% Pt/Al_2O_3 by SOMC.

Catalyst	Contribution	Coordination Number / N	R / Å	Debye-Waller ($x\ 10^{-4}$)/ $Å^2$	No. of runs
$PtSn/Al_2O_3$-1	Sn-O	5.8	2.05	4	1
$PtSn/Al_2O_3$-2	Sn-O	6.2	2.05	17	1
$PtSn/Al_2O_3$-3	Sn-O	6.7	2.04	14	1

Reference to Figures 3.28-3.30 indicate that the EXAFS data and corresponding Fourier transforms are almost identical in each case. The data in the above table indicates that the nearest neighbour to the Sn absorber is oxygen in all three samples and the Sn-O interatomic distance is equivalent to the bond distance in SnO_2. The results are similar to the results of the Sn doped Pd/Al_2O_3 catalysts which also indicate that the Sn exists as a SnO_2 species. Exposure of $PtSn/Al_2O_3$-2 to air resulted in an increase in Sn-O coordination number as expected. No Pt-Sn interaction could be observed as only the first coordination shell could be fitted.

No EXAFS data at the Pt L_{III}-edge was collected from the above $PtSn/Al_2O_3$ sample or the Pt L_{III}-edge and Fe K-edge of the $PtFe/Al_2O_3$ catalyst.

In summary, studies at the Pd K-edge of bimetallic 1.8 wt% $PdFe/Al_2O_3$ and $PdSn/Al_2O_3$ catalysts indicate the presence of oxygen atoms in the immediate

environment of the Pd atoms at all the stages of preparation and under a variety of treatment. The EXAFS data indicates the presence of Pd-O in the reduced catalyst, however, results in Section 3.3.2.4 suggest that this is most likely due to reoxidation after reduction, probably due to air leaking into the sample holders. It was not possible to determine whether Fe or Sn were present in the coordination sphere of Pd due to the presence of the dominant Pd-Pd interaction at an atomic distance similar to that expected for PdFe or PdSn. In addition, Sn K-edge and Fe K-edge EXAFS studies of bimetallic 1.8 wt% $PdSn/Al_2O_3$ and $PdFe/Al_2O_3$ catalysts, and the Sn K-edge studies of the 0.7 wt% $PtSn/Al_2O_3$ catalyst, indicated that the nearest neighbour in each case is oxygen with an interatomic distance consistent with either the formation of a SnO_2 and Fe_2O_3 phase. No evidence was found for the presence of a metal-metal interaction between the two metals in the bimetallic catalysts. However, given the limitations inherent in the EXAFS studies they cannot be taken to discount the evidence for the presence of bimetallic particles presented earlier via EDX and hydrogen chemisorption. Overall, if the apparatus had been available it would have been profitable to have reduced the catalysts *in situ* thus allowing EXAFS data to be collected directly for the catalysts in a reduced state [48] with ideally a large number of scans.

There are similarities between the present work and EXAFS analysis of $RuGe/Al_2O_3$ catalysts prepared by SOMC [49, 50]. Studies at the Ru K-edge did not indicate Ge species in the coordination sphere of the Ru atoms and Ge K-edge studies of the same catalysts indicates that Ge remains in the oxide form which strongly interacts with Ru (δ^+) on the surface of the Ru particles. The

main effect of the Ge is a lowering of the Ru coordination number. Indeed these two papers from the same group illustrate the difficulty in interpreting EXAFS data from bimetallic catalysts. In the earlier contribution [49] they erroneously considered the presence of Ge in the Ru environment, however this was corrected in the later paper [50] citing that the presence of Ru-Ru pairs at the Ru K-edge makes the detection of Ru-Ge contributions difficult.

3.4.2.5 Temperature programmed reduction (TPR)

The TPR profile obtained from the 4 wt% $PdFe/Al_2O_3$ and $PdSn/Al_2O_3$ catalysts, prepared by addition of half a monolayer of Sn or Fe to the 4 wt% Pd/Al_2O_3 catalyst are shown in Figure 3.31. The temperature range monitored was 77 K to 1073 K.

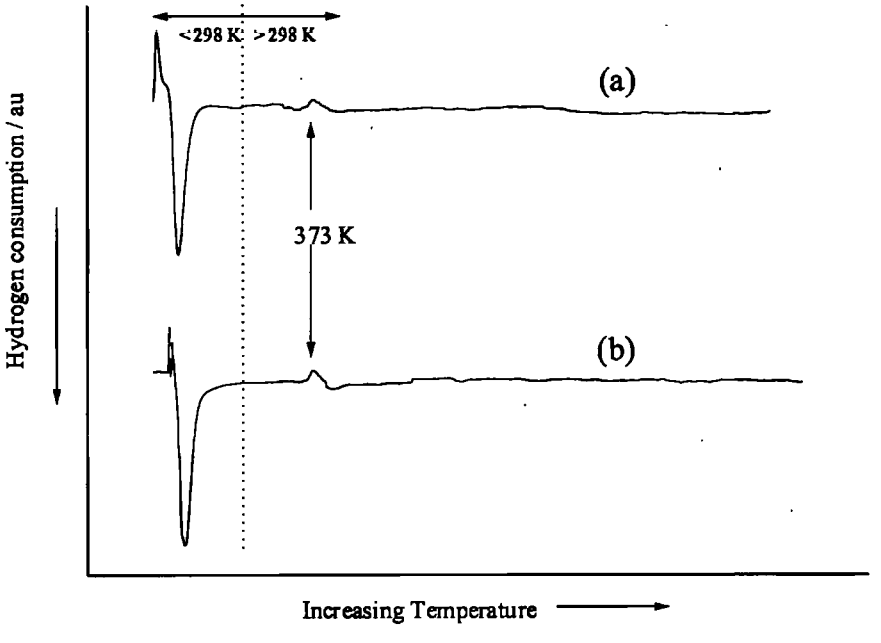

Figure 3.31 TPR profile for (a) 4 wt% $PdFe/Al_2O_3$, and (b) 4 wt% $PdSn/Al_2O_3$ bimetallic catalysts.

Inspection of the TPR profiles for the bimetallic catalysts indicates that both samples display a similar pattern. In both cases, reduction of PdO below room temperature, similar to the monometallic catalyst, is observed. The negative β-hydride peak is also observed indicating that the β-PdH phase formed by the monometallic catalyst is also formed by the bimetallic catalyst. This is a significant result since the formation of the β-PdH phase in bimetallic catalysts is often inhibited by the presence of an alloy phase [51]. It is thus reasonable to suggest that the presence of the hydride phase in the bimetallic catalysts may indicate the absence of a bulk alloy phase [51] which would be consistent with the surface nature of the reaction. No further reduction peaks are observed in either of the TPR profiles in the temperature range monitored (77 K to 1073 K). This is unexpected as reduction of the FeO_x and SnO_x, shown to exist by EXAFS studies, should be observed, however, it may be that the sensitivity of the TCD detector was not sufficient to record the small quantity of hydrogen which would have been consumed reducing the small amount of FeO_x or SnO_x phase present.

3.4.2.6 Mössbauer Spectroscopy

The 4 wt% Pd/Al_2O_3 catalyst, modified by addition of half a monolayer of Fe by SOMC, was studied using Mössbauer spectroscopy. The catalyst was chosen specifically to raise the Pd loading of the monometallic catalyst and also to enable a higher loading of Fe to be added to the catalyst hence improving the sensitivity of the experiment. Initial studies using lower loaded $PdFe/Al_2O_3$ catalysts failed to display any Fe phase in the ^{57}Fe Mössbauer spectrum.

PdFe bimetallic catalysts have been discussed at some length in the published literature and Mössbauer spectroscopy has been used in the characterisation of the catalysts in many of these studies. Before the Mössbauer spectrum obtained from the 4 wt% $PdFe/Al_2O_3$ catalyst is discussed, it is useful to review some of the data available from these literature Mössbauer studies. Table 3.17 summarises the Mössbauer data from a selection of reports on PdFe catalysts. Variation in the loading of the two metals, preparation technique, calcination or reduction treatments, etc., all contribute to the composition of the final catalyst prepared and hence there are a number of different Fe species in the catalysts. Table 3.17 the isomer shift (IS) is listed only for the contribution to the spectrum judged to originate from a PdFe interaction (as judged by the authors of the papers cited), although other Fe species were usually observed. A few significant points should be noted. PdFe interactions generally occur in the IS range 0.06 to 0.49 mm s^{-1}, although the majority of values are in the range 0.16 to 0.29 mm s^{-1}. It should be stressed that different IS values are obtained due to differences in the electronic environment of the Fe in the individual catalysts. Both bcc PdFe and fcc PdFe alloy contributions have been shown to exist and, as expected, different IS are observed for these two distinct alloys due to the different environment of the Fe in the alloys. It should be noted that in some cases the bimetallic contribution to the Mössbauer spectrum was designated as "PdFe" with no indication of the form of this interaction.

The other contributions from metallic Fe, Fe(II) and Fe(III), although not summarised in Table 3.17, depend on a number of factors as mentioned above. Characteristic isomer shifts for Fe(II) are generally in the range 1.0 to 2.0 mm s^{-1}

Table 3.17 Selection of Mössbauer data of supported PdFe catalysts from literature.

Catalyst	PdFe interaction	Isomer Shift / mm s^{-1}	Appearance	Other components	Reference
$PdFe/SiO_2$	PdFe	0.29	sextet	Fe^0 Fe(II)	[52]
$PdFe/SiO_2$	fcc PdFe alloy bcc PdFe alloy	0.42 0.49	singlet QS	Fe^0 Fe(II) Fe(III)	[53]
PdFe/NaY	PdFe	0.16-0.19	singlet	Fe (II) Fe(III)	[54]
PdFe/C	alloy	0.19	singlet	Fe^0 Fe(III)	[55]
PdFe/C	alloy PdFe	0.17 0.06	singlet	Fe^0	[56]
$PdFe/SiO_2$	PdFe superparamagnetic PdFe magnetically split	0.11-0.41 depending on Fe at% 0.22-0.28 depending on Fe at%	singlet QS		[57]
$PdFe/SiO_2$	PdFe superparamagnetic	0.13	singlet	Fe (II)	[58]

and Fe(III) in the range 0.4 to 1.1 mm s^{-1} with Fe^0 (a six-line magnetic hyperfine spectrum) and alloys in the range -0.1 to 0.4 mm s^{-1} [59]. The positive isomer shifts observed for PdFe catalysts compared to Fe^0 indicates a decrease in s-electron density at the Fe nuclei.

The literature results discussed above were typically obtained from PdFe catalysts prepared by traditional methods, such as co- or sequential impregnation, and we are not aware of any Mössbauer spectroscopy study in the literature, of PdFe catalysts prepared by SOMC. Thus, this is the first attempt to characterise PdFe catalysts, prepared by SOMC, using Mössbauer spectroscopy. Figure 3.32 shows the ^{57}Fe Mössbauer spectrum of the reduced 4 wt% $PdFe/Al_2O_3$ catalyst with a Pd loading of 4 wt% and half a monolayer of Fe deposited on the surface. The Mössbauer spectrum of $FeCl_3.6H_2O$ and the starting organometallic complex $Fe(C_5H_5)_2$ were also collected for comparison. The data from these three Mössbauer spectra, after the fitting procedure, are collated in Table 3.18.

By comparison of the Mössbauer spectrum shown and the data in Table 3.17 a number of points can be made. The 4 wt% $PdFe/Al_2O_3$ catalyst was fitted satisfactorily to a singlet with isomer shift 0.27 mm s^{-1}. Unambiguously the singlet cannot be attributed to unreacted ferrocene - a doublet with isomer shift 0.42 mm s^{-1} with QS of 0.36 mm s^{-1} and a singlet at 0.36 mm s^{-1}. Likewise the singlet cannot be attributed to Fe(III) (compare Fe(III) in $FeCl_3.6H_2O$ -an asymmetric doublet with IS 0.37 mm s^{-1} with QS 0.97 mm s^{-1}). It is also clear that the contribution does not originate from metallic Fe or Fe(II) [59], by comparison with the characteristic Mössbauer spectrum and isomer shifts of Fe^0

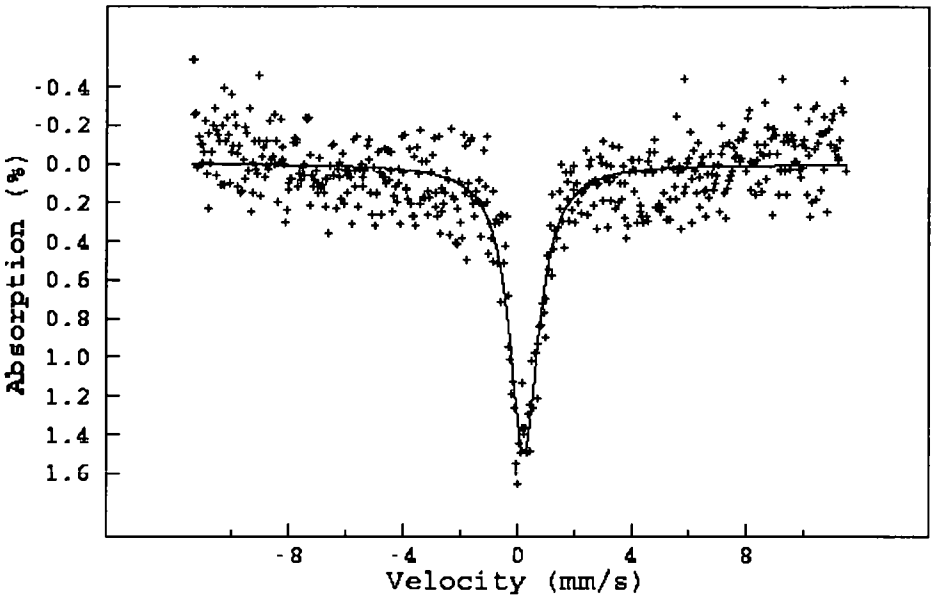

Figure 3.32 ^{57}Fe Mössbauer spectrum of reduced 4 wt% $PdFe/Al_2O_3$ catalyst collected for 7 days at room temperature.

Table 3.18 Summary of ^{57}Fe Mössbauer data from a reduced 4 wt% $PdFe/Al_2O_3$, $FeCl_3.6H_2O$ and $Fe(C_5H_5)_2$. IS is isomer shift and QS is quadropolar shift (both in mm s^{-1}).

Sample	Appearance	IS / mm s^{-1}	QS / mm s^{-1}	Interpretation
$PdFe/Al_2O_3$	Singlet	0.27	-	PdFe interaction
$FeCl_3.6H_2O$	Asymmetric Doublet	0.37	0.97	Fe^{3+}
$Fe(C_5H_5)_2$	Doublet	0.42	2.42	Fe^{3+}
	Singlet	0.36		

or Fe(II) species. It is therefore likely that the singlet in the Mössbauer spectrum of the $PdFe/Al_2O_3$ catalyst must be due to an interaction between Pd and Fe, indeed the isomer shift is in the region attributed to PdFe interactions or alloys in the literature. Although we do not believe that our catalyst is an 'alloy' type catalyst, a strong interaction between the two metals is thought to be present. Indeed other techniques such as TEM/EDX and hydrogen chemisorption have confirmed that a PdFe interaction does exist.

As a comparison, the Mössbauer spectrum of a $PtSn/Al_2O_3$ catalyst prepared using SOMC has been reported [60]. Identified from the spectra were a PtSn alloy, with a composition close to Pt_3Sn, and a non-stoichiometric SnO_2 phase with the alloy contribution being the dominant feature (80 %). The SnO_2 phase was believed to have been formed by an oxygen impurity. This clearly illustrates the highly selective reaction between the Pt surface and the organometallic precursor of the Sn.

In the present work due to the low signal-to-noise ratio of the data collected for the $PdFe/Al_2O_3$ catalyst (due to the low loading of the Fe) it is not possible to exclude the possibility that Fe(II) or Fe(III) is present. Nevertheless, even if Fe cations were present they must be present in only very small quantities and the great majority of the iron is in the form of PdFe bimetallic particles. The absence of any evidence of Fe(II) or Fe(III) in the bimetallic catalyst is significant and, indirectly may provide further evidence for a PdFe interaction. At the reduction temperature (623 K) of the catalyst before collection of the Mössbauer data, it is probable that a significant proportion of the iron would remain in an unreduced

state if Pd was not present as demonstrated by Garten and Ollis [61]. It has often been proposed that the presence of a noble metal (Pd or Pt) promotes the reduction of a less noble metal (Fe) in the presence of hydrogen. Strong evidence for this cooperative effect exists mainly from TPR and Mössbauer studies. The hydrogen adsorbs dissociatively on the noble metal surface and the hydrogen ions produced are believed to reduce the Fe cations. It has been argued that only Fe in contact with Pd can be reduced and if the Fe was not in contact with the Pd then the dissociated hydrogen would have to diffuse over the surface of the support to reach the oxidised Fe. Experimental evidence, however, shows that hydrogen migration over the alumina support is unlikely due to the poor electronic conductivity properties of the support [62]. In summary, reduction of Fe by hydrogen at low temperatures in PdFe bimetallic catalysts can only take place when the two metals are in intimate contact. Therefore the absence of any observable quantities of oxidised Fe in the ^{57}Fe Mössbauer spectrum of $PdFe/Al_2O_3$ indicates that the Fe has been reduced and, hence, that an interaction of Pd and Fe must be present.

In conclusion, the Mössbauer spectrum obtained from the reduced 4 wt% $PdFe/Al_2O_3$ bimetallic catalyst displays a singlet with IS 0.27 mm s^{-1} which can be attributed to a PdFe interaction, in agreement with literature data. This is further evidence for the selective deposition of Fe on Pd using surface organometallic chemistry.

3.4.2.7 *Electron paramagmetic resonance spectroscopy (EPR)*

The catalyst examined above by Mössbauer spectroscopy has also been studied by EPR in an attempt to gain further information about the chemical nature of the iron in the $PdFe/Al_2O_3$ catalyst. Again before the results are presented previous EPR studies of PdFe catalysts will be discussed. EPR studies of PdFe catalysts are characterised by broad resonance signals at about $g = 2.1$. Sancier and Inami [63] found that small amounts of Fe in Pd catalysts produced an intense EPR signal with a g value of 2.1 after reduction at 773 K, which was not present in Fe samples without any Pd. Xu *et al.* also observed an EPR signal with $g = 2.1$ in their PdFe/Zeolite Y catalysts which they attribute to either PdFe alloy particles or to metallic Fe [54]. Furthermore, Bagguley *et al.* demonstrated that bulk PdFe alloys exhibit EPR signals at $g = 2.1$ [64]. Fe(III) is characterised by a signal at $g = 4.2$ [66].

The EPR spectrum of the 4 wt% $PdFe/Al_2O_3$ catalyst after exposure to air is displayed in Figure 3.33 and Table 3.19 summarises the information obtained from this spectrum.

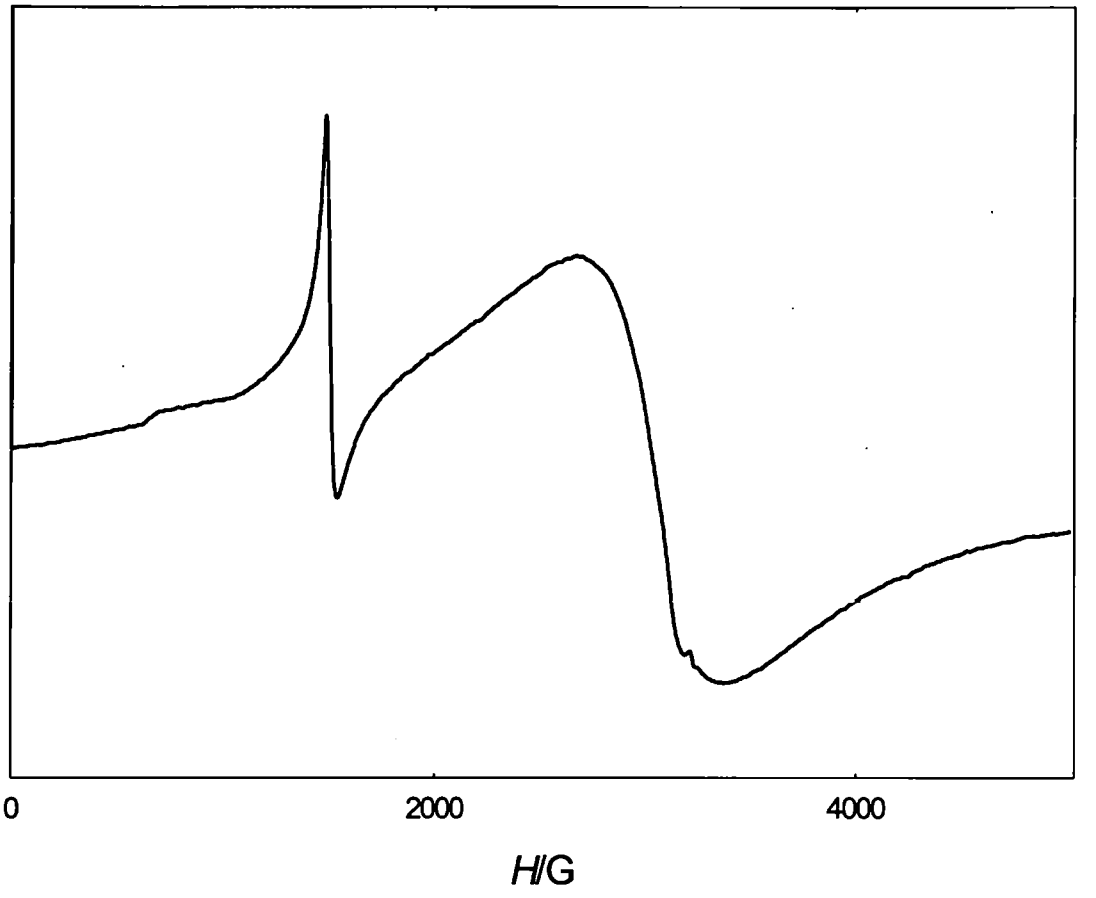

Figure 3.33 EPR spectrum of 4 wt% PdFe/ Al_2O_3 catalyst after exposure to air.

Table 3.19 EPR spectroscopy parameters of 4 wt% PdFe/Al_2O_3 catalyst.

Band/ g	Assignment
2.13	$PdFe^0$ interaction
4.29	Fe(III)

The signal at $g = 4.29$ can be unambiguously assigned to Fe(III) which indicates the presence of Fe_2O_3 in the exposed catalyst. It is important to note that Fe(III) was not observed (or at least to any significant extent) in the corresponding

Mössbauer spectrum of the same catalyst in the reduced state and this will be discussed later. The signal at $g = 2.14$ can be assigned to a PdFe interaction. The presence of a PdFe interaction confirms the Mössbauer data discussed above. Thus the EPR spectrum of the 4 wt% $PdFe/Al_2O_3$ catalyst after reduction but exposed to air indicates that iron exists in at least two different oxidation states. The assignments point to a portion of the Fe in a zero valent state with a g value typical of a PdFe interaction, $PdFe^0$, and there is also a portion that is oxidised in air and is present as Fe_2O_3.

The data from the Mössbauer and EPR experiments illustrate that the composition of the catalyst is highly dependent on whether the catalyst has been reduced or is in an oxidised state. The catalyst in a reduced form examined by Mössbauer spectroscopy displayed only a PdFe interaction with no evidence for oxidised Fe. However, after exposure to air, EPR spectroscopy indicates that as well as a PdFe interaction there is a Fe_2O_3 phase present. Hence a portion of the Fe can be oxidised or reduced depending on the chemical treatment. It should also be mentioned that Mössbauer spectroscopy is a much less sensitive technique than EPR spectroscopy so it may be possible that in the reduced state the catalyst still contained small quantities of Fe(III) below the level of detection of the Mössbauer experiment.

3.4.3 Structure of bimetallic catalysts prepared using SOMC

At this point the information obtained from the preparation and characterisation of the bimetallic catalysts will be summarised and some of the models described

in the literature for bimetallic catalysts prepared by SOMC will be discussed. Our attention will focus on two of the systems considered. First the Fe-containing catalysts will be considered since, until this work, no reports have appeared in the literature concerning the use of ferrocene to modify supported metal catalysts by SOMC then, secondly, the PtSn combination will be discussed.

Reaction of ferrocene with the alumina support alone was found to be minimal, hence the iron deposited must be initially, at least, on the surface of the metal particles. Evolution of an alkyl group in the gas phase during the reaction of ferrocene and M/Al_2O_3 (where M is Pd or Pt) suggests a selective reaction between ferrocene and the reduced surface of the parent metal resulting in the formation of MFe bimetallic particles. A reaction has been proposed (reaction (3.8)) to account for the deposition of Fe on the surface of the metal particles, similar to that previously forwarded by Renouprez *et al.* to account for the deposition of Ni on Pd using nickelocene [9]. The general mechanism provided in the literature for the SOMC reaction (reactions (3.1) and (3.2)) may be applicable to the reaction of ferrocene with M/Al_2O_3 as evidenced most notably by evolution of alkyl species in the gas phase. However, no direct evidence for this mechanism was gained since the presence of a surface intermediate species such as $Pd\text{-}Fe(C_5H_5)$ was not confirmed. Strong evidence for the formation of bimetallic PdFe particles on the alumina support from Mössbauer and EPR spectroscopy has been presented. The presence of a Fe(III) species, probably Fe_2O_3, has been confirmed by EXAFS and EPR data and complimentary evidence from Mössbauer and EPR spectroscopy indicates that the amount of

Fe(III) present depends critically on whether the catalyst has been reduced or oxidised. EDX analysis has shown the presence of the two metals in an individual particle, although these may have been in the form of metal oxides since this analysis was carried out after exposure of the sample to air. Although the characterisation has concentrated on the PdFe catalysts, it is anticipated that the PtFe catalysts also consist of $PtFe^0$ particles with a Fe_2O_3 component. There is no literature available to make direct comparisons between the structure of our Fe-containing catalysts, although Renouprez *et al.* concluded from STEM and XRD that the preparation of PdNi catalysts using the SOMC reaction between nickelocene and Pd/SiO_2 led to a homogeneous solid solution with no pure metal particles and EXAFS confirmed the presence of a PdNi interaction.

Several groups have studied the structural characteristics of PtSn bimetallic catalysts prepared by SOMC in detail. The greater volume of studies concerning PtSn catalysts is probably due to the greater importance of this particular combination of metals in industrial applications. Cabellero *et al.* also used EXAFS to study $PtSn/Al_2O_3$ catalysts prepared by SOMC [66] and concluded that the PtSn in their catalyst is a complex system containing PtSn clusters bound to the Al_2O_3 surface by $Pt\text{-}O\text{-}Sn^{2+}$ bonds, which stabilise the metallic particles leading to a high dispersion. A similar study has been published by Didillion *et al* [10]. They prepared $PtSn/Al_2O_3$ catalysts in a similar way to the method used in this work using $Pt(acac)_2$ to prepare the monometallic catalyst and tetrabutyl tin to modify the monometallic catalysts by a SOMC reaction. They propose that the structure of the catalyst depends critically on the particle size of the monometallic catalysts. For highly dispersed catalysts they claim that the Pt is

probably in interaction with tin oxide, similar to the conclusions reached Cabellero *et al.* [66]. Only when the Pt particle size is greater than 2 nm do $PtSn^0$ interactions occur. Therefore, according to these models our PtSn catalysts, which hydrogen chemisorption and TEM measurements indicate are highly dispersed, should have $Pt\text{-}O\text{-}Sn^{2+}$ interactions present. Our EXAFS data indicates that Sn is coordinated to oxygen therefore the existence of such an interaction is feasible, however, unfortunately our EXAFS data was not of a sufficient quality to determine if the oxygen is then coordinated to Pt. Indeed due to the low loading of this catalyst the only other characterisation method which has provided useful information about the structure of the PtSn catalyst is hydrogen chemisorption. This data indicated that the amount of hydrogen adsorbed decreased after deposition of Sn; this is most easily explained by assuming that the Sn is deposited on the Pt physically blocking the hydrogen adsorption sites. Therefore the only conclusions that we can make about the structure of the PtSn catalyst are that Sn is deposited on the Pt surface and secondly a SnO_2 phase is present.

In an attempt to rationalise the structure of the catalysts with regard to the presence of a bimetallic interaction and a second metal oxide the studies of Ruiz *et al.* should be considered [51]. They prepared $RuGe/Al_2O_3$ catalysts by addition of Ge to Ru/Al_2O_3 using SOMC and one conclusion they reported was that the Ru particles are partially covered by a layer of GeO_x. A similar situation may be envisaged to occur in the present study. To illustrate this we may again consider the PdFe catalysts. After the SOMC reaction and reduction a certain quantity of the Pd particle surface sites are covered by Fe in a reduced state,

giving a $PdFe^{o}$ interaction. This interaction has been confirmed by Mössbauer spectroscopy. Exposure of the catalyst to air results in the oxidation of this surface Fe, as evidenced by EXAFS and EPR. However, the Fe remains in contact with the Pd and a $PdFeO_x$ interaction is now present. This particular model satisfactorily accounts for the information gained from the characterisation studies. Another possible structure for the PdFe catalysts has been described by Pârvulescu *et al* [67]. They prepared $PdFe/Al_2O_3$ catalysts by a successive impregnation technique and claim that the catalysts consist of an interaction of palladium and iron through oxygen ions. This interaction can be represented as $Pd\text{-}O\text{-}Fe^{\delta+}$ which clearly resembles the interaction postulated by other authors for the PtSn system. In the present work the presence of this interaction would explain the EXAFS data which indicated that both metals have oxygen as nearest neighbours. However, such an interaction would not allow for direct contact between the Pd and Fe which has been indicated by Mössbauer and EPR data. Overall this model is not consistent with the results of the present work.

3.5 Conclusions

A range of alumina supported Pd and Pt-based bimetallic catalysts have been prepared by SOMC using ferrocene and tetrabutyl tin to deposit the Fe and Sn respectively, and characterised using a range of techniques.

i) Using the reaction conditions employed during the SOMC reaction only negligible amounts of Fe and Sn were deposited on alumina by reaction

of $Fe(C_5H_5)_2$ or $Sn(C_4H_9)_4$ with the support. Reaction of the Fe and Sn precursors is believed to result in the selective deposition of the metal onto the surface of a reduced Pd or Pt monometallic catalyst.

ii) Preparation of $PdFe/Al_2O_3$ and $PtFe/Al_2O_3$ by SOMC using ferrocene has been reported for the first time and in the case of the PdFe catalyst strong evidence has been presented for the formation of 'bimetallic' particles from EDX, Mössbauer and EPR spectroscopy. The Fe is proposed to deposit on the Pd or Pt particles by a SOMC reaction between the ferrocene and hydrogen preadsorbed on the parent metal surface (shown below) which is followed by hydrogenolysis of the $Fe\text{-}(C_5H_5)$ bond to yield a bimetallic particle:

$$Fe\text{-}(C_5H_5)_2 + 2H_{ads} \rightarrow Fe + 2C_5H_6$$

iii) The oxidation state of the Fe component of the 4 wt% $PdFe/Al_2O_3$ catalyst was found to depend on whether the catalyst was in a reducing or oxidising environment. Mössbauer spectroscopy showed only a PdFe interaction after reduction and EPR has indicated that the same catalyst after exposure to air, consists of a PdFe interaction and a Fe(III) component. EXAFS data indicates the presence of a Fe_2O_3 phase. Thus when reduced the catalysts consists of Fe deposited on the surface of the Pd particles, however, after exposure to air FeO_x is now in contact with the Pd surface.

3.6 References

1 Miura, H., Suzuki, T., Ushikuba, Y., Sugiyama, K., Gonzalez, R. D., and Matsuda, T., *J. Catal.* **85**, 331 (1984).

2 Inoue, T., Tomishige, K., and Iwasawa, Y., *J. Chem. Soc., Faraday Trans.* **92**, 461 (1996).

3 Candy, J. P., Didillon, B., Smith, E. L., Shay, T. B., and Bassett, J. M., *J. Mol. Catal.* **86**, 179 (1994).

4 Travers, C. H., Bournonville, J.P., and Martino, G., *in* "Proceedings, 8th International Congress on Catalysis, Berlin, 1984", **4**, 891, Elsevier, Amsterdam, 1984.

5 Margitfalvi, J., Hegedus, M., Gobolos, S., Kern-Talas, E., Szedlacsek, P., Szabo, S., and Nagy, F., *in* "Proceedings, 8th International Congress on Catalysis, Berlin, 1984", **4**, 903, Elsevier, Amsterdam, 1984.

6 Nuzzo, R. G., Dubois, L. H., Bowles, N. E., and Trecoster, M. A., *J. Catal.* **85**, 207 (1984).

7 Yermakov, Y. I., Kuznetsov, B. N., and Ryndin, Y. A., *React. Kin. Catal. Lett.*, **2**, 151 (1975).

8 Pleass, C. M., and Schimmel, D. G., *J. Catal.* **24**, 424 (1972).

9 Aduriz, H. R., Bodnariuk, P., Coq, B., and Figuéras, F., *J. Catal.* **119**, 97 (1989).

10 Faudon, J. F., Senocq, F., Bergeret, G., Moraweck, B., Clugnet, G., Nicot, C., and Renouprez, A., *J. Catal.* **144**, 460 (1993).

11 Merlen, E., Beccat, P., Bertolini, J. C., Delichère, P., Zanier, N., and Didillon, B., *J. Catal.* **159**, 178 (1996).

12 Margitfalvi, J. L., Jalett, H. P., Tàlas, E., Baiker, A., and Blaser, H. U., *Catal. Lett.* **10**, 325 (1991).

13 Margitfalvi, J. L., Kolosova, I., Tàlas, E., and Göbölös, S., *Appl. Cat. A: Gen.* **154**, L1 (1997).

14 Miura, H., Taguchi, H., Sugiyama, K., Matsuda, T., and Gonzalez, R. D., *J. Catal.* **124**, 194 (1990).

15 Ferretti, O. A., Lucas, C., Candy, J. P., Basset, J. M., and Le Peltier, F., *J. Mol. Cat. A: Chem.* **103**, 125 (1995).

16 Didillon, B., Houtman, C., Shay, T., Candy, J. P., and Basset, J. M., *J. Am. Chem. Soc.* **115**, 9380 (1993).

17 Nédez, C., Théolier, A., Lefabvre, F., Choplin, A., Basset, J. M., and Joly, J. F., *J. Am. Chem. Soc.* **115**, 722 (1993).

18 Coq, B., Goursot, A., Tazi, T., Figuéras, F., and Salahub, D. R., *J. Am. Chem. Soc.* **113**, 1485 (1991).

19 Miura, H., *Catalysis Today* **28**, 215 (1996).

20 Agnelli, M., Candy, J. P., Basset, J. M., Bouronville, J. P., and Ferretti, O. A., *J. Catal.* **121**, 236 (1990).

21 Schwarz, J. A., Contescu, C., and Contescu, A., *Chem. Rev.* **95**, 477 (1995).

22 Acres, G. J. K., Bird, A. J., Jenkins, J. W., and King, F., *in* "Specialist Periodicals Reports (Catalysis)", (C. Kembell, and D. A. Dowden, Eds.), **4**, The Royal Society of Chemistry, Cambridge, 1981.

23 Brunelle, J. P., *Pure Appl. Chem.* **50**, 1211 (1978).

24 Gonzalez, R. D., and Miura, H., *Catal. Rev.-Sci. Eng.* **36**, 145 (1994).

25 Sánchez Sierra, M. C., García Ruiz, J., Proietti, M. G., and Blasco, J., *J. Mol. Cat. A: Chem.* **96**, 65 (1995).

26 Boitiaux, J.P., Cosyns, J., and Vasudevan, S., *in* "Preparation of Catalysis III" (G. Poncelet, P. Grange, and P. A. Jacobs, Eds.), p123, Elsevier Science Publishers B.V., Amsterdam, 1983.

27 Lesage-Rosenberg, E., Vlaic, G., Dexpert, H., Lagarde, P., and Freund, E., *Appl. Cat.* **22**, 211 (1986).

28 Kunimori, K., Uchijima, T., Yamada, M., Matsumoto, H., Hattori, T., and Murakami, Y., *Appl. Cat.* **4**, 67 (1982).

29 Curtis Conner, W., and Falconer, J. L., *Chem. Rev.* **95**, 759 (1995).

30 Ho, V.-S., Wang, C.-B., and Veh, C.-T., *J. Mol. Cat. A: Chem.* **112**, 287 (1996).

31 Dalla Betta, R. A., and Boudart, M., *in* "Proceedings,. 5th International Congress on Catalysis", p1329, North Holland, Amsterdam, 1973.

32 Kip, B. J., Duivenvoorden, F. B. M., Koninsberger, D. C., and Prins, R., *J. Catal.* **105**, 26 (1996).

33 Shaplygin, I. S., Aparnikov, G. L., and Lazarev, V. B., *J. Inorg. Chem.* **23**, 488 (1978).

34 Hwang, C. P., and Yeh, C. T., *J. Mol. Cat. A: Chem.* **112**, 295 (1996).

35 Mill, G. A., Weller, S., and Cornelius, E. B., Actes du Zieme Congr. Intern. de Catalysts, **2**, Paris, (1962).

36 Teo, B. K., "EXAFS: Basic Principles and Data Analysis", Springer, Berlin, 1984.

37 Menacherry, P. V., Fernández-García, M., and Haller, G. L., *J. Catal.* **166**, 75 (1997).

38 Harada, M., Asakura, K., Ueki, Y., and Toshima, N., *J. Phys. Chem.* **96**, 9730 (1992).

39 Kuchubey, D. I., Pavlova, S. N., Novgorodov, B. N., Kryukova, G. N., and Sadykov, V. A., *J. Catal.* **161**, 500 (1996).

40 Pinna, F., Selva, M., Signoretto, M., Strukul, G., Boccuzzi, F., Benedetti, A., Canton, P., and Fagherazzi, G., *J. Catal.* **150**, 356 (1994).

41 Noronha, F. B., Schmal, M., Nicot, C., Moraweck, B., and Frety, R., *J. Catal.* **168**, 42 (1997).

42 Jung, H. J., Vannice, M. A., Mulay, L. N., Stanfield, R. M., and Delgass, W. N., *J. Catal.* **76**, 208 (1982).

43 Topsøe, H., Topsøe, N., and Bohlbro, H., *Stud. Surf. Sci. Cat.* **7**, 247 (1981).

44 Coq, B., Crabb, E., Warawdekar, M., Bond, G.C., Slaa, J.C., Galvagno, S., Mercadante, L., García-Ruiz, J., and Sánchez Sierra, M.C., *J. Mol. Cat.* **92**, 107 (1994).

45 Tauster, S. J., Fung, S. C., and Garten, R. L., *J. Am. Chem. Soc.* **100**, 170 (1978).

46 Bartholemew, C. H., Pannell, R. B., and Butler, J. L., *J. Catal.* **65**, 335 (1982).

47 Inorganic Crystal Structure Data File (ICSD), Chemical Database Service, Central Laboratory of the Research Councils Daresbury Laboratory.

48 Kampers, F. W. H., Maas, T. M. J., van Grondelle, J., Brinkgreve, P., and Koningsberger, D. C., *Rev. Sci. Instrum.* **60**, 2635 (1989).

49 Sánchez, M. C., Garcia, J., Blasco, J., and Proietti, M. G., *Physica B* **208 & 209**, 705 (1995).

50 Sánchez Sierra, M. C., Ruiz, J. G., Proietti, M. G., and Blasco, J., *J. Mol. Cat. A: Chem.* **108**, 95 (1996).

51 Xu, L., Lei, G.-D., Sachtler, W. M. H., Cortright, R. D., and Dumesic, J. A., *J. Phys. Chem.* **97**, 11517 (1993).

52 Niemantsverdriet, J. W., van Kaam, J. A. C., Flipse, C. F. J., and van der Kraan, A. M., *J. Catal.* **96**, 58 (1985).

53 Niemantsverdriet, J. A., Van Grondelle, J., and Van Der Kraan, A.M., *Hyperfine Interactions* **28**, 867 (1986).

54 Xu, L., Lei, G. D., Sachtler, W. M. H., Cortright, R. D., and Dumesic, J. A., *J. Phys. Chem.* **97**, 11517 (1993).

55 Guerrero-Ruiz, A., Sepulveda-Escribano, A., and Rodriquez-Ramos, I., *Appl. Cat. A: Gen.* **81**, 81 (1992).

56 Wunder, R., Phillips, J., *J. Phys. Chem.* **98**, 12329 (1994).

57 Lietz, G., Nimz, M., Völter, J., Lázár, K., and Guczi, L., *Appl. Cat.* **45**, 71 (1988).

58 Lietz, G., Nimz, M., Völter, J., Lázár, K., and Guczi, L., *Hyperfine Interactions* **41**, 657 (1988).

59 Niemantsverdriet, J. W., "Spectroscopy in Catalysis, An Introduction." VCH, Weinheim, 1995.

60 Vértes, C., Tálas, E., Czakó-Nagy, I., Ryczkowski, J., Göbölös, S., Vértes, A., and Margitfalvi, J., *Appl. Catal.* **66**, 149 (1991).

61 Garten, R. L., and Ollis, D. F., *J. Catal.* **35**, 232 (1974).

62 Vannice, M. A., and Neikam, W. C., *J. Catal.* **20**, 260 (1971).

63 Sancier, K. M., and Inami, S. H., *J. Catal.* **11**, 135 (1968).

64 Bagguley, D. M. S., Crossley, W. A., and Liesegang, J., *Proc. Phys. Soc.* **90**, 1047 (1967).

65 Martens, J. H. A., Prins, R., and Niemantsverdriet, J. W., *J. Catal.* **108**, 259 (1987).

66 Caballero, A., Dexpert, H., Didillon, B., LePeltier, F., Clause, O., and Lynch, J., *J. Phys. Chem.* **97**, 11283 (1993).

67 Pârvulescu, V. I., Filoti, G., Pârvulescu, V., Grecu, N., Angelescu, E., and Nicolescu, I. V., *J. Mol. Cat.* **89**, 267 (1994).

CHAPTER 4

Catalyst Testing

4 Catalyst Testing

The results from the hydrogenation of 1, 3-butadiene and crotonaldehyde will be presented and discussed in this chapter. Both reactions are of fundamental interest to the catalytic chemist and have generated a large number of publications in the catalysis literature over a number of years.

The investigation of the hydrogenation of 1, 3-butadiene is presented in Section 4.2 followed by that for the hydrogenation of crotonaldehyde in Section 4.3. In each case a brief review of the literature is given in the introduction to each section with emphasis on studies involving Pd- or Pt-based catalysts. Section 4.1 provides a summary of the catalysts that were used in the testing experiments.

4.1 Catalysts

Table 4.1 lists the catalysts considered in this chapter together with the metal loadings and dispersion values derived from hydrogen chemisorption experiments. The preparation and characterisation of these catalysts was considered in detail in Chapter 3 and some details will be repeated here where necessary.

Table 4.1 List of alumina supported Pd and Pt mono- and bimetallic catalysts used in catalyst testing experiments.

Catalyst (MM'/Al_2O_3)	M assay / wt%	M' assay / wt%	H/M
Pd/Al_2O_3	1.8	-	0.45
$PdFe/Al_2O_3$	1.8	0.23	0.36
$PdSn/Al_2O_3$	1.8	0.37	0.16
Pt/Al_2O_3	0.7	-	1.1
$PtFe/Al_2O_3$	0.7	0.23	0.41
$PtSn/Al_2O_3$	0.7	0.36	0.44

All the catalysts were prepared by SOMC. Emphasis will be placed in particular on the results obtained from the 1.8 wt% Pd/Al_2O_3 and 0.7 wt% Pt/Al_2O_3 catalysts and the corresponding bimetallic catalysts obtained by addition of 0.5 of a monolayer (ML) of Fe or Sn to these monometallic Pd or Pt catalysts (Table 4.1). The Pd monometallic catalyst consists of small Pd particles with particle size between 3-7 nm, with an average particle size of 4.9 nm. The Pd-based bimetallic catalysts consist of bimetallic particles with probably the existence of SnO_x or FeO_x phases on the surface of the Pd particles in air. The Pt monometallic catalysts are highly dispersed (mean diameter ca. 1 nm) and, similarly, it is believed for the bimetallic catalysts that a Sn or Fe phase is present on the surface of the Pt particles. It should be emphasised that in this chapter a generic term will be used for the iron or tin species deposited on the Pd or Pt catalysts, that is Fe or Sn.

4.2 Hydrogenation of 1,3-Butadiene

4.2.1 Introduction

Removal of 1,3-diolefin contaminants from industrial olefin feedstocks, using selective hydrogenation, is an important reaction in the manufacture of olefinic compounds [1]. 1,3-butadiene (hereafter referred to as butadiene) contains two sites of unsaturation, therefore the molecule can be semi-hydrogenated (where only one of the sites of unsaturation is hydrogenated) or fully hydrogenated (both double bonds are hydrogenated). This gives four possible products: 1-butene; cis-2-butene; trans-2-butene and n-butane, shown below in Scheme 4.1.

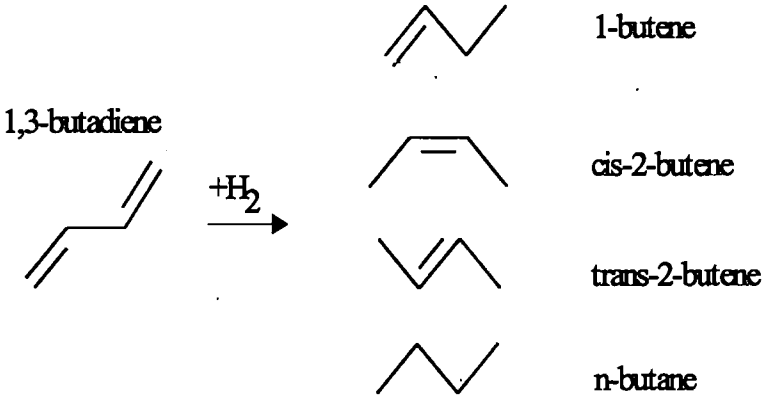

Scheme 4.1 Possible products from the hydrogenation of butadiene. Note for simplicity only the anti-form of butadiene is shown in the above scheme although the syn-form also exists and the interconversion of these two forms controls the stereoselectivity of the products (see below).

1-butene is the desired product of the hydrogenation reaction due to the commercial importance of this monomer in the polymer industry. Palladium-based catalysts have long been used as selective hydrogenation catalysts to remove undesirable 1,3-olefin impurities from olefin feedstocks. However, Pd catalysts are limited by their tendency to isomerise, oligomerise and polymerise the hydrogenation products and to further hydrogenate the n-butenes (where n-butene is taken to mean any of the butene isomers) to the saturated hydrocarbon (n-butane). With this in mind, many attempts have been made using bimetallic catalysts to prevent these unwanted side reactions.

Before discussing butadiene hydrogenation in more detail it is useful to discuss very briefly the mechanism of catalytic hydrogenation, in general terms. It should be noted that some of the points made here concerning catalytic hydrogenation will also be relevant to the hydrogenation of crotonaldehyde discussed in Section 4.3. In general it is agreed that catalytic hydrogenation occurs by addition of hydrogen atoms to adsorbed hydrocarbon molecules [2]. More specifically, this is believed to take place by four separate steps illustrated below in Scheme 4.2 for the hydrogenation of the simplest 1,3-diolefin, i.e. 1,3-butadiene: i) adsorption of the reactant on the catalyst surface (configuration I), ii) formation of a half hydrogenated state (configuration II), iii) reaction of the half hydrogenated state to give the product (configuration III), and finally iv) desorption. In addition, it is known that the first hydrogen is exclusively added to a terminal carbon [3].

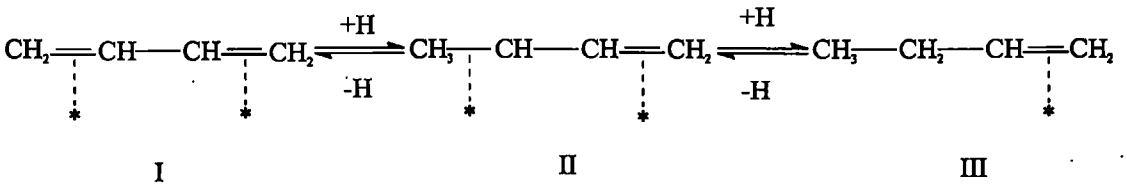

Scheme 4.2 Illustration of the general steps in catalytic hydrogenation where * represents an adsorption site.

In the above example, the hydrogenation would be termed a 1,2-addition since hydrogen was added to the first and second carbons. A similar mechanism occurs, known as a 1,4-addition, when hydrogen is added to both terminal carbons. Both 1,2 and 1,4-additions are important in butadiene hydrogenation as will become apparent in later sections. The reaction is believed to follow Langmuir-Hinshelwood type kinetics with the hydrocarbon and hydrogen competing for the same sites on the catalyst surface [4].

The initial di-π-adsorbed butadiene species can be adsorbed on the metal surface in two forms: anti- and syn-butadiene (structures I and II in Scheme 4.3 below).

Scheme 4.3 Anti- and syn-di-π-adsorbed butadiene.

The mechanism for butadiene hydrogenation is accepted by most workers in the field [2,3,5]. 1-butene is produced from either syn- or anti-adsorbed butadiene by a 1,2-addition of hydrogen. Trans- and cis-2-butene are formed by 1,4-addition of two hydrogen atoms to the anti- and syn-forms of butadiene, respectively (as illustrated in Scheme 4.4 below), or by isomerisation of 1-butene.

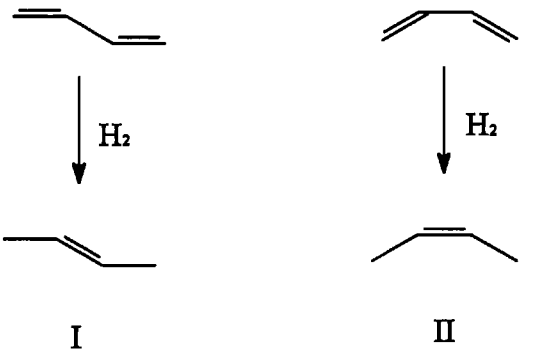

Scheme 4.4 Representation of hydrogenation of anti-butadiene to give trans-2-butene (configuration I) and syn-butadiene to give cis-2-butene (configuration II) by a 1,4 addition of hydrogen.

The isomerisation of 1-butene is expected to proceed via at least two different mechanisms: i) an intramolecular hydrogen shift; and ii) an associative mechanism with the formation of a half hydrogenated intermediate. In the gas phase, butadiene is believed to exist predominantly as the anti conformation (95 %) [6]. If the butadiene adsorbed reflects this ratio and no (or very little) interconversion between the two conformations occurs, then a high trans- to cis-2-butene ratio will be expected. N-butane can be formed by the hydrogenation of any of the three n-butene isomers.

The hydrogenation of butadiene has been studied for many years and in particular the period from 1960 onwards. A selection of these studies will be discussed in order to highlight some of the main aspects of butadiene hydrogenation over Pd and Pt monometallic catalysts. Much of the initial work was carried out by Bond and co-workers [2]. They studied the reaction over a range of group VIII metals, supported on alumina, and found that of the group VIII metals only Pd was completely selective for the hydrogenation to n-butenes without further hydrogenation to n-butane. All other group VIII metals, including Pt, produced n-butane as an initial product. Additionally, over Pd catalysts a high trans- to cis-2-butene ratio was observed in the products and this was regarded as a direct reflection of the ratio of the conformation of adsorbed butadiene, syn- or anti-adsorbed butadiene, on the surface of the catalysts. The high trans- to cis-2-butene ratio was taken to indicate that interconversion of the anti- and syn- forms of butadiene did not occur on the surface of the Pd. Lower ratios were observed on other group VIII metals indicating that conformational interconversion occurs on these metal surfaces. On Pt catalysts a trans- to cis-2-butene ratio of close to unity is commonly observed [2].

Bond *et al.* concluded that the higher selectivity of Pd catalysts to n-butene is explained by two effects: first, the absence of n-butane in the products is attributed to the absence of adsorbed - C_4H_9 (the final intermediate before n-butane formation) on the surface of the metal; second, to differences in the strength of adsorption of the reactants and products [2]. The strengths of

adsorption of the reactants and products on the palladium metal surface are as follows:

1,3-butadiene > n-butenes > hydrogen > n-butane

On Pd it is believed that the diene is more strongly adsorbed than the n-butenes which means that the n-butenes tend to desorb from the surface of the catalyst, by displacement by the more strongly adsorbed butadiene, before undergoing further hydrogenation. On Pt, the butadiene and n-butene adsorption strengths are more similar, and n-butenes on the surface may be further hydrogenated before desorbing. The stronger adsorption of butadiene than n-butenes on Pd was believed to be evidence for the interaction of both π-bonds of the butadiene with the surface. Indeed, a recent NEXAFS study [7] and theoretical calculations [8] have provided evidence for a di-π-adsorbed butadiene molecule on Pd(111).

Boitiaux and co-workers studied butadiene hydrogenation (and others) over Pd and Pt catalysts supported on alumina [5, 9-10]. They similarly found that butadiene hydrogenation over Pt produced n-butane as an initial product and that Pt catalysts with higher dispersions were less selective for n-butene formation than those with low dispersion. Pd catalysts were found to be 100 % selective to n-butenes and a high trans-/cis-2-butene ratio was again observed. These results are in qualitative agreement with the previous study mentioned.

Contradictory evidence exists, however, in the literature as to the degree of structure sensitivity of the reaction. Boitiaux *et al.* noted a marked decrease in activity for the reaction when the dispersion increased for a range of Pd/Al_2O_3

catalysts [5]. However, Borgna *et al.* found no such agreement between particle size and activity [11].

A low activity has been observed by many authors for highly dispersed Pd catalysts and the reason for this is also contentious. It has been claimed that the larger deactivation by smaller particles is due to stronger chemisorption of the unsaturated hydrocarbons on the smaller particles. Noupa *et al.* invoke an explanation in terms of hydrogen adsorption on different sized particles [12]. They claim that smaller Pd particles, which are essentially 2-dimensional islands of metal, cannot dissolve hydrogen and form hydrides whereas larger particles, which form 3-dimensional structures, can form the hydrides. This forms a source of hydrogen for the surface which prevents accumulation of adsorbed species on the surface and hence less deactivation.

General agreement is, however, found in the literature concerning the mode of deactivation of the catalysts in this reaction [1]. It is assumed that adsorption of oligomers of butadiene on the surface of the catalyst blocks the active sites responsible for the catalysis. It is also agreed that activity can be restored by purging the catalysts in a stream of gas (this can be nitrogen or hydrogen) free from hydrocarbons.

In summary, previous studies of butadiene hydrogenation over supported Pd and Pt monometallic catalysts highlight the following characteristics:

i) Pd is selective for hydrogenation to n-butenes whereas Pt produces significant amounts of n-butane.

ii) Pd is characterised by high trans- to cis-2-butene ratio whereas Pt catalysts display a ratio closer to unity.

Hydrogenation of butadiene has also been studied over a range of bimetallic systems although the majority of the reports concern Pd-based catalysts: for example, Pd-Au, Pd-Ag, Pd-Cu, Pd-Ni and Pd-Tl. No reports of butadiene hydrogenation using PdFe and PdSn bimetallic catalysts or any Pt-based bimetallic catalysts have been published in the literature as far as we are aware. The main aim of adding a second metal to Pd is to prevent further side reactions from occurring and to maximise the yield of 1-butene. Any studies relevant to the work presented here will be discussed at the appropriate point during the discussing of our results.

4.2.2 Experimental

The typical experimental conditions used for the catalyst testing are listed in Table 4.2.

Table 4.2 Main reaction conditions used for butadiene hydrogenation.

Reaction condition	Value
Mass of catalyst	0.1 g
Flow rate	60 cm^3 min^{-1}
C_4H_6:H_2 ratio	1:1.2
Reaction Temperature	298 K

In each test the first sample was taken after 1 minute on stream and every 20 minutes thereafter. Note, 20 minute intervals between samples was the minimum time adequate for satisfactory separation of the reactant and products in the GC column. In particular, n-butane and 1-butene eluted at similar retention times, as did the trans- and cis-2-butene isomers. The order the reactants and products eluted from the column was n-butane, 1-butene, trans-2-butene, cis-2-butene and then butadiene. No other products were observed.

The catalysts were maintained at a constant temperature of 298 K for collection of the data. This was the lowest temperature which could be easily maintained. At 273 K liquid butadiene condensed in the reactor around the catalyst.

To compare the activities of the different catalysts turnover frequencies (TOF) have been calculated, defined as the number of molecules converted per surface metal atom per second [13].

4.2.3 Results and discussion

Before the results are discussed, however, the conclusions from a series of control experiments will be presented:

i) No gas phase hydrogenation of butadiene occurred in the absence of a catalyst.

ii) No hydrogenation or isomerisation of butadiene occurred in the presence of a reduced Pt or Pd catalyst using nitrogen instead of hydrogen through the reactor.

iii) No reaction was observed on the alumina support, Fe/Al_2O_3 or Sn/Al_2O_3 at the temperatures studied.

The hydrogenation of butadiene over the Pd- and Pt-based catalysts can therefore be attributed to the presence of the noble metal and hydrogen from the gas phase.

4.2.3.1 Palladium-based catalysts

Figures 4.1, 4.2 and 4.3 display the data for the Pd/Al_2O_3, $PdFe/Al_2O_3$ and $PdSn/Al_2O_3$ catalysts respectively. In each Figure the Selectivity / % (left hand Y- axis), and the Butadiene conversion / % (right hand Y-axis) are plotted against time on stream (in minutes). Product selectivity is determined by the following equation:

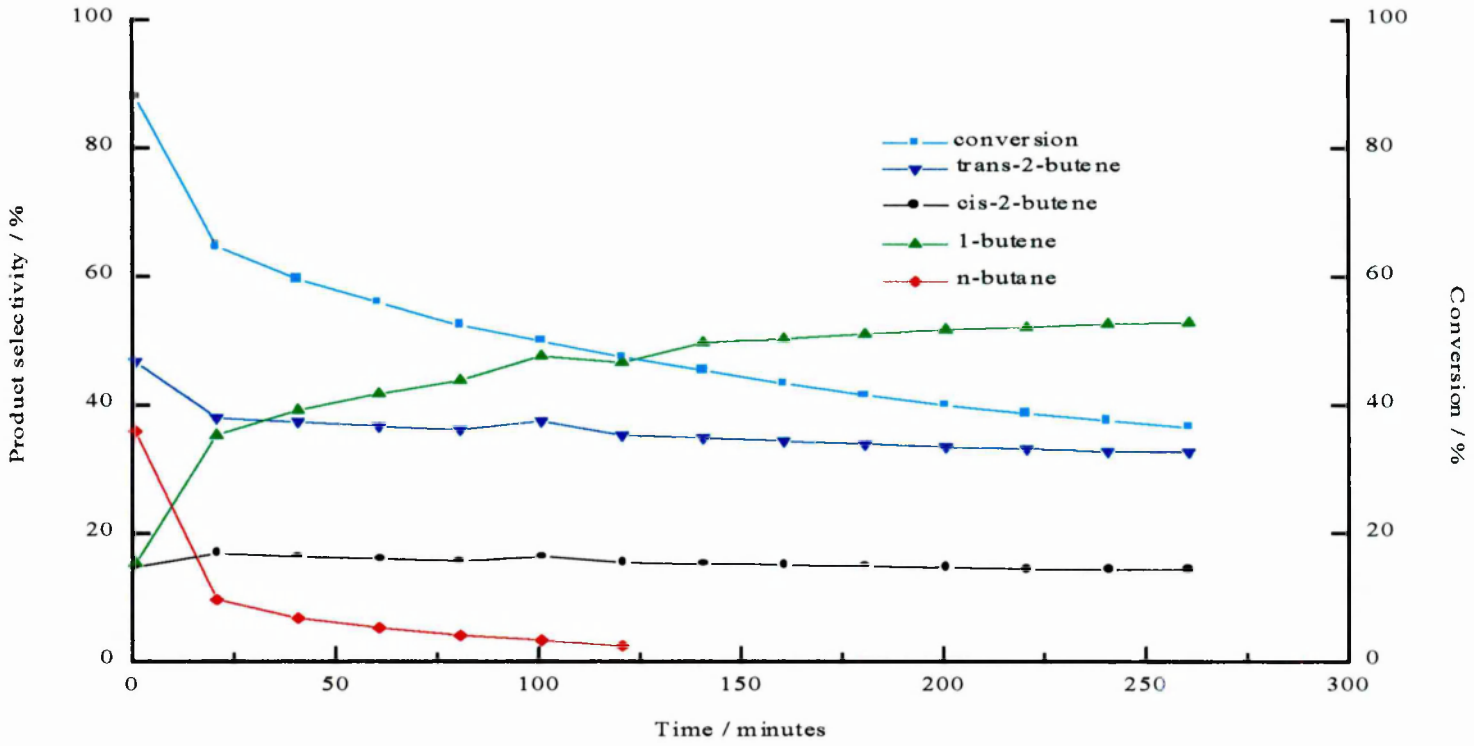

Figure 4.1 Data obtained from hydrogenation of butadiene over 1.8 wt% Pd/Al_2O_3 catalyst at 298 K displaying product selectivity and butadiene conversion versus time on stream.

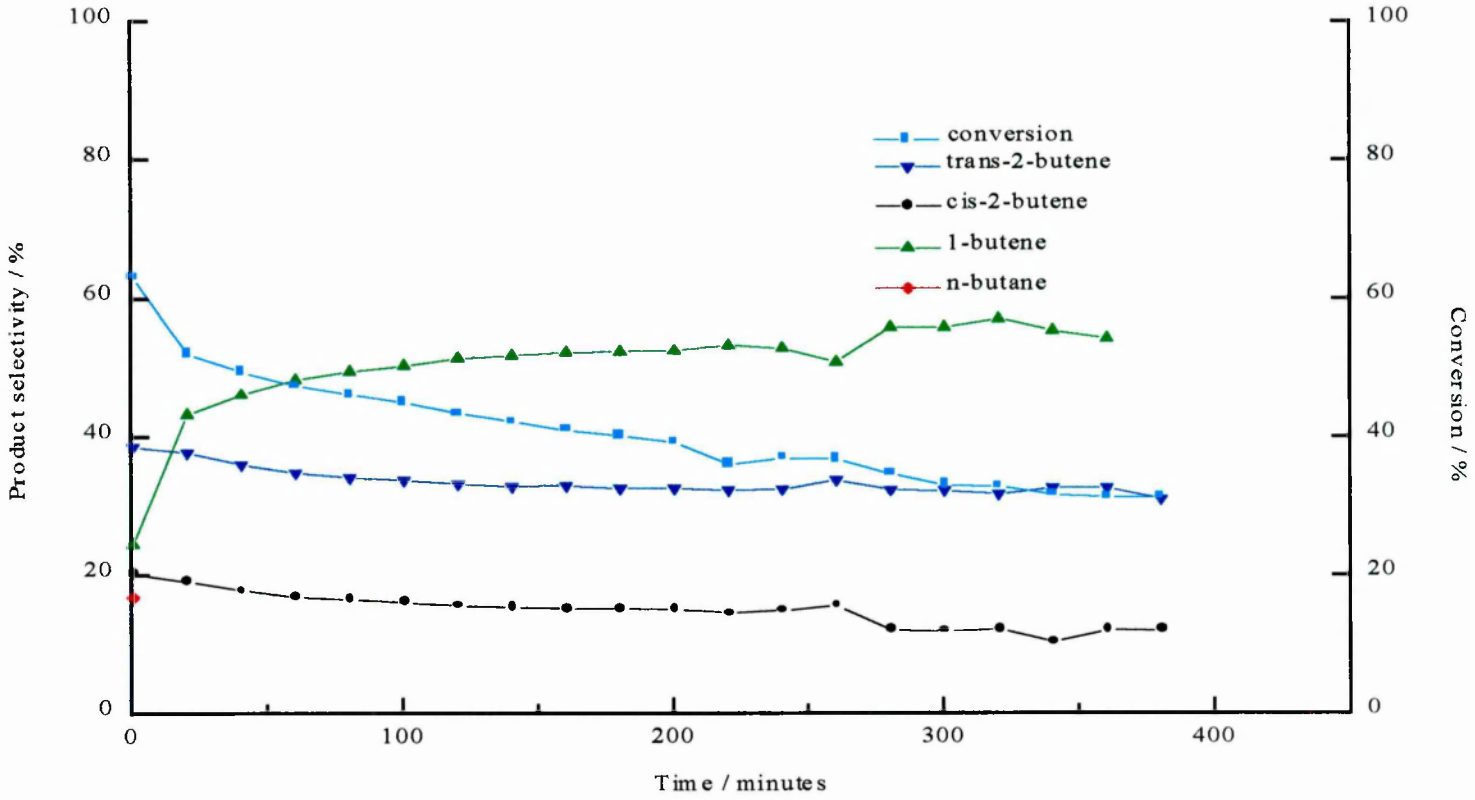

Figure 4.2 Data obtained from hydrogenation of butadiene over 1.8 wt% $PdFe/Al_2O_3$ catalyst at 298 K displaying product selectivity and butadiene conversion versus time on stream.

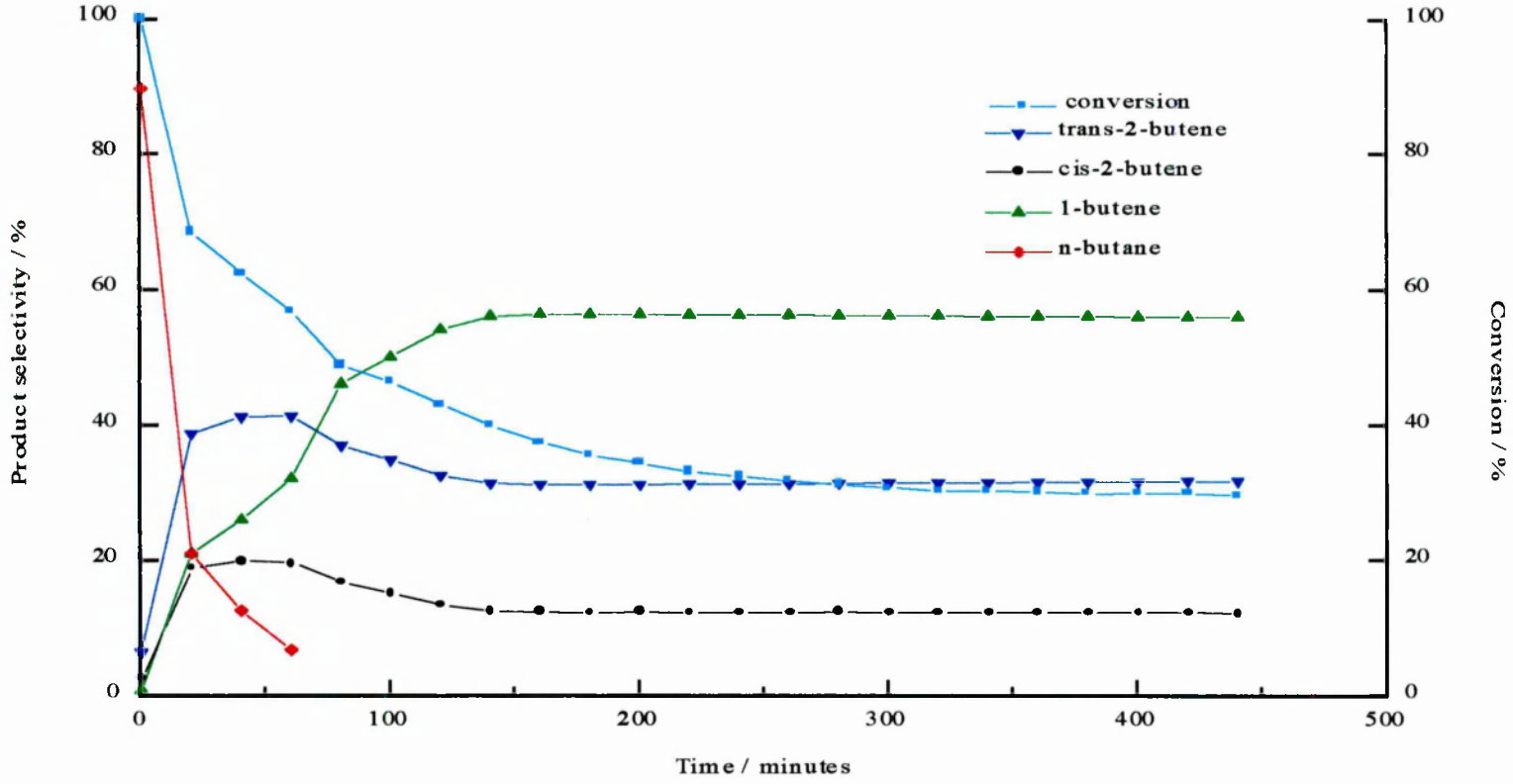

Figure 4.3 Data obtained from hydrogenation of butadiene over 1.8 wt% $PdSn/Al_2O_3$ catalyst at 298 K displaying product selectivity and butadiene conversion versus time on stream.

$$S_i = \frac{C_i}{\sum C_p}.100 \qquad (4.1)$$

where C_i is the concentration of product i and C_p is the total concentration of the products.

Monometallic catalyst

The profile for the monometallic 1.8 wt% Pd/Al_2O_3 catalyst is shown in Figure 4.1 with respect to time on stream. It can be seen that the conversion is initially very high with a value of just under 90 % at 1 min which decreases exponentially with time, falling to approximately 65 % for the second sample after 21 min on stream. This decay gradually slows down approaching a value of 37 % after 260 min. The deactivation of Pd catalysts in this reaction has been previously attributed to butadiene oligomerisation which blocks the catalytically active sites [1]. The product distribution also changes significantly over the first two samples. Initially trans-2-butene was the major product (46.8 %) with n-butane (36 %), 1-butene (15.4 %) and cis-2-butene (14.8 %). The selectivity to 1-butene then increased mainly at the expense of that to n-butane. After 20 min a more gradual increase is observed for 1-butene and a decrease for n-butane until 141 min where it is no longer observed. The selectivities to cis- and trans-2-butene are more steady decreasing only slightly over time, with a trans/cis ratio of approximately 2.3. The increase in 1-butene at the expense of n-butane would suggest that sites responsible for further hydrogenation of 1-butene are gradually poisoned/removed as the reaction proceeds. After 200 min on stream, chosen to represent steady selectivities to allow a comparison of the catalysts, the

selectivities were approximately 51 % to 1-butene, 34 % to trans-2-butene and 15 % to cis-2-butene at a conversion of 40 %. This is the order of selectivity generally reported in the literature. The TOF for the Pd monometallic catalyst after 200 minutes is 0.05 s^{-1}.

In comparing these results with the literature two main differences are observed. First, the trans- to cis-2-butene ratio at 2.3 is much lower than is generally quoted for other Pd catalysts which can be as high as 16 [2]. It is probable that here there is limited interconversion between the syn- and anti- forms of butadiene allowing a change in the configuration of the adsorbed butadiene (see Schemes 4.3 and 4.4). Second, the formation of n-butane in the initial part of the catalyst test at high conversion has not been widely reported as Pd is considered to be an active catalyst for the partial-hydrogenation of butadiene. It should be stated that direct comparison between the results quoted by different groups is difficult due to the variation in experimental conditions used by each group, although qualitative comparison can however be justified. It should be noted that in our experiment an excess of hydrogen was available and the formation of n-butane over a Pd catalyst has been attributed to a slight excess of hydrogen in the gas phase resulting in a lower butadiene coverage and allowing total hydrogenation and isomerisation of n-butenes [14]. In addition, the comparison of selectivities obtained at the high conversion reported here might be significant – attempts to reduce the conversion by reducing temperature or further diluting the system were not successful. The significant changes in selectivity and activity observed during the first few samples are consistent with modification of the catalyst

surface, by carbon laydown, during the initial part of the test. The initial samples taken when the catalyst is operating in a non steady state regime are not representative of either the activity or selectivity of the catalyst. Initially the 'clean' surface is more active (as judged by higher conversion) although not completely selective for butene formation. After a certain time on stream it can be assumed that the catalyst surface has been modified or conditioned in such a way that results in a less active catalyst surface which is, however, more selective for n-butene formation. The modification of the catalyst surface can be assumed to be caused by laydown of (hydro) carbonaceous deposits on the metal particles. A similar conclusion was reached by Ponec *et al.* [15] concerning the hydrogenation of acetylene over Pd surfaces. They noted that complete selectivity to the alkene was only observed after an initial conditioning period in which significant carbon laydown occurred as shown by carbon mass balance studies.

Bimetallic catalysts

The profiles for the PdFe and PdSn bimetallic catalysts are shown in Figures 4.2 and 4.3 respectively. In both cases an exponential decay is observed in conversion similar to that observed by the monometallic catalyst. Both bimetallic catalysts display the initial non steady state profile previously observed for the monometallic catalyst during which the surface of the catalysts are modified. The selectivities then settle down and the catalysts are completely selective for n-butene formation. The PdFe bimetallic catalyst displays an initial

conversion about 25 % lower than the monometallic catalyst although after a short period the conversions are much closer. N-butane is formed in much lower yields (< 20 %) than over the monometallic catalyst and was only observed in the sample taken after 1 min of reaction, after 21 min no n-butane was observed in the product stream. The 1-butene, trans-2-butene and cis-2-butene selectivity patterns are very similar to the trends shown by the monometallic catalyst with a rapid increase in selectivity to 1-butene at the expense of n-butane over 20 min. The conversion and selectivities after 200 min for each of the Pd-based catalysts are shown in Table 4.3.

The $PdSn/Al_2O_3$ bimetallic catalyst is initially the most active catalyst displaying 100 % conversion at 1 min (Figure 4.3). However the conversion drops rapidly so that after 200 min a lower butadiene conversion compared to the Pd/Al_2O_3 and the $PdFe/Al_2O_3$ catalysts is observed. The initial, very high, selectivity to n-butane (90 %) decreases rapidly so that after 61 minutes no n-butane is observed in the product stream. At this point the selectivity to n-butenes is 100 % and the order of selectivities to the three n-butene isomers observed, given in Table 4.3, is broadly similar to the other Pd-based catalysts.

Table 4.3 Comparison of activity and selectivity data for Pd-based catalysts for hydrogenation of 1,3-butadiene after 200 minutes on stream.

Catalyst	Conversion / %	Selectivity / %				Trans:cis ratio	Selectivity to n-butenes / %	TOF / s^{-1}
		n-butane	1-butene	trans-2-butane	cis-2-butene			
1.8 wt% Pd/Al_2O_3	40.0	0	51.5	33.7	14.8	2.3	100	0.05
1.8 wt% $PdFe/Al_2O_3$	39.5	0	52.5	32.7	17.8	1.8	100	0.07
1.8 wt% $PdSn/Al_2O_3$	34.3	0	56.4	31.4	12.2	2.6	100	0.13
1.8 wt% $PdFe/Al_2O_3$[1]	27.9	0	56.9	30	13.1	2.3	100	0.05

Notes. [1]. Unreduced before test. See text.

Effect of reduction before catalyst test

To examine the effect that prereduction has on the activity of the catalyst an unreduced 1.8 wt% $PdFe/Al_2O_3$ catalyst (taken from the same batch as the above $PdFe/Al_2O_3$ catalyst) was also tested for the butadiene hydrogenation reaction. Again the selectivity data is shown (Figure 4.4). Table 4.3 displays the data obtained after 200 minutes on stream. Unfortunately the first sample taken was after 21 minutes which meant we were unable to observe whether the n-butane observed in Figure 4.2 was reproduced. Nevertheless it can be seen that the conversion of the unreduced catalyst was much lower than the corresponding reduced catalyst but the product selectivities are broadly similar. This implies that prereduction of the catalysts before the catalytic reaction is necessary to achieve maximum activity although prereduction does not alter the selectivities.

The results for all the catalysts at 200 min are given in Table 4.3. Table 4.3 does highlight some differences between the $PdSn/Al_2O_3$ catalyst and the other Pd-based catalysts; the conversion after 200 minutes on stream is slightly lower and a higher selectivity to 1-butene and a higher trans-/cis-2-butene ratio are observed. Table 4.3 also lists the TOF for each of the Pd catalysts. The most significant point is that the value for the PdSn catalyst is approximately double that of the monometallic catalyst and the PdFe catalyst which are broadly similar. This is due to the decrease in specific surface area of Pd, measured by H/M. A similar rate of reaction is observed for each catalyst when the total Pd content is considered and it is only when the rate is expressed in terms of the number of

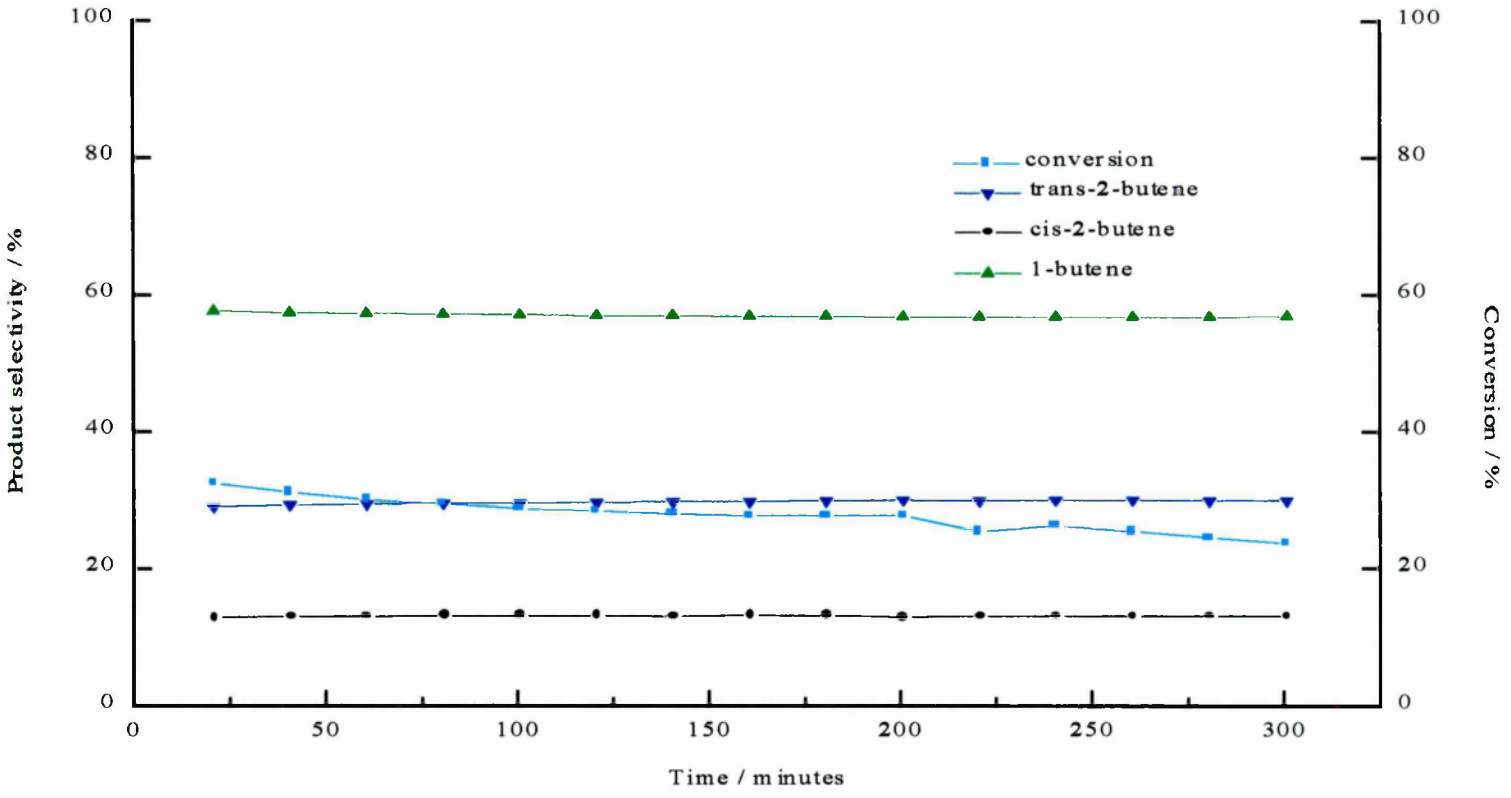

Figure 4.4 Data obtained from hydrogenation of butadiene over 1.8 wt% Pd/Al_2O_3 catalyst at 298 K (unreduced before test) displaying product selectivity and butadiene conversion versus time on stream.

exposed surface Pd atoms that the values vary greatly. It would then appear that addition of an inactive metal onto the surface of the Pd, blocking some of the active catalytic sites, has the effect of increasing the activity of the remaining Pd surface atoms. A similar situation has been reported by Jackson *et al.* for the hydrogenation of propyne over supported palladium catalysts. In their model, however, instead of a second metal blocking the active sites, carbon deposition is responsible for a reduction in reaction rate which is compensated for by an increase in the specific activity of the remaining sites [16].

Thus to summarise, there are a number of points to note:

i) After an initial period of about 1 - 2 h, the absolute conversion and selectivities of the catalysts are broadly similar, with complete selectivity to n-butenes in the order:

1-butene > trans-2-butene > cis-2-butene

The TOF, however, varies significantly for the PdSn catalyst.

ii) The initial activities and product distribution of the catalysts are significantly different, with the Fe catalyst less active than the monometallic and the Sn catalyst more so. A comparison of the ratio of 1-butene to 2-butene for the PdSn and Pd catalysts versus conversion illustrates the difference in the product distribution for these materials, (a difference which can not be explained simply by hydrogenation of 1-butene to n-butane).

In an attempt to rationalise the data obtained from the bimetallic catalysts it has been necessary to consider reports in the literature of bimetallic catalysts other than PdFe and PdSn since no work has previously been reported for such catalysts. This will be limited to studies of Pd plus another metal which is itself inactive for the reaction. It should also be noted that no reports of butadiene hydrogenation have been reported for any combination of metals prepared by SOMC, hence the following discussion relates to catalysts prepared by traditional techniques.

An early study by Wells *et al.* [3] compared Pd and PdAu alloys. The main effect of the Au was to alter the distribution of the 2-butenes as the temperature (and therefore conversion) was increased while the selectivity to 1-butene remained unchanged. However, at low Au levels no change in the product distribution was observed. From this work it was concluded that the presence of Au had little effect on the ability of Pd to form the butadiene surface species prior to hydrogenation. Our results appear similar with little change in the product distribution once the reaction has settled down (after approximately 100 min) which might suggest that the Fe and Sn have little influence at this point. Another study of the effect of Au and Ag on Pd/Al_2O_3 was carried out by Miura *et al.* [17]. They reported that the main effect of Au and Ag was a decrease in the activity of the Pd but also importantly the formation of n-butane was suppressed even at high conversion (90%). This differs significantly from our results where it appears that the more rapid decrease in n-butane observed for the bimetallic catalysts may be a factor of the more rapid decrease in conversion of the

catalysts. Figure 4.5 shows that the relationship between n-butane selectivity and conversion is similar for all the Pd based catalysts, with no total hydrogenation at conversions below about 45 %. PdCu bimetallic systems have been considered in a number of publications. Furlong *et al.* [18] studied the gas phase reaction and found that addition of Cu alters the selectivity of the Pd catalyst by increasing the selectivity to n-butenes without total hydrogenation and isomerisation. They believe that the hydrogen sorption data may explain the results since Cu reduces the amount of hydrogen adsorbed. The difference in the product distribution may imply a subtle change in the relative concentration of surface species influenced by either geometric or electronic differences caused by the Pd-Cu interactions. They also observed extensive deactivation of the catalysts which they attribute to accumulation of small amounts of higher molecular weight oligomerised olefins on the surface. A similar study by Schmal *et al.* [19] noted that addition of Cu to niobia supported Pd decreased the activity of the catalysts and increased the selectivity to 1-butene and the trans/cis ratio. The change in activity was attributed to a geometric site blocking mechanism and the changes in selectivity to electronic effects.

In all cases the order of selectivity of the n-butenes appears to have been the same as for our catalysts: 1-butene > trans-2-butene > cis-2-butene although the ratios of these vary throughout. It would appear that the deactivation of all the catalysts with respect with time may be attributed to deposition/modification of the surface by a carbonaceous overlayer. As the conversion decreases total hydrogenation to n-butane also decreases. The initially lower overall activity for

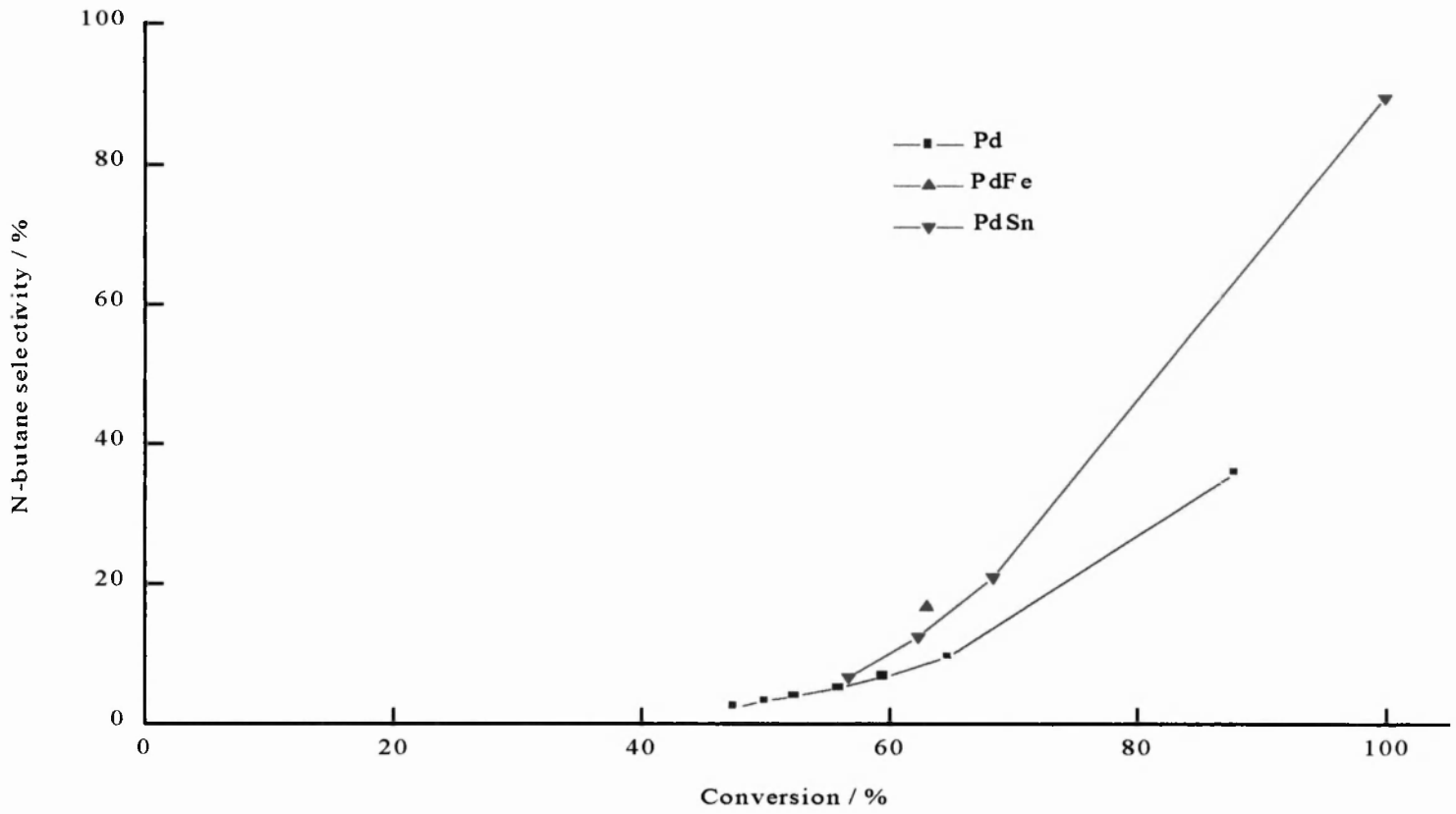

Figure 4.5 Figure displaying relationship between n-butane selectivity versus conversion for Pd-based catalysts.

the PdFe catalyst along with the lower H:Pd ratio can be explained by surface blocking of the palladium sites by the iron. Indeed the TOF for the Pd and PdFe catalysts calculated for the sample taken after 1 min of reaction are very similar (0.12 s^{-1} versus 0.11 s^{-1}). Thus the similar activity in terms of TOF would suggest that the decreased activity, in terms of conversion, for the PdFe catalyst is purely a geometric effect of Fe blocking the Pd sites. That the Pd and PdFe catalysts are so similar after the initial period suggests that the iron may deposit on some of the same sites as the carbon, and after a certain time the same number of sites are covered. A similar geometric effect is likely to be relevant for the PdSn catalyst, however the higher initial activity, both overall and TOF (the initial TOF for the PdSn catalyst is 0.19 s^{-1}) of the PdSn catalyst suggests that another factor is also significant. The increase in the specific activity of this catalyst suggests that even though the number of sites available to chemisorb hydrogen has decreased the activity of these sites appears to have increased. This increase is unlikely to be due to activity on tin alone as experiments on Sn/Al_2O_3 have shown this to be inactive. The tin-palladium interaction may influence the adsorption characteristics of the different hydrocarbons, possibly due to an electronic effect. The rapid deactivation of this catalyst suggests that these sites are poisoned by a similar mechanism although this may be more pronounced for this catalyst. The TOF is still significantly higher even after 200 min when the overall activity and product distribution of all the catalysts are similar. The TOF is of course based on the number of sites calculated from chemisorption experiments performed on a 'clean' surface and may not reflect the number of sites under the reaction conditions when some coverage by the carbonaceous layer is proposed. It is also

possible that the second metal may be removed over time and so the similar results reported after 200 min are in all cases due to monometallic palladium. This alternative explanation can not be ruled out as no characterisation or reactivation of the materials after the run was performed.

4.2.3.2 Platinum-based catalysts

The results from the platinum based catalysts listed in Table 4.1 are shown in Figures 4.6 - 4.9. The conditions used for the butadiene hydrogenation are listed in Table 4.2. Again the selectivity and conversion data are displayed against time on stream, all data obtained at 298 K. Each catalyst will be discussed in turn and any differences between the catalysts highlighted.

Monometallic catalyst

The Pt/Al_2O_3 monometallic catalyst (Figure 4.6) displayed a high initial conversion (> 80 %) and high selectivity to n-butane (ca. 95 %). The conversion decreased rapidly over the first 41 min on stream then declined more gradually and stabilised at about 25 - 28 % after approximately 100 min displayed no deactivation thereafter for the length of the experiment. The selectivity to the n-butenes is initially very low however this increases until it is approximately steady after 41 min. No cis-2-butene is observed in the first sample taken after 1 min within the limits of detection by GC. The n-butane formation decreases from 95 % to about 68 % during the first 100 min. After this point the

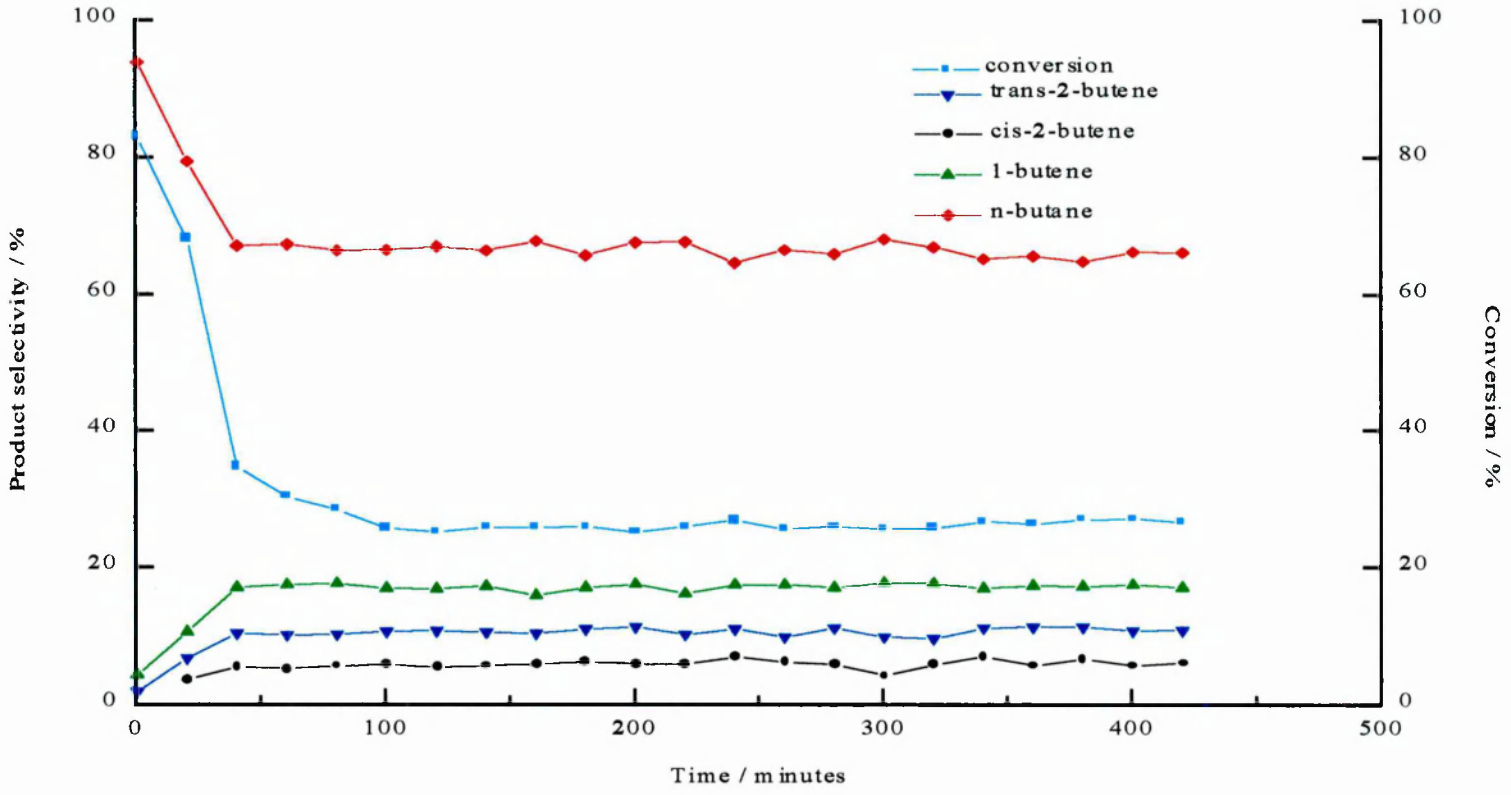

Figure 4.6 Data obtained from hydrogenation of butadiene over 0.7 wt% Pt/Al_2O_3 catalyst at 298 K displaying product selectivity and butadiene conversion versus time on stream.

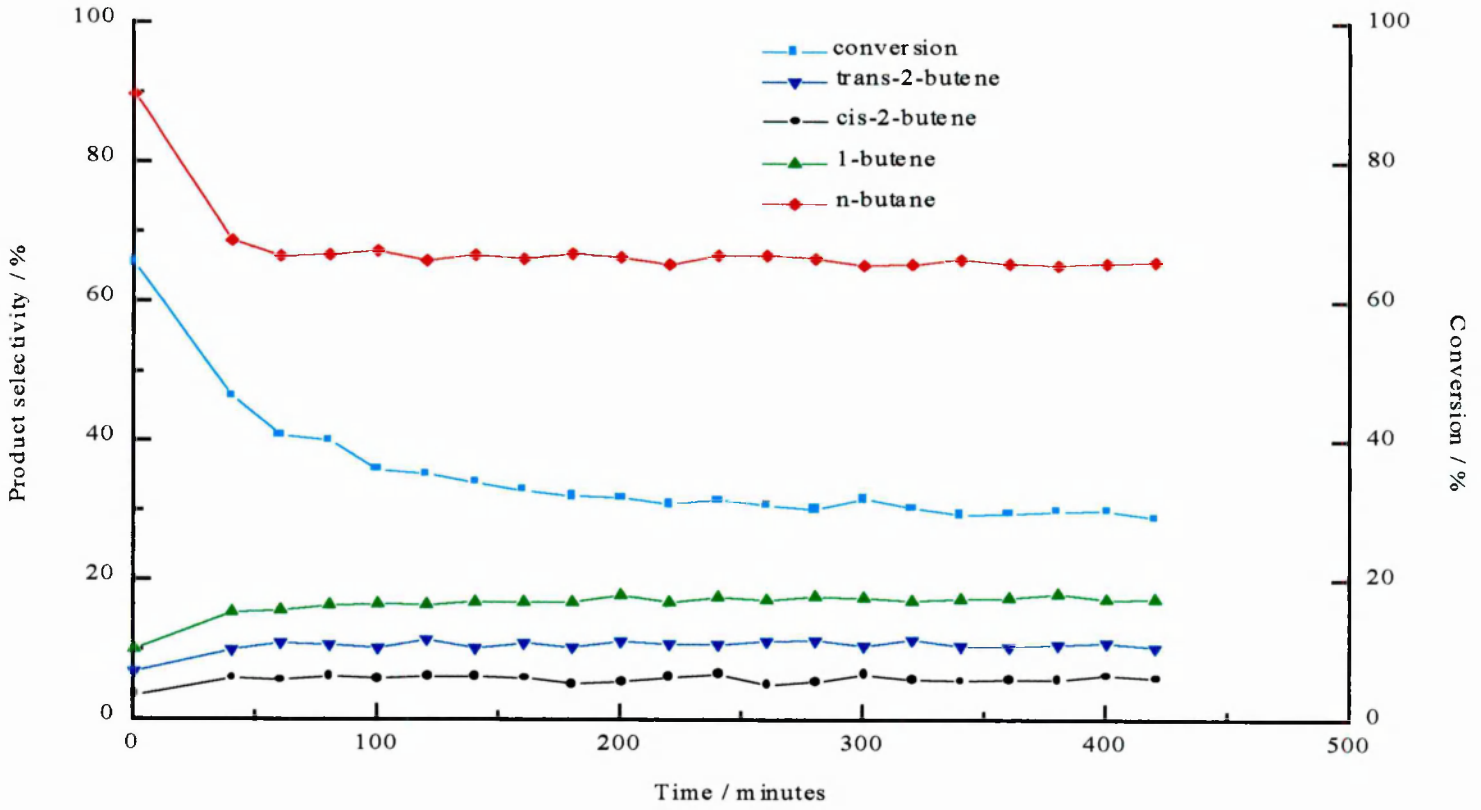

Figure 4.7 Data obtained from hydrogenation of butadiene over 0.7 wt% Pt/Al_2O_3 catalyst (regenerated after test) at 298 K displaying product selectivity and butadiene conversion versus time on stream.

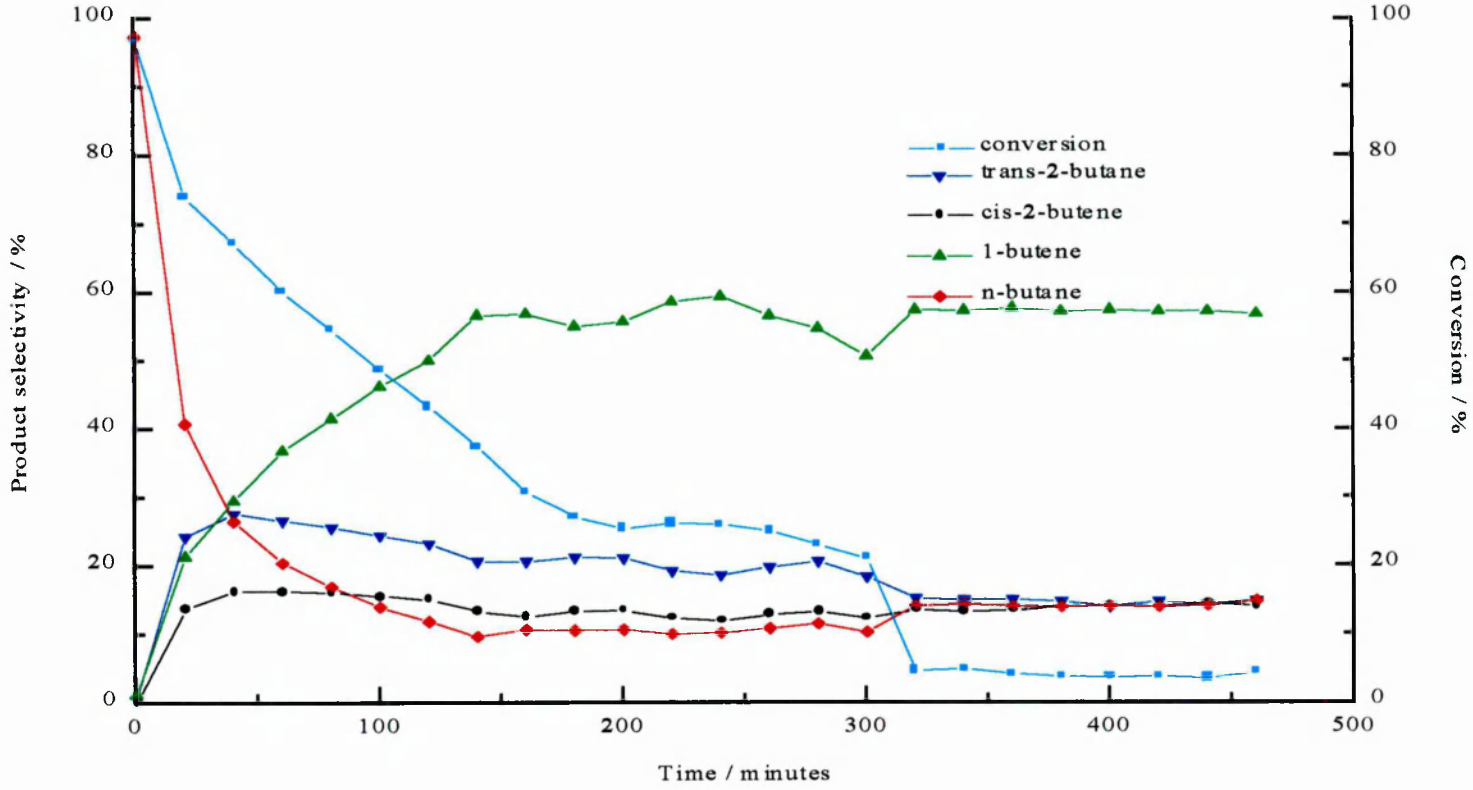

Figure 4.8 Data obtained from hydrogenation of butadiene over 0.7 wt% $PtFe/Al_2O_3$ catalyst displaying product selectivity and butadiene conversion versus time on stream.

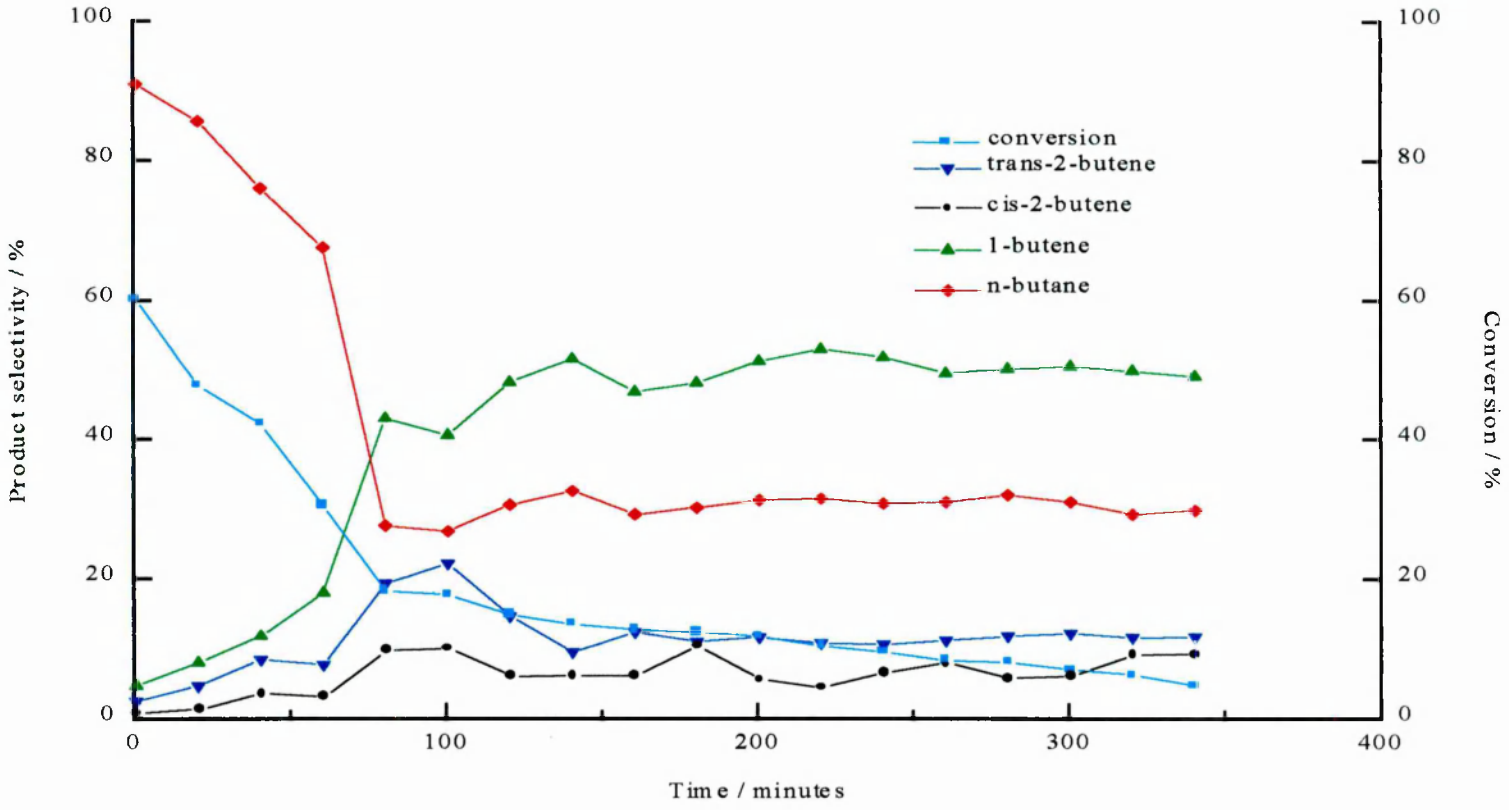

Figure 4.9 Data obtained from hydrogenation of butadiene over 0.7 wt% $PtSn/Al_2O_3$ catalyst at 298 K displaying product selectivity and butadiene conversion versus time on stream.

selectivities are fairly constant for the duration of the test as the system reaches steady state, with the selectivity to n-butenes about 33 %. At steady state the selectivity order for the monometallic catalyst is:

n-butane > 1-butene > trans-2-butene > cis-2-butene

The trans- to cis-2-butene ratio is about 1.9 which is lower than the value obtained for the Pd monometallic catalyst, as expected from previous comparisons of butadiene hydrogenation over Pd and Pt catalysts. A TOF of 0.07 s^{-1} is calculated for the 0.7 wt% Pt/Al_2O_3 catalyst using the data obtained after 200 minutes on stream. This is slightly higher than the value obtained for the Pd monometallic catalyst (0.05 s^{-1}) which is perhaps surprising when one considers the higher fundamental activity for Pd to hydrogenate olefinic double bonds. Indeed, Ouchaib *et al.* for butadiene hydrogenation reported a TOF for Pd/SiO_2 of 0.2 s^{-1} and for Pt/SiO_2 a value of 0.015 s^{-1} was obtained [4]. They attributed the lower activity of Pt to the lower hydrogen coverage on the Pt catalyst in the presence of butadiene, arising from a smaller heat of adsorption. However our experiments were performed in an excess of hydrogen which would be expected to have an effect on the kinetics and the adsorption characteristics of the reaction. The validity of comparisons of TOF's of catalysts with different metals, different metal loadings and different dispersions is unclear.

The selectivity results for Pt/Al_2O_3 are in general agreement with previous results discussed in the literature. Bond *et al.* observed for a Pt/Al_2O_3 catalyst a trans- to cis-2-butene ratio of between 0.9 to 1.8 with selectivity to butenes of 50–92 % depending on temperature [2]. The most notable feature of these results is the

high yield of n-butane observed throughout the duration of the catalyst test. The most likely reason for this is related to the strength of adsorption of the reactants and products as will be discussed below.

Effect of rereducing catalyst in situ

The effect of re-reducing the catalyst *in situ* after an initial test was also investigated to see if reactivation was possible. The Pt/Al_2O_3 catalyst used in the test described above was re-reduced using the standard reducing conditions without exposure of the catalyst to air and the catalyst test repeated. The results of this test are shown in Figure 4.7. It can be seen that after this reduction step the butadiene conversion is restored to a level greater than at the end of the first catalyst test but lower than the initial conversion on the 'fresh' catalyst. The selectivities are almost identical after steady state is reached (Table 4.4). It should however be noted that the conversion for the reactivated catalyst continues to decrease with increasing time on stream.

Bimetallic catalysts

The $PtFe/Al_2O_3$ catalyst (Figure 4.8) displayed a high conversion (ca. 97 %) and a selectivity to n-butane of 97 % for the sample taken after 1 minute. The conversion decreases with time, however, although the decline was significant it did not follow the exponential profile obtained for the monometallic catalyst, maintaining a steady decrease over about 180 min instead of the initial very rapid

Table 4.4 Comparison of activity and selectivity data for Pt-based catalysts for hydrogenation of 1, 3-butadiene after 200 minutes on stream.

Catalyst	Conversion / %	Selectivity / %				trans:cis ratio	Selectivity to n-butenes / %	1-butene/ 2-butenes	TOF / s^{-1}
		n-butane	1-butene	trans-2-butene	cis-2-butene				
0.7 wt% Pt/Al_2O_3	24.9	66.8	16.8	10.8	5.6	1.9	33.2	1.02	0.07
0.7 wt% Pt/Al_2O_3[1]	31.8	67.0	16.7	10.7	5.6	1.9	33	1.02	0.09
0.7 wt% $PtFe/Al_2O_3$	24.9	10.3	55.8	20.8	13.1	1.6	89.7	1.6	0.17
0.7 wt% $PtSn/Al_2O_3$	11.9	31.4	51.1	11.7	5.7	2.1	68.6	2.9	0.07

Notes. [1]. Rereduced *in situ* after test. See text.

decline. At 320 min however, a sudden drop to just 5 % was observed. The selectivity to n-butane, however, dropped very rapidly and after the first 41 minutes on stream 1-butene is the major product with the following order of product selectivity:

1-butene > trans-2-butene > cis-2-butene > n-butane

The major observation for this catalyst compared to the monometallic is the suppression of the formation of n-butane. Table 4.4 displays the data taken after 200 min on stream and the higher selectivity to the olefin products is observed. A lower trans-/cis-2-butene ratio compared to the monometallic catalyst but higher ratio of 1-butene/2-butene should also be noted. The conversion for both the catalysts after 200 min on stream is identical, although the TOF for the bimetallic is more than doubled, again reflecting the difference in the number of exposed Pt atoms on the fresh catalysts. It can also be noted that after 320 min on stream when the conversion drops, the selectivities to n-butane, trans- and cis-2-butenes are almost identical at 14-15 %, while 1-butene remains the major product.

$PtSn/Al_2O_3$ (Figure 4.9) displays a lower butadiene conversion than the monometallic Pt/Al_2O_3 but a similar high initial selectivity to n-butane is observed. The conversion profile with respect to time shows the more gradual decrease observed with the PtFe catalyst, but remains the lowest of the three catalysts. The overall conversion is approximately half that of the Pt and PtFe catalysts at 200 min, however the TOF is similar to that over the monometallic. As observed for the Pt/Al_2O_3 and the $PtFe/Al_2O_3$ catalysts the high n-butane

selectivity dropped rapidly levelling off at about 30 % after 80 min, with a corresponding increase in the n-butene formation. After 200 min the selectivity order is:

1-butene > n-butane > trans-2-butene > cis-2-butene

This catalyst is more selective for n-butene formation than the monometallic catalyst, however, n-butane is still significant. The ratio of 1-butene/2-butene is the highest for this catalyst.

From the figures and Table 4.4, it is evident that the selectivities are very different for each of the Pt-based catalysts. With regard to the n-butenes the order of selectivity is the same as for the Pd-based catalysts, i.e. 1-butene > trans-2-butene > cis-2-butene although the values are very different, however, the selectivity to the fully hydrogenated product varies in its placement for each catalyst. For the monometallic catalyst n-butane is the major product, for PtFe it is a minor product and for PtSn it is the second most abundant product after 1-butene. Differences between the product selectivity between the Pt catalysts may be electronic in origin. A change in the electronic properties of the catalysts will affect the strength of adsorption of the reagent and products on the catalyst surface. Therefore, addition of a second metal may alter the selectivity of the catalysts due to modification of the strength of adsorption of butadiene and/or the products. The 1-butene yields of the bimetallic catalysts are both much improved, and indeed similar, which implies that addition of Sn or Fe to Pt alters the strength of adsorption such that the 1-butene formed by 1,2-addition of hydrogen to adsorbed butadiene has a greater chance of desorbing from the

catalyst surface before undergoing further hydrogenation. The 2-butene yields for the two bimetallic catalysts however vary, with that for the PtSn resembling that of the monometallic. This might suggest that the Fe also inhibits further hydrogenation of 2-butene or enhances 1,4 addition of hydrogen. This difference between the two metals provides further evidence for an electronic effect rather than solely a geometric effect.

An electronic effect may also be invoked in trying to explain the activity profile of the catalysts, particularly the PtFe catalyst with 100 % initial conversion and higher TOF, even at 'steady state'. The effect of Sn more closely resembles the effect of Cu on the Pd catalysts discussed in the previous section in reducing activity and changing the selectivity profile. Deactivation, probably due to deposition of a carbonaceous layer, is evident for all the catalysts, however, the magnitude of deactivation appears to be greater (but the decline more gradual) for the two bimetallic catalysts. Interestingly, the rate of decline more closely resembles that of the reactivated monometallic catalyst than the fresh catalyst. The fact that the reactivated catalyst did not achieve the initial conversion of the fresh catalyst might suggest that irreversible modification of the surface has occurred. Reactivation appears, at least temporarily, to enhance the activity. At this point, little can be said about the causes of the difference in the activities of the catalysts other than it would appear that geometric and electronic effects of the second metal are likely to play a role. The significant differences between the monometallic and bimetallic catalysts, even after 480 min, suggests, at least for

the Pt catalysts, that the second metal is not lost (at least not all) during the reaction.

To summarise, the activity and selectivity of the Pt-based catalysts depends strongly on the presence of a second metal. On the monometallic Pt/Al_2O_3 catalyst n-butane is the major product and selectivity to n-butenes is only 33%. Addition of Fe or Sn to Pt/Al_2O_3 changes the selectivity of the catalyst, most notable by decreasing the formation of n-butane, with a resultant increase in selectivity to n-butenes of 68.6 % and 89.7 % for the PtSn and PtFe catalysts respectively. Indeed, the Fe doped sample is almost three times more selective than the monometallic catalyst.

4.2.4 Conclusions

The addition of Fe or Sn to Pd/Al_2O_3 and Pt/Al_2O_3 appear to have varying effects on the activity and selectivity of the catalysts depending on the metals.

i) For all the catalysts a deactivation with respect to time was observed, attributed to deposition of a carbonaceous overlayer. Although some of the activity can be recovered on reactivation, this deposition appears to lead to irreversible modification at least under our conditions.

ii) For the Pd catalyst the most significant difference was the initial activity of the bimetallics. For PdFe, a decrease in overall initial activity was observed leading to a suppression of n-butane formation which can be attributed to geometric effects. The decreased initial activity of the PdFe

catalyst is due to a site blocking mechanism as shown by a comparison of the initial TOF. For PdSn an increase is observed suggesting electronic effects may be important. For both catalysts after approximately 100 min, the overall activity and product distribution closely resembled that of the monometallic.

iii) Differences in the activity of the Pt bimetallics can be explained in a similar manner, although the second metal appeared to change the deactivation profile slightly, and the effects of the metals were reversed. The major change for the Pt catalysts, however, was a change in the selectivity and suppression of total hydrogenation. For PtFe the yield of both 1-butene and 2-butene increased and for PtSn just the 1-butene. This can be attributed to different electronic effects of the two metals and subtle changes to the strength of adsorption of butadiene and its hydrogenation products.

4.3 Hydrogenation of Crotonaldehyde

4.3.1 Introduction

The selective hydrogenation of an α, β-unsaturated aldehyde to the corresponding unsaturated alcohol is an important reaction in the fine chemical industry [20]. Unsaturated alcohols are important intermediates in the production of perfumes, flavourings, pharmaceuticals and other chemicals. Unfortunately it is thermodynamically more favourable to hydrogenate the olefinic (C=C) double bond of an α, β-unsaturated aldehyde rather than the carbonyl functional group (C=O) [21]. The hydrogenation of both C=C and C=O groups are thermodynamically possible but the free energy for the C=C bond hydrogenation is higher by about 10 kcal mol^{-1} [22]. The selective hydrogenation of the carbonyl group of α, β-unsaturated aldehydes therefore serves as a challenge for catalyst chemists.

Hydrogenation of an α, β-unsaturated aldehyde (hereafter the term unsaturated aldehyde will be taken to mean an α, β-unsaturated aldehyde) as well as producing an unsaturated alcohol, may produce a saturated aldehyde and, as secondary products, a saturated alcohol and, by hydrogenolysis, the corresponding hydrocarbon. The reaction scheme shown below (Scheme 4.5) illustrates the hydrogenation of crotonaldehyde, an unsaturated aldehyde.

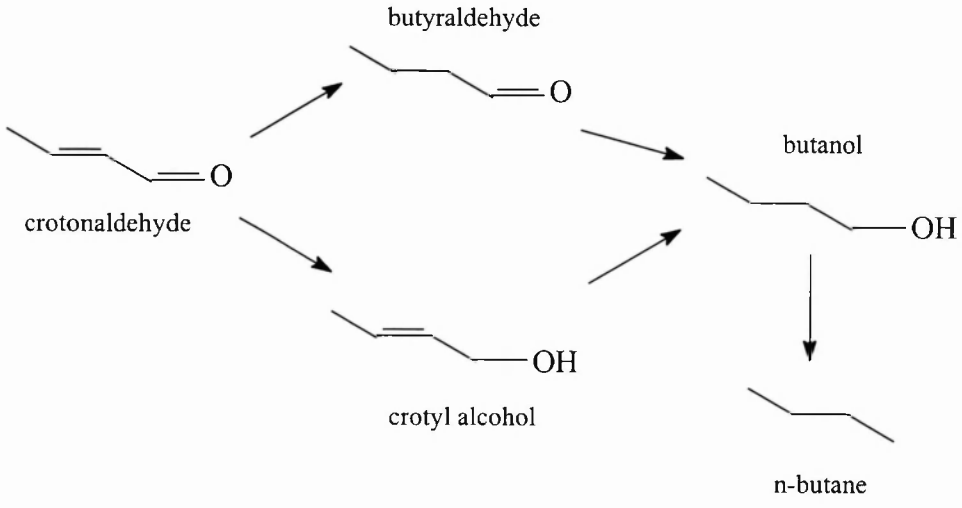

Scheme 4.5 Illustration of hydrogenation of crotonaldehyde, an unsaturated aldehyde.

The comments made in Section 4.2.1 concerning the mechanism of catalytic hydrogenation are also relevant here and are covered in the following statements. The hydrogenation of the olefinic double bond of the unsaturated aldehyde is proposed to occur by two different mechanisms. One mechanism involves a 3,4-addition (where atom 1 is the oxygen of the carbonyl group) of hydrogen to the adsorbed C=C group and the other a 1,4-addition leading to the formation of an enol which isomerises to give the same saturated aldehyde as the 3,4-addition process. Hydrogenation of the carbonyl group involves a 1,2-addition of hydrogen to crotonaldehyde. After the initial hydrogenation, producing either the aldehyde or the unsaturated alcohol, further hydrogenation of the remaining unsaturated bond produces the saturated alcohol [23].

We have chosen to study crotonaldehyde as a representative member of the unsaturated aldehyde family; the hydrogenation of crotonaldehyde and other unsaturated aldehydes has been widely studied in the catalysis literature and where relevant the hydrogenation of unsaturated aldehydes other than crotonaldehyde will be discussed. Before the results from the gas phase hydrogenation of crotonaldehyde over the catalysts are reported and discussed (Section 4.3.3), the appropriate literature will be briefly summarised to highlight relevant factors involved in controlling the activity and selectivity of Pt-group metals in the hydrogenation of unsaturated aldehydes.

The literature contains many reports of attempts to design catalysts that are active for the selective hydrogenation of unsaturated aldehydes to unsaturated alcohols. A chemical reduction method using $NaBH_4$ [24], can be used to selectively reduce the carbonyl group, however, a catalytic process is desirable due to lower costs. A homogeneous catalytic method using a Ru complex is another common method used [25], however, due to difficulty in separating the catalyst from the reaction medium, the usefulness of this method is limited, therefore a heterogeneous catalytic route is preferred. In this respect most reports concern the use of platinum group metals on high surface area supports.

Pt catalysts supported on silica or alumina are typically characterised by a low selectivity to the unsaturated alcohol when hydrogenating an unsaturated aldehyde. In these cases the reduction of the olefinic bond to form the saturated aldehyde is often followed by reduction of the carbonyl group to form the

saturated alcohol e.g., [23, 26]. However, a few authors report an enhanced selectivity to the unsaturated alcohol on supported Pt catalysts either by using a support which interacts strongly with the metal or by increasing the Pt particle size. For example, Lercher *et al.* studied the activity and selectivity of Pt/TiO_2 and Pt/SiO_2 catalysts towards crotonaldehyde hydrogenation [23]. They demonstrated that Pt supported on titania exhibited activity for the selective hydrogenation of crotonaldehyde to crotyl alcohol. This was attributed to the formation of a $Pt\text{-}TiO_x$ interface, after high temperature reduction, which enhances adsorption of crotonaldehyde through the carbonyl group due to the existence of Ti cations on the Pt surface. Assuming that the double bond adsorbed on the surface is the bond hydrogenated, then the formation of the unsaturated alcohol is favoured. Over Pt/SiO_2 they found that the selectivity to the unsaturated alcohol and the activity increased with increasing Pt particle size suggesting that the reaction is structure sensitive. They also noted a high initial selectivity to the hydrocarbon product (> 80 %) which decreased rapidly with time on stream. It was suggested that on small Pt particles crotonaldehyde is adsorbed through both double bonds and therefore the formation of the saturated aldehyde is observed since the hydrogenation of the C=C group is thermodynamically favoured. However, on large particles, the adsorption of crotonaldehyde via the carbonyl group is enhanced, with a resultant increase in yield of the unsaturated alcohol. This they related to the proportion of Pt(111) surfaces present. Increasing the particle size increases the number of Pt(111) faces. Smaller particles containing relatively fewer Pt(111) surfaces, consisting instead of corners and edges, are less active for the adsorption and hydrogenation

of the carbonyl group [23]. The lower activity of smaller particles is attributed to the faster deactivation of the highly exposed surface atoms.

It has also been shown that modifying a Pt catalyst by addition of a second metal can increase the yield of the unsaturated alcohol. Reports of both PtFe and PtSn bimetallic catalysts exist in the literature and are relevant to this work. A review of the role of promoters in the hydrogenation of unsaturated aldehydes has been presented by Ponec [27]. It is the intention to discuss these promoted Pt catalysts further at the relevant point in the discussion of results.

As the number of studies increases, using a variety of different metals and supports, then the mechanism of the reaction and the factors involved in the selectivity pattern observed become clearer. Many factors are discussed, however, consideration of the geometric and electronic properties of the surface of the catalyst, after appropriate characterisation, in most cases, allows the results to be explained.

Very few reports exist in the literature concerning the hydrogenation of unsaturated aldehydes on palladium-based catalysts. This is primarily because Pd catalysts are known to be very ineffective at hydrogenating carbonyl groups either as part of unsaturated aldehydes or isolated groups such as in ketones [21]. Delbecq and Sautet have studied the mode of adsorption of unsaturated aldehydes on Pd(111) in an attempt to understand these results [28]. They believed that the unsaturated aldehyde adsorbs through both double bonds on the

Pd surface so therefore the C=C bond is hydrogenated first, again for thermodynamic reasons. Only a couple of papers discuss Pd bimetallic catalysts and they will be discussed at a later point.

4.3.2 Experimental

The catalysts investigated here were listed in Table 4.1 and the procedures used to obtain the results discussed in this section were described in Chapter 2. It should be noted that no attempt was made to investigate the reaction conditions, such as crotonaldehyde/hydrogen ratio, flow rate, etc, in order to optimise the activity/selectivity of the catalysts. A set of conditions were chosen (listed in Table 4.5 below) and each catalyst was tested using these standard conditions.

Table 4.5 Main reaction conditions used for hydrogenation of crotonaldehyde.

Reaction Condition	Value
Mass of catalyst	0.1 g
Flow rate	60 cm^3 min^{-1}
Temperature	298-363 K

It should be noted that we are unable to quote a value for the ratio of $C_4H_7O:H_2$ since the temperature of the saturator vessel (273 K) was actually below the freezing point of crotonaldehyde (281 K), thus the partial pressure of crotonaldehyde was unknown.

4.3.3 Results and discussion

The results from the hydrogenation of crotonaldehyde on Pt-based catalysts will be presented first (Section 4.3.3.1) followed by the results from the Pd-based catalysts (Section 4.3.3.2).

The same control experiments described in Section 4.2.3 were repeated for crotonaldehyde hydrogenation which confirmed that (i) no gas phase reaction occurred in the absence of a catalyst, (ii) no reaction occurred over either the alumina support, a Fe/Al_2O_3 or Sn/Al_2O_3 catalyst at the temperatures studied and (iii) no reaction occurred using nitrogen as the reactor gas.

4.3.3.1 Platinum-based catalysts

Monometallic catalyst

Figure 4.10 displays the product selectivity and conversion data for the 0.7 wt% Pt/Al_2O_3 catalyst. At 363 K the conversion is low (< 5 %) and the main products are butyraldehyde and n-butane. Initially a significant amount of butanol is formed (27 %), however, this decreases rapidly so that after 30 min on stream no butanol is observed in the gas phase product stream. An important finding is that at this temperature and conversion no detectable selective hydrogenation of the carbonyl functional group of crotonaldehyde is observed during the test. With increasing time on stream the selectivity to n-butane increases at the expense of that to butyraldehyde. This suggests that the surface of the catalyst is modified, probably by deposition of a carbonaceous overlayer, with a resultant alteration in product selectivity. After 200 min the conversion was 2.9 % with a selectivity of 50.1 % to butyraldehyde and 49.9 % to n-butane (although the selectivity to n-butane continues to increase after this point and that to butyraldehyde decrease). When compared to previous literature reports of hydrogenation of unsaturated aldehydes on supported Pt catalysts, the absence of hydrogenation of the C=O group is expected, however, the high selectivity to the hydrocarbon product observed in this work is unusual. A high initial selectivity of n-butane up to 80 % has been previously reported on a Pt/SiO_2 catalyst [23] although this decreased rapidly with time on stream. It may be assumed that in the present work that

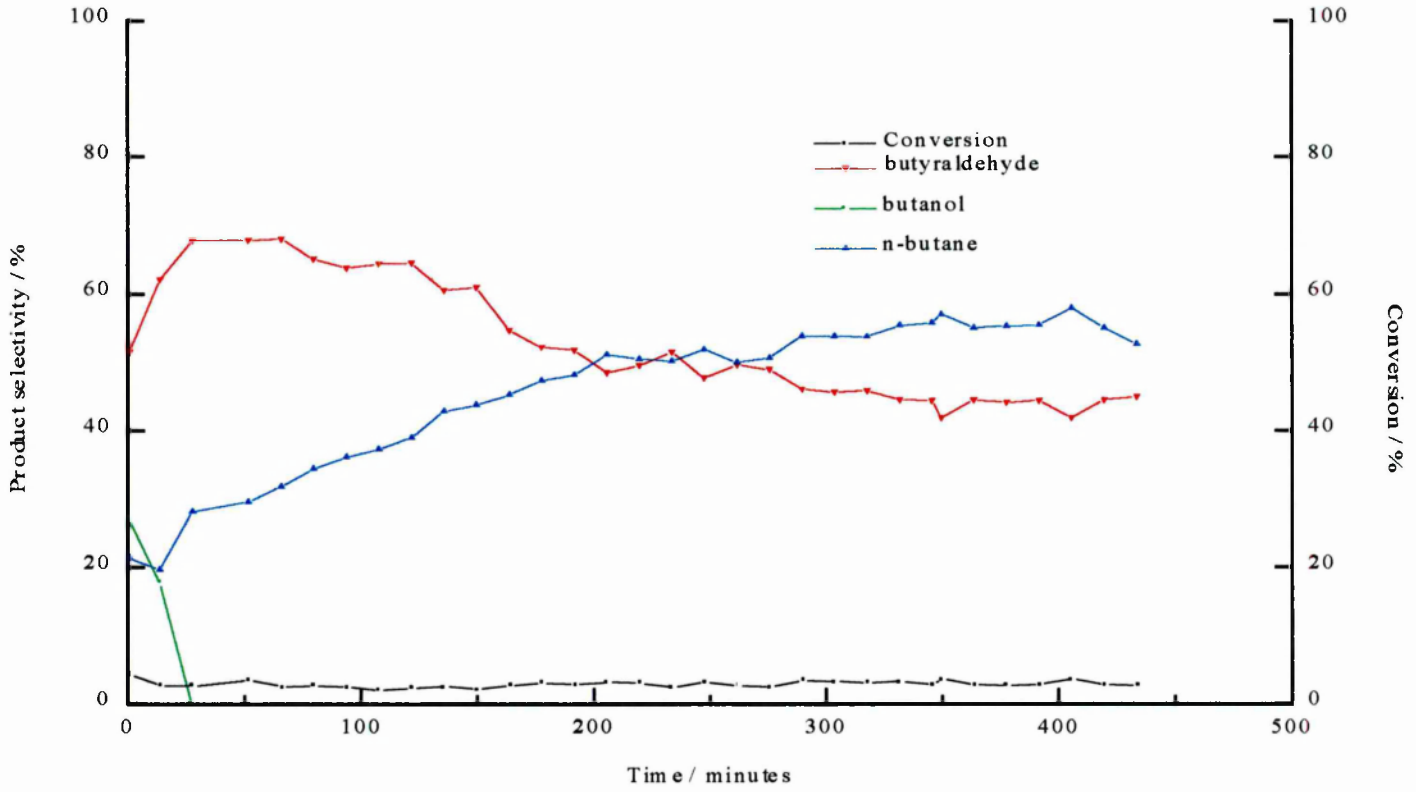

Figure 4.10 Data obtained from hydrogenation of crotonaldehyde over 0.7 wt% Pt/Al_2O_3 catalyst at 363 K displaying product selectivity and crotonaldehyde conversion versus time on stream.

either the reaction conditions used or the structure of the parent Pt catalyst is favourable for the hydrogenolysis reaction yielding n-butane. As mentioned previously direct comparison between different studies is difficult due to the different experimental conditions, however as a comparison Lercher *et al.* reported at 353 K in the gas phase 90 % selectivity to butyraldehyde (< 10 % conversion) but only 2 % to n-butane [23].

Increasing the temperature of the catalyst increases the conversion of crotonaldehyde, however, no hydrogenation of the C=O group is observed, instead the selectivity to n-butane increases.

In summary the data from the hydrogenation of crotonaldehyde over the 0.7 wt% Pt/Al_2O_3 monometallic catalyst is characterised by high selectivity to butyraldehyde and n-butane and, after a short time on stream, no hydrogenation of the C=O group of crotonaldehyde is observed. These results agree with previous literature data that report that small Pt particles supported on 'non-reducible' supports display poor activity for the hydrogenation of the C=O bond of unsaturated aldehydes.

Bimetallic catalysts

In Figure 4.11 the data obtained from the hydrogenation of crotonaldehyde on 0.7 wt% $PtFe/Al_2O_3$ is displayed and the selectivity data after 200 min is listed in Table 4.6. At 323 K the conversion of crotonaldehyde is greater than for the monometallic catalyst at 363 K clearly indicating that addition of Fe to Pt/Al_2O_3 increases the activity of the Pt towards hydrogenation of crotonaldehyde. Significant differences between the selectivity data for the monometallic and bimetallic catalyst are also observed. The order of selectivity of the 0.7 wt% $PtFe/Al_2O_3$ catalyst at 323 K is:

butyraldehyde > butanol > crotyl alcohol > n-butane

The major difference in the selectivity data between this catalyst and the monometallic is the significant decrease in n-butane formation on the bimetallic catalyst which remains constant throughout at ca. 5 %. An important observation is the formation of crotyl alcohol with an initial selectivity up to 15 %, although this does decrease with time on stream to ca. 6 %. Also butanol, formed by hydrogenation of both unsaturated double bonds, is observed with selectivities of 15-17 % throughout the duration of the test in contrast to the monometallic catalyst data (Figure 4.10) where no butanol is observed after a short time on stream. The main product is butyraldehyde, similar to the monometallic catalyst, although again a change in selectivity is observed in that the selectivity is greater for the bimetallic. Although the activity of this catalyst is not high it is clear that no deactivation occurs during the time of the experiment, which is in contrast to

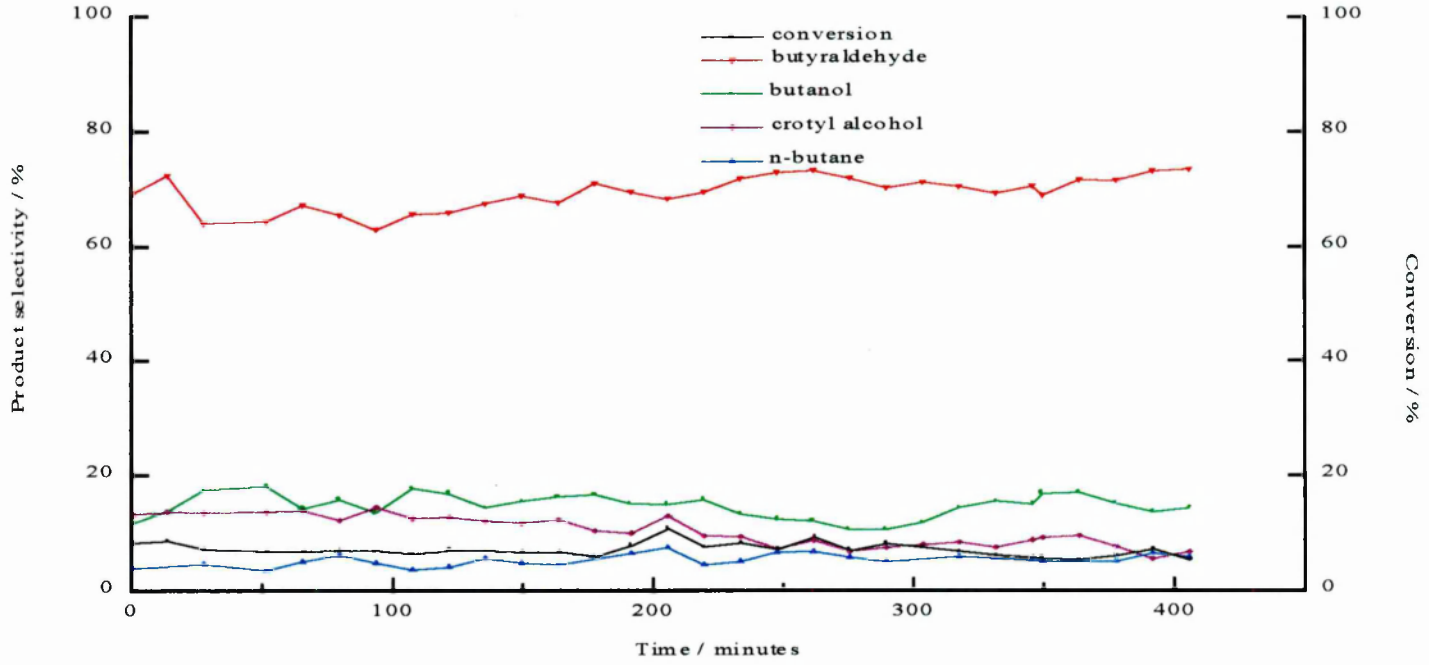

Figure 4.11 Data obtained from hydrogenation of crotonaldehyde over $PtFe/Al_2O_3$ catalyst at 323 K displaying product selectivity and crotonaldehyde conversion versus time on stream.

Table 4.6 Comparison of selectivity data for Pt-based catalysts for hydrogenation of crotonaldehyde after 200 minutes on stream.

Catalyst	Temperature / K	conversion / %	Selectivity / %			
			butyraldehyde	butanol	crotyl alcohol	n-butane
0.7 wt% Pt/Al_2O_3	363	2.9	50.1	-	-	49.9
0.7 wt% $PtFe/Al_2O_3$	323	7.7	67.1	14.7	11.4	6.8
0.7 wt% $PtSn/Al_2O_3$	363	11.3	71.7	7.6	11.3	9.4

many studies of crotonaldehyde hydrogenation which report significant deactivation with time on stream [23].

From the present results it is clear that addition of Fe or FeO_x to the surface of a 0.7 wt% Pt/Al_2O_3 catalyst modifies the activity and selectivity of the monometallic catalyst in the hydrogenation of the unsaturated aldehyde crotonaldehyde. However this not the first report of modification of the catalytic properties of Pt by addition of Fe towards this class of reaction. Among the earliest contributions to the area of hydrogenation of unsaturated aldehydes using PtFe catalysts was by Adams and Tuley who found that Pt became selective for production of cinnamyl alcohol when hydrogenating cinnamaldehyde upon addition of $FeCl_2$ [29]. The group of Lercher *et al.* considered the gas and liquid phase hydrogenation of crotonaldehyde over Pt/SiO_2 doped by Fe [30]. They found an increase in selectivity to crotyl alcohol in both reaction media with the addition of Fe and noted that selectivity decreased with increasing temperature. In the gas phase they found that the TOF for the $PtFe/SiO_2$ catalyst is five times greater than the value for the monometallic. Although TOF's are not reported here it is clear that the PtFe catalyst is considerably more active than the monometallic sample, when one considers that the conversion for the PtFe sample is higher at 323 K than the conversion for the monometallic catalyst at 363 K. Indeed remembering that the Pt surface area in the bimetallic catalyst is approximately half that of the monometallic, then a large increase in the specific activity of the remaining $Pt_{surface}$ atoms is evident. Lercher *et al.* reported that the catalytic activity decreased by up to 80 % after 90 min on stream. This is clearly

not observed here (indeed the monometallic catalyst did not display significant deactivation either) hence the mode of deactivation of catalysts during this reaction needs consideration. It is believed that decarbonylation of crotonaldehyde and subsequent poisoning of the surface by adsorbed CO is responsible for the deactivation associated with this reaction [23]. Therefore it may be that the rate of decarbonylation of crotonaldehyde and adsorption of CO is greatly decreased on these Pt based catalysts and hence deactivation is not observed. Lercher *et al.* reported a selectivity to crotyl alcohol of 44 % and concluded that the increase in selectivity was attributed to the presence of a bimetallic phase which induces polarity on the alloy surface leading to an increase in the activation and hence hydrogenation of the carbonyl group [30]. Ponec *et al.* considered the hydrogenation of a series of unsaturated aldehydes [31]. They found that Fe increased the activity and selectivity of Pt/SiO_2 catalysts for hydrogenation of unsaturated aldehydes although this was only really significant when substituents other than hydrogen were attached to the olefinic carbons. For crotonaldehyde hydrogenation, $PtFe/SiO_2$ displayed a selectivity of ca. 28 % to crotyl alcohol compared with a value of 13 % obtained for the monometallic catalyst. It is clear from the present work and the studies described above that addition of Fe to Pt increases both the activity and the selectivity for the hydrogenation of unsaturated aldehydes to unsaturated alcohols. It is then necessary to consider the origin of this favourable enhancement of selectivity in terms of the geometric and electronic structure of the catalysts. Goupil *et al.* found a similar increase in activity and selectivity for a PtFe/C catalyst compared to Pt/C for liquid phase hydrogenation of

cinnamaldehyde [32]. Indeed a catalyst containing 20 atom% Fe is about 40 times more active than the Pt/C catalyst and a catalyst with 50 atom% Fe displays selectivity to cinnamyl alcohol of up to 90 %. XRD and magnetic measurements indicate that their PtFe catalyst was monocrystalline PtFe with alloy particles of uniform composition. XANES and EXAFS experiments indicate that a transfer of electrons from Fe to Pt occurs which was believed to be responsible for the enhanced activity and selectivity. Similar results were reported by Richard *et al.* who investigated the liquid phase hydrogenation of cinnamaldehyde on Pt/C catalysts modified by addition of $FeCl_2$ [33]. They observed an increase in the activity and selectivity upon addition of Fe with an optimum ratio of Fe:Pt of 0.2. They showed by XANES that Fe atoms on Pt are positively charged, either because they are incompletely reduced or because of an electron transfer between Fe and Pt. In this case Fe cations, Lewis acid sites, can act as an adsorption site for the carbonyl group of the unsaturated aldehyde via donation of an electron from the oxygen atom of the carbonyl group. The selectivity is further improved by a decreased rate of hydrogenation of the olefin group which they attribute to the higher charge density on Pt. This decreases the probability of activation of the olefin group since the first step in the activation is a transfer of electron density from the π-electrons of the olefin group to the metal. In addition, Gallezot and Richard also claim that electron transfer to the platinum from the iron increases the H^- character of the neighbouring chemisorbed hydrogen promoting the attack by the hydride on the electropositive carbon of the C=O [22]. A study has been published which considered the adsorption of unsaturated aldehydes on Pt(111) and $Pt_{80}Fe_{20}(111)$ from a

theoretical perspective [34]. This showed that crotonaldehyde is less strongly adsorbed on the alloy and has a more pronounced tendency to adsorb through the carbonyl group of crotonaldehyde on the alloy thus explaining the higher activity and greater selectivity towards the unsaturated alcohol of the alloy.

Clearly, the present study has shown that addition of Fe to the surface of alumina supported Pt by SOMC increases the rate of hydrogenation of the carbonyl formed by hydrogenation of crotonaldehyde compared to a Pt/Al_2O_3 catalyst, as observed by the increased yields of butanol and crotyl alcohol. In Chapter 3 the Fe was shown to deposit on the surface of the Pt particles although it is not clear whether the Fe would be fully reduced prior to the catalyst test. However it is probable that the mode of adsorption of crotonaldehyde on the catalyst surface is modified such that the adsorption of the carbonyl group is more favoured. The increased activity of the bimetallic catalyst compared to the monometallic catalyst is more difficult to explain. Examination of the literature, however, reveals that addition of Fe to Pt catalysts increases the activity of the Pt for hydrogenation of unsaturated aldehydes. This was clearly illustrated in the examples of $PtFe/SiO_2$ (hydrogenation of crotonaldehyde) [30], PtFe/C (hydrogenation of cinnamaldehyde) [33] and $Pt_{80}Fe_{20}$ single crystals (hydrogenation of crotonaldehyde and methylcrotonaldehyde) [35]. Since XANES studies have proved the existence of an electronic transfer from Fe to Pt, it is therefore likely that the modification of the electronic properties of Pt, resulting in modification of the strength of adsorption of crotonaldehyde, is

responsible for the increase in activity observed. It is also possible that the presence of a second metal prevents deposition of polymeric substances on the catalysts allowing more of the catalyst surface to participate in the reaction, hence increasing catalytic activity. The decreased selectivity to n-butane exhibited by the bimetallic catalyst is explained by considering the size of the Pt ensembles required for the hydrogenolysis reaction. It is widely accepted that the hydrogenolysis reaction requires a certain number of adjacent Pt atoms. By depositing Fe on the Pt surface, resulting in the partitioning of the Pt surface, fewer of the multi atom ensembles required for the hydrogenolysis will exist, thus decreasing the formation of n-butane, i.e. a traditional site isolation explanation [15]. Therefore, indirectly, the decreased selectivity of the bimetallic catalyst to n-butane may also confirm the presence of the second metal on the surface of the Pt particles. The above hypothesis is well illustrated if one considers the data of Ponec and Marinelli [36]. They studied acrolein hydrogenation over a PtSn catalyst. After calcination in air - inducing segregation of the two metals – significant amounts of the hydrogenolysis product of acrolein (propane) are formed. However, if the catalyst is reduced instead of calcined so that the two metals are still associated with each other, the amount of propane produced is significantly suppressed.

The corresponding data for the 0.7 wt% $PtSn/Al_2O_3$ at 363 K is shown in Figure 4.12 and the conversion and selectivity data are shown in Table 4.6. Again clear differences between the monometallic catalyst and this catalyst are observed. At 363 K the conversion is slightly higher than the monometallic catalyst. Again no

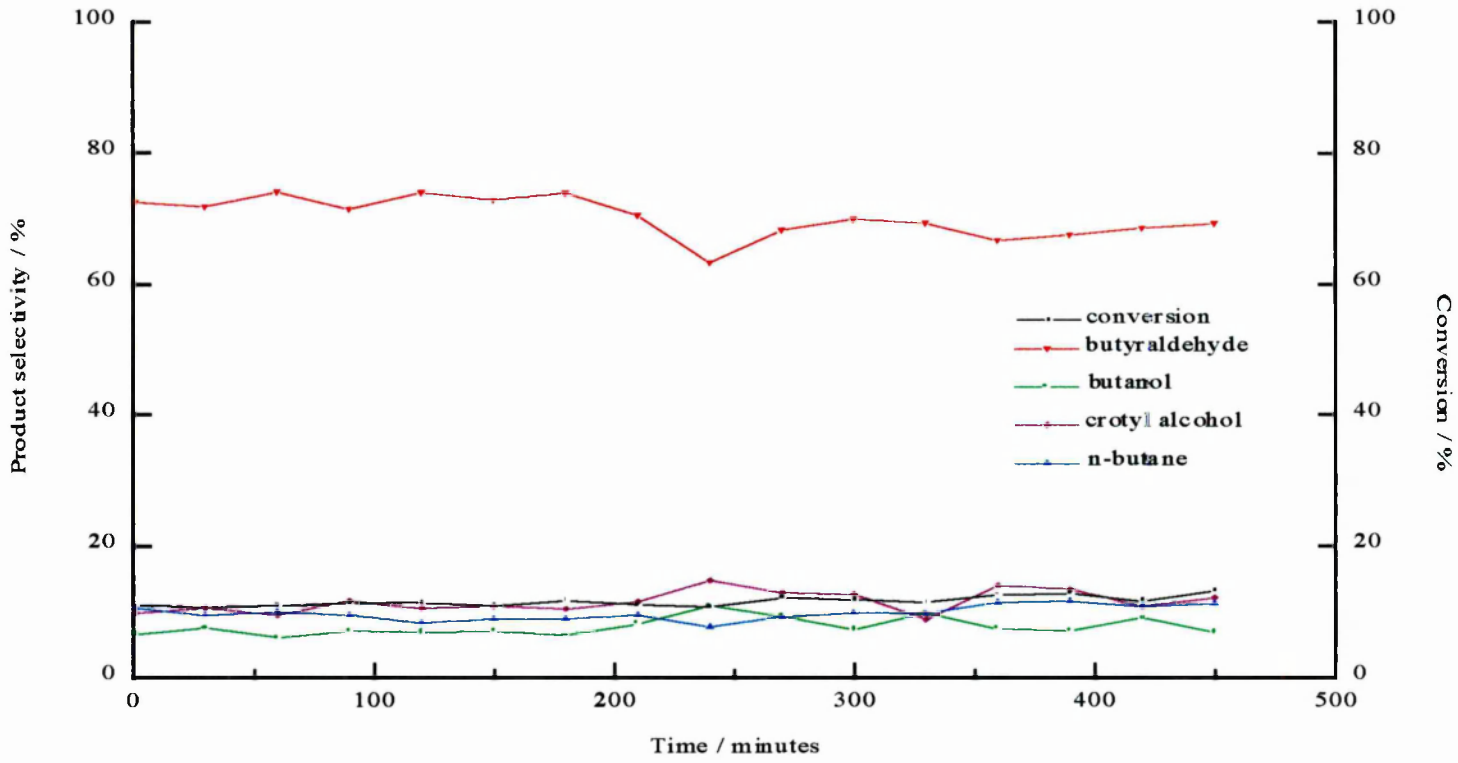

Figure 4.12 Data obtained from hydrogenation of crotonaldehyde over 0.7 wt% $PtSn/Al_2O_3$ catalyst at 363 K displaying product selectivity and crotonaldehyde conversion versus time on stream.

deactivation was observed for the duration of the test. The order of selectivity for the $PtSn/Al_2O_3$ catalyst is as follows:

butyraldehyde > crotyl alcohol > n-butane > butanol

Compared to the parent monometallic catalyst the Sn modified Pt catalyst clearly exhibits an enhanced activity for hydrogenation of the carbonyl group of crotonaldehyde. Both crotyl alcohol (selectivity up to 15 %) and butanol are observed for the duration of the test in contrast to the monometallic catalyst. Again the selectivity to butyraldehyde is increased and the selectivity to n-butane is greatly reduced. The selectivity to butanol is greater than the monometallic but less that PtFe, however it should be remember that the PtFe was tested at a lower temperature.

A number of groups have also studied the hydrogenation of unsaturated aldehydes on PtSn bimetallic catalysts. Poltarzewski *et al.*, for instance, found that addition of a small amount Sn to Pt supported on Nylon caused an increase in selectivity to the unsaturated alcohol in the case of hydrogenation of acrolein and cinnamaldehyde [37]. The higher selectivity was mainly a result of a large increase in the rate of hydrogenation of the carbonyl group which they attributed to the acidic properties of Sn activating the C=O group and, in parallel, an electronic interaction between the Sn and Pt poisoned the sites responsible for hydrogen activation. Stronger electron density on Pt leads to a more nucleophilic chemisorbed hydrogen which can attack the electropositive carbon of the carbonyl group precipitating addition of hydrogen to the oxygen of the carbonyl

group to form the unsaturated alcohol. Galvagno *et al.* claim that addition of Sn to Pt has two effects: i) activation of carbonyl group (as before) and ii) deactivation of the sites responsible for addition of hydrogen to multiple bonded carbon [38]. The same group characterised the PtSn bimetallic catalysts using electron microscopy and confirmed the presence of ionic tin on the surface of Pt particles [39]. Lercher *et al.* studied crotonaldehyde hydrogenation over PtSn supported on SiO_2 and compared the results with the corresponding monometallic catalysts [30]. They found the monometallic Pt catalyst was only active for hydrogenation of the olefinic group however addition of Sn not only increases the rate of reaction ten-fold but also improves the yield for crotyl alcohol from 0 % for the monometallic catalyst to 31 % for the $PtSn/SiO_2$, although butyraldehyde remained the dominant product (> 60 %). They agreed with others that the enhancement of C=O group hydrogenation is due to the presence of Lewis acid sites on the catalysts (Sn cations). The same group carried out an *in situ* XANES study in which they showed that the interaction between the free electron pairs of the oxygen of various oxygen containing unsaturated hydrocarbon molecules and the unoccupied electronic sites above the Fermi level of the Pt is very small. This might help to explain the requirement for polarity on the surface of the catalyst, which would act as electron pair acceptor sites for the electron pair of the oxygen of the carbonyl group. With regard to the higher activity of the PtSn catalysts compared with the monometallic sample it is claimed that the presence of Sn on the surface prevents deposition of polymeric substances on the surface. Therefore in this work it is

likely that the presence of Sn on the Pt surface acts as a Lewis acid and promotes the hydrogenation of the carbonyl group of crotonaldehyde.

Comparison of results from Pt-based catalysts

Based upon conversion of crotonaldehyde, the activity of the Pt-based catalysts can be ranked as:

$$PtFe/Al_2O_3 > PtSn/Al_2O_3 > Pt/Al_2O_3$$

An enhancement of activity is observed for both bimetallic catalysts compared to the monometallic catalyst although it is significantly greater for the Fe-doped catalyst. The enhanced activity is probably due to an alteration in the electronic properties of Pt which affects the strength of adsorption of crotonaldehyde on the Pt surface. Both bimetallic catalysts exhibit selectivity to crotyl alcohol which is not observed by the monometallic catalyst although the yield of both products from hydrogenation of the carbonyl group - butanol and crotyl alcohol - is greater for the PtFe catalyst. Hence the order of catalytic activity for hydrogenation of the C=O bond is:

$$PtFe/Al_2O_3 > PtSn/Al_2O_3 >> Pt/Al_2O_3$$

Modification of the catalytic properties of the monometallic catalyst by addition of Fe or Sn is likely to be due to an alteration of the mode of adsorption of

crotonaldehyde on the Pt surface, and in particular adsorption of C=O must be more favourable on the bimetallic surface compared to the monometallic surface. The change in the adsorption is probably due to the presence of Lewis acid sites formed by metal cations of the second metal, in agreement with previous literature results. The selectivity to n-butane is suppressed on both bimetallic catalysts and the reason for this is likely to be due to site isolation as discussed above. No deactivation of the catalysts was observed at the temperature of reaction although changes in selectivity were observed with time on stream. It is clear that on all the Pt-based catalysts deactivation with time on stream is not observed although this may be due to the low concentration of crotonaldehyde used in our experiment. The activity of the bimetallic catalysts is greater than the monometallic which may be due to an electronic effect of the second metal or it may be related to the decreased hydrogenolysis capability of the bimetallic catalyst which would result in a decreased deposition of carbonaceous deposits on the surface.

The selectivity to the unsaturated alcohol on the bimetallic catalysts is modest and although the yields do not compare favourably with some of the selectivities reported in the literature for similar catalysts, it is anticipated that the selectivity may be improved by altering the ratio of Pt to the second metal, which has been shown to be an important factor in determining the selectivity to the unsaturated alcohol.

In all cases increasing the temperature of the catalyst does not increase the selectivity to crotyl alcohol, instead on the bimetallic catalysts the selectivities to butyraldehyde and butanol increase.

In summary, both bimetallic catalysts display higher activity than the monometallic catalysts used as the 'parent' catalyst. We have also demonstrated that addition of Fe or Sn to Pt increases the hydrogenation of the carbonyl group compared to the monometallic catalyst with a maximum selectivity to crotyl alcohol of about 15 %. The formation of n-butane was greatly suppressed on the bimetallic catalysts.

4.3.3.2 Palladium-based catalysts

The catalysts discussed in this section are the monometallic 1.8 wt% Pd/Al_2O_3 catalyst and the corresponding bimetallic catalysts 1.8 wt% $PdFe/Al_2O_3$ and 1.8 wt% $PdSn/Al_2O_3$. The metal loadings and Pd dispersion values were given Table 4.1. All the results discussed below were obtained using the conditions listed in Table 4.5. It should be mentioned here that all the Pd-based catalysts displayed very high conversions at 298 K (see below) and that under normal circumstances it would have been preferable to record the selectivities at much lower conversions (usually at 10 % conversion or below) in order to operate in a differential reactor mode where secondary effects are not as significant [13]. In

this work in an attempt to reduce the conversion the reactor containing the catalyst was placed in an ice bath however this resulted in the formation of liquid crotonaldehyde around the catalyst. Hence 298 K was the lowest easily obtainable temperature at which to record the data. Another method attempted to reduce the activity was to reduce the mass of the catalyst and to dilute it with the inert support. However it was found that non-reproducible data was obtained using that procedure. Hence the conditions listed in Table 4.5 were used to obtain the results presented here.

Monometallic catalyst

The data for the 1.8 wt% Pd/Al_2O_3 monometallic catalyst are presented in Figure 4.13 and the conversion and selectivity data at 298 K after 200 min on stream are listed in Table 4.7. At this temperature the conversion is over 90 % which decreases only slightly during the test and the order of selectivity is as follows:

butyraldehyde >> n-butane > crotyl alcohol ~ butanol

Selectivity to butyraldehyde was greater than 95 % with only small amounts of the other products formed, with the selectivity towards crotyl alcohol and butanol typically less than 1 %. It should also be noted that initially the selectivity to butyraldehyde increased in parallel to a decrease in n-butane selectivity and conversion. This would tend to indicate that a short induction period is observed during which the Pd surface, initially active for the hydrogenolysis reaction, is

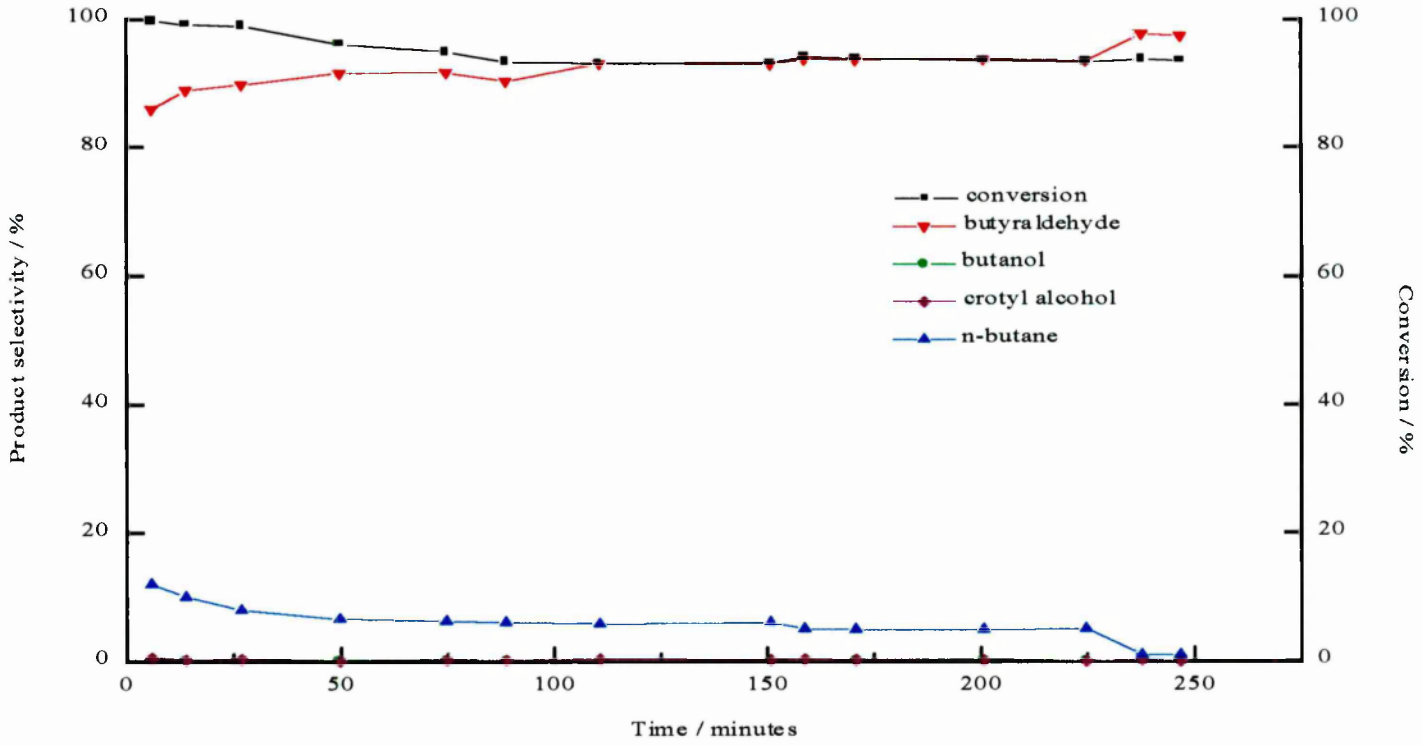

Figure 4.13 Data obtained from hydrogenation of crotonaldehyde over 1.8 wt% Pd/Al_2O_3 catalyst at 298 K displaying product selectivity and crotonaldehyde conversion versus time on stream.

Table 4.7 Comparison of selectivity data for Pd-based catalysts for hydrogenation of crotonaldehyde after 200 minutes on stream.

Catalyst	Temperature / K	conversion / %	Selectivity / %			
			butyraldehyde	butanol	crotyl alcohol	n-butane
1.8 wt% Pd/Al_2O_3	298	94.2	95.6	0.3	0.4	3.7
1.8 wt% $PdFe/Al_2O_3$	298	98.6	94.5	4.1	0.5	0.9
1.8 wt% $PdSn/Al_2O_3$	298	87.8	98.6	0.7	0.7	-

modified in such a way that the hydrogenolysis reaction is somewhat suppressed. The hydrogenolysis reaction requires an ensemble of Pd atoms, however, it is probable that deposition of carbon on the Pd surface causes a dilution in the number of Pd ensembles active for the hydrogenolysis reaction, therefore a decrease in the formation of n-butane with increasing time on stream would be expected. These results, therefore, confirm the high activity of Pd towards hydrogenation of olefinic double bonds, and poor activity for hydrogenation of a carbonyl group. As discussed by Delbecq and Sautet the likely reason for this is related to the adsorption of the unsaturated aldehyde on the Pd surface through both double bonds and the C=C bond is hydrogenated in preference to the C=O bond for thermodynamic reasons [28].

Bimetallic catalysts

The $PdFe/Al_2O_3$ data at 298 K are displayed in Figure 4.14 and Table 4.7. Total conversion is observed during the first 60 min of the reaction then the conversion decreases slightly and thereafter remains steady at 97-99 %. The order of selectivity is shown below:

butyraldehyde >> butanol ~ crotyl alcohol ~ n-butane

Selectivity to butyraldehyde is > 95 % for the greater part of the test and selectivity to the unsaturated alcohol is less than 1 %, similar to the results obtained from the parent monometallic catalyst. One difference between the

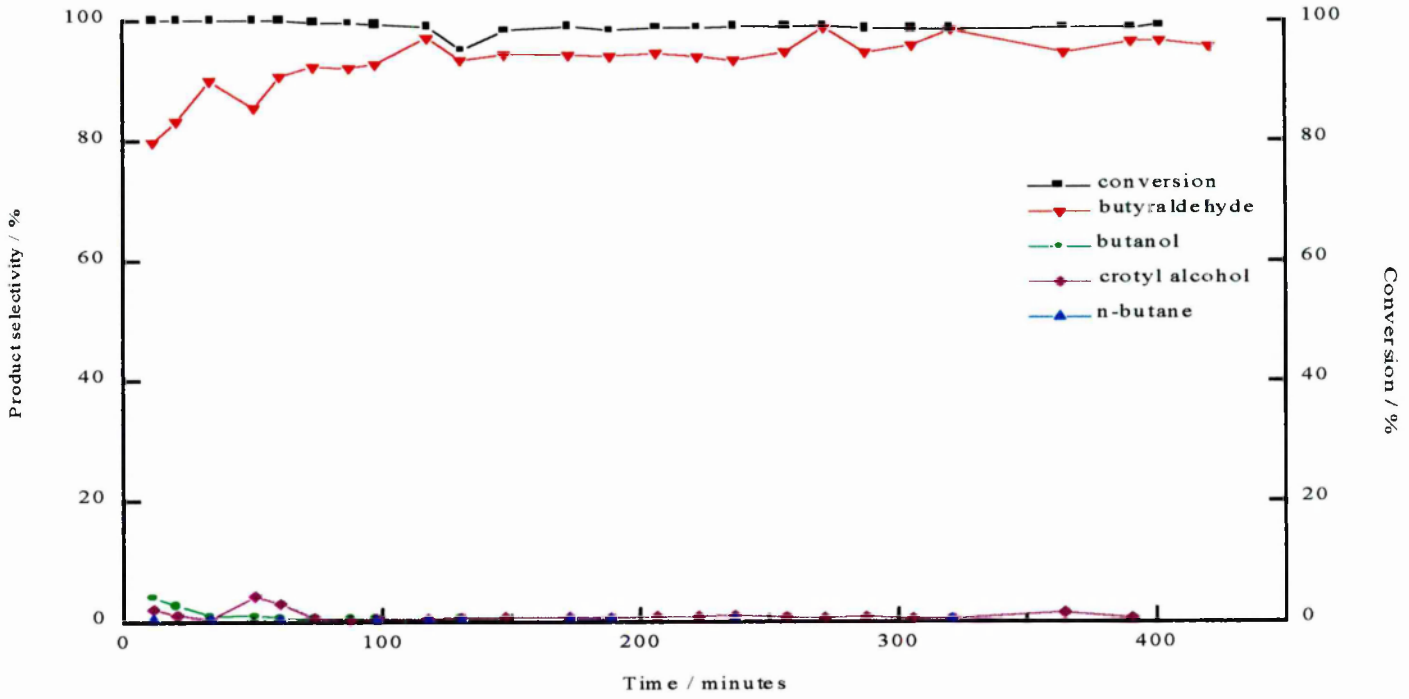

Figure 4.14 Data obtained from hydrogenation of crotonaldehyde hydrogenation over 1.8 wt% $PdFe/Al_2O_3$ catalyst at 298 K displaying product selectivity and crotonaldehyde conversion versus time on stream.

monometallic catalyst and the Fe modified bimetallic catalyst is the lower yield of n-butane formed on the bimetallic catalyst, which can be explained by a site isolation phenomena in which the Fe partitions the Pd surface into smaller Pd ensembles as discussed above for the Pt-based catalysts. It can also be seen that the yield of butanol is marginally higher on the bimetallic catalyst than the monometallic catalyst, which indicates that addition of Fe slightly increases the rate of hydrogenation of the C=O group.

Again at these high conversions the slight differences in selectivity are not that very informative due to secondary effects. The theoretical study by Delbecq and Sautet, discussed earlier, also considered the adsorption of crotonaldehyde on a PdFe surface [28]. They state that upon addition of Fe to Pd the adsorption of the C=O bond is enhanced but the C=C is also stabilized so the adsorption mode involving both double bonds would still be preferred and hence the C=C bond would still be hydrogenated preferentially and so the selectivity to the unsaturated alcohol would not change. The only experimental study of the hydrogenation of unsaturated aldehydes over PdFe catalysts was by Aramendía *et al.* which involved the liquid phase hydrogenation of citral [40]. It was found that the activity/selectivity varied with the $Pd/Fe^{\delta+}$ ratio. It should be noted that this study involved the addition of a solution of $FeCl_2$ into a liquid phase batch reactor containing the reduced Pd catalyst rather than a bimetallic catalyst prepared by a traditional technique. Hence, the extent of the interaction between the Pd and Fe is uncertain. However, a model, similar to that suggested for the Pt

bimetallic catalysts, is proposed whereby unreduced $Fe^{\delta+}$ located on the Pd surface activates the carbonyl bond for hydrogenation. The maximum selectivity to the unsaturated alcohol is about 35 % and occurs at a Pd/Fe^{2+} ratio close to unity. Hence the study by Aramendía *et al.* indicates that the presence of unreduced $Fe^{\delta+}$ on the surface of Pd can increase the selectivity to the unsaturated alcohol in the case of the liquid phase hydrogenation of citral. In the present work no such enhancement is observed however due to differences between the two studies, this is perhaps not surprising.

The selectivity and conversion data at 298 K for the 1.8 wt% $PdSn/Al_2O_3$ catalyst are shown in Figure 4.15 and Table 4.7. The conversion of crotonaldehyde decreases with time on stream, from initially almost 100 % to ca. 75 % after 480 min. The selectivity to butyraldehyde is > 98 % for the major part of the test. The selectivity to the other products is thus less than 2 % and n-butane is not formed after ca. 160 min. Again selectivity to the products obtained from hydrogenation of the carbonyl group is very low. No reports of hydrogenation of unsaturated aldehydes over PdSn catalysts have been found in the literature.

To summarise, the Pd-based catalysts are characterised by high conversion of crotonaldehyde with high selectivity to butyraldehyde and low selectivity to crotyl alcohol and butanol. The three Pd catalysts display similar activity although the PdSn deactivates at a faster rate than the Pd monometallic and PdFe catalysts. These results clearly show that the hydrogenation of the C=C bond is

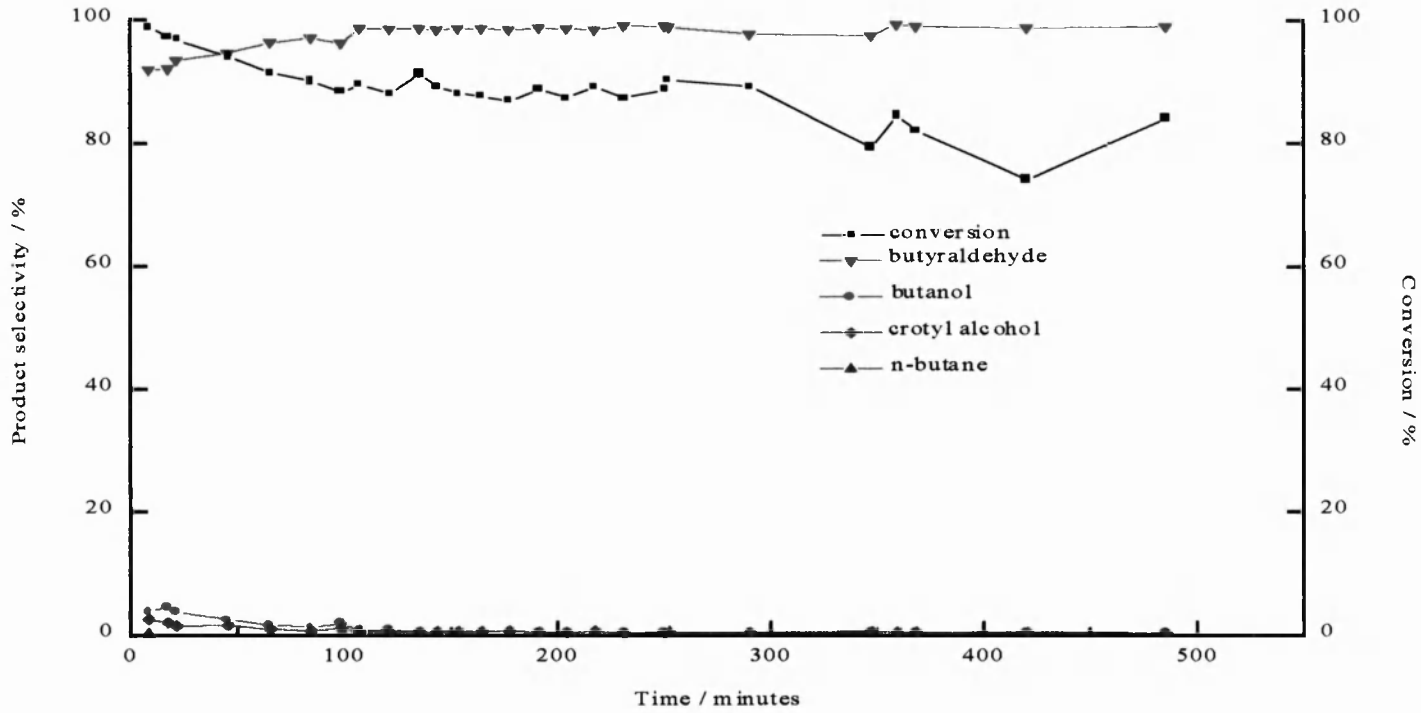

Figure 4.15 Data obtained from hydrogenation of crotonaldehyde over 1.8 wt% $PdSn/Al_2O_3$ catalyst at 298 K displaying product selectivity and crotonaldehyde conversion versus time on stream.

much more favourable compared to the hydrogenation of the C=O group on the Pd catalysts. These results are in agreement with previous literature studies concerning the hydrogenation of olefinic and carbonyl groups on Pd catalysts. Addition of Fe or Sn to the monometallic Pd catalyst does not increase the yield of the unsaturated alcohol under our conditions. The only difference observed upon addition of Fe or Sn to the Pd/Al_2O_3 catalyst is a decreased yield of the hydrogenolysis product (n-butane) and the reason for this is discussed above. It would have been preferable to have studied the selectivities at lower conversions than were achieved here although for the reasons discussed above this was not possible.

4.3.4 Conclusions

Crotonaldehyde hydrogenation has been studied over Pt and Pd based catalysts and the main conclusions include:-

i) For the Pt catalyst the activity and selectivity was modified by addition of Fe or Sn, most noticeable by a significant decrease in the yield of n-butane. A slight increase in the overall activity of the bimetallics was also observed as well as an increased yield of butanol and crotyl alcohol. The suppression of n-butane formation over the bimetallic catalysts is attributed to a traditional site isolation phenomena and the increased hydrogenation of the carbonyl group to enhanced adsorption of crotonaldehyde through the carbonyl group due to

electronic effects. The increased activity of the bimetallics may be due to either electronic or geometric effects.

ii) The data for the Pd-based catalysts are all very similar and characterised by high conversion and high selectivity to butyraldehyde. This reflects the fundamental ability of Pd to hydrogenate olefin bonds in preference to carbonyl bonds. This also serves to indicate that the mode of adsorption of crotonaldehyde on the monometallic catalyst is not significantly altered by addition of Fe or Sn to the surface of the Pd catalyst.

4.4 References

1 Goetz, J., Murzin, D. Y., and Touroude, R. A., *Ind. Eng. Chem. Res.* **35**, 703 (1996).

2 Bond, G. C., Webb, G., Wells, P. B., and Winterbottom, J. M., *J. Chem. Soc.* 3218 (1965).

3 Joice, B. J., Rooney, J. J., Wells, P. B., and Wilson, G. R., *Discuss. Faraday Soc.* **41**, 223 (1966).

4 Ouchaib, T., Massardier, J., and Renouprez, A., *J. Catal.* **119**, 517 (1989).

5 Boitiaux, J. P., Cosyns, J., and Robert, E., *Appl. Cat.* **35**, 193 (1987).

6 Smith, L. B., and Massintil, J. L., *J. Am. Chem. Soc.* **83**, 4301 (1961).

7 Bertolini, J.-C., Cassuto, A., Jugnet, Y., Massardier, J., Tardy, B., and Tourillon, G., *Surf. Sci.* **349**, 88 (1996).

8 Sautet, P., and Paul., J. F., *Catal. Lett.* **9**, 245 (1991).

9 Boitiaux, J. P., Cosyns, J., and Vasudevan, S., *Appl. Cat.* **6**, 41 (1983).

10 Boitiaux, J. P., Cosyns, J., and Robert, E., *Appl. Cat.* **32**, 169 (1987).

11 Borgna, A., Moraweck, B., Massardier, J., and Renouprez, A. J., *J. Catal.* **128**, 99 (1991).

12 Noupa, C., Rousset, J. L., Tardy, B., and Bertolini, J. C., *Catal. Lett.* **22**, 197 (1993).

13 Farrauto, R. J., and Bartholomew, C. H., "Fundamentals of Industrial Processes." Blackie Academic and Professional, London, 1997.

14 Sarkany, A., Zsoldos, Z., Furlong, B., Hightower, J. W., and Guczi, L., *J. Catal.* **141**, 566 (1993).

15 Den Hartog, A. J., Deng, M., Jongerius, F., and Ponec, V., *J. Mol. Cat.* **60**, 99 (1990).

16 Jackson, S. D., Casey, N. J., and Huntington, I. J., *Stud. Surf. Sci. Catal.* **88**, 313 (1994).

17 Miura, H., Terasaka, M., Oki, K., and Matsuda, T., *in* "New Frontiers in Catalysis, Proc. 10th Int. Con. Cat." (L. Guczi, *.et al.*, Eds.), p2379, Elsevier Science Publishers, 1993.

18 Furlong, B. K., Hightower, J. W., Chan,T. Y-L., Sarkany, A., and Guczi, L., *Appl. Cat. A: Gen.* **117**, 41 (1994).

19 Pereira, M. M., Noronha, F. B., and Schmal, M., *Catal. Today* **16**, 407 (1993).

20 Bauer, K., and Garbe, D., *in* "Common Fragrance and Flavour Materials." VCH, New York, 1985.

21 Rylander, P., "Catalytic Hydrogenation over Platinum Metals." Academic Press, New York, 1967.

22 Gallezot, P., and Richard, D., *Science and Technology* **47**, 283 (1994).

23 Englisch, M., Jentys, A., and Lercher, J. A., *J. Catal.* **166**, 25 (1997).

24 Chaikin, S. W., and Brown, W. G., *J. Am. Chem. Soc.* **71**, 122 (1949).

25 Hotta, K., *J. Mol. Cat.* **29**, 105 (1985).

26 Coloma, F., Sepúlveda-Escribano, A., Fierro, J. L. G., and Rodríguez-Reinoso, *Appl. Cat. A: Gen.* **148**, 63 (1996).

27 Ponec, V., *Appl. Cat. A: Gen.* **149**, 27 (1997).

28 Delbecq, F., and Sautet, P., *J. Catal.* **152**, 217 (1995).

29 Tuley, W. F., and Adams, R., *J. Am. Chem. Soc.* **47**, 3061 (1925).

30 Englisch, M., Ranade, V. S., and Lercher, J. A., *J. Mol. Cat. A: Chem.* **121**, 69 (1997).

31 Marinello, T. B. L. W., Nabuurs, S., and Ponec, V., *J. Catal.* **151**, 431 (1995).

32 Goupil, D., Fouilloux, P., and Maurel, R., *React. Kinet. Catal. Lett.* **35**, 185 (1987).

33 Richard, D., Ockelford, J., Giroir-Fendler, and Gallezot, P., *Catal. Lett.* **3**, 53 (1989).

34 Delbecq, F., and Sautet, P., *J. Catal.* **164**, 152 (1996).

35 Beccat, P., Bertolini, J. C., Gauthier, Y., Massardier, J., and Ruiz, P., *J. Catal.* **126**, 451 (1990).

36 Marinelli, T. B. L. W., and Ponec, V., *J. Catal.* **156**, 51 (1995).

37 Poltarzewski, Z., Galvagno, S., Pietropaola, R., and Staiti, P., *J. Catal.* **102,** 190 (1986).

38 Galvagno, S., Poltarzewski, Z., Donato, A., Neri, G., and Pietropaolo, R., *J. Mol. Cat.* **35**, 365 (1986).

39 Neri, G., Donato, A., Milone, C., Pitropaolo, R., and Schwank, J., *Mater. Chem. Phys.* **44**, 145 (1996).

40 Aramendía, M. A., Borau, V., Jiménez, C., Marinas, J. M., Porras, A., and Urbano, F. J., *J. Catal.* **172**, 46 (1997).

CHAPTER 5

Preparation, characterisation and testing of carbon supported PtSn bimetallic catalysts

5.1 Introduction

This chapter will consider the application of surface organometallic chemistry to modify a 'real' catalyst (19.1 wt% Pt/C) used as an electrocatalyst for the hydrogen-oxygen solid polymer fuel cell. A comparison of a PtSn/C catalyst prepared using SOMC will be made with a catalyst with a similar loading prepared using a more traditional hydrolysis/precipitation route. In addition, the effect of varying the $Sn/Pt_{surface}$ ratio on the catalyst properties will also be considered. This work is also of fundamental interest as it involves expanding the SOMC method to higher loadings and a different support than have previously been reported.

The preparation of these catalysts by SOMC will be considered only briefly as the technique was considered in detail for lower loaded alumina supported catalysts in Chapter 3. The main bulk of this chapter will concentrate on characterisation and evaluation of the catalysts using a variety of techniques of which CO stripping cyclic voltammetry is perhaps the most interesting.

Background

The development of fuel cells for transportation is a current major technical challenge for scientists and engineers, particularly in light of increasingly stringent legislation requiring substantial decreases in emissions from vehicles.

Fuel cells offer a number of benefits as an alternative to the internal petrol combustion engine, including low or even zero emissions, higher efficiency and reliability. One fuel cell which is particularly well suited for transportation is the hydrogen-oxygen solid polymer fuel cell (SPFC). The basic components of a SPFC fuel cell are shown in Figure 5.1 [1].

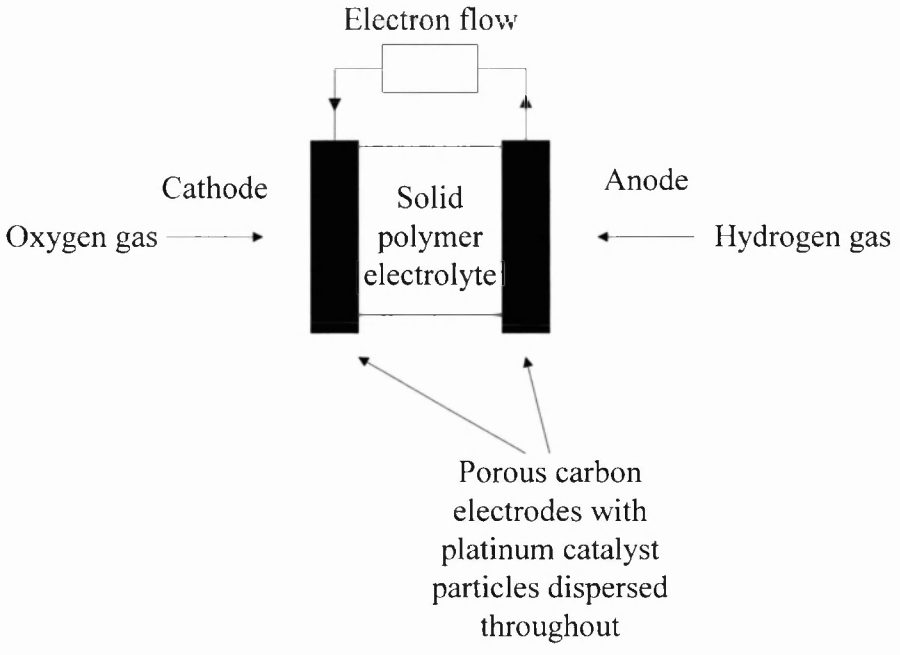

Figure 5.1 Schematic diagram of the basic construction of a solid polymer fuel cell.

The fuel cell consists of a porous carbon anode and cathode impregnated with platinum particles, linked by a load, and separated by an electrolytic polymer membrane. It operates on the principle of producing power, in the form of electricity, by combining oxygen and hydrogen to form water, in the reverse reaction of the electrolysis of water. If clean sources of H_2 and O_2 are available it

is possible, using a catalyst, to combine the two gases efficiently.

When an acid electrolyte is used, hydrogen gas dissociates at the anode to form protons (H^+) and an equal number of electrons (e^-) (5.1):

$$H_2 \rightarrow 2H^+ + 2e^- \qquad (5.1)$$

The electrons flow through an external load from the anode to cathode where they react with oxygen (O_2) and water (H_2O), from the electrolyte, to form hydroxyl ions (OH^-) (5.2):

$$\tfrac{1}{2}\, O_2 + H_2O + 2e^- \rightarrow 2OH^- \qquad (5.2)$$

The protons formed in reaction (5.1) pass through the electrolytic membrane, combining with the OH^- anions (formed in reaction (5.2)), in the electrolyte, to form water, with the overall reaction (5.3):

$$H_2 + \tfrac{1}{2}\, O_2 \rightarrow H_2O \qquad (5.3)$$

However, before vehicles powered by fuel cells become a commercial reality several technical problems must be overcome. One of the ongoing areas to be addressed is the CO tolerance of the anode electrocatalyst [2]. As the storage and distribution of hydrogen is complex it is likely that the anode fuel will be

provided by on-board generation of hydrogen through the reforming of hydrocarbons such as methanol [3]. The reformate typically contains 20-25 % CO_2 and small amounts of CO (1-2.5 %). Although further processing can reduce the CO content in the anode fuel stream to ten's of ppm [4], even at these levels the platinum electrocatalyst needed to catalyse the anodic fuel cell reaction is sensitive to poisoning at the operating temperature (353 K) of the fuel cell resulting in degradation of the fuel cell performance [5]. CO is preferentially adsorbed at these temperatures blocking the access of hydrogen to the catalyst surface. A possible solution to the problem is to bleed low levels of O_2 into the CO-containing H_2 feedstream [6] however this leads to loss of efficiency. A more sophisticated approach is to design a CO tolerant electrocatalyst capable of operating in the presence of at least 100 ppm of CO. In the development of such reformate tolerant hydrogen oxidation catalysts a key aspect is to maximise the number of hydrogen oxidation sites while minimising the CO coverage of the surface. Research efforts have concentrated on modifying the platinum catalyst by the addition of a second metal or metal oxide. One approach would be to alloy the Pt with an element which enhances the activity of the Pt for electrooxidation of CO, forming CO_2 which does not poison the electrode. A number of elements form alloys with Pt such as Ru [7] and Sn [8, 9] and these elements have been examined in the literature for this potential application. PtRu alloy catalysts have been shown to alleviate the substantial deactivation observed by platinum electrodes in the presence of small concentrations of CO. However, at higher concentrations of CO, competitive adsorption between OH and CO on

the Ru surface, results in a requirement for higher potentials for CO electrooxidation. Hence an alloying element which does not adsorb CO, so that CO adsorption does not interfere with OH_{ads}, is sought. In this respect PtSn catalysts may appear as an appropriate combination since CO is not adsorbed on Sn [10]. Indeed, Gasteiger *et al.* found that polycrystalline Pt_3Sn alloys display activity for CO electrooxidation four orders of magnitude greater than pure Pt [9]. They postulated that the high activity of Pt_3Sn was due to a unique state of CO_{ad} adsorbed on Pt sites adjacent to Sn atoms and the ability of Sn atoms to activate water at low potentials. It is clear that intimate contact between the Pt and Ru or Pt and Sn appears to be vital. Other reformate tolerant catalysts reported in the literature include Pt catalysts promoted with SnO_2 or WO_3 [11]. These oxide doped catalysts also promote the electrochemical oxidation of CO and again it is important that the Pt and metal oxide are in intimate contact.

The rate determining step appears to be the chemisorption and activation of H_2O on the promoter in close proximity to adsorbed CO. The reaction is believed to proceed as follows (5.4):

$$CO + H_2O \rightarrow CO_2 + 2H^+ + 2e^- \qquad (5.4)$$

On pure Pt, competitive adsorption of CO and H_2O results in negligible H_2O coverage's at low potentials. Thus promoters which are less susceptible to CO adsorption but able to adsorb water are sought.

5.2 Characterisation of the carbon supported platinum (Pt/C) monometallic catalyst

Before the tin doped catalysts are discussed it is first necessary to describe the properties of the 'parent' monometallic platinum catalyst supported on carbon (Vulcan XC-72R). The Pt/C catalyst was kindly prepared and supplied by Johnson Matthey (JM). A brief description of the patented preparation procedure was given in Chapter 2, Section 2.1.1 and the appropriate patent reference listed. The loading of the active metal was 19.1 wt% as determined by ICP-AES. The following sections describe the results from the characterisation of the Pt/C catalyst. The electrochemical data presented below was collected at the Johnson Matthey Technology centre (JMTC).

5.2.1 X-ray powder diffraction

The XRD powder pattern of the 19.1 wt% Pt/C catalyst scanned from $0° < 2\theta < 70°$ is shown in Figure 5.2 (a) with that of the carbon support (b) shown for comparison. It can clearly be seen that additional reflections are observed in the Pt/C sample and these were matched to metallic Pt according to the JCPDS file 4-0802. The three main reflections originate from the crystal planes Pt(111), Pt(200) and Pt(220). Other planes would be expected to be present at $2\theta > 70°$ (not scanned). Therefore it is evident that the Pt exists as the metal in air at room temperature although it is expected that the surface Pt atoms will be oxidised,

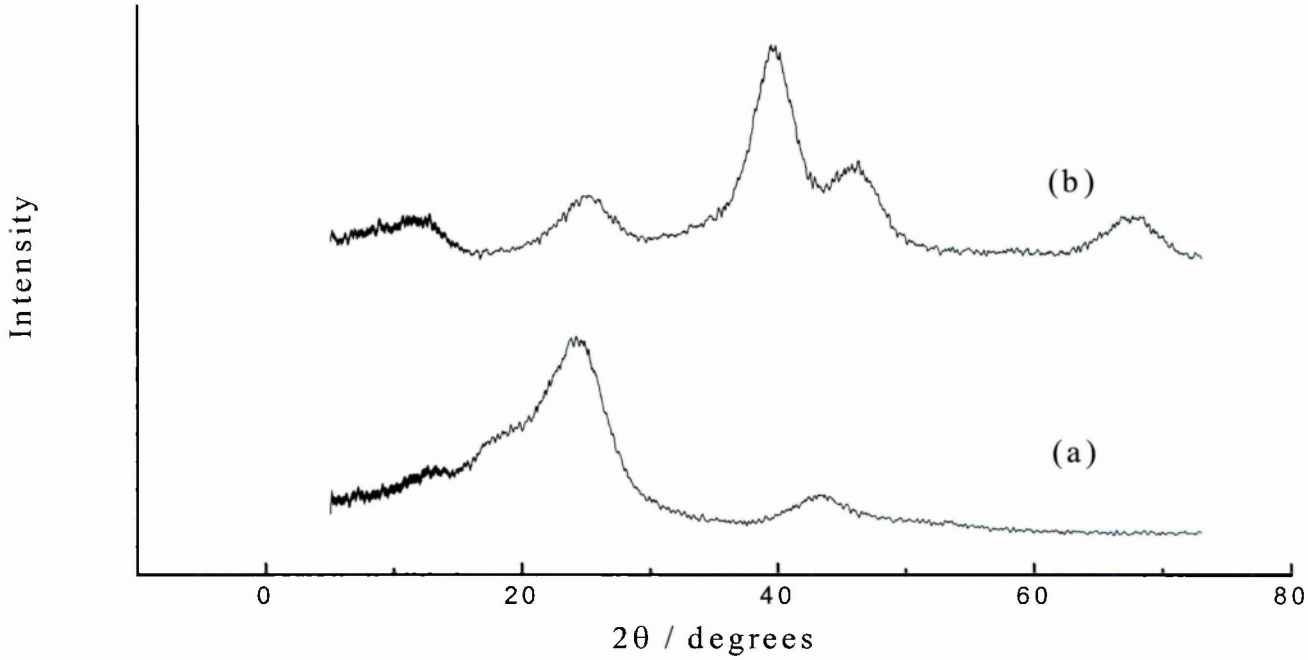

Figure 5.2 XRD powder patterns of (a) carbon support as supplied by JMTC, (b) 19.1 wt% Pt/C monometallic catalyst as supplied by JMTC.

PtO_x.

The average platinum particle size was calculated from its XRD powder pattern using the Scherrer equation [12] (equation 5.5):

$$D = \frac{K\lambda}{\beta \cos\theta} \tag{5.5}$$

where D is the mean crystallite size, K is a constant (which is approximately equal to unity), λ is the wavelength of the X-rays, β is the X-ray diffraction broadening (determined by measuring the peak width at half maximum height) and θ is the angle of reflection of the peak observed.

The Pt(111) reflection with 2θ equal to 39.26° was used, giving a value of 1.9 nm. This is in reasonable agreement with the value of 2.2 nm determined by XRD at Johnson Matthey.

5.2.2 Transmission electron microscopy

A representative electron micrograph of the 19.1 wt% Pt/C catalyst is shown in Figure 5.3. The magnification was 200 000 x and the small Pt particles are easily distinguishable from the carbon support.

The particle size distribution, obtained after counting over 200 particles, is shown in the histogram in Figure 5.4.

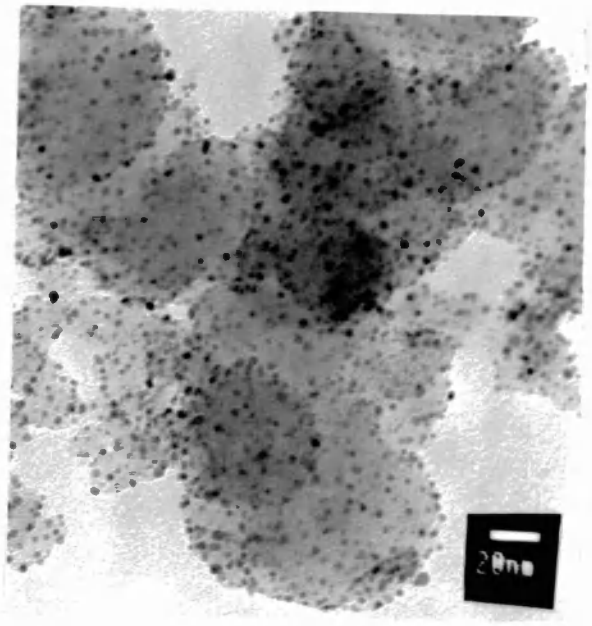

Figure 5.3 Representative electron micrograph of 19.1 wt% Pt/C catalyst.

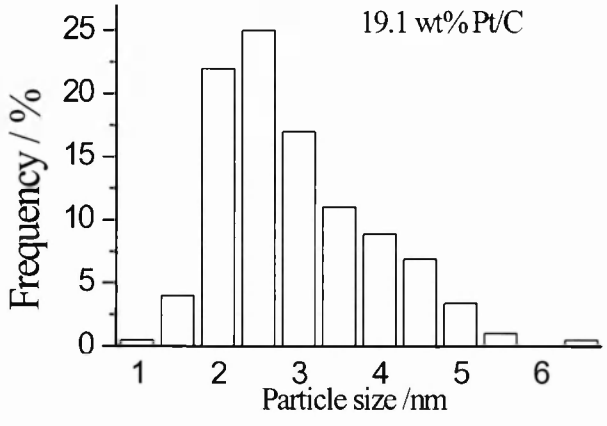

Figure 5.4 Particle size distribution of 19.1 wt% Pt/C catalyst.

From the analysis of the electron micrographs and the resulting particle size distribution, the average particle size ϕ_{AV} is calculated using equation (5.6):

$$\phi_{AV} = \frac{\sum_i n_i \phi_i}{\sum_i n_i} \tag{5.6}$$

where n_i is the number of particles with diameter ϕ_i.

The average particle size calculated using equation (5.6), is 3.2 nm. This is higher than both the value of 2.2 nm obtained by TEM at JMTC (although the particle size range observed is identical (1-6 nm)) and the value of 1.9 nm determined at the OU using XRD. Considering the particle size distribution shown in Figure 5.4 it can be seen that relatively few particles were observed below 2 nm. Since particles smaller than 2 nm are difficult to observe it suggests that the measurement process used at the OU is biased towards larger particles explaining the larger particle size obtained by TEM at the OU.

5.2.3 Hydrogen and carbon monoxide chemisorption

Both hydrogen and carbon monoxide chemisorption have been used to determine the dispersion of the 19.1 wt% Pt/C monometallic catalyst. The H_2 and CO chemisorption data (Table 5.1) generated from Pt/C catalyst agree well (0.27 for CO data, 0.28 for H_2 data) giving a value for the fraction of metal atoms exposed at the surface as 28 % (rounded up).

Table 5.1 H_2 and CO chemisorption data for 19.1 wt% Pt/C catalyst.

Catalyst	H/M	Amount H_2 adsorbed / moles (x 10^{-5})	CO/M	Amount CO adsorbed / moles (x 10^{-5})	CO:H ratio
Pt/C	0.27	1.17	0.28	2.33	1.98

A value for the average particle size can be determined from the dispersion values using the volume-area mean diameter (d_{va}) which is related to the dispersion, D, as shown in equation (5.7) [13]:

$$d_{va} = \frac{6\left(V_m / a_m\right)}{D} \qquad (5.7)$$

where a_m is the effective average area occupied by a metal atom in the surface and V_m is the volume per metal atom in bulk. For Pt the value quoted in the literature for 6 (V_m/a_m) is 1.13 nm [14]. A value for the volume average mean diameter of 4.2 nm is obtained using this technique which is approximately double the particle size obtained using the XRD data. Errors from the assumptions made in both equations may however be significant.

5.2.4 Electrochemical evaluation

The CO stripping voltammogram for the 19.1 wt% monometallic Pt/C catalyst is displayed in Figure 5.5. Cycle 1 is the CO electrooxidation cycle and cycle 2 shows the results from the LPSCV experiment between 0 and 1.2 V. Each cycle will be discussed in turn and the relevant features of the voltammogram highlighted.

i) Cycle 1 shows the CO electrooxidation peak at about 0.7-0.8 V and integration of this peak gives the CO adsorption charge (CO_{ox}) (Table 5.2) which can be expressed in terms of the number of surface Pt atoms and hence dispersion (if the initial loading is known). The sharp well defined peak indicates that CO oxidation occurs over a narrow potential range. The peak maximum occurs at 0.79 V which agrees well with the potential found in the literature for CO oxidation on Pt catalysts [15]. It should also be noted that the absence of current in the anodic scan (area of voltammogram with $I > 0$), in the region associated with H_{ads} oxidation in the CO stripping cycle, indicates that all the Pt adsorption sites are occupied by CO and no hydrogen is adsorbed [16].

ii) At the start of cycle 2 at 0 V, it is assumed that Pt is in the zero valent state. Increasing the potential, in the anodic sweep, two peak maxima can be observed, although not well defined, in the H oxidation region between 0 and 0.4 V. These correspond to the removal of weakly and strongly adsorbed hydrogen. This is followed by the region known as the double layer region.

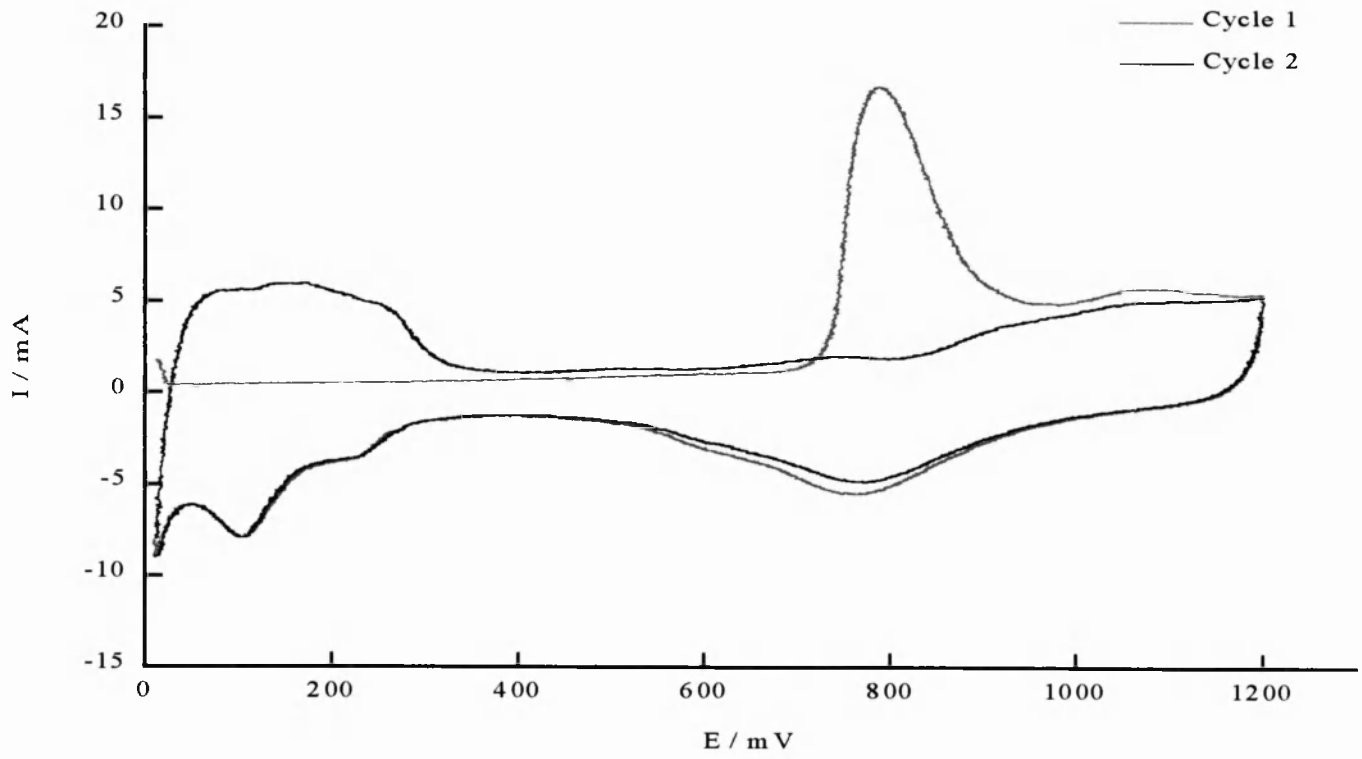

Figure 5.5 CO stripping voltammogram (Cycle 1) of 19.1 wt% Pt/C catalyst in 1 M H_2SO_4 followed by one cycle of linear potential sweep voltammetry (Cycle 2) at 10 msV^{-1} at 303 K.

Finally, oxidation of the surface Pt is indicated by the charge between 0.9 and 1.2 V resulting in the formation of PtO_x (believed to be about two thirds of monolayer) [17].

The cathodic region (area of voltammogram with $I < 0$) is dominated by the reduction of the PtO_x surface overlayer at about 0.9 to 0.6 V (although not at the opposite potential to that corresponding to oxidation of the Pt) followed by redeposition of H on the surface of the Pt between 0.4 and 0 V. Clearly, Pt reduction can be seen to be take place in two stages as indicated by the two peaks in this region which, as previously discussed, are attributed to strongly and weakly bound hydrogen. However, no third, intermediate, hydrogen adsorption is observed, as might be expected from comparable literature reports. The hydrogen coverage in region I varies from a monolayer coverage at 0 V to zero at about 0.4 V.

The major difference between this voltammogram and that of polycrystalline platinum is a loss of definition, for example, the distinction between the different H adsorbed species is not so clear. This reflects the less well defined surface for the Pt/C catalyst. The nature of the carbon support will also affect the appearance of the voltammogram [18] although since the same support was used throughout variation due to the support between this and the doped catalysts should not arise.

Integration of the hydride adsorption region (the area on the cathodic scan

between 0.35 and 0.05 V) also gives a charge (Table 5.2) which can be interpreted as a surface area and hence dispersion (if initial Pt loading is known). Note, that two potential cycles were made after the initial CO electrooxidation sweep and that the charge of the hydride region was integrated for each cycle, although only the first cycle is displayed in Figure 5.5 for clarity.

Table 5.2 Data from cyclic voltammetry experiments of 19.1 wt% Pt/C monometallic catalyst.

CO_{ox} charge / mC cm^{-2}	H_{ads} charge (1^{st}cycle) / mC cm^{-2}	H_{ads} charge (2^{nd} cycle) / mC cm^{-2}	CO:H charge ratio
141.5	72.4	73.3	1.95:1.00 1.93:1.00

A CO:H charge ratio of 2 is expected when one considers the stoichiometry of adsorption of CO and H_2, assuming that all Pt surface sites adsorb equally and that the adsorption of Pt:CO and Pt:H in both cases is 1:1. This ratio is indeed observed (within experimental error) for the monometallic Pt/C catalyst (Table 5.2). It should also be noted that the CO:H ratio for the Pt/C catalyst obtained from both chemisorption (Table 5.1) and CV are in good agreement. Using the CV charge data to calculate the dispersion, a value of 45 % is obtained, which in turn gives an average measure of diameter of 2.5 nm. These values clearly do not agree with those derived from the gas adsorption experiments, repeated in Table

5.3 with the average particle size values estimated from the XRD and TEM data.

The mean diameter derived from the CV is, however, closer in line with the values obtained from the electron microscopy and XRD measurements. This might suggest that the dispersion value obtained by CV gives a more accurate indication of the metal dispersion than that obtained from the gas adsorption experiments. Such a difference may be due to the more severe conditions used in the chemisorption experiment, such as outgassing at 523 K under dynamic vacuum, followed by reduction at 473 K, which may promote sintering of the Pt crystallites. Kuster *et al.* compared the Pt particle size in a Pt/graphite catalyst by CO chemisorption and TEM and also found that the diameter derived from the chemisorption technique was greater than the diameter estimated from TEM measurements [19]. They state that this may be due to the assumption made in the chemisorption procedure that the particles are hemispherical and that the assumed stoichiometry of CO adsorption on Pt particles may be incorrect for small particles. On the other hand, Marin *et al.* in a comparison of the two techniques concluded that CV provides a more accurate measure of particle size than CO chemisorption, although they generally found reasonable agreement between the two [18].

Table 5.3 Physical property data for 19.1 wt% Pt/C catalyst supplied by JMTC. Column JM displays data collected at JMTC and column OU displays data obtained at the Open University.

Physical Property	OU	JM
Average XRD crystallite size / nm	1.9	2.2
Dispersion[1]	0.28	0.45
d_{va}[2] / nm	4.2	2.5
Average TEM particle size / nm	3.2	2.2
Particle size distribution / nm	1-6	1-6

Notes. [1]. Dispersion value derived by JM on basis of electrochemical results and at OU by CO and H_2 gas chemisorption data. [2]. Volume area mean diameter derived from dispersion data using equation (5.7).

5.3 Carbon supported platinum tin (PtSn/C) bimetallic catalysts

5.3.1 The PtSn/C catalysts: Preparation

A range of catalysts of different Sn loadings were prepared from the parent Pt/C catalyst using SOMC and are listed in Table 5.4. The precursor used was $Sn(C_4H_9)_4$. Descriptions of the experimental procedure and the chemistry

involved, can be found in Chapter 2 and Chapter 3, respectively, and are not repeated here. In addition, results for a PtSn/C catalyst prepared at Johnson Matthey by a hydrolysis/precipitation reaction are also included.

Table 5.4 Pt mono- and bi-metallic catalysts supported on carbon.

Catalyst	Coverage of Sn / ML	Assay / wt% Pt	Assay / wt% Sn	Theoretical / wt% Sn	Pt:Sn atomic ratio
Pt/C[1]	-	19.1	-	-	-
PtSn/C[1]	-	18.2	2.5	-	4.46:1
0.33 PtSn/C[2]	0.33	18.7	1.6	1.6	6.98:1
0.5 PtSn/C[2]	0.5	18.7	2.1	2.4	5.44:1
0.75 PtSn/C[2]	0.75	17.6	3.6	3.6	2.99:1
1 PtSn/C[2]	1	17.6	4.6	4.8	2.32:1

Notes. [1]. Prepared at JMTC by hydrolysis / precipitation traditional method.

[2]. Tin added using surface organometallic chemistry.

Using the SOMC reaction different coverage's of Pt by Sn were achieved by varying the quantity of $Sn(C_4H_9)_4$ introduced to the monometallic catalyst. A dispersion value of 45 % was used for the monometallic catalyst in the calculation of the volume of organometallic precursor added. For ease of identification, the bimetallic catalysts prepared by SOMC will, hereafter, be

designated by the nominal monolayer coverage (ML) of the second metal. For example, 0.5 PtSn/C represents the bimetallic catalyst prepared by modification of the 19.1 wt% Pt/C catalyst with addition of sufficient $Sn(C_4H_9)_4$ to give half a monolayer (0.5 ML) coverage of the Pt. Also note, that after preparation of the PtSn/C catalysts it was necessary to expose the catalysts to air. Since the Sn is believed to be oxidised the bimetallic catalysts should be described, more correctly, as $PtSnO_x/C$ species rather than PtSn/C, however, for simplicity the latter designation will be used.

Before any discussion of the preparation and characterisation of the PtSn/C catalysts are presented it is first necessary to establish whether Sn can be deposited on a sample of Pt-free carbon support using $Sn(C_4H_9)_4$ under the reaction conditions typically used in the SOMC reaction.

5.3.2 Reaction of n-tetrabutyl tin with carbon support

A SOMC preparation procedure was used to deposit Sn onto a sample of Pt-free support. A sample of the carbon support was reduced in the normal manner (473 K, 3 h, flow 100 cm^3 min^{-1} H_2) and 100 μl $Sn(C_4H_9)_4$ in heptane added. The sample was then allowed to react for 48 h under hydrogen, initially at room temperature then at 353-363 K for 8 h. This preparation route was identical to the procedure used to prepare the bimetallic catalysts by SOMC. As discussed in Chapter 3 the mechanism postulated for the SOMC reaction involves a selective

reaction between the organometallic species, in our case $Sn(C_4H_9)_4$, and hydrogen preadsorbed on the surface of the parent metal. It has previously been established that no reaction occurs between $Sn(C_4H_9)_4$ and alumina support under our reaction conditions. Establishing whether the organometallic species will be deposited on the support in the absence of the parent metal is fundamental to understanding the reaction and its mechanism for the Pt catalyst supported on carbon.

A guide to the course of the reaction is gained from analysis of the gases exiting the reactor. It was observed that butane was evolved for the initial 1-2 hours of the reaction which suggests some reaction has occurred with hydrogenolysis of the butyl groups. Thereafter, only a small amount of butyl groups were observed in the gas phase, even after heating to 353-363 K.

The catalyst was then washed in heptane to remove any unreacted $Sn(C_4H_9)_4$. The amount of Sn added would correspond, if it was all deposited on the carbon support, to 4.5 % by weight of the support. The XRD powder pattern of this sample is shown in Figure 5.6 (a) with that of the support (b). Clearly no additional features are present in the XRD pattern of the carbon support after reaction with the $Sn(C_4H_9)_4$ when compared with that of the carbon support alone, although this does not exclude the presence of a highly dispersed tin phase. TEM/EDX analysis of the sample also failed to show the presence of Sn particles on the support. However, ICP-AES analysis revealed the presence of 1.15 wt%

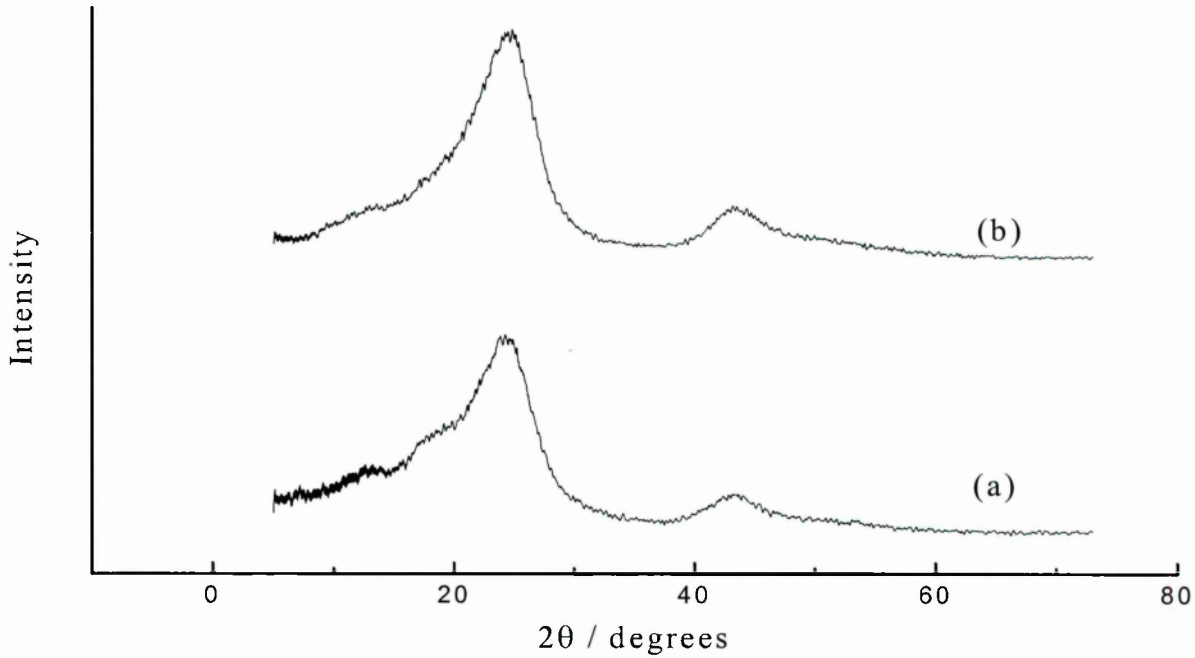

Figure 5.6 XRD powder patterns of (a) carbon support as supplied by JMTC, (b) carbon support after reaction with $Sn(C_4H_9)_4$.

Sn. This corresponds to a deposition of about a quarter of the Sn available. Assuming that all the unreacted Sn had been removed, it appears that the $Sn(C_4H_9)_4$ has reacted to a limited extent with the carbon support. This may not be surprising when one considers the surface of the support. The organometallic precursor, $Sn(C_4H_9)_4$, requires sites on the carbon support for the hydrogenolysis of a Sn-C bond. The reduced surface may have oxygenated organic groups on the surface such as carbonyl groups or phenolic groups and some of these may assist in the deposition of $Sn(C_4H_9)_4$. However, considering that only a quarter of the available Sn is deposited this would indicate that either i) the number of the sites available for deposition is small or ii) the reaction between the $Sn(C_4H_9)_4$ and the support is slow and has a high activation energy. That the reaction was mainly confined to the first few hours of reaction might suggest the existence of a finite number of sites on the surface suitable for reaction with $Sn(C_4H_9)_4$ which are consumed within the first few hours of reaction. It is also possible that the Sn precursor was deposited intact on the support surface and was not removed during the washing process and Sn was then deposited during the reduction procedure.

5.3.3 Characterisation of PtSn/C catalysts by traditional methods

The data for the assay/wt% Sn and the theoretical/wt% Sn for the PtSn/C bimetallic catalysts are displayed in Table 5.4. It can be seen that in general there is good agreement between the two values. The general agreement between the

theoretical and actual loadings indicate that no loss of Sn occurs during the preparation of PtSn/C bimetallic catalysts by SOMC.

In this section the results from the characterisation of the PtSn catalysts prepared using SOMC will be presented. In the following section the results from the electrochemical evaluation of the catalysts will be presented. It should be noted that there was an insufficient quantity of each of the PtSn/C catalysts available to allow characterisation of each sample by the range of traditional techniques (XRD, TEM and chemisorption) used in this work. The following sections will therefore discuss the data gained from each technique for the applicable catalysts.

5.3.3.1 X-ray powder diffraction

The XRD powder patterns of the carbon support, Pt/C monometallic catalyst and the PtSn/C bimetallic catalysts with coverage's of 0.33 and 0.5 are shown in Figure 5.7. Clearly no additional reflections are observed on comparing the monometallic and bimetallic catalysts, indicating that the Sn from the organometallic precursor has been deposited on the catalyst in a highly dispersed form. If the proposed mechanism for the deposition of the Sn on the surface of the Pt catalyst is correct, in that the Sn is deposited homogeneously on the surface of the Pt particles in a layer one atom thick, then one would not expect this phase to be observed by XRD.

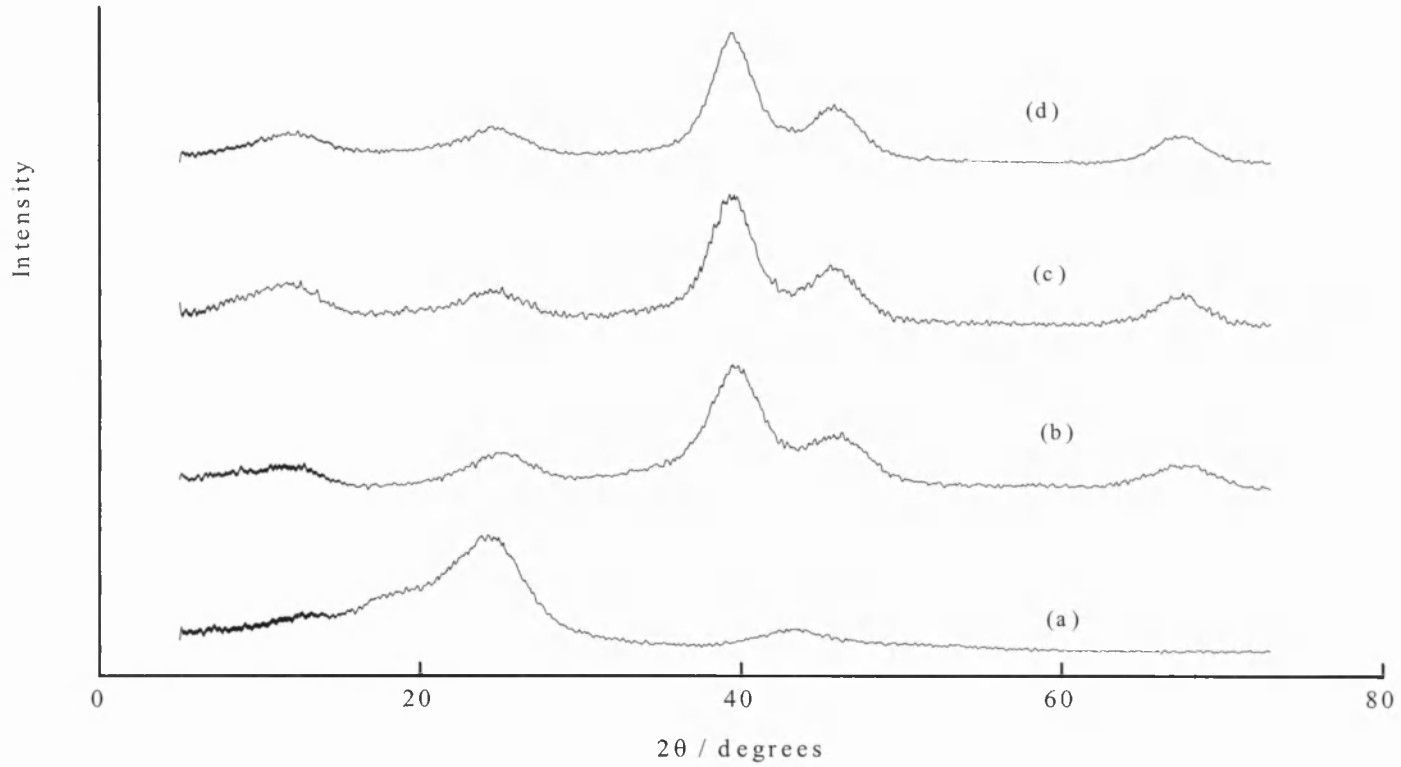

Figure 5.7 XRD powder patterns of (a) carbon support, (b) 19.1 wt% Pt/C monometallic catalyst, (c) 0.33 PtSn/C, and (d) 0.5 PtSn/C.

The average crystallite size for the bimetallic catalysts examined by XRD has been determined using the Scherrer equation (5.5) and these results are given in Table 5.5 together with the Pt/C data.

Table 5.5 Results from calculation of mean particle size using the Scherrer equation for Pt/C and a selection of PtSn/C catalysts.

Catalyst	D / nm
Pt/C	1.9
0.33 PtSn/C	2.5
0.5 PtSn/C	2.7

Clearly an increase in the mean particle size is observed upon depositing Sn on the surface of the Pt particles, when compared to the Pt/C monometallic catalyst. Furthermore, as the coverage of the second metal increases, the particle size also increases.

5.3.3.2 *Transmission electron microscopy and energy dispersive X-ray analysis*

A representative electron micrograph for each of the PtSn/C bimetallic catalysts prepared by SOMC - with the exception of the 0.5 PtSn/C - are shown in Figures 5.8 to 5.10. The particle size distribution estimated for each catalyst are shown

Figure 5.8 Representative electron micrograph of 0.33 ML PtSn/C catalyst.

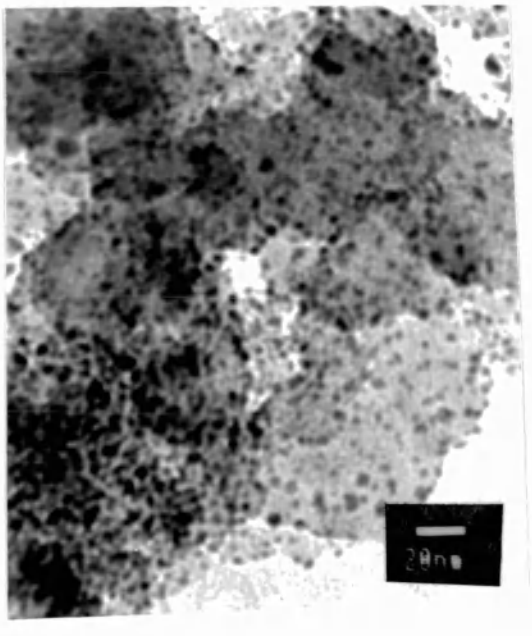

Figure 5.9 Representative electron micrograph of 0.75 ML PtSn/C catalyst.

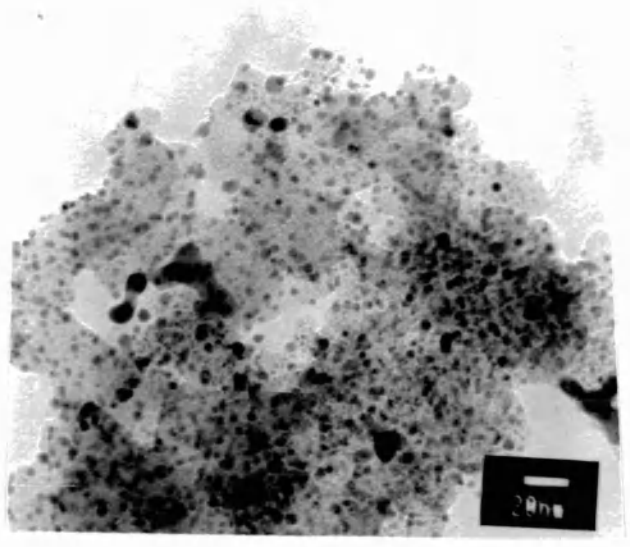

Figure 5.10 Representative electron micrograph of 1 ML PtSn/C catalyst.

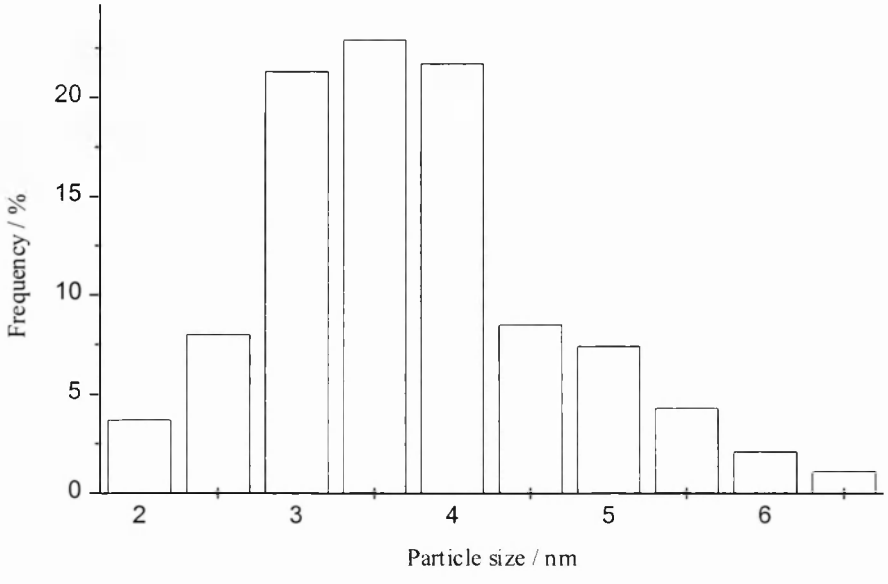

Figure 5.11 Particle size distribution of 0.33 ML PtSn/C catalyst.

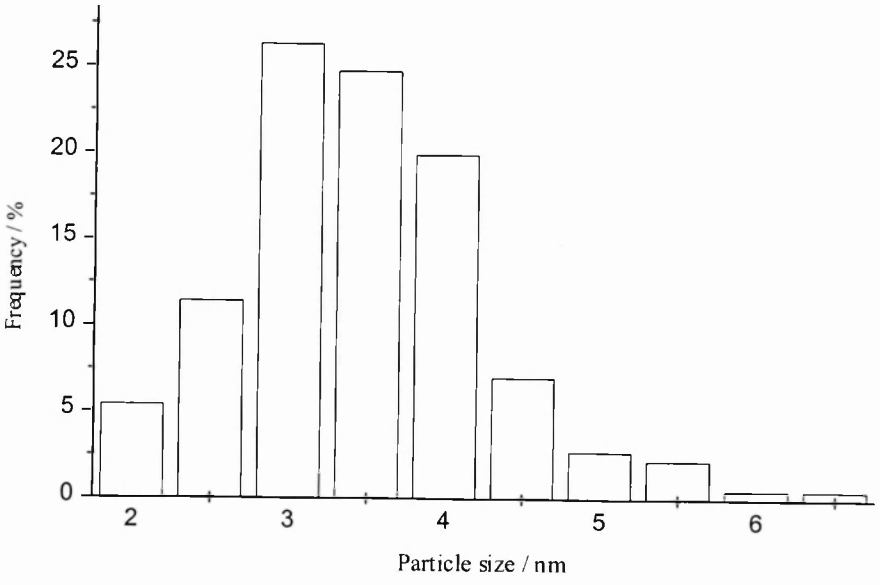

Figure 5.12 Particle size distribution of 0.75 ML PtSn/C catalyst.

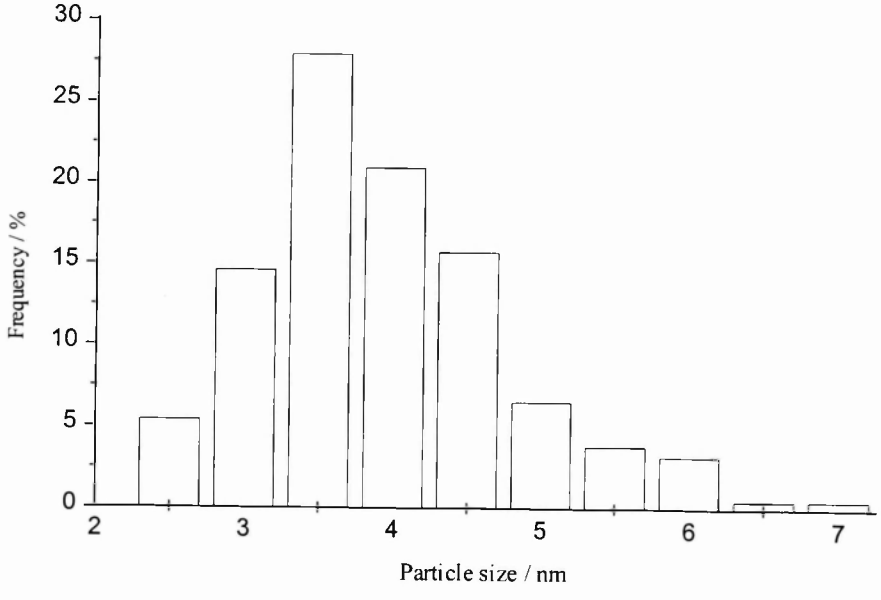

Figure 5.13 Particle size distribution of 1 ML PtSn/C catalyst.

in Figures 5.11 to 5.13. In general, the catalyst samples appear, by visual inspection, to be very similar with most of the particles being spherical in nature. The average particle size for each sample was estimated using equation (5.6) calculated, after measuring at least 200 particles, and the results presented in Table 5.6.

Table 5.6 Particle size analysis calculated from TEM for PtSn/C catalysts with various Sn coverage's.

Catalyst	Particle Size distribution / nm	Mean Particle Size / nm
Pt/C	1-6	3.2
0.33 ML PtSn/C	2-6	3.4
0.75 ML PtSn/C	2-6	3.7
1 ML PtSn/C	2-7	4.1

Clearly an increase in particle size of the bimetallic catalysts compared with the monometallic 19.1 wt% Pt/C (mean particle size 3.2 nm determined by TEM at OU or 2.2 nm determined by TEM at JMTC) is identified. For each of the catalysts the particle size distribution is narrow and the majority of particles are within 1 nm of the average particle size. It is also apparent that the increase in particle size is greater for higher coverage's of Sn which would be expected as more tin is being put down. Plotting the average particle size determined by

TEM in Figure 5.14 against the nominal tin coverage, an almost linear relationship is observed.

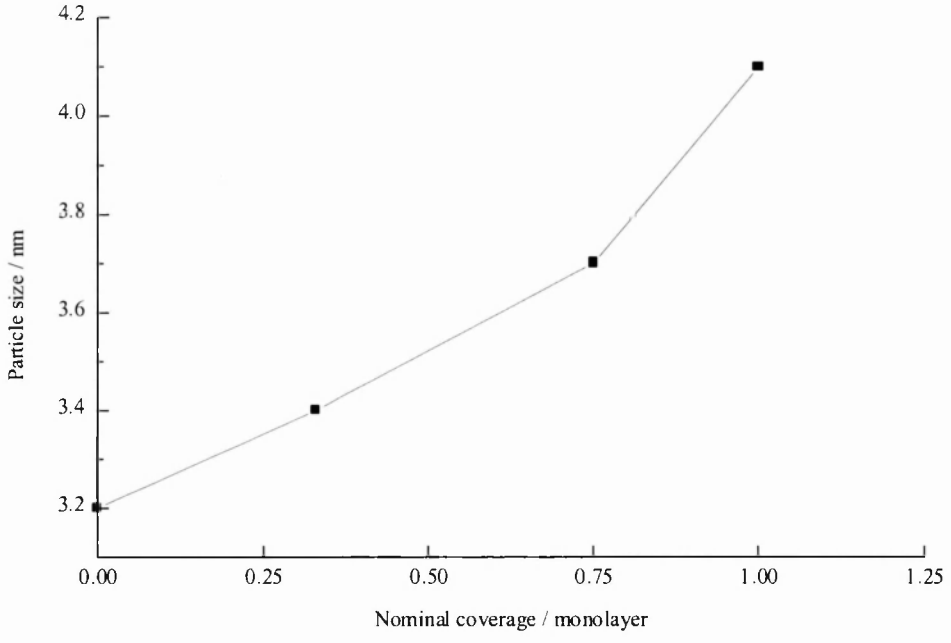

Figure 5.14 Comparison of particle size of PtSn/C catalysts with different monolayer coverage's as determined by TEM

Comparing the average crystallite size estimated by XRD (Table 5.5) with the particle size determined by TEM, in all cases the TEM value is larger than that obtained by XRD. It has already been stated that the average particle size of the monometallic catalyst measured by TEM at the OU is greater than the value obtained at JMTC and the value calculated using XRD. This is believed to be due to an inherent bias in the measurement process used at the OU to determine particle size. However, even if the actual values are a little high, the trend

showing an increase in particle size with coverage is still valid.

Coq *et al.* reported, by TEM analysis, an increase in particle size from 2.8 nm for a Pd monometallic catalyst to 3.4 nm for a PdSn bimetallic catalyst prepared by SOMC. They claim this increase in particle size corresponds to the addition of an atomic monolayer of the second metal to the Pd particles [20]. Similarly, Candy *et al.* observed an increase from 1.4 nm to 2.2 nm in the case of a $RhSn/SiO_2$ catalyst prepared by addition of $Sn(C_4H_9)_4$ to Rh/SiO [21]. In our case an increase from 3.2 nm to 4.1 nm was observed by TEM measurements for addition of nominally a monolayer of Sn to Pt/C which clearly is in line with these two reports.

EDX analysis of different areas of each catalyst was carried out. The EDX analysis from the 0.75 ML PtSn/C catalyst is shown below in Figure 5.15. This was obtained by reducing the size of the beam so that it focused on a single metal particle. The presence of Pt and Sn in the same metal particle can clearly be seen. This EDX spectrum was reproduced on analysing another particle. Significantly no isolated Sn (or SnO_x) particles were observed on the catalyst surface, which suggests that the Sn deposited on the Pt/C is preferentially deposited on the Pt particles rather than on the C support. The absence of any evidence for Sn on the support by EDX analysis does not exclude the possibility that some of the Sn was deposited on the support below detection limits of the technique.

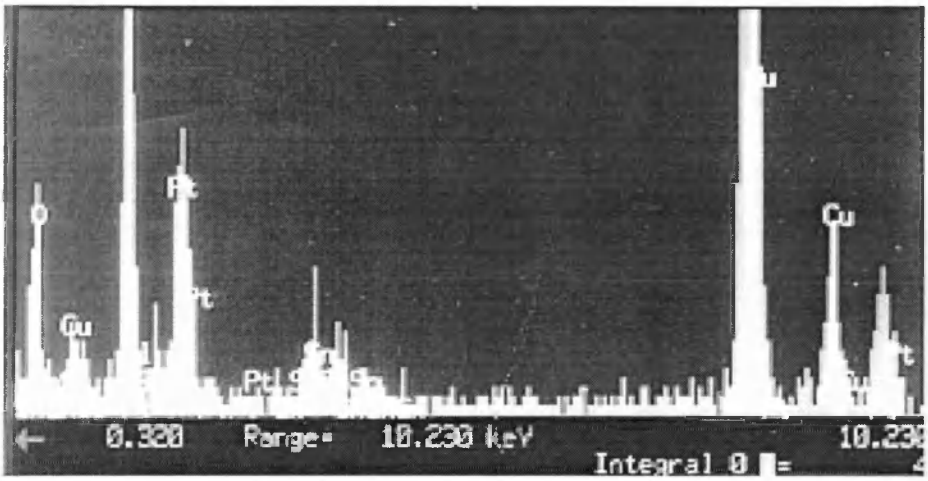

Figure 5.15 EDX analysis one metal particle contained in 0.75 PtSn/C catalyst.

Similar EDX spectra were obtained by analysis of the 1 ML catalyst. It was not possible, however, to confirm the presence of bimetallic particles in the case of 0.33 PtSn/C, probably due to the low Sn loading.

5.3.3.3 Hydrogen and carbon monoxide chemisorption

Both H_2 and CO chemisorption have been used to determine the dispersion of the PtSn/C bimetallic catalysts. The H_2 and CO chemisorption data for these catalysts is presented in Table 5.7 with the corresponding data for the carbon support and the 19.1 wt% Pt/C monometallic catalyst.

Table 5.7 H_2 and CO chemisorption results for carbon support, Pt/C and PtSn/C catalysts.

Catalyst	H/M	Amount H_2 adsorbed / moles H_2 (x 10^{-5})	CO/M	Amount CO adsorbed / moles CO (x 10^{-5})	CO:H
Carbon support	-	0	-	0.045	-
Pt/C	0.27	1.17	0.28	2.33	1.98
0.33 PtSn/C	0.15	0.68	0.16	1.43	2.08
0.75 PtSn/C	0.07	0.35	0.12	1.29	3.69
1 PtSn/C	0.09	0.54	0.11	1.26	2.33

It was confirmed that the carbon support did not adsorb H_2 and only a negligible volume of CO was chemisorbed under our conditions. Furthermore, it is well known that Sn does not adsorb H_2 or CO [10]. The H_2/CO chemisorbed can, therefore, be attributed to the Pt metal particles present at the catalyst surface.

The CO and H_2 chemisorption results are plotted in Figure 5.16 for the different catalysts.

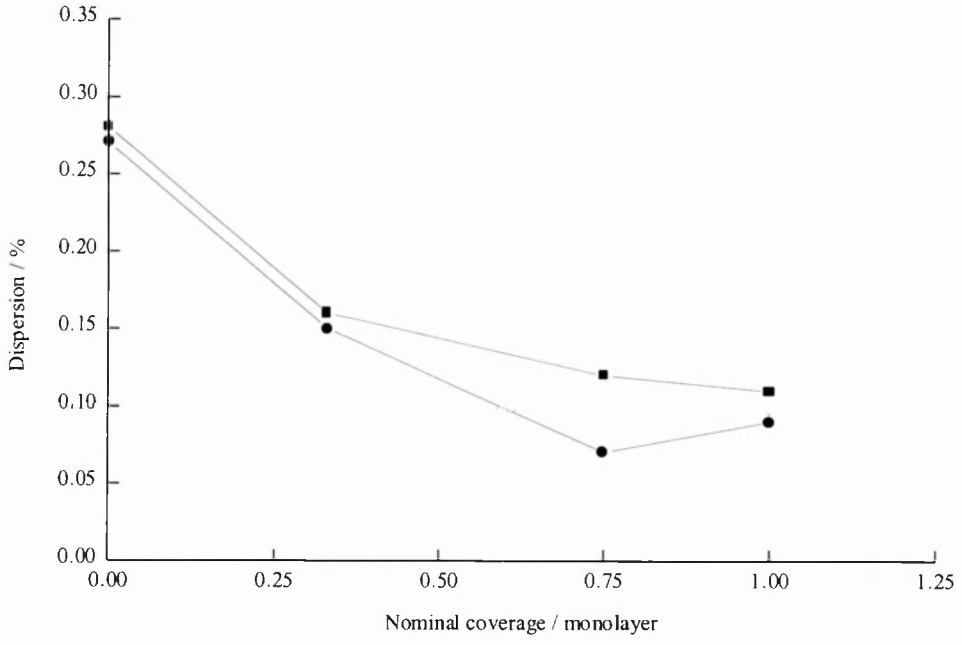

Figure 5.16 Comparison of dispersion values for the PtSn/C catalysts determined by H_2 (circles) and CO chemisorption (squares).

It can be seen that, in general, the dispersion values for the PtSn/C catalysts with different coverage's are generally in reasonable agreement for the two chemisorption methods, with the exception of the 0.75 ML sample. This is reflected in the ratio of the number of moles of CO adsorbed to the number of moles of H_2 adsorbed by the catalyst (CO:H) given in the final column in Table 5.7. The chemisorption data indicates a CO:H ratio greater than 2 for the PtSn/C catalysts at higher Sn coverage's. The exceptionally high value observed for the 0.75 ML catalyst may be due to a smaller uptake of H_2 than expected and unfortunately due to time constraints it was not possible to repeat the hydrogen chemisorption on this sample. A low adsorption of H_2 compared to CO has

previously been observed on PtSn catalysts, e.g., [22], and Vannice *et al.* noted that hydrogen adsorption on $PtSn/Al_2O_3$ was significantly suppressed compared to the Pt/Al_2O_3 catalyst [23] and Sn has even been described as a 'drastic poison' for the hydrogen adsorption on Pt catalysts [24]. It has been speculated that the reason for this may be due to an ensemble effect of the Sn on the surface of the Pt particles [10]. Assuming that dissociative adsorption of H_2 requires the presence of two adjacent Pt atoms, it was shown that increasing the interatomic distance between Pt atoms decreases the H_2 adsorption. Similarly deposition of Sn on the Pt surface is envisaged to isolate Pt atoms from each other, increasing the Pt-Pt distance and thus decreasing the H_2 adsorption. CO adsorption requires only one Pt atom so therefore will not be affected by isolation of Pt atoms.

A general trend is clear with the amount of H_2 or CO adsorbed by the catalysts decreasing as the tin content increases. The obvious explanation is that the Sn is preferentially deposited on the surface of the Pt covering some of the H_2 or CO adsorption sites. It is clear from inspection of Figure 5.16 that addition of a small amount of Sn (0.33 ML) results in a sharp decrease in the volume of H_2 or CO adsorbed. Further addition of Sn causes a further decrease in the dispersion, until a plateau is reached at about 10 % dispersion. At this point further addition of Sn only causes a slight decrease in the dispersion. At the nominal monolayer coverage about 10 % of the surface Pt sites are still available for H_2 and CO adsorption.

These results are in agreement with the results of Candy *et al.* where a comparison was made of CO chemisorption data obtained from a series of RhSn catalysts prepared by SOMC [21]. They also observed a sharp decrease in the volume of CO chemisorbed after addition of small amounts of Sn, followed by a plateau at higher loadings. They found that at nominal Sn coverage of a monolayer almost 30 % of the Rh was still accessible to CO.

Note, a decrease in dispersion could also be attributed to other effects. In particular an increase in particle size (i.e. sintering) would result in a smaller ratio of surface atoms to the total number of atoms, that is, a decrease in dispersion. However, it is believed that under the conditions experienced during the preparation of the bimetallic catalysts, no significant sintering occurs. Measurement of metal particle size by TEM and XRD indicates that the increase in particle size required for the observed decrease in dispersion is not realised. Indeed, it was shown in Chapter 3, that no increase in particle size was observed after subjecting a Pd/Al_2O_3 catalyst to the reaction conditions used in the SOMC reaction. Another possible reason for a decrease in CO and H_2 adsorbed would be the existence of a strong metal support interaction [25]. However, this is not thought to be important here due to the low temperature of the reduction and the nature of the support (as discussed in Chapter 3).

It should be clear that particle size calculations from dispersion data are not valid in the case of bimetallic particles since hydrogen does not adsorb on both

constituent atoms and it is not possible to calculate a value for V_m/a_m (see equation (5.7)) when the exact composition of the particles is not known.

5.3.4 Characterisation of PtSn/C by electrochemical methods

The first section of the electrochemical results (5.3.4.1) will compare two PtSn/C with similar loadings, one prepared using the SOMC method (OU) and the other prepared by a more conventional route (JM). Then a series of PtSn/C catalysts with varying coverage's of Sn - prepared by SOMC - will be discussed (5.3.4.2).

5.3.4.1 Comparison of PtSn/C catalysts prepared by a SOMC route and traditional hydrolysis/precipitation route

Catalysts

For convenience, the assay data of the catalysts that will be discussed here is reproduced in Table 5.8.

Table 5.8 Assay data for two PtSn/C catalysts prepared by different routes.

Catalyst	Assay / wt% Pt	Assay / wt% Sn	Pt:Sn atomic ratio
PtSn/C (OU)	18.7	2.1	5.44:1
PtSn/C (JM)	18.2	2.5	4.46:1

The catalyst designated as PtSn/C (OU) was prepared using SOMC and the coverage of Sn corresponds to nominally 0.5 ML. The catalyst designated PtSn/C (JM) was prepared by a conventional hydrolysis/precipitation method. It can be seen that the JM catalyst has a slightly higher loading of the second metal and therefore a lower Pt:Sn atomic ratio. In this section the analysis of the two PtSn/C catalysts by CV will be presented; no other characterisation techniques were used to compare the two PtSn/C catalysts.

The cyclic voltammograms generated for the PtSn/C (OU) and PtSn/C (JM) catalysts are shown in Figures 5.17 and 5.18. The *onset potential* or the potential at which the CO oxidation reaction was initiated and the position of the CO electrooxidation peak are listed in Table 5.9, together with the values for the Pt/C monometallic catalyst. The CO electrooxidation stripping cycle is shown as cycle 1 and then the second and fifth linear potential sweep cycles (at 10 mV s^{-1}) are also shown.

Table 5.9 Comparison of onset potential and peak position for CO oxidation for Pt/C, and PtSn/C (OU) and PtSn/C (JM) catalysts.

Catalyst	Onset potential / V	Peak position / V
Pt/C	0.70	0.79
PtSn/C (OU)	0.30	0.67
PtSn/C (JM)	0.36	0.67, 0.76

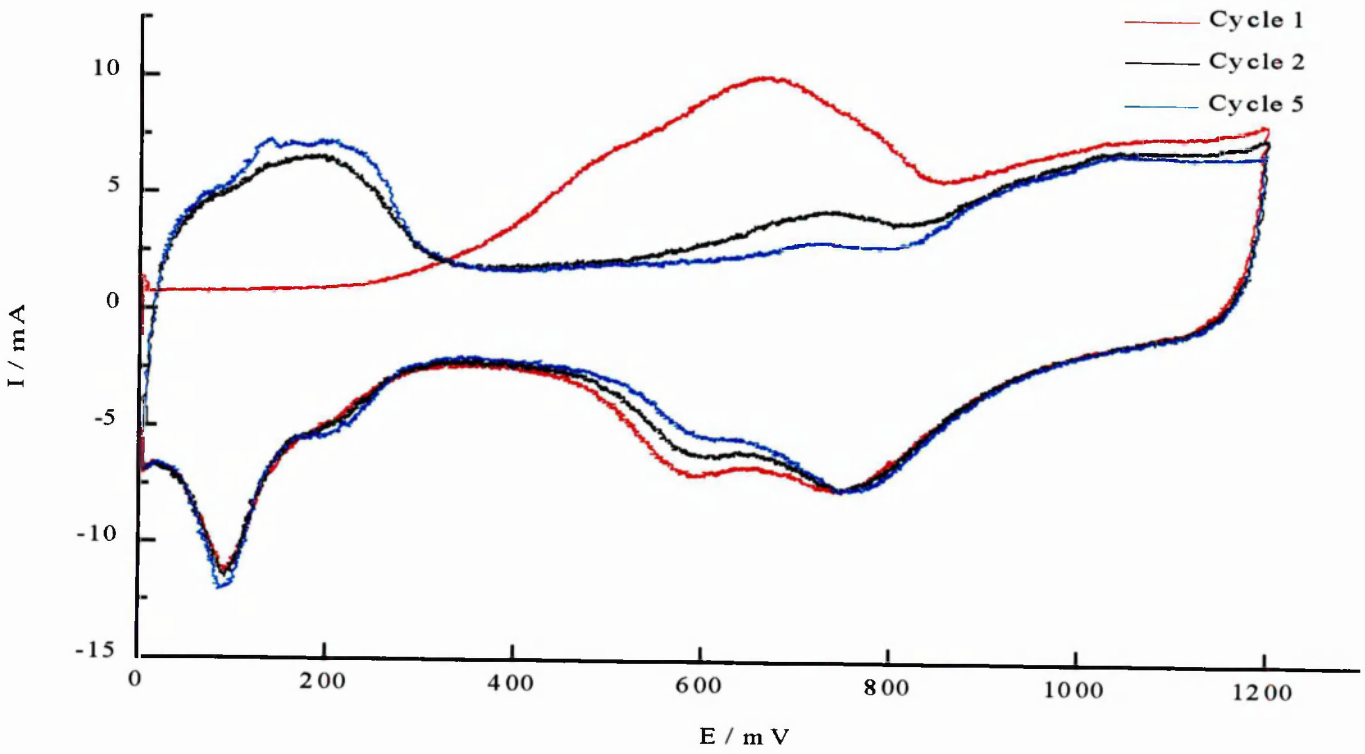

Figure 5.17 CO stripping voltammogram (Cycle 1) of PtSn/C catalyst (OU) in 1 M H_2SO_4 followed by the 2nd and 5th cycle of linear potential sweep voltammetry at 10 mVs^{-1} at 303 K.

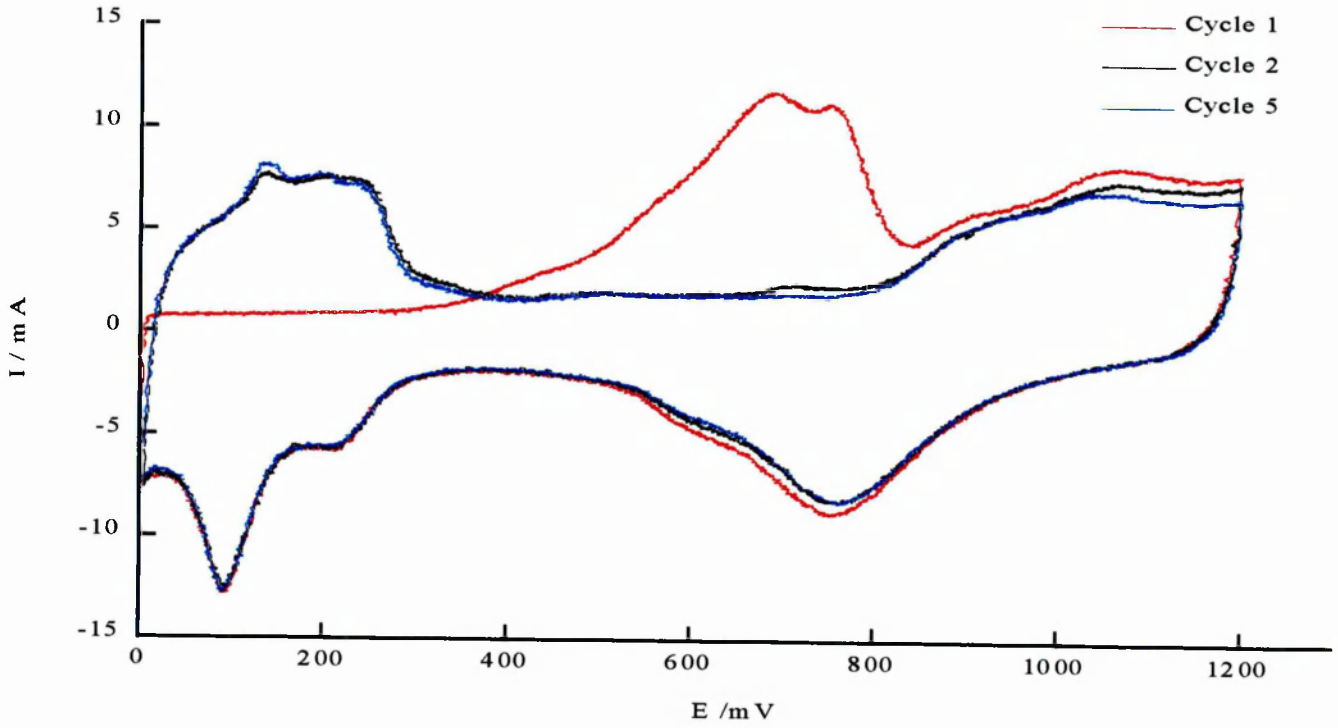

Figure 5.18 CO stripping voltammogram (Cycle 1) of PtSn/C catalyst (JM) in 1 M H_2SO_4 followed by the 2nd and 5th cycle of linear sweep voltammetry a 10 mVs^{-1} at 303 K.

Comparing the voltammograms of the tin doped catalysts (Figures 5.17 and 5.18) with the corresponding voltammogram for the Pt/C catalyst (Figure 5.5) and the data in Table 5.9, a number of differences can be observed.

i) First, it is clear, considering the CO stripping cycle (cycle 1), that both PtSn/C catalysts show enhanced activity for CO electrooxidation compared to the monometallic Pt/C catalyst, with a significant decrease in the onset potential for CO oxidation. Such enhanced activity for CO electroooxidation on PtSn surfaces has previously been reported [8, 9]. Moreover, the CO oxidation envelope is more pronounced at lower potentials for the OU catalyst than the JM catalyst which suggests that CO oxidation is promoted more readily on the OU catalyst than the JM catalyst. A slight shoulder is observed at ca. 0.5 V for the OU catalyst (Figure 5.17) and the interpretation of this shoulder will be discussed later in Section 5.3.4.2. The two peak maxima in the CO oxidation region observed for the JM catalyst have previously been observed on Pt catalysts and are believed to be due to CO oxidation on different crystal faces of Pt [26]. CO will have different strengths of adsorption on the different planes and therefore will require different potentials for oxidation [11].
ii) Second, as might be expected, additional peaks are observed for Sn reduction and oxidation in the potential cycling voltammograms (cycles 2 and 5). In the anodic region, oxidation of the Sn species is observed with a peak at ca. 0.6-0.8 V. This region is more pronounced for the OU catalyst than the JM catalyst. Similarly the SnO_x reduction peak at about 0.5 V in the cathodic

sweep is larger for the OU catalyst than the JM catalyst. These values for Sn/SnO_x oxidation and reduction potentials are in agreement with literature values [18]. Significantly only Sn deposited on the surface of the Pt particles are involved in the electrochemical processes as shown by Marin *et al.* [18], who deposited Sn on Pt-free support and obtained a voltammogram identical to that of the carbon support indicating that isolated Sn species on the support cannot be oxidised or reduced in the range of the voltammogram. This is particularly important in our research and we will assume that observation of electrochemical processes involving Sn species indicates the existence of an interaction between the Sn and Pt. Assuming that only Sn in contact with Pt at the catalyst surface takes part in the processes observed, the larger peaks indicate that more Sn is in contact with the Pt in the OU catalyst than the JM catalyst. This is despite the fact that the loading is actually greater for the JM catalyst. In the case of the OU catalyst it can be noted that from cycles 2-5 that a smaller amount of Sn is reduced in each cycle indicating that Sn is either i) oxidatively removed under these reaction conditions (as might be expected from the literature [22]) or ii) the Sn moves from the surface into the bulk of the Pt particles and therefore will not be available for the surface oxidation- reduction reactions.

iii) Similarly the Pt oxidation and PtO_x reduction areas are smaller for the OU catalyst as would be expected indicating that less of the Pt is accessible to the electrolyte indicating that more of this surface is covered by Sn.

All of these features, noted in i) to iii) above, are observed by inspection and comparison of the different sets of voltammograms, however, it is also possible to quantify these effects. In essence, this involves measurement of the charge transferred to or from the electrode, at various points on the voltammogram. Integration of the peaks associated with CO oxidation and hydride adsorption allows quantitative evaluation of the Pt metal surface area and degree of coverage of the Pt by Sn.

The CO_{ox} and the hydride adsorption charges calculated from the integration of the peaks in the three cycles shown in Figures 5.17 and 5.18 for the OU and JM doped catalysts are shown in Table 5.10. Note that higher charges associated with CO_{ox} and H_{ads} for these tin doped catalysts compared to the corresponding charges quoted in Table 5.2 for the Pt/C monometallic catalyst are due to a higher loading of the platinum on the electrode for these catalysts.

Table 5.10 Cyclic voltammetry results from PtSn/C bimetallic catalysts prepared by OU and JM method.

Catalyst	CO_{ox} charge / mC cm^{-2}	H_{ads} charge (1^{st} cycle) / mC cm^{-2}	H_{ads} charge (2^{nd} cycle) / mC cm^{-2}	H_{ads} charge (5^{th} cycle) / mC cm^{-2}	CO:H charge ratio
PtSn/C (OU)	240.4	106.8	113.8	121.7	2.25:1.00 2.11:1.00 1.98:1.00
PtSn/C (JM)	240.2	121.5	123.3	127.0	1.98:1.00 1.95:1.00 1.89:1.00

Integration of the peak areas associated with the the hydride adsorption reactions gives a charge which can be converted to actual area of surface Pt in $m^2 g^{-1}$, using the relationship (5.8) given below [27].

The number of Pt atoms (N_H^o) is given by:

$$N_H^o = \frac{Q_H^o(\mu C)}{1.6x10^{-13}} \qquad (5.8)$$

where Q_H^o is the amount of charge passed on formation of a monolayer of hydrogen and can be used to calculate the Pt surface area assuming that one Pt atom occupies 7.6 Å or that there is 1.31 x 10^{15} Pt atoms per cm^2. A similar equation exists to calculate the number of Pt atoms from the CO_{ox} charge.

The data obtained using these relationships, using the data from Tables 5.2 (monometallic Pt/C catalyst) and 5.10, is displayed in Table 5.11.

Table 5.11 Real Pt metal area derived from cyclic voltammetry results for Pt/C and PtSn/C catalysts.

Catalyst	Area from H_{ads} area[1] / m^2g^{-1}	Area from CO_{ox} area / m^2g^{-1}
Pt/C	99	96
PtSn/C (OU)	57	63
PtSn/C (JM)	68	65

Note. [1]. H_{ads} calculated from H charge from cycle 1.

It can be seen that both the OU and JM bimetallic catalysts have a lower Pt metal area than the monometallic Pt/C catalyst as would be expected. The OU bimetallic Pt surface area is in fact about one-third lower than that of the monometallic catalyst, although this might be expected to be lower considering

that every second Pt surface atom should be covered by a Sn atom. However, this still indicates that the SOMC reaction is indeed selective with the Sn reacting and depositing only on the Pt surface. Moreover, the OU bimetallic catalyst has a lower Pt surface area than the JM catalyst indicating again that more of the Pt surface is covered by Sn despite the fact that the OU catalyst has a slightly lower loading of Sn (2.1 wt% versus 2.5 wt%). Thus, the data clearly indicates that the OU method of preparing Sn doped Pt/C catalysts using SOMC allows a greater degree of control and is more successful in preparing a catalyst with the two metals in contact with each other.

From Table 5.10 it can be seen that the OU catalyst has a CO:H charge ratio greater than the expected value (2:1) for the first two cycles. The H_{ads} charge increases however as the number of cycles increases to give a CO:H charge ratio 1.98:1.00 for the 5th cycle. Similar results were observed for a second sample of each catalyst. That more hydrogen is adsorbed by the catalyst in each successive cycle further suggests that Sn is being removed from the Pt surface, exposing more Pt during each successive cycle. This can be explained by either oxidation of Sn and dissolution into the electrolytic solution or movement of Sn from the surface into the bulk of the Pt particles thus exposing previously covered Pt. This removal of Sn from the surface may also account for the higher value for the Pt metal area, given in Table 5.11, than was expected. Note also that the increase in H_{ads} is similar in moving from the 1st to the 2nd cycle compared to moving from the 2nd cycle to the 5th cycle. This indicates that some of the Sn is easily removed

from the Pt surface initially then further Sn removal from the surface is much slower. This is probably due to the presence of strong and weakly adsorbed Sn on the Pt surface.

The origin of the CO:H charge ratio of greater than 2 observed for the OU catalyst has previously been discussed in 5.3.3.3 in connection with the observation that gas chemisorption results display a similar CO:H ratio for the PtSn/C catalysts prepared by SOMC. The H_{ads} charge for the JM catalyst increases only slightly over the three cycles displayed indicating that the potential cycling does not expose significant amounts of fresh Pt. The charge ratio is much closer to 2:1 in line with the results from the Pt/C monometallic catalyst.

5.3.4.2 Comparison of PtSn/C catalysts prepared by SOMC with different Sn monolayer coverage's

In an effort to see the effect of coverage with activity a range of catalysts with different nominal coverage's were prepared.

The assay data of the catalysts to be discussed in this section is listed in Table 5.4. Comparison will often be made between the PtSn/C catalysts and the 19.1 wt% Pt/C monometallic catalyst and the data for this and the 0.5 PtSn/C catalyst (designated as PtSn/C (OU) in previous section) will be repeated here where

necessary.

The range of PtSn/C bimetallic catalysts were examined for the CO electrooxidation and subsequent linear potential sweep cyclic voltammetry (LPSCV) experiments. The voltammograms for the 0.33 ML, 0.75 ML, and 1 ML PtSn/C bimetallic catalysts are shown in Figures 5.19 to 5.21 respectively. The corresponding voltammograms for the 19.1 wt% Pt/C and 0.5 PtSn/C catalysts were shown in Figures 5.5 and 5.17. For each voltammogram, the CO electrooxidation stripping cycle and one cycle of linear potential cycling are shown. In the following discussions it should be remembered, firstly, that only atoms on the surface of the particles are involved in the oxidation and reduction procedures and, secondly, only Sn in physical contact with Pt participates in the electrochemical reactions, i.e., no oxidation or reduction of isolated particles of Sn or SnO_x is observed at the potentials used in this work. The onset potentials and CO electrooxidation peak maxima are listed in Table 5.12 for the range of PtSn/C catalysts, with the data for the monometallic catalyst and 0.5 PtSn/C catalyst.

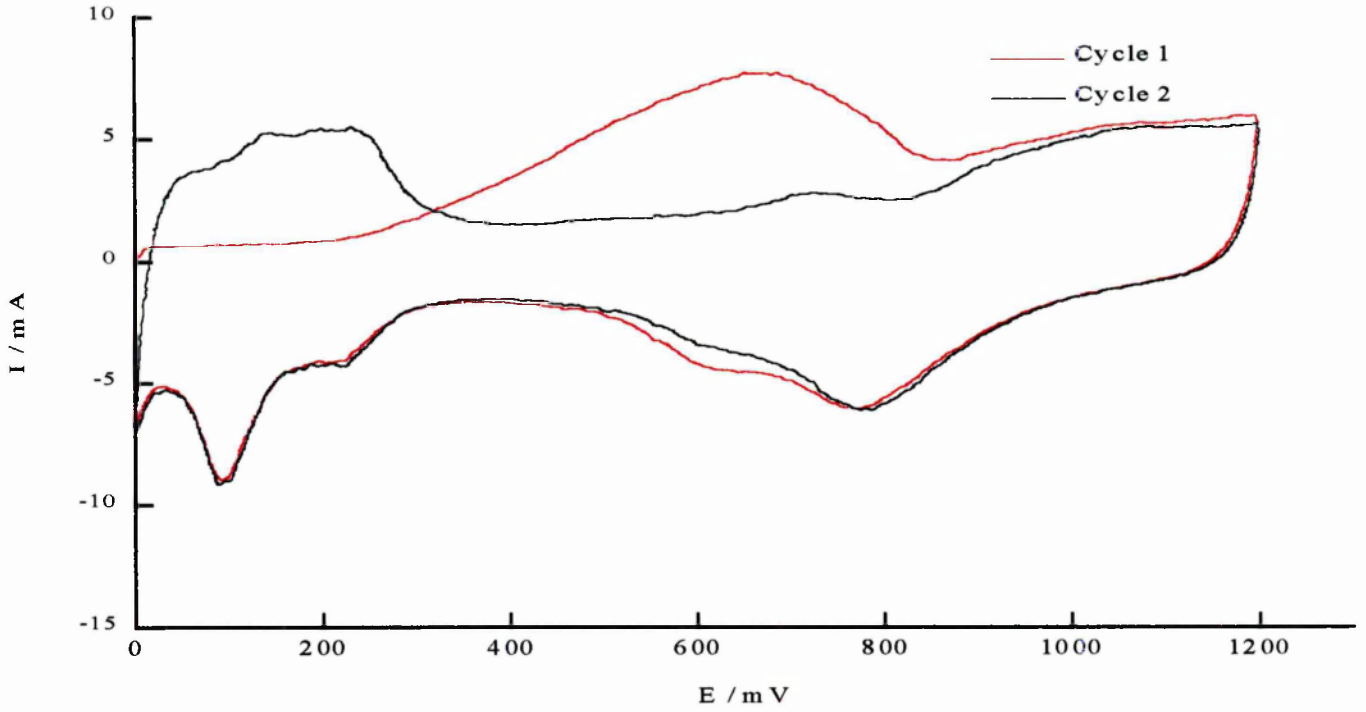

Figure 5.19 CO stripping voltammogram (Cycle 1) of 0.33 PtSn/C catalyst in 1 M H_2SO_4 followed by one cycle of linear potential sweep voltammetry (Cycle 2) at 10 mVs^{-1} at 303 K.

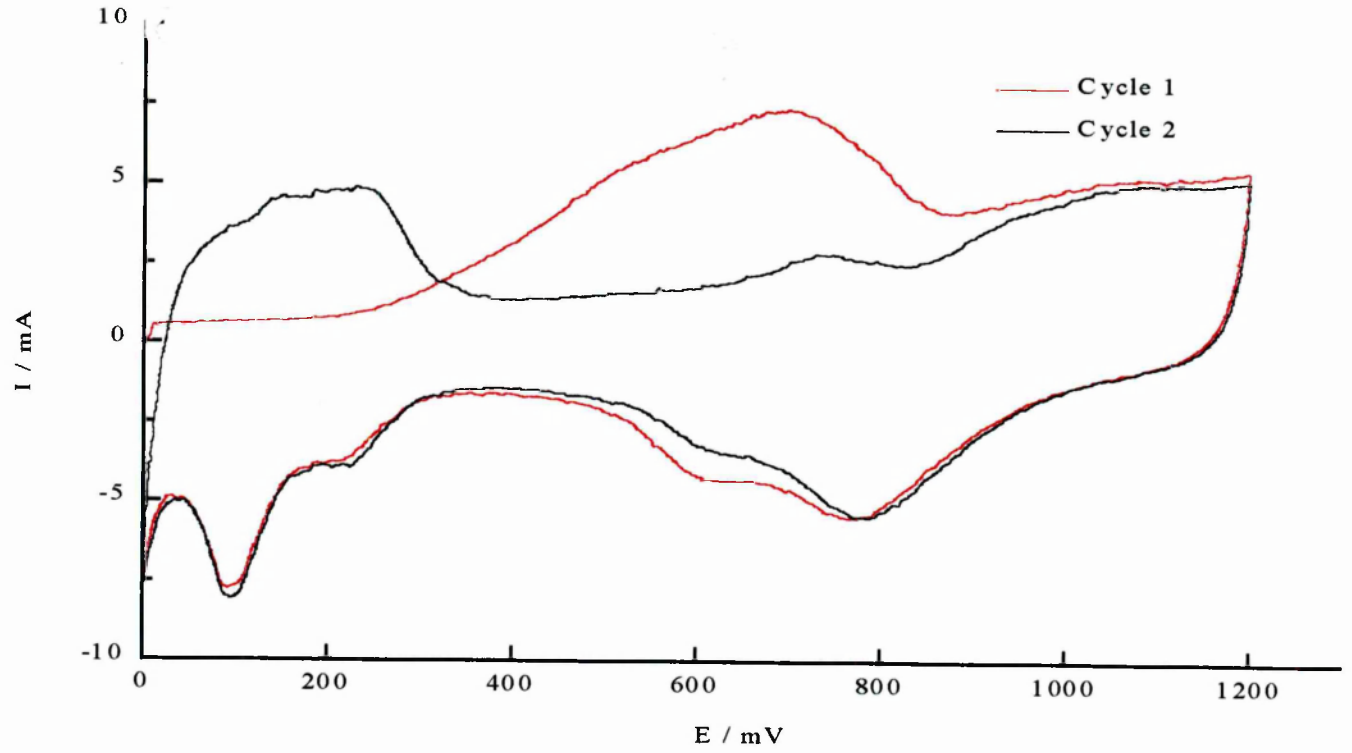

Figure 5.20 CO stripping voltammogram (Cycle 1) of 0.75 PtSn/C catalyst in 1 M H_2SO_4 followed by one cycle of linear potential sweep voltammetry (Cycle 2) at 10 mVs^{-1} at 303 K.

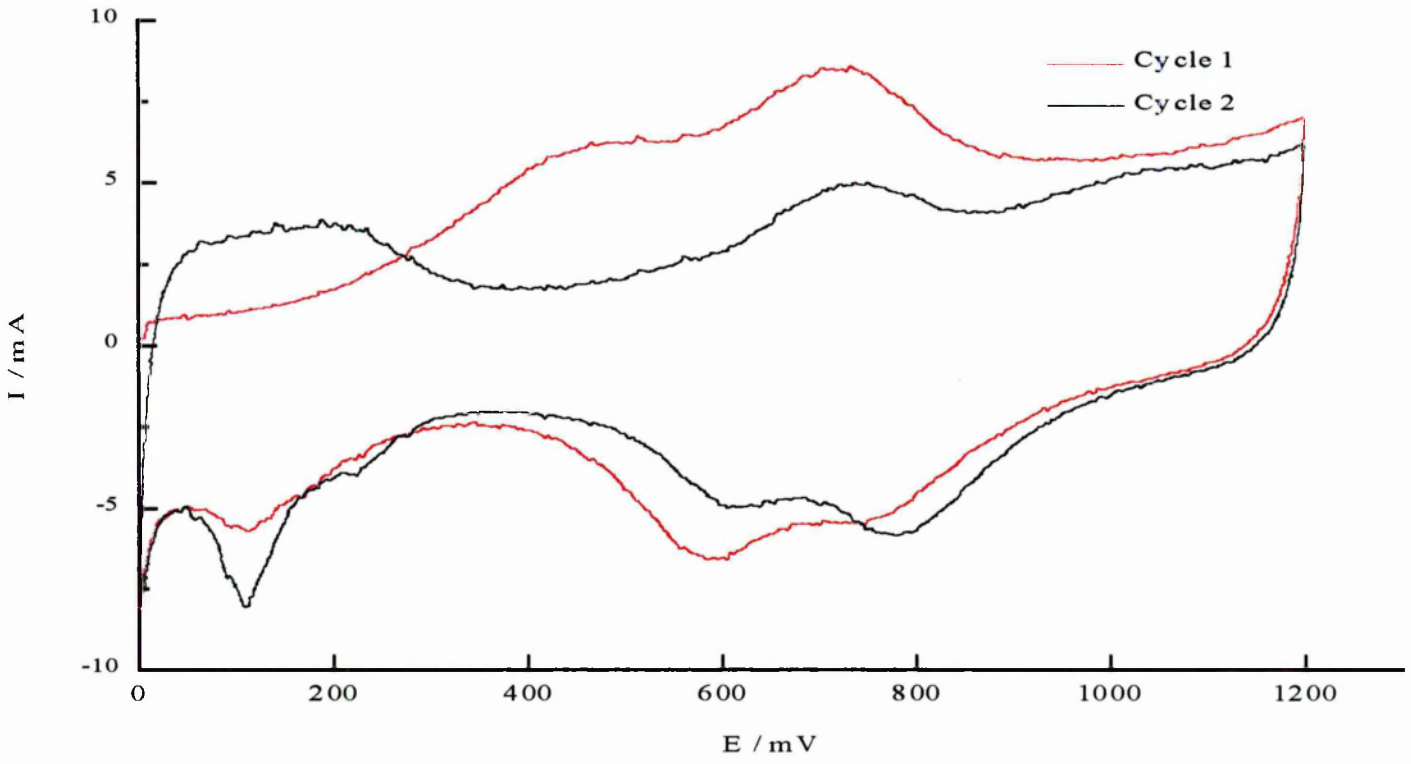

Figure 5.21 CO stripping voltammogram (Cycle 1) of 1 PtSn/C catalyst in 1 M H_2SO_4 followed by one cycle of linear potential sweep voltammetry (Cycle 2) at 10 mVs^{-1} at 303 K.

Table 5.12 Comparison of onset potential and peak position for CO oxidation for Pt/C, and range of PtSn/C catalysts.

Catalyst	Onset potential / V	Peak position / V
Pt/C	0.70	0.79
0.33 PtSn/C	0.32	0.67
0.5 PtSn/C	0.30	0.67
0.75 PtSn/C	0.32	0.70
1 PtSn/C	0.27	0.73

By comparison of the Figures 5.5, 5.17 and Figures 5.19 to 5.21 and Table 5.12 the following observations can be made:

i) With respect to CO electrooxidation, it is clear that both the onset potential and peak position for the PtSn/C catalysts are lower than the corresponding values for the monometallic Pt/C catalyst, confirming that addition of different coverage's of Sn promotes the activity of the Pt surface for electrooxidation of CO. The promotion of CO oxidation on the PtSn catalysts is speculated to be due to adsorption of H_2O on Sn sites adjacent to CO adsorbed on Pt and subsequent reaction of the H_2O and CO on adjacent sites. The onset potentials and peak positions, respectively, are plotted against nominal monolayer coverage in Figure 5.22, respectively. This emphasises the decrease in both peak potential and onset potential for the Sn containing catalysts compared to the

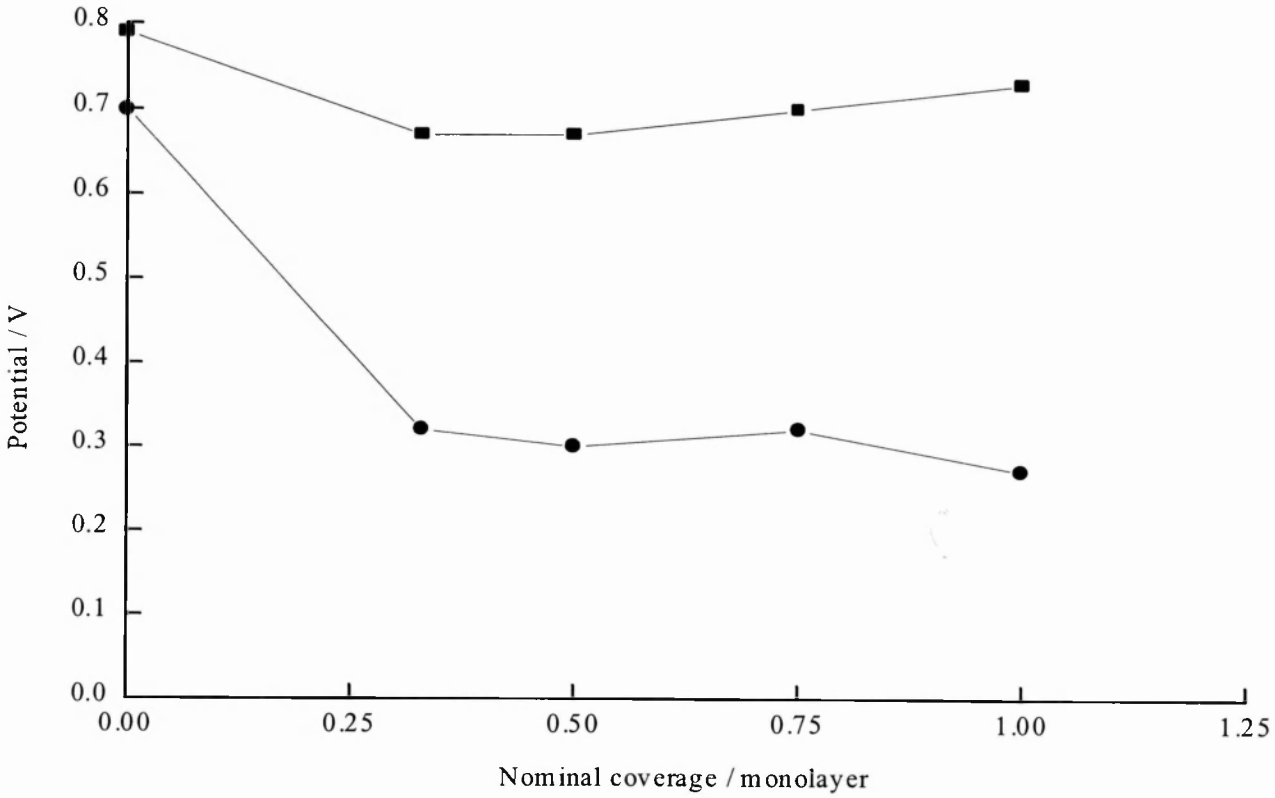

Figure 5.22 Plot of peak potentials (squares) and onset potentials (circles) for electrooxidation of CO on PtSn/C catalysts.

monometallic catalyst. With respect to the peak positions, after an initial decrease for the 0.33 ML catalyst compared to the Pt/C catalyst, further addition of Sn has the effect of slightly raising the potential of the main CO electrooxidation peak, however, it still remains significantly below the maximum of the monometallic catalyst. In terms of the onset potential, a more dramatic decrease is observed on addition of 0.33 ML of Sn to the monometallic catalyst. However, at higher coverage's the potentials are rather similar. It appears, therefore, that there is significant impact on peak position and onset potentials on addition of 0.33 ML but thereafter further addition of Sn does not have such a dramatic effect. Such a trend has already been observed for the chemisorption data of this range of catalysts where addition of 0.33 ML Sn decreases the fraction of surface Pt atoms rapidly and further addition of Sn does not decrease the dispersion at the same rate. It is therefore possible that the activity and Sn coverage are related. For all the bimetallic catalysts a shoulder is observed at ca. 0.5 V, which increases in magnitude as the tin loading increases. Significantly the shoulder is not observed during the CO electrooxidation cycle for the Pt monometallic catalyst. It is unlikely to be attributed to oxidation of adsorbed Sn species when one considers cycle 2 - it is clear that Sn oxidation occurs at about 0.6 to 0.8 V. It is probable that two different CO_{ads} species exist on the surface of the Pt particles. Therefore, the shoulder observed in the voltammogram is due to oxidation of a weakly adsorbed CO species. The weakly bound CO

species is believed to be adsorbed on Pt sites where Sn is in close association.

ii) In region I (0 to 0.4 V) of the voltammogram which corresponds to PtH_{ads} oxidation (anodic sweep) and hydrogen deposition on Pt (cathodic sweep), it is evident that the area of the voltammogram of these processes decreases as the tin monolayer coverage increases. This can be understood if we consider that as more Pt sites are covered with Sn (by increasing the nominal coverage) then fewer Pt sites are exposed at the surface and hence available to adsorb/desorb hydrogen.

iii) Between 0.6 and 0.8 V the oxidation of Sn (anodic scan) - probably corresponding to the oxidation of Sn(II) to Sn(IV) - and reduction of SnO_x (cathodic scan) can be observed. Clearly increasing the nominal monolayer coverage of Sn increases the size of the peak associated with these processes again indicating that more Sn is in contact with the Pt.

iv) With reference to the region (0.75 to 1.2 V) attributed to Pt oxidation (anodic scan) and PtO_x reduction (cathodic scan) the catalyst with the least Sn (0.33 ML) has the largest area and the sample with the most Sn (1 ML) has the smallest peak area. This again confirms that the higher loaded catalysts have fewer exposed surface Pt sites.

v) The loss of Sn from the surface of the Pt catalyst seen for the 0.5 ML catalysts is again seen here for the other PtSn catalysts and is particularly noticeable for the 1 ML. An increase in the hydride adsorption charge and a decrease in the charge associated with SnO_x reduction region are

observed going from the first to the second cycle as discussed previously in Section 5.3.4.1.

In addition to the observations above the following quantitative observations can also be made.

It is possible to calculate the Pt area uncovered between cycles by comparing the Pt-hydride area on two successive cycles. The difference between the two can be taken to be the amount of Sn removed from the surface during the potential cycle. This gives an indication of the strength of adsorption of the deposited Sn on the Pt surface. The results from this comparison are listed in Table 5.13 for the 0.33, 0.5, 0.75 and 1 ML PtSn/C bimetallic catalysts.

Table 5.13 Comparison of the Pt area uncovered between successive cycles.

Nominal Coverage / ML	Pt area uncovered between cycles 2 & 3/ %
0.33	5
0.5	5
0.75	3
1	15

Clearly the 0.33, 0.5 and 0.75 ML catalysts lose a similar quantity of Sn between the cycles, whereas, it appears that three times more Sn is removed for the 1 ML catalyst. It is probable that on the Pt surface, different Sn species exist with different strengths of adsorption. This is analogous with the situation where strongly and weakly bound hydrogen on the Pt surface have been shown to exist. The existence of different Sn species has been shown experimentally [19]. Hence it is clear that the 1 ML catalyst has a higher proportion of the weakly bound Sn species than the other catalysts [28].

It is possible to estimate the coverage of Pt by Sn derived by comparing the Pt-hydride adsorption area in the presence and absence of Sn using equation (5.9) below:

$$\theta_{Sn} = 1 - \frac{N_H^{Sn}}{N_H^0} \qquad (5.9)$$

where θ_{Sn} is the Sn coverage, N_H^{Sn} is the Pt-hydride area in the presence of Sn i.e., PtSn/C, and N_H° is the Pt-hydride area in the absence of Sn i.e., Pt/C, and these results are shown in Table 5.14.

Table 5.14 Comparison of experimental Pt coverage by Sn for range of PtSn/C catalysts.

Nominal Coverage / ML	Experimental Sn coverage / %
0.33	60
0.5	61
0.75	64
1	79

Clearly, addition of just a small amount of Sn (0.33 ML) causes a large number of Pt surface sites to be covered. Addition of further Sn does not cover the Pt sites at the same rate and at a nominal monolayer coverage it is not possible to cover all the Pt sites and therefore Pt sites are still exposed at the surface and available to adsorb hydrogen. This agrees with our previous results from the chemisorption of H_2 and CO that indicate that addition of a small amount of Sn decreased the surface Pt atoms exposed quite quickly. A plateau was then reached where further addition of Sn only decreased the number of Pt atoms slightly and at a nominal monolayer coverage about 10 % of Pt were still accessible to the adsorbing molecule. It has been observed experimentally that the stoichiometry of adsorption of Sn on Pt is 2:1 [29], i.e., one Sn atom covers two Pt atoms, hence a quantity of Sn equal to 0.5 ML should be sufficient to cover all the Pt surface atoms. A reason for the experimental observation that even at a nominal monolayer Sn coverage some of the Pt is still exposed could be

the inefficient packing geometry of the Sn on the Pt leaving gaps on the surface. Another possibility is the build up of mulitilayers of Sn rather than a monolayer which will leaving gaps where the Pt surface is exposed. The results of Pradier *et al.* may assist the interpretation of the data. In their study 2 monolayers of Sn were deposited on a Pt (533) surface and they found that at this level Sn formed "an island-type growth" of Sn atoms leaving the Pt atoms exposed at the surface rather than covering all of the Pt particles [30]. Therefore, in our case, at higher Sn loadings it may be possible that these island-type areas of Sn may exist on the Pt surface, thus explaining the ability of the Pt particles at monolayer coverage to adsorb H_2 and CO. These islands might form during the SOMC reaction itself, or due to Sn migration during the reduction procedure.

Similar trends are also apparent when one considers the data for the onset and peak potentials shown in Figure 5.22. Clearly addition of small amounts of Sn has the effect of decreasing both the onset and peak potentials significantly. However, further addition of Sn does not decrease the potentials similarly.

The original aim of this particular work was to compare the CO electrooxidation activity of a series of PtSn/C catalysts prepared by SOMC, with a PtSn/C catalyst prepared by a hydrolysis/precipitation method and a monometallic Pt/C catalyst. It is clear from the above data that the PtSn catalysts prepared by SOMC have a significantly lower onset potential (by about 0.4 V) than the Pt/C catalyst, and marginally lower onset potential than the traditionally prepared PtSn sample.

However even the lowest onset potentials observed here are still higher than those reported in the literature for PtSn alloy surfaces (onset potential 0.25 V) by Gasteiger *et al.* [8, 9].

5.4 Conclusions

A Pt/C catalyst has been modified by addition of different monolayer coverage's of Sn using SOMC and the catalysts characterised and tested by a range of traditional techniques and electrochemical methods. The main conclusions are summarised below:

i) Characterisation of the PtSn/C catalysts, prepared by SOMC, by traditional methods has confirmed the deposition of the Sn on the surface of the Pt particles. H_2 and CO chemisorption reveals that addition of 0.33 ML Sn results in a large decrease in the number of exposed Pt sites, however, addition of further Sn does not cover up the Pt surface at the same rate. TEM and XRD measurements indicate that the Pt particle size increases as the monolayer coverage of Sn increases.

ii) Comparison of two PtSn/C catalysts with similar loadings, one prepared by SOMC and the other by a hydrolysis/precipitation method, indicates that both catalysts are more active for the electrooxidation of CO than the Pt monometallic catalyst. Moreover, the catalyst prepared by SOMC is

more active than the traditionally prepared catalyst. The data indicates that the SOMC method is more successful in preparing a catalyst with the two metals in close contact than the more conventional hydrolysis/precipitation method.

iii) A range of PtSn/C catalysts, with Sn coverage varying from 0.25 to 1 ML, again exhibit greater CO electrooxidation activity than the monometallic catalyst. The most dramatic improvement in activity was observed by addition of 0.33 ML Sn. From a comparison of the Pt-hydride adsorption areas it is clear that addition of small amounts of Sn decreases the Pt surface area significantly although, even at nominally monolayer coverage some exposed Pt sites are still present. A higher proportion of weakly bound tin was found to be present on the catalyst with the highest coverage.

5.5 References

1 For introduction to fuel cells see the special issue of *Catalysis Today* **38**(4), (1997), dedicated to the subject.

2 Igarashi, H., Uchida, H., Suzuki, M., Sasaki, Y., and Watanabe, M., *Appl. Cat. A: Gen.* **159**, 159 (1997).

3 Frelink, T., Visscher, W., and van Veen, J. A. R., *J. Electroanal. Chem.* **382**, 65 (1995).

4 Gottesfeld, S., and Pafford, J. A., *J. Electrochem. Soc.* **135**, 2651 (1988).

5 Igarashi, H., Fujino, T., and Watanabe, M., *J. Electroanal. Chem.* **119,** 391 (1995).

6 Tobias, H., Paffett, M. T., Pappin, P. A., Valerio, J., and Gottesfeld, S., *in* "Proceedings of the Workshop on Direct Methanol-Air Fuel Cells" (A. R. Landgrebe, R. K. Sen, D. J. Wheeler, Eds.), The Electrochemical Society, New Jersey, (1992).

7 Gasteiger, H. A., Markovic, N., Ross, P. N., and Cairns, E. J., *J. Phys. Chem.* **98**, 617 (1994).

8 Markovic, N. M., Widelôv, A., Ross, P. N., Monteiro, O. R., and Brown, I. G., *Catal. Lett.* **43**, 161 (1997).

9 Gasteiger, H. A., Markovic, N., and Ross, P. N., *J. Phys. Chem.* **99**, 8945 (1995).

10 Verbeek, H., and Sachtler, W. M. H., *J. Catal.* **42**, 257 (1976).

11 Trasatti, S. M, and Petrii, J., *J. Electroanal. Chem.* **327**, 353 (1992).

12 Azaroff, L. V., and Buerger, M. J., "The Powder Method in X-Ray Crystallography." McGraw-Hill, New York, 1958.

13 Anderson, J. R., "Structure of Metallic Catalysts." Academic Press, London, New York, San Francisco, 1975.

14 Kunimori, K., Uchijima, T., Yamada, M., Matsumoto, H., Hattori, T., and Murakami, Y., *Appl. Catal.* **4**, 67 (1982).

15 Bett, J., Kinoshita, K., Routsis, K., and Stonehart, P., *J. Catal.* **31**, 325 (1973).

16 de Becdelièvre, A. M., de Becdelièvre, J., and Clavier, J., *J. Electroanal. Chem.* **294**, 97 (1990).

17 Thompsett, D., private communication.

18 de Bruijin, F. A., Kuster, B. F. M., and Marin, G. B., *Appl. Cat. A: Gen.* **145**, 351 (1996).

19 Vleeming, J. H., Kuster, B. F. M., Marin, G. B., Oudet, F., and Courtine, P., *J. Catal.* **166**, 148 (1997).

20 Aduriz, H. R., Bodnariuk, P., Coq, B., and Figuéras, F., *J. Catal.* **119**, 97 (1989).

21 Didillon, B., Houtman, C., Shay, T., Candy, J. P., and Basset, J. M., *J. Amer. Chem. Soc.* **115**, 9380 (1993).

22 Lamy-Pitara, E., El Ouazzani-Benhima, L., Barbier, J., Cahoreau, M., and Caisso, J., *Appl. Cat. A: Gen.* **81**, 47 (1992).

23 Passos, F. B., Schmal, M., and Vannice, M. A., *J. Catal.* **160**, 106 (1996).

24 Birchem, T., Pradier, C. M., Berthier, Y., and Cordier, G., *J. Catal.* **161**,

68 (1996).

25 Tauster, S. J., Fung, S. C., and Garten, R. L., *J. Amer. Chem. Soc.* **100**, 170 (1978).

26 Beden, B., Lamy, C., de Tacconi, N. R., and Arvia, A. J., *Electrochimica Acta* **35**, 691 (1990).

27 Lamy, E., Barbier, J., and Lamy, C., *J. Chim. Phys.* **77**, 967 (1980).

28 Bowles, B. J., and Cranshaw, T. E., *Phys. Lett.* **17**, 258 (1965).

29 Szabos, S., *J. Electroanal. Chem.* **172**, 355 (1984).

30 Birchem, T., Pradier, C. M., Berthier, Y., and Cordier, G., *J. Catal.* **146**, 503 (1994).